WIDE FIELD/PLANETARY CAMERA OPTICS STUDY

(NASA-CR-158578) WIDE FIELD/PLANETARY CAMERA OPTICS STUDY Final Report (Eastman Kodak Co.) 230 p HC A11/MF A01 CSCL 20F

N79-23778

Unclas
G3/74 25181

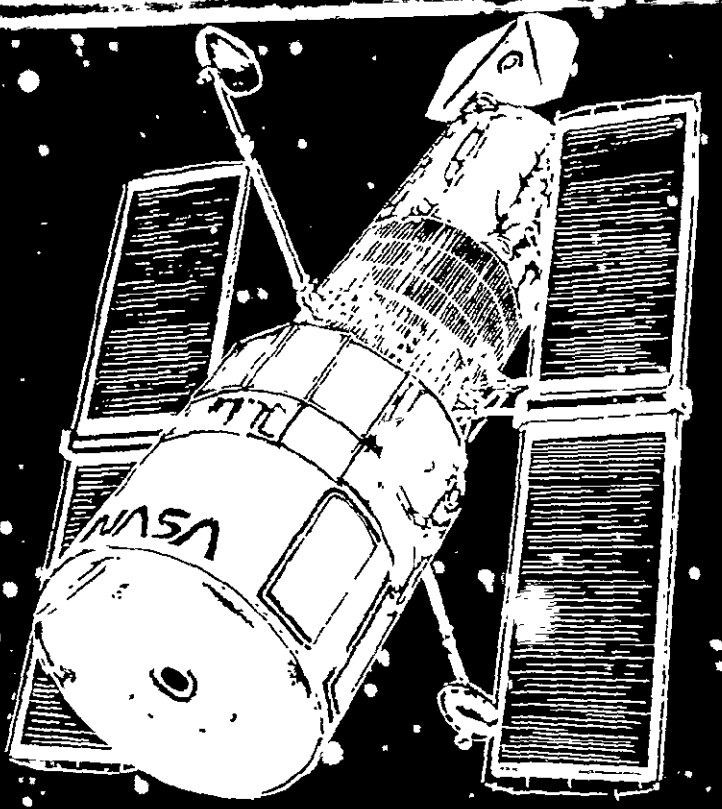

Kodak

JPL Subcontractor Report

JPL FILE NO. 9950-59

TITLE WIDE FIELD/PLANETARY CAMERA OPTICS STUDY

AUTHOR(S) Eastman Kodak Company

SUBCONTRACTOR Eastman Kodak Company/ Kodak Apparatus Division

SUBCONTRACTOR REPORT NO. Final Report

REPORT DATE March 23, 1979 PERIOD COVERED ---

JPL CONTRACT NO. 955182 PAGE COUNT 230

4/23/79KW

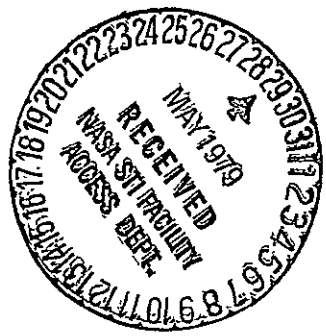

This document has been released for external distribution.

9950-59

WIDE FIELD/PLANETARY CAMERA OPTICS STUDY

FOR

CALIFORNIA INSTITUTE OF TECHNOLOGY
JET PROPULSION LABORATORY
PASADENA, CALIFORNIA

CONTRACT NO. 955182

BY

EASTMAN KODAK COMPANY
KODAK APPARATUS DIVISION
ROCHESTER, NEW YORK

23 MARCH 1979

P. A. JONES
STUDY MANAGER

L. P. MITCHELL
GOVERNMENT PROJECTS

TABLE OF CONTENTS

LIST OF FIGURES

LIST OF TABLES

1.0 INTRODUCTION

1.0 INTRODUCTION

This document constitutes the final report for the Wide Field Planetary Camera Optics Study, sponsored by California Institute of Technology Jet Propulsion Laboratory and conducted by Eastman Kodak Company.

1.1 BACKGROUND

The Wide Field/Planetary Camera (WF/PC) will be used with the Space Telescope (ST) to obtain high angular resolution astronomical information over a wide field. The Jet Propulsion Laboratory design concept employs internal optics to relay the ST image to a CCD detector system.

1.2 PROGRAM

The purpose of the Wide Field/Planetary Camera Optics Study was to:

1. Establish design feasibility of the baseline optical design concept.
2. Optimize the baseline optical design, if necessary.
3. Calculate design performance data for the optimized design.
4. Perform optical sensitivity and tolerance analysis.
5. Establish feasibility of a pyramid mirror as a focus mechanism.
6. Establish manufacturability of the unmounted optical components.
7. Establish detailed techniques for acceptance testing of the two mirror Cassegrain relays.
8. Provide detailed optical component drawings.

1.3 PROGRAM SCHEDULES

The start of contract was 11 August 1978. Two technical briefings were held at the Jet Propulsion Laboratory. The first briefing was on 12 October 1978

and covered the analyses and optimization of the baseline design concept. The second briefing was on 9 January 1979 and covered optical design performance predictions, sensitivity and tolerance analyses, manufacturability of the optical components, and acceptance testing of the two mirror Cassegrain relays.

1.4 ACKNOWLEDGEMENTS

The following people contributed to this study:

Study Manager	-	Peter A. Jones
Optical Design	-	Richard A. Stark
Optical Fabrication	-	John E. Schlauch
Optical Testing	-	John J. Hannon
		Alexander Zanolli
System Engineering	-	Peter A. Jones
		Stanley E. Ekiert

1.5 STUDY RESULTS

The primary and secondary mirror surfaces in the wide field camera have been changed in the optical design from conic aspheres to general aspheres. This design change increases the off-axis performance with a minor reduction in on-axis performance. The planetary camera is optimized with no changes in the design necessary.

The unmounted optical components are within the state-of-the-art; however, a development program will be needed to manufacture the aspherical surfaces.

Stringent performance requirements of the combined Optical Telescope Assembly (OTA)-Wide Field/Planetary Camera (WF/PC) demand quantitative interferometric testing throughout the buildup of the WF/PC.

2.0 OTA OPTICAL CONFIGURATION

2.0 OTA OPTICAL CONFIGURATION

The OTA optical configuration is a catoptric Ritchey-Chretien version of the Cassegrain telescope (figure 2.0-1). The configuration consists of hyperbolic primary and secondary mirrors. The conic shapes have been chosen to simultaneously correct spherical aberration and coma. The aberrations of astigmatism, field curvature, and distortion are present off-axis in predictable amounts. Field curvature and astigmatism appear as two well-defined curved focal surfaces (two concave prolate spheroids), shown in figure 2.0-2. At a semi-field angle of 15.6 arcminutes (edge of tracking field of fine guidance sensor), the primary astigmatism is 0.73 λ rms (λ = 0.6328 Angstroms) with a residual coma of 0.2 λ rms. At a semi-field angle of 7.8 arcminutes (inside data field of axial scientific instrument) the primary astigmatism is 0.18 λ rms with a residual coma on the order of 0.002 λ rms.

An optical control subsystem is provided on the OTA. Its purpose is to (1) sense the condition of primary mirror position, (2) sense the condition of secondary mirror optical axis to primary mirror optical axis alignment, (3) sense the condition of focus, (4) define the relative positions of the OTA focal surfaces mounted on the focal plane structure, (5) provide the means for primary mirror position adjustment and, (6) provide means by which alignment and focus can be adjusted.

Under orbital operational conditions for up to ten hours of observation, the optical control subsystem will be used to maintain the on-axis static wavefront error to be less than 0.075 λ rms. However, it is anticipated that the on-axis static wavefront error should be less than 0.05 λ rms. Coupled with a worst case image stability requirement of 0.007 arcseconds (overall Space Telescope), 70 percent of the encircled energy in the star image will occur in a radius of 0.1 arcseconds.

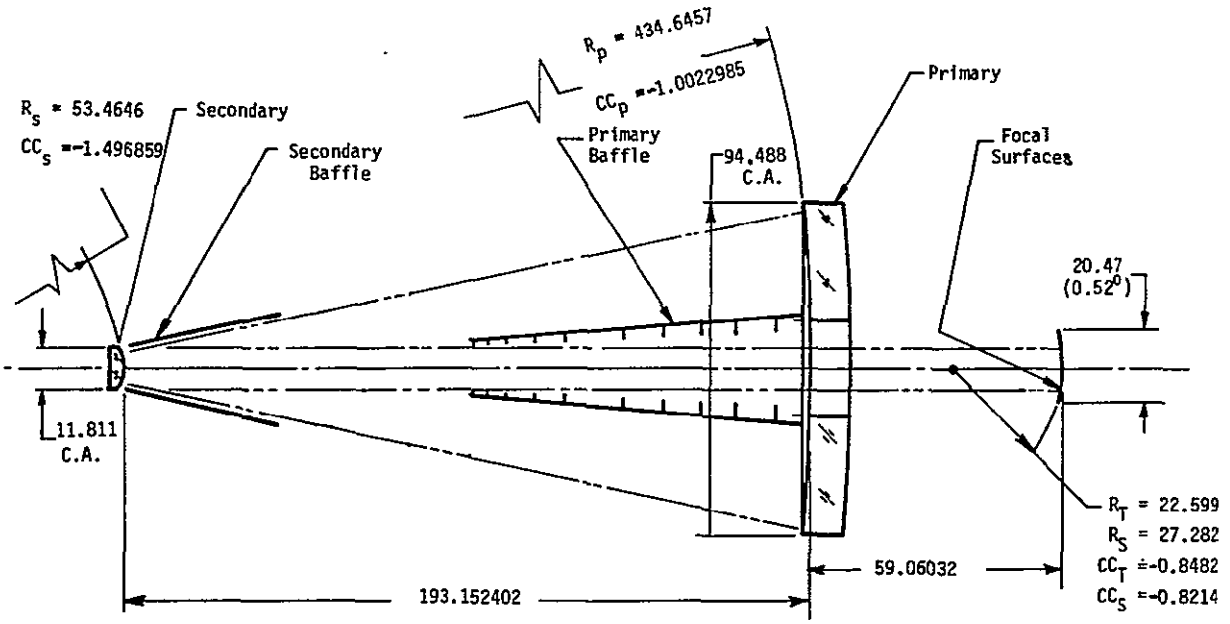

SYSTEM FOCAL RATIO - $f/24$
SYSTEM FOCAL LENGTH - 2267.7

OTA OPTICAL CONFIGURATION

Figure 2.0-1

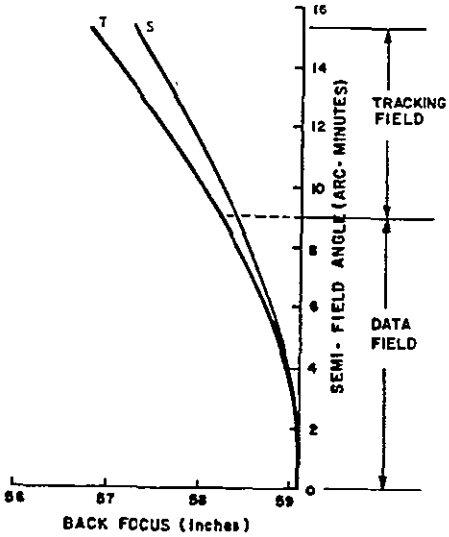

$X_S = (1.833 \times 10^{-2})Y^2 + (1.099 \times 10^{-6})Y^4 + (1.318 \times 10^{-10})Y^6 + (1.977 \times 10^{-14})Y^8$

$X_T = (2.212 \times 10^{-2})Y^2 + (1.644 \times 10^{-6})Y^4 + (2.443 \times 10^{-10})Y^6 + (4.539 \times 10^{-14})Y^8$

FOCAL PLANE TOPOGRAPHY

Figure 2.0-2

In figure 2.0-3 is shown the designed, static, on-axis geometric mean MTF for the OTA. The geometric mean is an average of the sagittal and tangential MTF's which are independently calculated. In an operational (dynamic) condition, the designed MTF will be reduced by manufacturing, alignment, and focus errors as well as pointing stability error. As noted, the OTA is designed to have an on-axis, static wavefront error of no more than 0.05 λ rms (λ = 6328 Angstroms) with an autocorrelation length of 0.125. The predicted "manufactured" on-axis, static MTF is shown in figure 2.0-3. The overall system is designed to have a pointing stability error of no greater than 0.007 arcseconds. Also shown in figure 2.0-3 is the predicted on-axis, operational MTF performance.

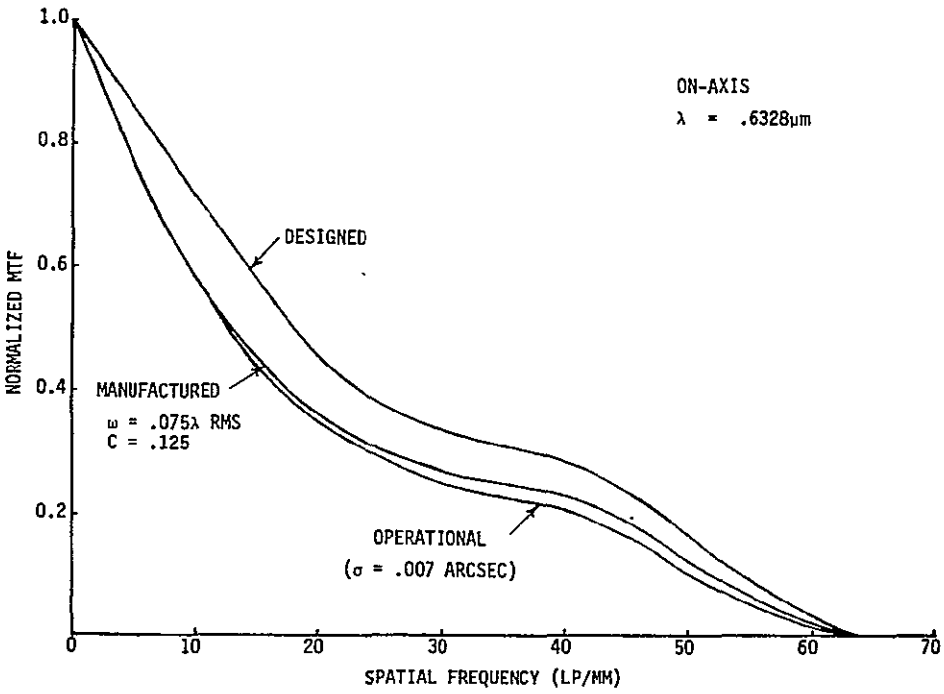

OTA PERFORMANCE PREDICTION

Figure 2.0-3

The Space Telescope is expected to make exposures on the day side of the orbit when stray light from the sun or the earth could limit the sensitivity of its instruments. Therefore, an extensive system of light shields and baffles to protect the focal surface from stray light has been specified for the OTA.

One of the principal advantages of a space telescope is that ultraviolet measurements can be made without detriment due to absorption or turbulent effects from an intervening atmosphere. (Of special astronomical interest is the Lyman Alpha line at 1215 Å.) To meet the overall wavelength requirements, a coating of aluminum with a protective overcoating of magnesium fluoride has been specified for the mirror surfaces.

2.1 PARAXIAL EVALUATION OF OTA OPTICS

The locations of optical images are calculated by paraxial ray trace equations. These equations are:

$$y_i = y_{i-1} + (nu)_{i-1}\ (t/n)_{i-1}$$

$$(nu)_i = (nu)_{i-1} + y_i\ (n_{i-1} - n_i)r_i$$

Where:

y_i = ray height on i-th surface

u_i = ray slope following i-th surface

n_i = refractive index following i-th surface

t_i = thickness between i-th surface and next surface

r_i = vertex radius of curvature of i-th surface

Thickness and index are positive (+) in the region where the ray travels from left to right and the vertex radius of curvature is positive (+) if its center-of-curvature lies to the right of the vertex.

2.1.1 OTA Focal Surface Location, Focal Length and *f*-number

For the OTA, the following surface subscripts will be used:

0 - object surface
1 - entrance pupil/primary mirror
2 - secondary mirror
3 - exit pupil
4 - image surface

The OTA lens prescription is:

$r_1 = -1104.0$ cm $t_1 = -490.6071$ cm $n_1 = -1.0$

$r_2 = -135.8$ cm $(t_2 + t_3) = 640.61992$ cm $n_2 = n_3 = +1.0$

Let an axial reference ray, parallel to the optical axis ($u_0 = 0$) be incident upon the primary mirror. The height of this incoming ray, traveling left to right, is 100 units ($y_0 = y_1 = 100$). After reflection from the primary mirror, the ray slope is:

$$(nu)_1 = 0 + (100)(1 + 1)/(-1104.0) = -0.18115942$$

At the secondary mirror, the ray height is:

$$y_2 = 100 + (-0.18115942)(-490.6071/-1) = 11.121902 \text{ units}$$

And after reflection from the secondary mirror, the ray slope is:

$$(nu)_2 = (-0.18115942) + (11.121902)(-1 -1)(-135.8) = -0.017361156$$

At this point in the analysis, the location of the exit pupil is unknown; however, because it is a dummy surface causing no reflection or refraction of the ray, it can be neglected and the ray can be traced directly to the image surface. At the image surface, the ray height is:

$$y_4 = (11.121902) + (-0.017361156)(640.61992/1.0) = 0.000000 \text{ units}$$

A ray height of zero at the OTA image surface shows that incoming on-axis rays are brought to a focus at the prescribed image surface. The focal length (f) of the OTA can also be easily checked by the formula:

$$f = -y_1 / u_R$$

Where:

Surface 1 is the entrance pupil

Surface R is the exit pupil

Then, the calculated OTA focal length is:

$$f = -100/(-0.017361156) = 5760 \text{ cm}$$

The OTA system f-number is the ratio of system focal length divided by entrance pupil diameter. This diameter, 240 cm, is also the clear aperture diameter of the primary mirror. Thus 5760/240 = 24 and the system f-number is $f/24$.

2.1.2 OTA Exit Pupil

The exit pupil of the OTA is the image of its entrance pupil. The location of the exit pupil is found by tracing a chief ray through the optical system. Chief rays, by definition, pass through the centers of both the entrance and exit pupils. Thus, the height of a chief ray in the entrance pupil is zero ($\bar{y}_1=0$). Let the slope for an incoming reference chief ray be unity ($\bar{u}_0 = 1.0$).

Then, the slope for the chief ray after reflection from the primary mirror is:

$$(n\bar{u})_1 = 1.0 + (0)\ (1 + 1)/(-1104.0) = 1.0$$

The ray height of the chief ray at the secondary mirror is:

$$\bar{y}_2 = 0 + (1.0)(-490.6071/-1) = 490.6071 \text{ units}$$

After reflection from the secondary mirror, the slope of the chief ray is:

$$(n\bar{u})_2 = 1.0 + (490.6071)(-1 - 1)/(-135.8) = 8.225436$$

The height of the chief ray on the next surface is then calculated. This next surface is the exit pupil and the chief ray height is, by definition, zero at that surface ($\bar{y}_3 = 0$). Thus, equation (1) is written:

$$0 = 490.6071 + (8.225436)(t_2/1)$$

Solving for the unknown distance t_2:

$$t_2 = -(490.6071)/(8.225436) = -59.645118 \text{ cm}$$

The exit pupil, therefore, is located 59.645118 cm from the secondary mirror vertex. The minus sign means that this exit pupil is a virtual image of the entrance pupil and is located to the left of the secondary mirror.

Finally, the spacing t_3 between the exit pupil and the image surface is solved:

$$t_3 = (t_2 + t_3) - t_2 = (640.61992) - (-59.64512) = 700.26504 \text{ cm}$$

Now that t_2 and t_3 are known, the height (y_3) of the axial ray on the exit pupil can be calculated. Using equation (1):

$$y_3 = 11.121902 + (-0.017361156)(-59.645118/1) = 12.15741 \text{ units}$$

The actual diameter (Dep') of the OTA exit pupil in centimeters is found by scaling y_3 by the ratio of actual entrance pupil diameter (240 cm) divided by axial ray height (100 units) used at the entrance pupil:

$$\text{Dep}' = (12.15741)(240/100) = 29.17778 \text{ cm}$$

In summary, the above paraxial evaluation of the OTA verified the location of the OTA focal surface and the values of OTA focal length and f-number with respect to the OTA lens prescription which was provided. Also, the above evaluation determined the location and diameter of the OTA exit pupil.

2.1.3 OTA Conic Constants

The OTA is a two-mirror Ritchey-Chretien (RC) optical system. An RC system is corrected for third-order spherical aberration and coma by adjustment of the conic constants for the two mirrors. The following sets of equations are used to calculate these conic constants (K). Subscript 1 refers to the first mirror (primary) and subscript 2 refers to the second mirror (secondary).

$$B_1 = (nu)_0 + y_1/r_1$$

$$B_2 = (nu)_2 + y_2/r_2$$

$$A_1 = (n\bar{u})_0 + \bar{y}_1/r_1$$

$$A_2 = (n\bar{u})_2 + \bar{y}_2/r_2$$

$$B_1' = (nu)_1 - (nu)_0$$

$$B_2' = (nu)_2 - (nu)_1$$

$$C_1 = +2\,(y_1/r_1)^3$$

$$C_2 = -2\,(y_2/r_2)^3$$

$$E = B_1\,{}^2B_1'\,y_1 + B_2\,{}^2\,B_2'\,y_2 + R_s$$

$$F = A_1\,B_1\,B_1'\,y_1 + A_2\,B_2\,B_2\,y_2 + R_c$$

$$K_1 = (F\,y_2 - E\,\bar{y}_2)\,/C_1\,(y_1\,\bar{y}_2 - \bar{y}_1\,y_2)$$

$$K_2 = (F\,y_1 - E\,\bar{y}_1)\,/C_2\,(y_2\,\bar{y}_1 - \bar{y}_2\,y_1)$$

The application of these equations will be illustrated by calculating the conic constants for the OTA. The paraxial ray trace data generated in the preceding sections will be used. For those data, the subscripts coincide with those used in the above equation set.

$$B_1 = 0 + 100/(-1104) = -0.0905797101$$

$$B_2 = (-0.017361156 + 11.121902/(-135.8) = -0.0992602871$$

$$A_1 = 1 + 0/(-1104) = 1$$

$$A_2 = (8.225436) + 490.6071/(-135.8) = 4.612718032$$

$$B_1' = (-0.18115942) - 0 = -0.18115942$$

$$B_2' = (-0.017361156) - (-0.18115942) = 0.163798264$$

$$C_1 = 2\left[100/(-1104)\right]^3 = -0.0014863558$$

$$C_2 = -2\left[11.121902/(-135.8)\right]^3 = 0.0010986715$$

The quantities R_s and R_c are residual spherical aberration and residual coma, respectively. For the OTA, these two aberrations are corrected exactly. Hence, $R_s = 0$ and $R_c = 0$. Then:

$$E = -0.1306866124$$

$$F = 0.8068316434$$

And:

$$K_1 = -1.0022985$$

$$K_2 = -1.4968601$$

These conic constants agree exactly with those specified in the OTA lens prescription.

3.0 WF/PC OPTICAL CONFIGURATION

3.0 WF/PC OPTICAL CONFIGURATION

In order to meet the scientific objectives of the Space Telescope, the scientific instruments must introduce the least possible degradation to the image provided by the OTA. Ideally, all of the scientific instruments would be designed with their detector surfaces at the OTA focal surface (figure 3.0-1); however, there are two basic reasons for optics in the scientific instruments. The first is to correct the astigmatism in the OTA data field (figure 3.0-2). The Space Telescope optical system (OTA + scientific instrument) can then be considered field curvature limited (one well-defined image surface). In this case, the field curvature could be "accommodated" by a similarly curved detector surface. The second reason is to change the OTA system focal ratio ($f/24$). This will change the angular resolution and the field of view.

The scientific objectives of the WF/PC involve obtaining high angular resolution over the widest field of view possible ($\simeq$ 3 arcminutes). UV requirements prohibit system refractive elements. Reflective surfaces must be held to a minimum to meet the photometric requirements. The optical design concept is based on optimizing the image spot size to the CCD pixel size by changing the OTA focal ratio ($f/24 \rightarrow f/12.9$). To meet the field of view requirement (3 arcminutes x 3 arcminutes) with state-of-the-art CCD technology (800x800 array), the total field (1600x1600 array) is split into four fields via a four faceted reflective pyramid. The OTA focal ratio is changed and re-imaged at a second focal surface via a finite conjugate Cassegrain relay. One of the four optical paths is shown in Figure 3.0-3. To meet the angular resolution and field of view requirements of the planetary camera, a separate optical system ($f/30$) is used.

In the baseline design, the Cassegrain relays have been corrected for third order spherical aberration and coma. Astigmatism and field curvature are not controlled in the design. In the optimized design (see Section 6.1) for the wide field camera, these aberrations are balanced by changing the asphericity of the Cassegrain relay primary and secondary mirrors. It should be noted, however, that the WF/PC focal surface for the wide field camera is not flat (see section 7.2).

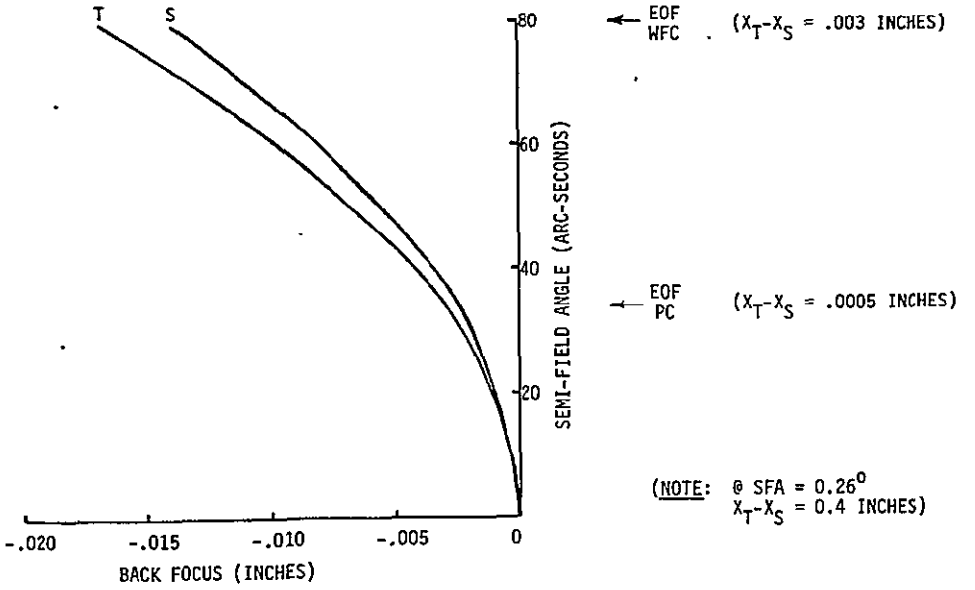

OTA FOCAL SURFACE CONTOUR

Figure 3.0-1

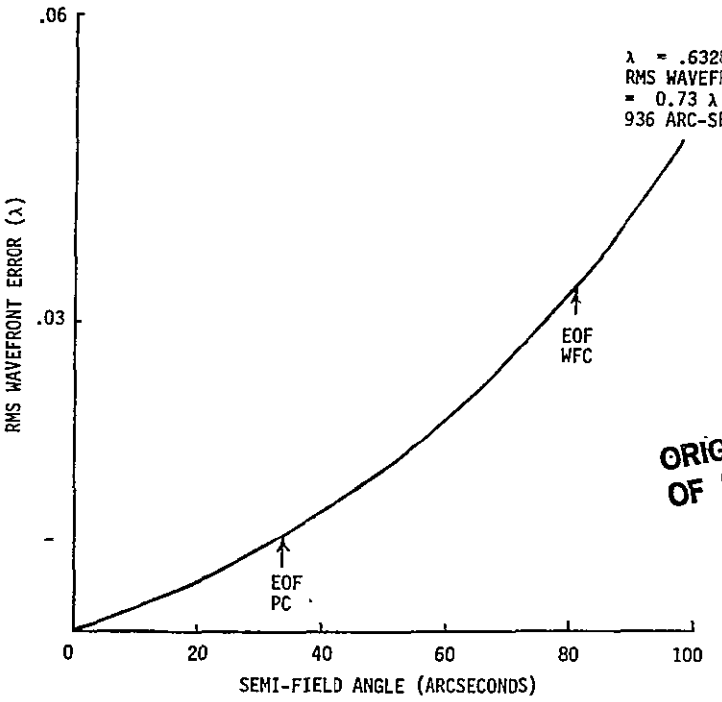

RMS WAVEFRONT ERROR VS SEMI-FIELD ANGLE
(OTA FOCAL SURFACE)

Figure 3.0-2

The Planetary Camera also has residual astigmatism and field curvature. However, the effect of these aberrations on image quality is negligible because this system operates at a higher f-number and has a smaller angular field.

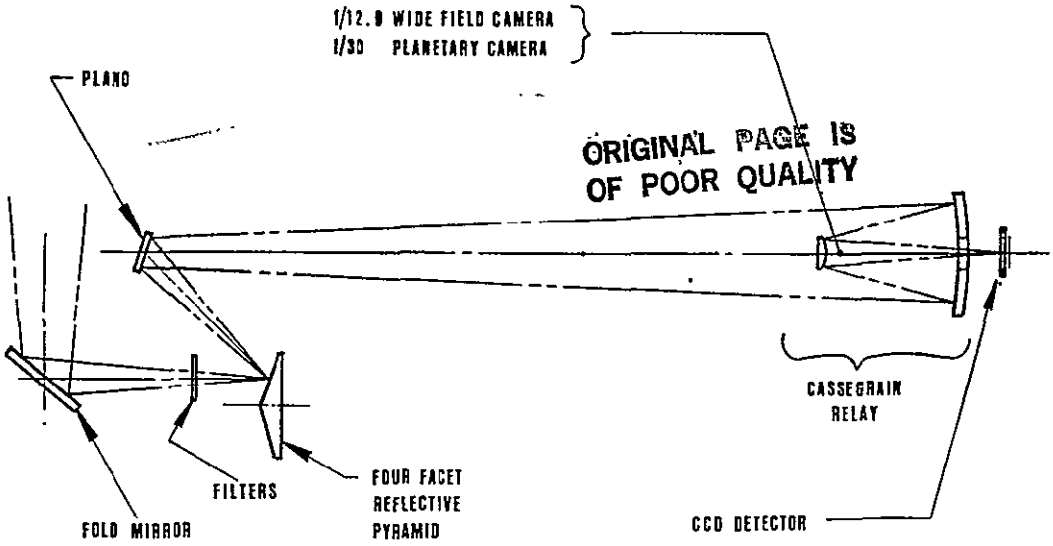

WF/PC OPTICAL CONFIGURATION

Figure 3.0-3

3.1 PARAXIAL EVALUATION OF WF/PC OPTICS

The following surface subscripts will be used for the WF/PC optics and OTA exit pupil:

3 - OTA exit pupil
4 - OTA image surface/field mirror (pyramid face)
5 - primary mirror
6 - secondary mirror
7 - primary mirror hole

8 - window (first surface)
9 - window (second surface)
10 - image surface (detector)

3.1.1 *f*/12.88 Focal Surface Location, Focal Length, and *f*-number

The lens prescription for this relay system is:

r_4 = 306.84 cm	t_4 = 113.0610 cm	n_4 = 1.0
r_5 = -40.5662 cm	t_5 = -16.2590 cm	n_5 = -1.0
r_6 = -28.5460 cm	t_6 = 16.2590 cm	n_6 = 1.0
r_7 = infinity	t_7 = 4.2227 cm	n_7 = 1.0
r_8 = infinity	t_8 = 0.2500 cm	n_8 = 1.387
r_9 = infinity	t_9 = 0.1011 cm	n_9 = 1.0

In the preceding section, an on-axis ray was made incident upon the OTA primary mirror at a height of 100 units. This same ray came to a focus (y_4 = 0) at the OTA focal surface and was incident upon that surface at a slope of $(nu)_3 = (nu)_2$ = -0.017361156. We will now continue this paraxial ray trace through the wide-field relay system where the relay is assumed to be in-line with the OTA.

After reflection from the field mirror, which is coincident with the OTA image surface, the reflected ray slope from equation (2) is:

$$(nu)_4 = (-0.017361156) + (0)(-1 \quad -1)/306.84 = -0.017361156$$

At the primary mirror of the relay lens, the ray height is:

$$y_5 = 0 + (-0.017361156)(113.0610/1.0) = 1.962870 \text{ units}$$

After reflection from the primary mirror, the ray slope is:

$$(nu_5) = -0.017361156 + (-1.962870)(1 + 1)/(-40.5662)$$
$$= + 0.079412496$$

The ray height at the secondary mirror is:

$$y_6 = -1.962870 + (0.079412496)(-16.2590)/(-1.0)$$
$$= -0.671702 \text{ units}$$

The ray slope, after reflection from the secondary mirror, is:

$$(nu)_6 = (0.079412496) + (-0.671702()-1 -1)/(-28.5460)$$
$$= + 0.032351479$$

At the primary mirror hole, the ray height is:

$$y_7 = 0.671702 + (0.032351479)(16.2590/1.0)$$
$$= -0.145699 \text{ units}$$

There is no refraction or reflection at the primary mirror hole, so the ray slope is unchanged:

$$(nu)_7 = (nu)_6 = +0.032351479$$

The ray height at the first surface of the window is:

$$y_8 = -0.145699 + (0.032351479)(4.2227/1.0)$$
$$= -0.009089 \text{ units}$$

Refraction at this surface changes the ray slope to the following value:

$$(nu)_8 = 0.032351479 + (-0.009089)(1.0 - 1.387)/\infty$$
$$= +0.032351479$$

The "optical slopes" $(nu)_7$ and $(nu)_8$ are equal. However, the geometric slopes u_7 and u_8 differ:

$$u_7 = (nu)_7/n_7 = 0.032351479/1.0 = 0.032351479$$
$$u_8 = (nu)_8/n_8 = 0.032351497/1.387 = 0.23324787$$

At the second surface of the window, the ray height is:

$$y_9 = 0.009089 + (0.032351479)(0.2500/1.387)$$
$$= -0.003257 \text{ units}$$

The ray slope following this refractive surface is:

$$(nu)_9 = 0.032351479 + (-0.003257)(1.387 - 1.0)/\infty$$
$$= 0.032351479$$

Finally, at the image (detector) surface, the ray height is:

$$y_{10} = -0.003257 + (0.032351479)(0.1011/1.0)$$
$$= 0.000013 \text{ units}$$

This value of ray height is significant, which means that the location of the detector in the lens prescription is not exactly at the paraxial focus. The exact spacing (t_9') between the window and the paraxial image surface is:

$$t_9' - y_9/(nu)_9 = -(-0.003257)/0.032351479 = 0.1007 \text{ cm}$$

The focal length, calculated from equation (3), for the OTA and relay lens system is:

$$f = -100/(0.032351479) = (-)\ 3091.0 \text{ cm}$$

In this instance, the minus sign for the focal length means that the relay lens inverted the image which was formed by the OTA. The focal length value itself is positive.

The f-number for the OTA and relay lens system is the ratio of system focal length divided by the 240 cm entrance pupil diameter. Thus, 3091/240 = 12.88 and the system f-number is 12.88.

3.1.2 *f*/12.88 Exit Pupil

The chief ray was traced through the OTA in section 2.0 of this report. This ray entered the system entrance pupil (OTA primary mirror aperture) at a unit slope ($n\bar{u}_1 = 1.0$) and emerged from the OTA exit pupil at a slope of 8.225436. The paraxial trace of this chief ray through the wide-field relay system is performed in exactly the same manner as that for the axial ray. Thus, ray height and slope data will be listed below without additional comments.

$\bar{y}_3 = 0$	$(n\bar{u})_3 = 8.22543$
$\bar{y}_4 = 5759.99$	$(n\bar{u})_4 = -29.3185$
$\bar{y}_5 = 2445.21$	$(n\bar{u})_5 = -149.873$
$\bar{y}_6 = 8.4327$	$(n\bar{u})_6 = -149.282$
$\bar{y}_7 = -2418.74$	$(n\bar{u})_7 = -149.282$
$\bar{y}_8 = -3049.11$	$(n\bar{u})_8 = -149.282$
$\bar{y}_9 = -3076.02$	$(n\bar{u})9 = -149.282$
$\bar{y}_{10} = -3091.05$	$(n\bar{u})_{10} = -149.282$

The location of the exit pupil for the OTA and relay lens system is $\bar{y}_{10}/(n\bar{u})_{10}$ or 20.7062 cm ahead of the image (detector) surface. The diameter of this exit pupil is the product of the entrance pupil diameter of 240 cm times exit pupil magnification, $-(n\bar{u}_1)/(n\bar{u})_{10}$, of 1/149.282. This computation yields an exit pupil diameter of 1.6077 cm.

The distance between the secondary mirror and the image surface is ($t_6 + t_7 + t_8 + t_9'$) or 20.8324 cm, and the distance between the exit pupil and the image surface, as just noted above, is 20.7062 cm. Thus, the system exit pupil is located at the relay secondary mirror.

3.1.3 *f*/12.88 Clear Aperture Sizes

Clear aperture heights are listed in table 3.1.3-1. For each surface, the axial ray height (y) and chief ray height ($\bar{y}$) are given. For this analysis, only the absolute values of these quantities are significant. The axial ray heights are scaled by the ratio of OTA primary mirror radius (120 cm) divided by input ray height (100 units) at the primary mirror. Thus, the axial ray height (Y), given in units of centimeters, is given by the expression: $Y = (120/100)y$. In a similar manner, the chief ray heights are scaled by the ratio of the tangent of the required semi-field angle Q_R (57.6 arcseconds)* divided by the input chief ray slope (1.0). Thus, the chief ray height ($\bar{Y}$), given in units of centimeters, is given by the expression: $\bar{Y} = (.000279091/1)\bar{y}$. These values of Y and $\bar{Y}$ are also listed in table 3.1.3-1. The clear aperture radius for each optical surface must accommodate both the axial beam height and the offset of this beam in the aperture due to field angle if vignetting is to be avoided. The radius of the axial beam is Y and the offset corresponding to a field angle of 57.6 arcseconds is $\bar{Y}$. Thus, the clear aperture height (Y_{CA}) is the sum of Y and $\bar{Y}$.

* $Q_R = \tan^{-1}\left[\frac{\text{Detector Semi-diagonal}}{\text{System Focal Length}}\right] = \tan^{-1}\left[\frac{\frac{1}{2}(1.22/\sin 45^0)}{3091.0}\right] = 57.567$ arcseconds

Table 3.1.3-1

CLEAR APERTURE HEIGHTS (Y_{CA}) FOR THE *f*/12.88 RELAY LENS

NO.	SURFACE	$\|y\|$	$\|\bar{y}\|$	Y	$\bar{Y}$	Y_{CA}
3	OTA EXIT PUPIL	12.16	0	14.59	0	14.59
4	RELAY FIELD MIRROR (PYRAMID)	0	5760	0	1.61	1.61
5	RELAY PRIMARY MIRROR	1.963	2445	2.36	0.68	3.04
6	RELAY SECONDARY MIRROR	.6717	8.433	0.81	0.00	0.81
7	RELAY PRIMARY MIRROR HOLE	.1457	2419	0.17	0.68	0.85
8	DETECTOR WINDOW (FRONT)	.0091	3049	0.01	0.85	0.86
9	DETECTOR WINDOW (BACK)	.0033	3076	0.00	0.86	0.86
10	DETECTOR FOCAL SURFACE	0	3091	0	0.86	0.86

$|y|$ = *reference axial ray height (absolute value in "units")*

$|\bar{y}|$ = *reference chief ray height (absolute value in "units")*

Y = *marginal axial ray height (centimeters)*

$\bar{Y}$ = *chief ray height coreesponding to "full field" (centimeters)*

Y_{CA} = *clear aperture height (centimeters)*

The OTA secondary mirror has a clear aperture radius of 15 cm. The maximum field angle (Q) this aperture can accommodate without vignetting is:

$$(120/100)\ y + (\tan Q/1)\bar{y} = 15.0$$

Where, for this mirror, y = 11.12 and $\bar{y}$ = 490.6. Solving for tan Q:

$$\tan Q = \left[15.0 - (120/100)(11.12)\right] /490.6 = 0.003375$$

or Q = 11.6 arcminutes. Thus, as expected, the OTA provides a completely unvignetted field of view for the WF/PC.

The clear aperture radii called out in the Baseline Optical Prescription equal or exceed their corresponding values of Y_{CA} in table 3.1.3-1. Thus, the optical prescription provides an unvignetted optical system.

Table 3.1.3-1 shows that the chief ray height $\overline{Y}$ on the relay secondary mirror is 0.0. This means that the illuminated area on the mirror remains stationary for all field angles, thereby minimizing the clear aperture radius. Since this mirror acts as an obstruction in the optical system, it is appropriate that its size be minimized. The 306.84 cm radius of curvature of each pyramid face causes the chief ray height $\overline{Y}$ to be zero at the secondary mirror. Thus, in effect, the curvature of the pyramid faces has been chosen to minimize the size of the relay secondary mirrors.

3.1.4 *f*/12.88 Field Coverage

The pyramid also acts as a field stop because it is located close to the OTA image surface. Thus, the size of the relayed image field depends upon the dimensions of the pyramid faces. The plane view of the pyramid is shown on the left side of figure 3.1.4-1. The diagonal of each quadrant has a length of 3.18 cm. The side view of the pyramid, also shown in figure 3.1.4-1, shows that the pyramid faces are inclined at an angle of 9.1056^{0}. The pyramid is centered on the OTA optical axis and is positioned longitudinally such that the center-point of each quadrant is coincident with the OTA image surface. The distance between the OTA exit pupil and this image surface is 700.2650 cm. A chief ray is shown which emerges from the center of the exit pupil (as all chief rays do) and intercepts the top corner of the upper quadrant. The slope of this chief ray is:

$$\tan Q' = 3.18/(700.2650 + 1.59 \tan 9.1056^{0}) = 0.004539486$$

This slope corresponds to $(n\overline{u})_3$ defined in the chief ray trace of the relay optics. That ray trace showed that if $(n\overline{u})_3$ has a value of 8.22543, the corresponding chief ray height $(\overline{y}_{10})$ at the image surface has a value of -3091.05. Thus, the chief ray height corresponding to tan Q' can be found

by scaling:

$$\overline{Y}_{10} = \overline{y}_{10} \quad \frac{\tan Q'}{(n\overline{u})_3} = 1.7059 \text{ cm or } 17.059 \text{ mm}$$

This distance, $\overline{Y}_{10}$, is the diagonal of the image field at the CCD detector. The image field is square because the pyramid face is square, so the edge dimension (d) of the image field is:

$$d = \overline{Y}_{10} \text{ Sin } 45^{o} = 12.06 \text{ mm}$$

The CCD detector, having a 12.2x12.2 mm active area, is then centered upon this 12.06x12.06 mm image field.

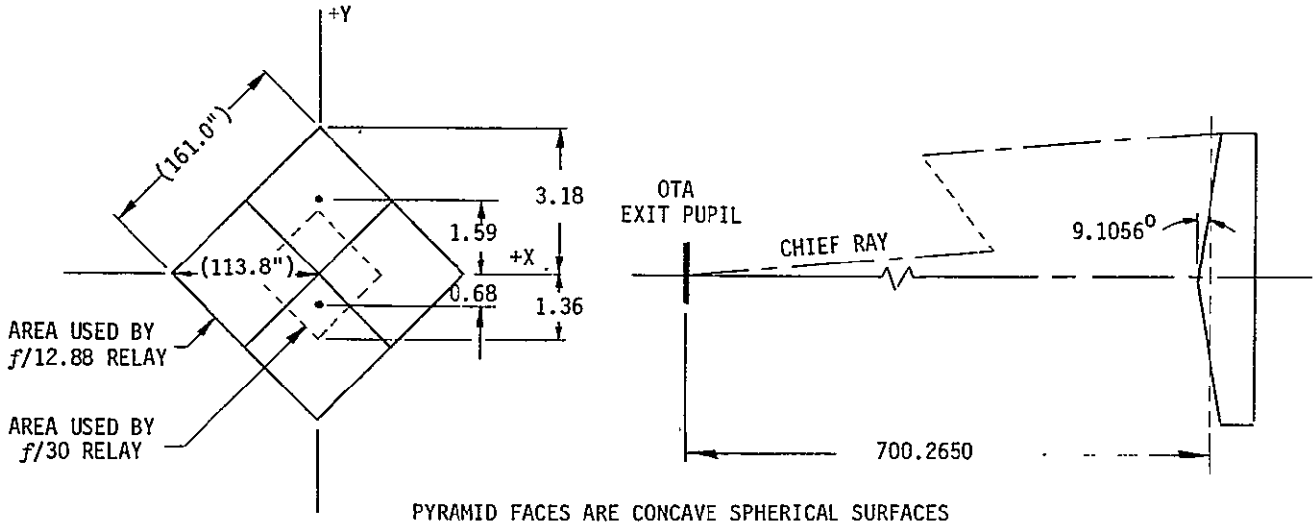

REFLECTING PYRAMID
(PHYSICAL DIMENSIONS AND ANGULAR DIMENSIONS IN OBJECT SPACE)

Figure 3.1.4-1

In object space, a chief ray slope of 1.0 at the OTA entrance pupil (primary mirror) results in a slope $(n\bar{u})_3$ of 8.22543 for this ray at the OTA exit pupil. Using these data, the input field angle (Q) corresponding to tan Q' can be found by scaling:

$$\tan Q = \tan Q' \quad \frac{1.0}{(n\bar{u})_3} \quad = 0.00055188$$

and:

$$Q = 113.83 \text{ arcseconds}$$

Thus, in object space, the corners of the pyramid correspond to a radial semi-field angle of 113.83 arcseconds. Or, expressing it another way, the perimeter of the circular OTA image field which corresponds to 113.83 arcseconds will circumscribe the pyramid.

Since the pyramid is square, a square angular field in object space can be defined. The angular length ℓ of this square field is:

$$\tan \ell = \tan Q / \sin 45^{\circ} = 0.00078048$$

And:

$$\ell = 161.0 \text{ arcseconds}$$

Thus, the full field of view of the OTA needs to be 161 arcseconds square to completely illuminate the pyramid. These angular dimensions are also shown in figure 3.1.4-1.

3.1.5 *f*/12.88 Aperture Obscurations

Obstructions within the clear apertures of the OTA and relay lens diffract light and, as a result, reduce image quality. The four principal obstructions in the OTA/relay system are: the OTA secondary mirror, the OTA primary mirror hole, the relay secondary mirror, and the relay primary mirror hole. The

overall obscuration caused by these obstructions is found by projecting all the obstructions onto the system entrance pupil (which is the OTA primary mirror).

The OTA secondary mirror obstruction is to have a maximum radius of 0.34 times the primary mirror radius. Hence, this obstruction radius is (0.34)(120) or 41 cm. Since this obstruction is in a region of parallel light, it projects directly onto the entrance pupil, so its obscuration radius is also 41 cm.

The OTA primary mirror hole is smaller than the secondary mirror obstruction and its obscuration will always lie within the secondary mirror obscuration. Therefore, the primary mirror hole can be neglected in this analysis.

The relay secondary mirror clear aperture radius Y_{CA} is 0.81 cm (from table 3.1.3-1). For this analysis, it will be assumed that the physical radius of the mirror equals the clear aperture radius. To project this obstruction onto the entrance pupil, the height of the axial ray (traced previously) at the obstruction needs to be calculated. The distance t_x between the field mirror (pyramid) and the obstruction is:

$$t_x = t_4 + t_5 = 113.0610 - 16.2590 = 96.8020 \text{ cm}$$

Ray height at the obstruction is found from ray trace equation (1)

$$y_x = y_4 + (nu)_4 \ (t/n)_x$$

$$y_x = 0 + (-0.017361156)(96.8020/1.0) = -1.680595 \text{ units}$$

The ray which intercepts the lower edge of the obstruction has a height Y_x of -0.81 cm. The corresponding height of this ray in the entrance pupil is:

$$Y = Y_x \ (y_1/y_x) = -0.82 \ (100/-1.680595) = 48 \text{ cm}$$

Thus, the obscuration radius of the relay secondary mirror obstruction, when projected onto the entrance pupil, is 48 cm.

The relay primary mirror hole requires a clear aperture radius Y_{CA} of 0.85 cm (from table 3.1.3-1). The ray height at this obstruction is y_5, which has a value of -1.962870 units. The ray which intercepts the lower edge of this obstruction has a height (Y_5), of -0.85 cm. By scaling, the corresponding height of this ray in the entrance pupil is:

$$Y = Y_5 \ (y_1/y_5) = -0.85 \ (100/ -1.962870) = 43 \text{ cm}$$

The obscuration radius of the relay primary mirror hole, therefore, is 43 cm when projected onto the entrance pupil.

With respect to on-axis imaging of the relay optics, the OTA secondary mirror obscuration and the relay primary mirror hole obscuration are contained within the relay secondary mirror obscuration. Thus, the effective on-axis obscuration is a circular opaque area, centered in the system clear aperture, having a radius of 48 cm at the entrance pupil.

The effect of the central obstruction is to increase the amount of diffraction in the lens. With respect to the image of a point source, such as a star, a central obstruction will narrow the core of the star image and intensify the diffraction rings. For an extended source, such as a planet, diffraction from a central obstruction will reduce the contrast of surface detail.

Mathematically, star image intensity given as a function of distance from its maxima is called the point spread function. The Fourier transform of the point spread function is a complex expression termed the optical transfer function. The modulus of this complex function is called the modulation transfer function (MTF) and the argument is called the phase transfer function. The lens MTF is a function that describes the amount of object modulation transferred to the image in terms of spatial frequency. For example, if a sine-wave pattern having a modulation of 60 percent were imaged by a lens such that its image would have a spatial frequency of 33 cycles/mm and modulation of 30 percent, the MTF of that lens would be 30%/60% or 0.50 at 33 cycles/mm.

The effect of a central obstruction upon the lens modulation transfer function is to reduce the MTF over the low and mid-frequencies and slightly increase the MTF for high frequencies. This effect is shown in figure 3.1.5-1 for the optical system which is comprised of the OTA and the *f*/12.88 relay optics. The dashed curve is on-axis MTF which would occur if the effective obscuration were due to the OTA secondary mirror. The solid curve is on-axis MTF for the actual system where the relay secondary mirror causes a larger obscuration. This larger obscuration (48-cm radius as compared to 41-cm radius for the OTA secondary mirror) causes MTF to drop from a value of 0.50 at 33 cycles/mm to a value of 0.45.

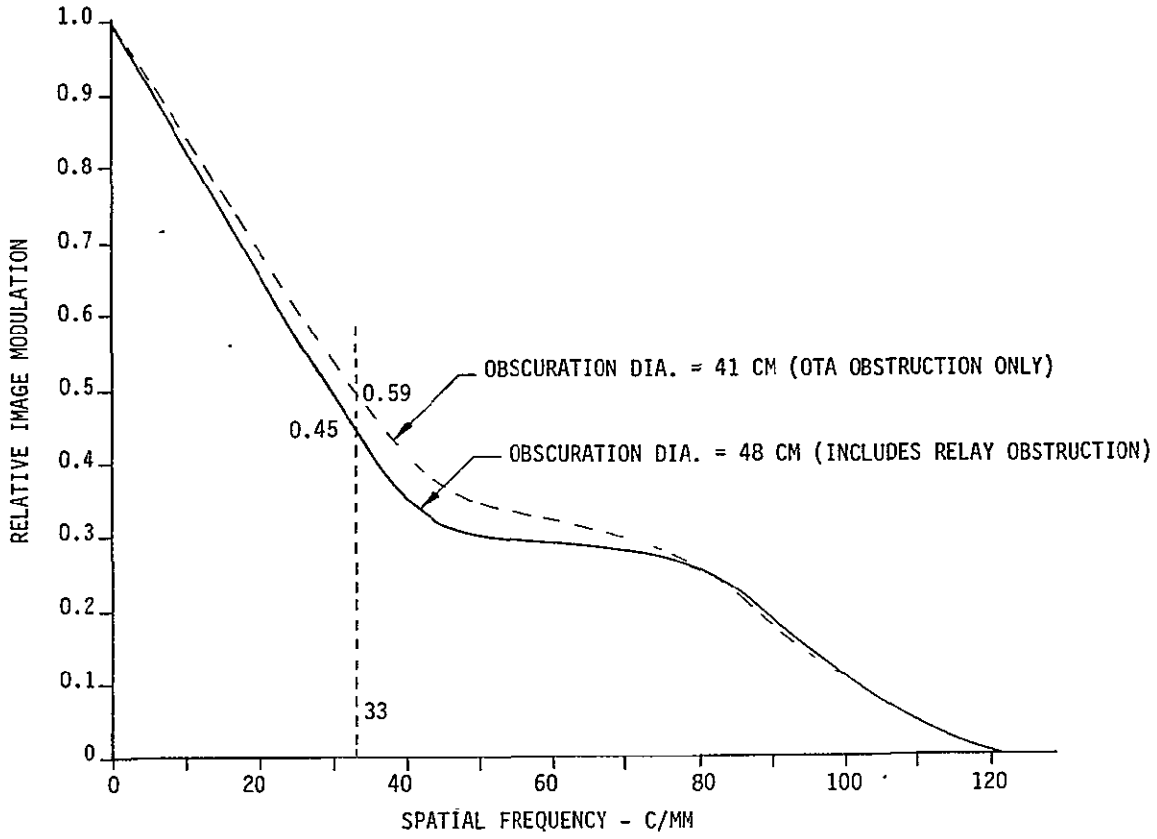

HYPOTHETICAL ABERRATION-FREE ON-AXIS MTF
FOR *f*/12.88 RELAY SYSTEM

Figure 3.1.5-1

The obscuration in the lens entrance pupil shifts laterally for off-axis field angles. Consequently, the OTA secondary mirror obscuration will move outside the perimeter of the relay secondary mirror obscuration and add to the overall obscuration. The amount of obscuration shift, $\bar{Y}o$, is given by the expression:

$$\bar{Y}o + -100\ (\bar{y}_x/y_x)\bar{U}o$$

where:

$\bar{y}_x$ = reference chief ray height at the obstruction

y_x = reference axial ray height at the obstruction

$\bar{U}o$ = tangent of the field angle

The above expression is valid for the two reference paraxial rays used. That is, an axial ray having a height of 100 units at the entrance pupil and a chief ray having a slope of 1.0 units at the entrance pupil.

To demonstrate this shifting of obscuration, data corresponding to the maximum OTA radial field angle has been calculated. This maximum field angle, as previously determined, is 113.83 arcseconds and the tangent of this angle is $\bar{U} = 0.00055188$. The reference chief ray height $\bar{y}_x$ at the OTA secondary mirror obstruction is found from paraxial ray trace equation (1) where t_x is the distance between the obstruction and the OTA primary mirror.

$$\bar{y}_1 = \bar{y}_x + (n\bar{u})_o\ (t/n)_x$$

$$\bar{y}_x = \bar{y}_1 - (n\bar{u})_o\ (t/n)_x = 0 - (1.0)(490.6071/1.0) = -490.6071 \text{ units}$$

Since this obstruction is located in the path of parallel input axial rays, $y_x = y_1 = 100$. Then, solving for the shift $\bar{Y}o$ of the OTA secondary mirror obscuration:

$$\bar{Y}o = -100\ (-490.6071/100)(0.00055188) = 0.2708 \text{ cm}$$

The optical axis of the relay lens is tilted with respect to the OTA optical axis. With respect to this tilted axis, the maximum field angle is ½(113.23 arcseconds) or 56.92 arcseconds and $\overline{U}o$ for the relay optics is 0.00027593. The reference chief ray height $\overline{y}_x$ at the relay lens secondary mirror obstruction is also found from paraxial ray trace equation (1) where t_x is the distance between the field mirror (pyramid) and the obstruction. This distance was previously calculated to be 96.8020 cm. Then:

$$\overline{y}_x = \overline{y}_4 + (n\overline{u}_4)\ (t/n)_x = 5759.99 + (-29.3185)(96.8020/1.0)$$

$$\overline{y}_x = 2921.90 \text{ units}$$

The reference axial ray height y_x at this obstruction has previously been calculated and is -1.680595 units. Then, solving for the shift $\overline{Y}o$ of the relay secondary mirror obscuration:

$$\overline{Y}o = -100\ (2921.90/-1.680595)(0.00027593) = 47.9735 \text{ cm}$$

For the relay primary mirror hole obstruction, $\overline{y}_x = \overline{y}_5 = 2445.21$ units and $y_x = y_5 = 1.962870$ units. Then, solving for the shift $\overline{Y}o$ of the relay primary mirror hole obstruction:

$$\overline{Y}o = -100\ (2445.21/-1.962870)(0.00027593) = 34.3735 \text{ cm}$$

Figure 3.1.5-2 shows these decentered obscurations in the system entrance pupil. The overall obscuration is larger than it was when viewed on-axis because much of the OTA secondary mirror baffle obscuration is now visible in the pupil. The shape of the overall obscuration has also lost the rotational symmetry it had when viewed on-axis. Diffraction from this asymmetric pupil causes asymmetry in both the image point spread function and the modulation transfer function. Consequently, the shape of the MTF curve will be azimuth-dependent.

This effect is shown in figure 3.1.5-3 where the diffraction limited off-axis MTF (solid lines) correspond to two different azimuths. The curve marked MTF(X) corresponds to image modulation for a sine wave object pattern that

runs parallel to the entrance pupil X-axis and MTF(Y) corresponds to a pattern running parallel to the pupil Y-axis. The dashed curve is what the MTF would be for any azimuth if the obscurations did not shift in the pupil.

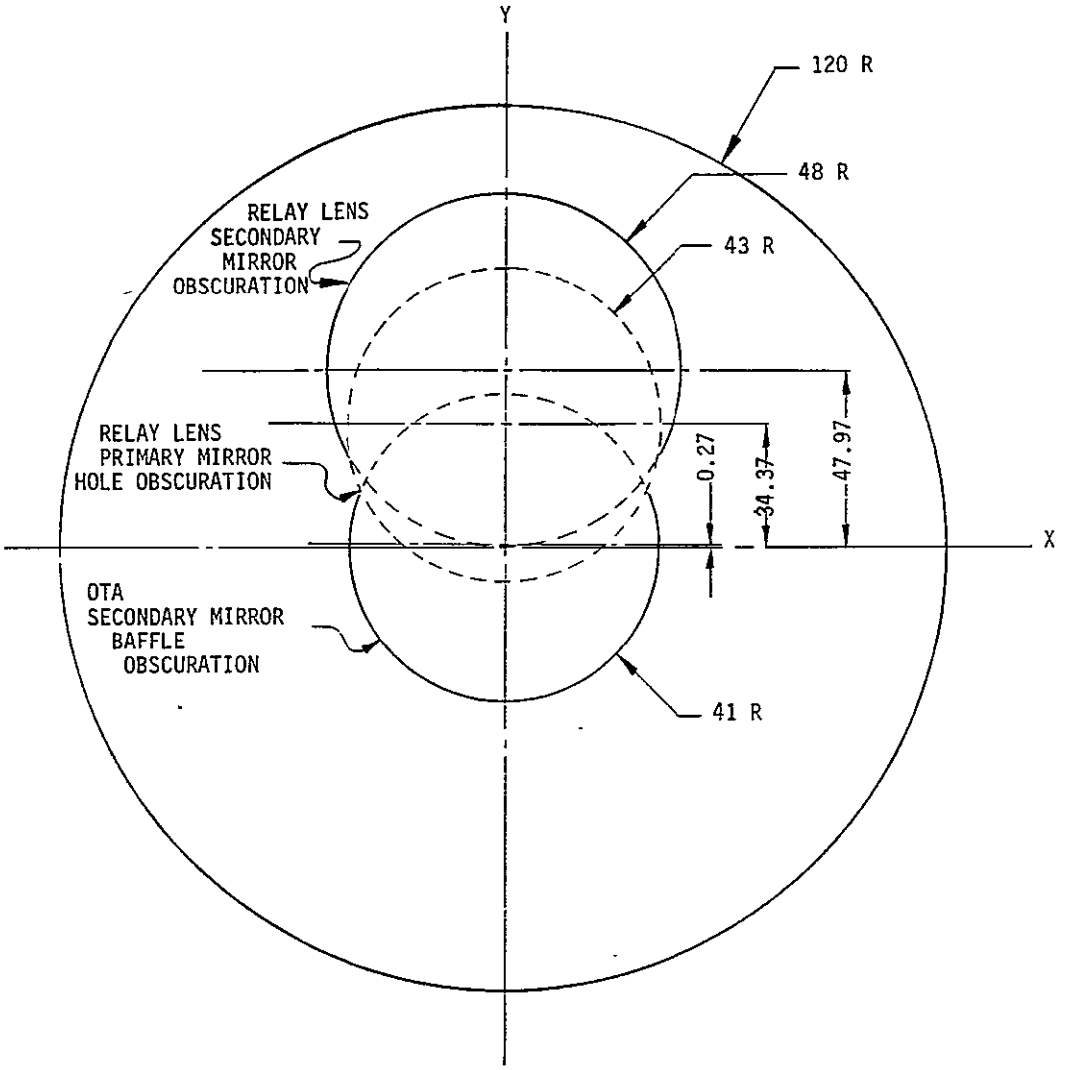

OTA + *f*/12.88 RELAY SYSTEM ENTRANCE PUPIL
INCLUDING OBSCURATIONS AT FULL-FIELD
(113.8 ARC SECONDS WRT OTA AXIS)

Figure 3.1.5-2

The off-axis MTF curves given in figure 3.1.5-3 are hypothetical in that they assume the optical system is completely free of wavefront aberrations. In the real system, however, aberrations such as astigmatism and field curvature will be present and will cause additional reduction in the MTF.

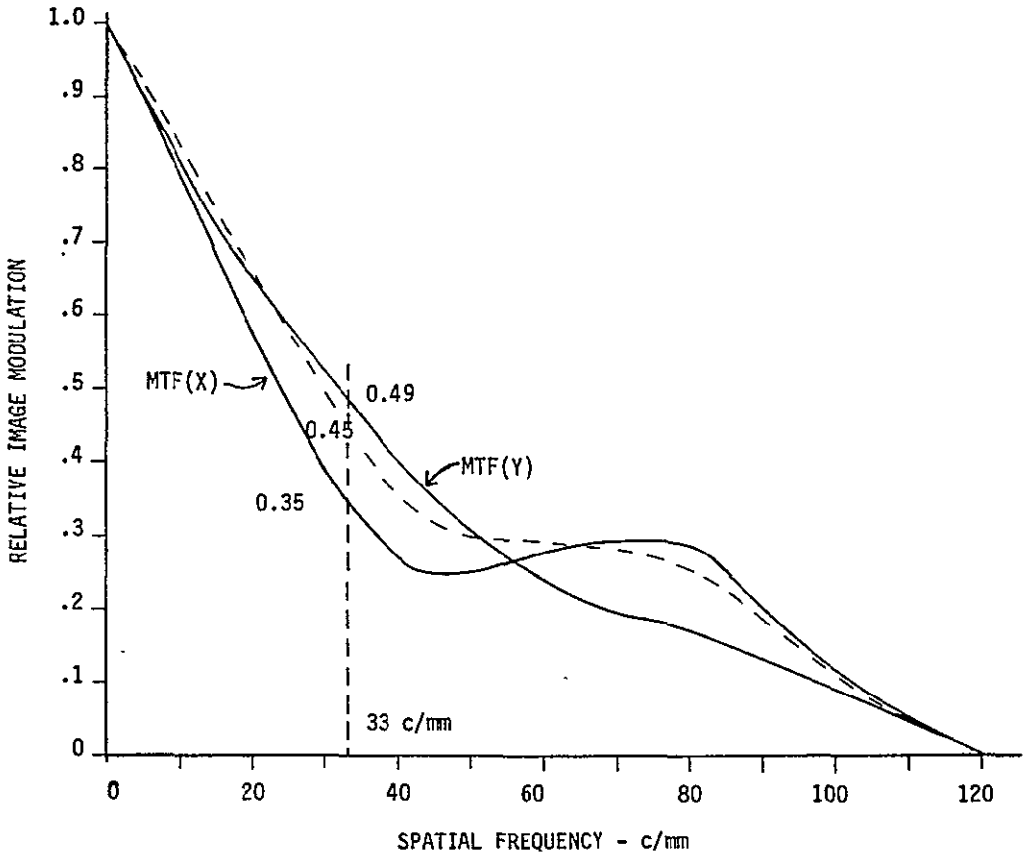

HYPOTHETICAL ABERRATION-FREE FULL-FIELD MTF
f/12.88 RELAY SYSTEM

Figure 3.1.5-3

3.1.6 *f*/30 Focal Surface Location, Focal Length, and *f*-number

The lens prescription for the *f*/30 relay system is:

r_4 = 306.84 cm	t_4 = 113.0570 cm	n_4 = 1.0
r_5 = -51.7800 cm	t_5 = -24.6470 cm	n_5 = -1.0
r_6 = -23.4330 cm	t_6 = 24.6470 cm	n_6 = 1.0
r_7 = infinity	t_7 = 12.6637 cm	n_7 = 1.0
r_8 = infinity	t_8 = 0.2500 cm	n_8 = 1.387
r_9 = infinity	t_9 = 0.1011 cm	n_9 = 1.0

The ray heights and slopes for the reference axial ray are:

y_4 = 0	$(nu)_4$ = -0.017361156
y_5 = -1.962800214	$(nu)_5$ = +0.0584519075
y_6 = -0.5221360499	$(nu)_6$ = +0.0138877416
y_7 = -0.179844883	$(nu)_7$ = +0.0138877416
y_8 = -0.0039746898	$(nu)_8$ = +0.0138877416
y_9 = -0.001471492	$(nu)_9$ = +0.0138877416
y_{10} = -0.0000674413	$(nu)_{10}$ = +0.0138877416

The calculated paraxial back focus is:

$$t_9' = y_9/(nu)_9 = 0.0160 \text{ cm}$$

The focal length for the OTA and relay system is:

$$f = -100/(nu)_9 = (-)\ 7200.6 \text{ cm}$$

The f-number for the OTA and relay system is:

$$f\text{-number} = 7200.6/240 = 30.00$$

3.1.7 *f/30 Exit Pupil*

The ray heights and slopes for the reference chief ray are:

$\bar{y}_3 = 0$	$(n\bar{u})_3 = 8.225436$
$\bar{y}_4 = 5759.99$	$(n\bar{u})_4 = -29.3185$
$\bar{y}_5 = 2445.33$	$(n\bar{u})_5 = -123.769$
$\bar{y}_6 = -605.210$	$(n\bar{u})_6 = -175.424$
$\bar{y}_7 = -4928.876$	$(n\bar{u})_7 = -175.424$
$\bar{y}_8 = -7150.389$	$(n\bar{u})_8 = -175.424$
$\bar{y}_9 = -7182.008$	$(n\bar{u})_9 = -175.424$
$\bar{y}_{10} = -7200.602$	$(n\bar{u})_{10} = -175.424$

The location of the exit pupil for the OTA and relay lens system is $\bar{y}_{10}/(n\bar{u})_{10}$ or 41.0468 cm ahead of the image (detector) surface. The diameter of the exit pupil is 240/175.424 or 1.3681 cm.

3.1.8 *f*/30 Clear Aperture Sizes

Clear aperture heights are listed in table 3.1.8-1. These heights agree with those called out in the Baseline Optical Prescription.

Table 3.1.8-1

CLEAR APERTURE HEIGHTS (Y_{CA}) FOR THE *f*/30 RELAY LENS

NO.	SURFACE	$\|y\|$	$\|\bar{y}\|$	Y	$\bar{Y}$	Y_{CA}
3	OTA EXIT PUPIL	12.16	0	14.59	0	14.59
4	RELAY FIELD MIRROR (PYRAMID)	0	5760	0	0.69	0.69
5	RELAY PRIMARY MIRROR	1.963	2445	2.36	0.29	2.65
6	RELAY SECONDARY MIRROR	.5221	605.2	0.63	0.07	0.70
7	RELAY PRIMARY MIRROR HOLE	.1798	4929	0.22	0.59	0.81
8	DETECTOR WINDOW (FRONT)	.0040	7150	0.00	0.86	0.86
9	DETECTOR WINDOW (BACK)	.0015	7182	0.00	0.86	0.86
10	DETECTOR FOCAL SURFACE	0	7201	0	0.86	0.86

$|y|$ = *reference axial ray height (absolute value in "units")*
$|\bar{y}|$ = *reference chief ray height (absolute value in "units")*
Y = *marginal axial ray height (centimeters)*
$\bar{Y}$ = *chief ray height corresponding to "full field" (centimeters)*
Y_{CA} = *clear aperture height (centimeters)*

3.1.9 *f*/30 Field Coverage

The pyramid acts as a field stop. Since the pyramid is sized for the *f*/12.88 system, the relayed image field for the *f*/30 system exceeds the size of the CCD detector. In the WF/PC System optical schematic (JPL Drawing No. 10084811), the chief ray which becomes the optical axis of the tilted *f*/30 relay intercepts the pyramid at a height of 0.679. Using this value, the top corner of the detector would project onto the pyramid at a height of 2(0.679) or 1.358 cm.

The chief ray which emerges from the center of the exit pupil and intercepts this projected corner of the detector has a slope of

$$\tan Q' = 1.358/(700.2650 + 0.679 \tan 9.1056^{0}) = 0.001938965$$

The height of this chief ray at the detector is

$$\overline{Y}_{10} = \overline{y}_{10} \frac{\tan Q'}{(n\overline{u})_3} = 1.6974 \text{ cm or } 16.974 \text{ mm}$$

This distance, $\overline{Y}_{10}$, is the diagonal of the image field at the CCD detector. The image field is square, and the edge dimension (d) of the image field is:

$$d = \overline{Y}_{10} \text{ Sin } 45^{0} = 12.00 \text{ mm}$$

The input field angle Q (at the OTA entrance pupil) corresponding to Q' is:

$$\tan Q = \tan Q' \left[\frac{1.0}{(n\overline{u})_3}\right] = 0.00023573$$

and:

$$Q = 48.62 \text{ arcseconds}$$

The square angular field in object space corresponding to this radial field angle is:

$$\tan \ell = \tan Q/\text{Sin } 45^{0} = 0.000333373$$

and:

$$\ell = 68.8 \text{ arcseconds}$$

Thus, the full field of view of the OTA needs to be 68.8 arcseconds square for the *f*/30 relay system.

3.1.10 *f*/30 Aperture Obscurations

The following calculations determine the obscuration radius (Y) of the relay secondary mirror obstruction when projected onto the entrance pupil:

$$t_x = t_4 + t_5 = 113.0570 - 24.6770 = 88.4100 \text{ cm}$$

$$y_x = y_4 + (nu)_4 \, (t/n)_x = 0 + (-0.017361156)(88.4100/1.0)$$

$$= -1.534900 \text{ units}$$

$$Y = Y_x \, (y_1/y_x) = -0.70(100/ -1.534900) = 46 \text{ cm}$$

Similarly, the obscuration radius (Y) of the relay primary mirror hole, when projected onto the entrance pupil, is:

$$Y = Y_5(y_1/y_5) = -0.81(100/ -1.962800) = 41 \text{ cm}$$

The lateral shift $\overline{Y}o$ of the OTA secondary mirror obscuration at full field ($\overline{U}o$ = tan 48.62 arcseconds)

$$\overline{Y}o = -100(\overline{y}_x/y_x)\overline{U}o = -100(-490.6071/100)(0.00023573)$$

$$= 0.1157 \text{ cm}$$

With respect to the tilted axis of the relay lenses, the maximum field angle is ½(48.62 arcseconds) or 24.31 arcseconds and $\overline{U}o$ is 0.00011786. The following calculations determine the lateral shift $\overline{Y}o$ of the relay secondary mirror obscuration:

$$\overline{y}_x = \overline{y}_4 + (n\overline{u})_4 \, (t/n)_x = 5759.99 + (-29.3185)(88.4100/1.0)$$

$$= 3167.94 \text{ units}$$

$$\overline{Y}o = -100(3167.94/-1.534900)(0.00011786) = 24.3256 \text{ cm}$$

For the relay primary mirror hole obstruction, $\overline{y}_x = \overline{y}_5 = 2445.33$ units and $y_x = y_5 = -1.962800$ units. The solving for the shift $\overline{Yo}$ of the relay primary mirror hole obstruction:

$$\overline{Yo} = -100(2445.33/-1.962800)(0.00011786) = 14.68 \text{ cm}$$

3.1.11 WF/PC Preliminary Conic Constants

Each of the WF/PC relay systems consist of four mirrors: a curved field mirror (pyramid face), a plano folding mirror, curved primary mirror, and curved secondary mirror. Also, each system includes a plano cover plate for the detector made of MgF_2.

The cover plate introduces a small amount of spherical aberration and coma which can be compensated by adjustment of the relay primary and secondary mirror conic constants. The spherical aberration contribution for this cover plate is:

$$SA = \left[(n^2 - 1)/n^3\right] (nu)^4 T$$

where:

n = refractive index of the plate material
T = thickness of the plate
(nu) = optical slope of axial reference ray

The plate thickness T is 0.25 cm and, for this analysis, a refractive index n of 1.387 will be assumed. Using these values, the above equation becomes:

$$SA = 0.0865514 (nu)^4$$

For the *f*/12.88 relay, the axial ray optical slope (nu) at the cover plate has been shown previously to be 0.032351479. Thus, for this relay, the spherical aberration contribution is 9.48×10^{-8} units.

Similarly, for the $f/30$ relay, the optical slope (nu) is 0.013887416 and the resulting spherical aberration contribution is 3.22×10^{-9} units.

The coma contribution for the cover plate is:

$$\text{Coma} = \left[(n^2 - 1)/n^3\right] (n\bar{u})(nu)^3 \, T$$

Where:

$(n\bar{u})$ = optical slope of reference chief ray

and using the given values of plate thickness and index, this equation becomes:

$$\text{Coma} = 0.0865514 \, (n\bar{u})(nu)^3$$

For the $f/12.88$ relay, the chief ray optical slope $(n\bar{u})$ at the cover plate is -149.282. Thus, for this relay, the coma contribution is -4.37×10^{-4} units.

Similarly, for the $f/30$ relay, the optical slope $(n\bar{u})$ is -175.424 and the resulting coma contribution is -4.07×10^{-5} units.

Spherical aberration and coma contributions from the field (pyramid) mirror are negligible because the OTA is focused on this surface. Also, no aberrations are produced at the folding mirror because its surface is plano.

The preliminary conic constants for the primary and secondary relay mirrors are chosen to correct spherical aberration and coma for the overall system. The equations for calculating the conic constants were given in equation set (4).

Solving these equations for the $f/12.88$ system:

$$B_1 = (-0.017361156) + (-1.962870)/(-40.5662) = 0.0310256784$$

$$B_2 = (0.032351479) + (-0.671702)/(-28.5460) = 0.0558819912$$

$$A_1 = (-29.3185) + (2445.21)/(-40.5662) = -89.59552866$$

$$A_2 = (-149.282) + (8.4327)/(-28.5460) = -149.5774074$$

$$B_1' = (0.079412496) - (-0.017361156) = 0.096773652$$

$$B_2' = (0.032351479) - (0.079412496) = -0.047061017$$

$$C_1 = +2\left[(-1.962870)/(-40.5662)\right]^3 = 0.0002265748$$

$$C_2 = -2\left[(-0.671702)/(-28.5460)\right]^3 = -0.000026057$$

The residual spherical aberration R_s is given a value equal to the cover plate spherical aberration:

$$R_s = SA = 9.48 \times 10^{-8}$$

Similarly, the residual coma aberration R_c is:

$$R_c = Coma = +4.37 \times 10^{-4}$$

Then:

$$E = -0.000084039$$

$$F = +0.2633640285$$

and:

$K_1 = -0.47828$ primary mirror conic constant

$K_2 = -7.35155$ secondary mirror conic constant

The prescribed conic constants for the primary mirror and secondary mirror are -0.479 and -7.314, respectively. These values are very close to those

calculated above.

For the $f/30$ relay system, a similar set of calculations as those above gave a primary mirror conic constant of -0.28312 and a secondary conic constant of -2.43835. The prescribed conic constants are -0.284 and -2.420.

This evaluation of conic constants show that the prescribed $f/12.88$ and $f/30$ relays have virtually zero third-order spherical aberration and coma.

4.0 SYSTEM PERFORMANCE SPECIFICATIONS

4.0 SYSTEM PERFORMANCE SPECIFICATIONS

In order to realize the Space Telescope objectives of high angular resolution over a wide field, extended wavelength coverage and faint object detection, the performance of the Wide Field/Planetary Camera must be matched to that of the Optical Telescope Assembly (OTA).

The capability of the Space Telescope is limited by three parameters of the OTA and the Wide Field/Planetary Camera. The first two, manufacturing limitation of the optics and UV cutoff of the optics coating, impose the static limitations. These two limitations, coupled with the third limitation -- pointing stability of the Space Telescope (SSM + OTA + WF/PC), constitute the dynamic limitation.

The inability of a static manufactured optical system to perfectly match the designed system results in degradation of performance. For a manufactured optical system, the modulation transfer function (MTF) can be calculated and compared with the designed MTF. (The ratio of manufactured MTF to designed MTF is called the optical quality factor, "OQF".) For performance "prediction" purposes, the OQF can be expressed as follows:

$$OQF = \exp^{-(2\pi\omega)^2} \quad \left[1-\phi(\nu)\right]$$

where ω is the rms wavefront error in units of wavelength and $\phi(\nu)$ is the autocorrelation function. $\phi(\nu)$ is usually expressed as follows:

$$\phi(\nu) = \exp - \frac{2\lambda^2 f\#^2 \nu^2}{C^2}$$

where λ is the wavelength; $f\#$ is the system focal ratio; ν is the spatial frequency; and C is the autocorrelation length.

It should be noted that these empirical performance prediction equations have agreed closely in past experience with calculated "static" manufactured results. Shown in figure 4.0-1 is the theoretical designed MTF for a combined OTA with planetary camera at the center of the CCD. To create this hypothetical

"best" case condition, a simple scaling relationship was used ($f/30 \div f/24$). This assumes the WF/PC optics design does not increase the central obstruction due to the OTA, and the WF/PC optics design is diffraction-limited. (Actual design performance data without this assumption is given in section 10.1.) Using the performance "prediction" equations, the effect of "static" manufacturing errors on the planetary camera theoretical design (ω=0) is shown in figure 4.0-1. The effect on the resultant star spot size is shown in figure 4.0-2. Inherent in the manufacture of a combined OTA with WF/PC is a maximum rms wavefront error of 0.075 λ due to the OTA alone. The addition of an independent WF/PC optical system to the OTA must minimize any wavefront error increase to the inherent 0.075 λ rms wavefront error. Shown in figure 4.0-3 is the preliminary system static wavefront budget for the combined OTA with WF/PC (see section 8.5). Shown in figures 4.0-4 and 4.0-5 are the manufactured performance specifications for the OTA with wide field and planetary cameras. The manufactured system specification for a combined OTA with WF/PC can be stated as follows:

> *The OQF (at the center of the CCD array) of a combined OTA with wide field/planetary camera optical assembly at a wavelength of 0.6328 microns shall be greater than 63 percent.*

Shown in figures 4.0-6 and 4.0-7 are the manufactured performance specifications for the wide field and planetary cameras without the OTA. In this case, the manufactured system specification can be stated as follows:

> *The OQF (at the center of the CCD array) of the Wide Field/Planetary Camera optical assembly at a wavelength of 0.6328 microns shall be greater than 79 percent.*

In the change from a static manufacturing environment to a dynamic operational environment, the imaging performance will be further degraded by image motion. This degradation would not be verified by test. For "prediction" purposes, however, a Gaussian model combining linear and non-linear image motions is usually used:

$$\tau_\sigma = \exp- (2\pi^2\sigma^2\nu^2 f\#^2)$$

where τ_σ is the MTF degradation factor resulting from an image motion and σ is the pointing stability error. The predicted effect of image motion on the manufactured performance of a combined OTA with WF/PC is also shown in figures 4.0-4 and 4.0-5 (see section 10.0).

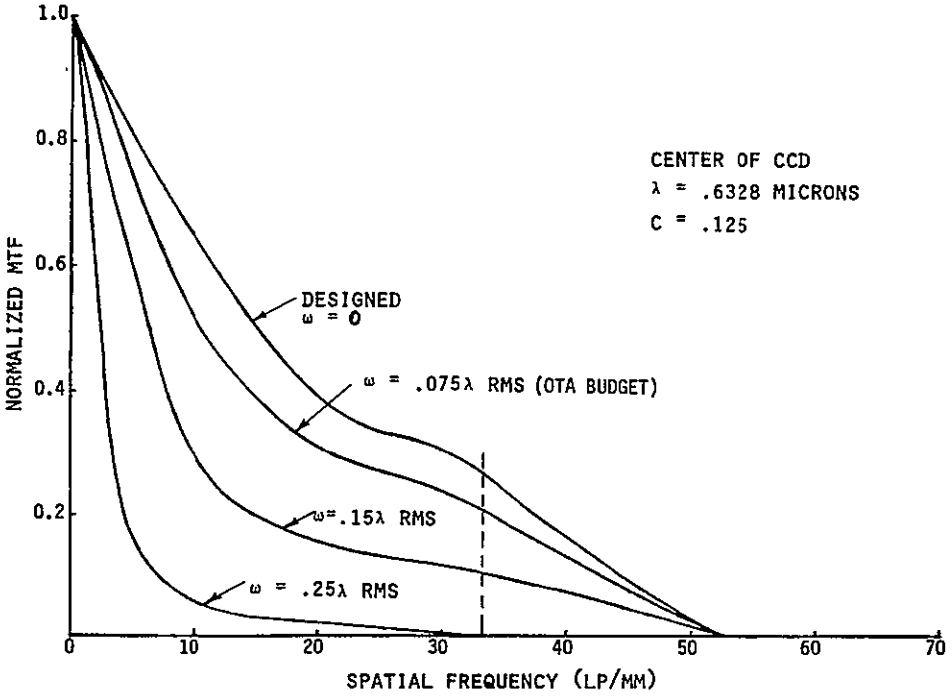

EFFECT OF STATIC MANUFACTURING WAVEFRONT ERROR
ON COMBINED OTA WITH PLANETARY CAMERA

Figure 4.0-1

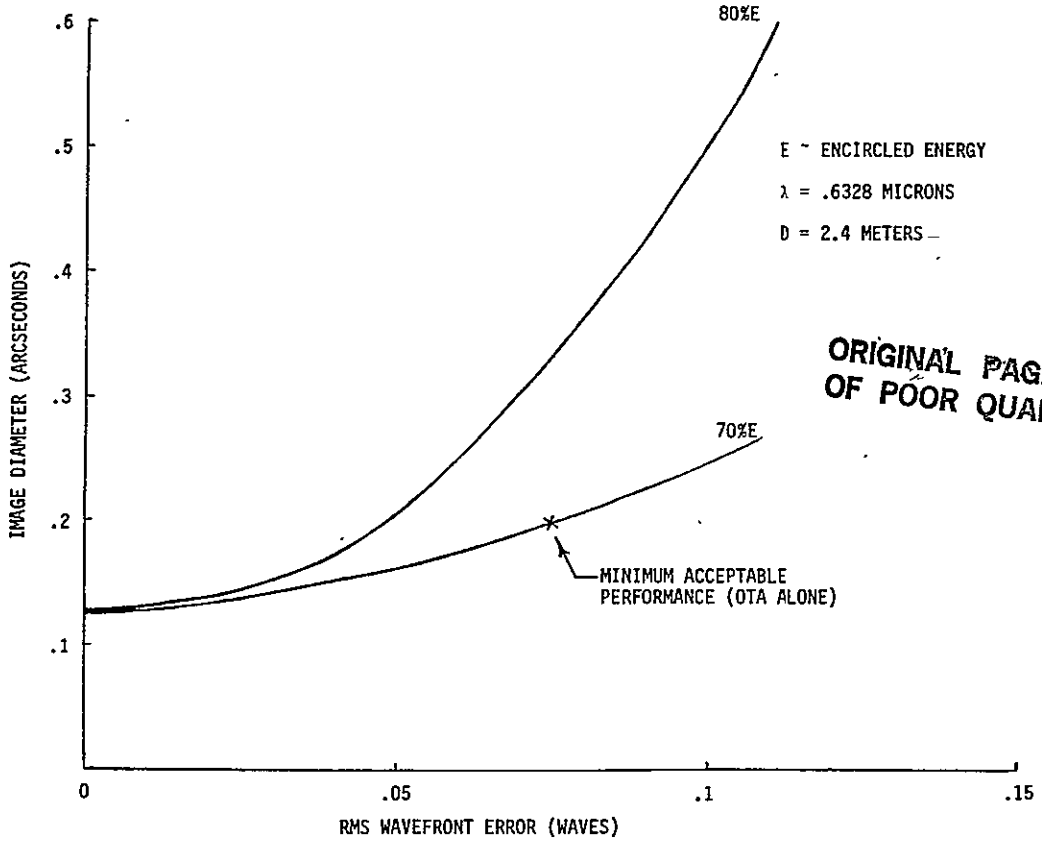

STAR SPOT SIZE WITH MANUFACTURING ABERRATIONS IN OPTICS

Figure 4.0-2

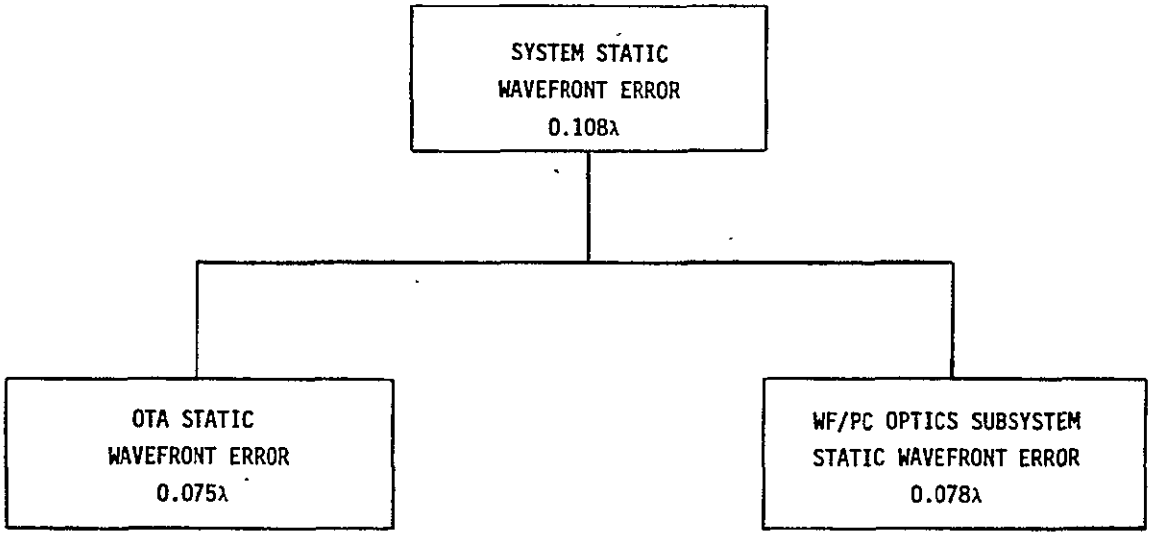

SYSTEM WAVEFRONT ERROR
(RMS ERROR AT 0.6328 μm)

Figure 4.0-3

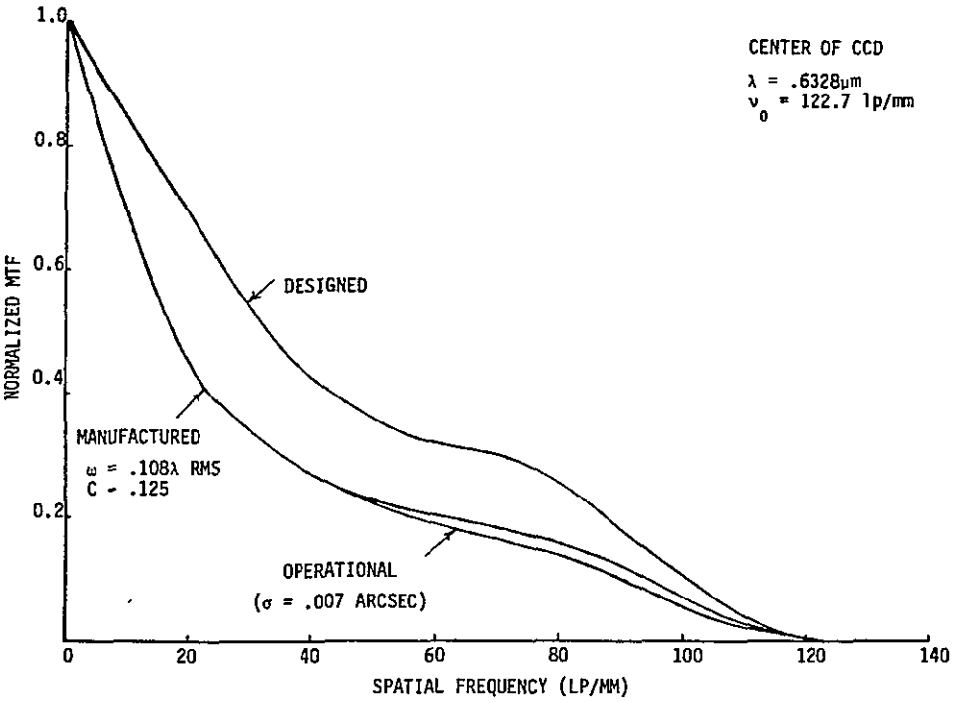

WIDE FIELD CAMERA PERFORMANCE SPECIFICATIONS
(WITH OTA)

Figure 4.0-4

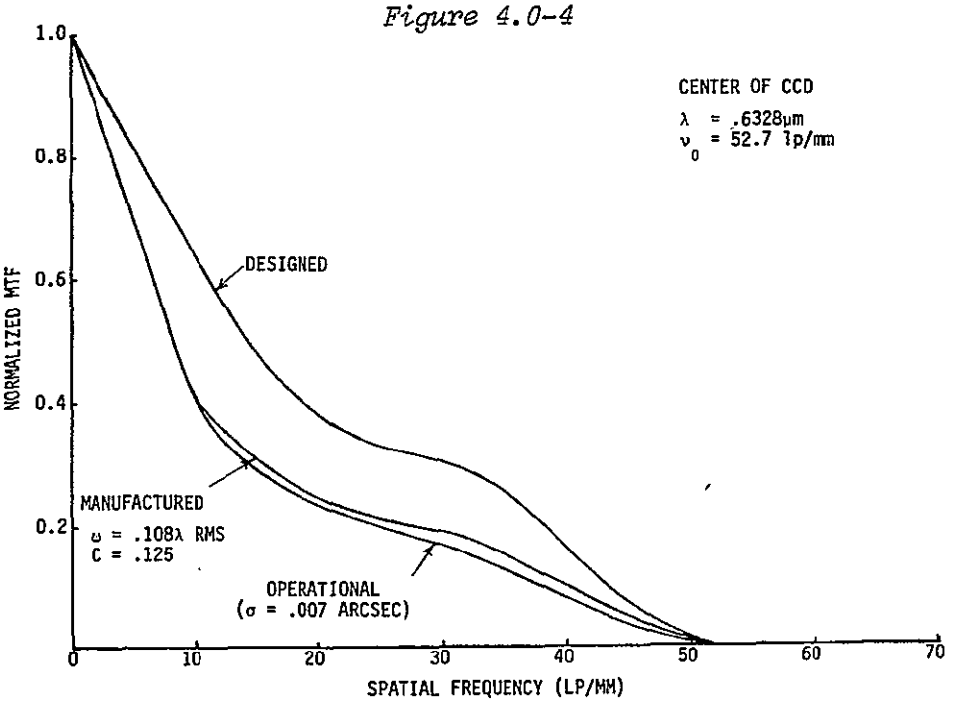

PLANETARY CAMERA PERFORMANCE SPECIFICATIONS
(WITH OTA)

Figure 4.0-5

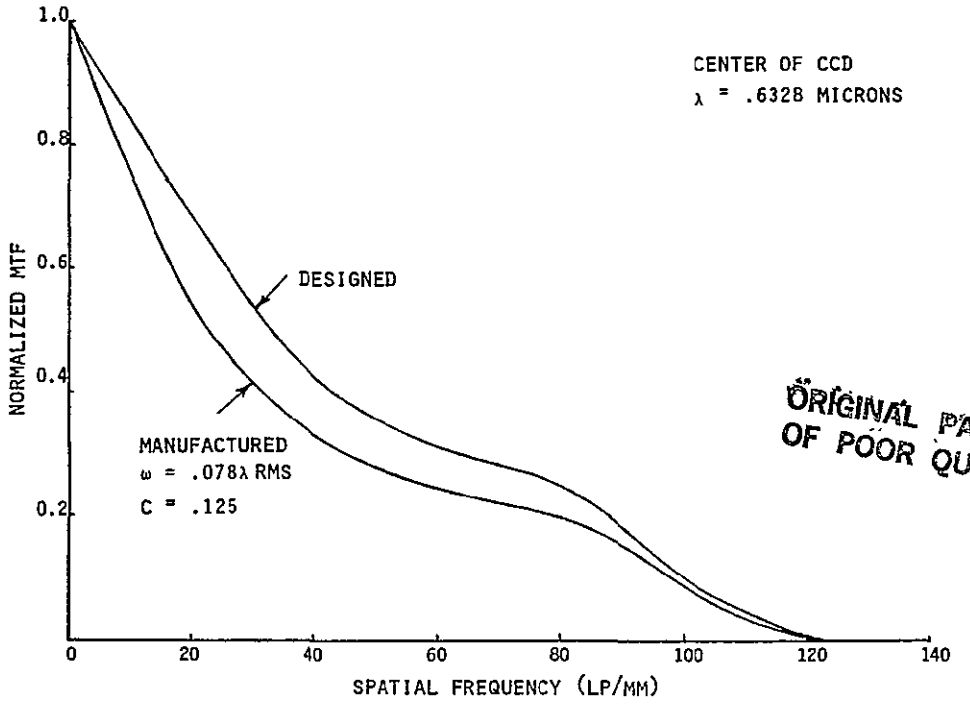

WIDE FIELD CAMERA PERFORMANCE SPECIFICATIONS
(WITHOUT OTA)

Figure 4.0-6

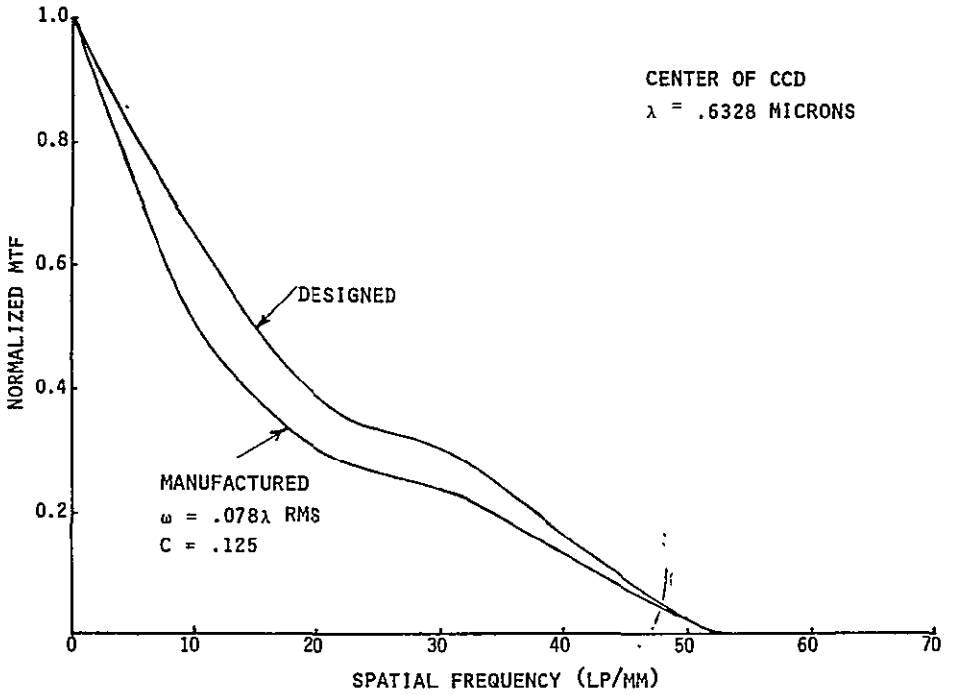

PLANETARY CAMERA PERFORMANCE SPECIFICATIONS
(WITHOUT OTA)

Figure 4.0-7

5.0 OPTICAL CRITIQUE OF BASELINE DESIGN

5.0 OPTICAL CRITIQUE OF BASELINE DESIGN

To critique an optical design, specialized optical analysis software is utilized to predict optical imaging performance under theoretical design, simulated manufacturing and simulated operational conditions.

The questions to be addressed include:

a. What are the system performance merit functions?
b. What is the predicted "designed" system performance?
c. What is the system fabrication tolerance?
d. What is the predicted "manufactured" system performance?
e. What is the operational (dynamic) tolerance?
f. What is the predicted "operational" system performance?

For most imaging devices, MTF analyses serve as useful performance merit functions. System performance specifications have been established in section 4.0. The six basic questions have been addressed in figures 4.0-4 and 4.0-5, and serve as theoretical upper limit goals for the optical critique of the baseline design.

The calculation of data such as spot diagrams, wavefront optical pathlength differences (OPD), and modulation transfer functions (MTF) require the tracing of many exact trigonometric rays. Also, extensive data processing is required such as numerical integration. Consequently, the use of large-scale computer programs is required.

STAR is an Eastman Kodak Company proprietary program which traces exact trigonometric rays thorugh an optical system and calculates ray intercept points and wavefront OPD. There are no restrictions on lens element tilt and decenter because this program uses exact trigonometric expressions throughout.

BFLT5 is also an Eastman Kodak Company proprietary program. This program is more extensive than STAR. In addition to ray intercept points and wavefront OPD, BFLT5 calculates spot diagrams and diffraction-based MTF. Trigonometric approximations are used in its tilt and decenter routines, however, so the magnitudes of lens element tilts and decenters are restricted.

The tilted OTA + f/12.88 relay system was modeled on both STAR and BFLT5. Wavefront OPD's were calculated using both programs, and compared. No significant difference was found between the STAR data and the BFLT5 data. This showed that errors due to tilt and decenter approximations in BFLT5 were negligible. After the accuracy of BFLT5 was established, this program was used to calculate spot diagrams and MTF.

5.1 WIDE FIELD CAMERA MATH MODEL

The following six mirrors were incorporated in the BFLT5 math model: OTA primary mirror, OTA secondary mirror, pyramid field mirror, folding mirror, relay primary mirror, and relay secondary mirror. Initially, all the mirrors were aligned to a common optical axis. A full-aperture (40x40 array size) ray trace of this in-line system showed all rays converging to the expected focus, thereby forming an aberration-free on-axis image point.

The field mirror was then decentered upward by 1.59 cm and tilted 9.1056 degrees about its decentered vertex to simulate one of the concave pyramid faces.

A single chief ray, passing through the vertex of the OTA primary mirror (which is also the system entrance pupil) was traced. The input angle of this ray was adjusted until it intercepted the pyramid face at a height of 1.59 cm (for the f/12.88 relay system). This input field angle was 0.015816 degrees.

After reflection from the pyramid face, this chief ray traveled to the folding mirror at an angle of 18.34 degrees relative to the OTA optical axis. The folding mirror was tilted about its chief ray intercept point by 18.34/2 or 9.17 degrees. This tilt caused the chief ray, after reflection from the folding mirror, to be parallel to the OTA optical axis, but displaced from it by a distance of 6.64 cm.

The segment of the chief ray which was made parallel to the OTA axis is the optical axis of the relay mirrors.* The primary and secondary mirrors of the relay lens and the cover glass were shifted upward 6.64 cm to center them on the relay optical axis. The two relay mirrors and cover glass were shifted as a unit along their optical axis until the prescribed back focal distance was achieved.

Focus was checked by tracing a set of parallel input rays entering the OTA at a field angle of 0.015816 degrees. It was verified that the OTA brought these rays to a focus on the pyramid face at a height of 1.59 cm from the OTA axis. After reflection from the pyramid, the rays diverged to the relay primary mirror via the folding mirror. The relay primary and secondary mirrors refocused the rays and formed a point image on the relay optical axis. This image was formed 0.1009 cm behind the cover glass.

A fixed plano image surface was then placed 0.1009 cm behind the cover glass. This surface simulates the CCD detector. Two "dummy" surfaces were also added to the math model. One of these surfaces, located 490.6 cm in front of the OTA primary mirror, contained the OTA central obstruction. The second surface, located 16.26 cm in front of the relay primary mirror, contained the obstruction caused by the relay secondary mirror. These dummy surfaces do not refract or reflect rays; instead, they block rays which fall within their obstruction perimeters. A third obstruction, caused by the relay primary mirror hole, was specified on the relay primary mirror surface.

5.2 WIDE FIELD CAMERA PERFORMANCE PREDICTION

The tilted optical system comprised of the OTA plus baseline *f*/12.88 relay design was evaluated. Shown in figure 5.2-1 is the actual system MTF compared with the design MTF specification. It should be noted, however, that there was virtually no difference between the actual system MTF and the theoretical

---

* *Relay lens axis, in JPL design, is inclined 1.7254 degrees to the OTA optical axis. In the math model, it is convenient to make these axes parallel. This does not affect optical performance because the folding mirror is plano.*

aberration-free MTF (optical performance at the center of the CCD was diffraction-limited; the spot diagram was a single point.) The difference between the design specification MTF and the theoretical aberration-free MTF is the increase in central obscuration due to the secondary mirror of the relay (see figure 3.1.5-2).

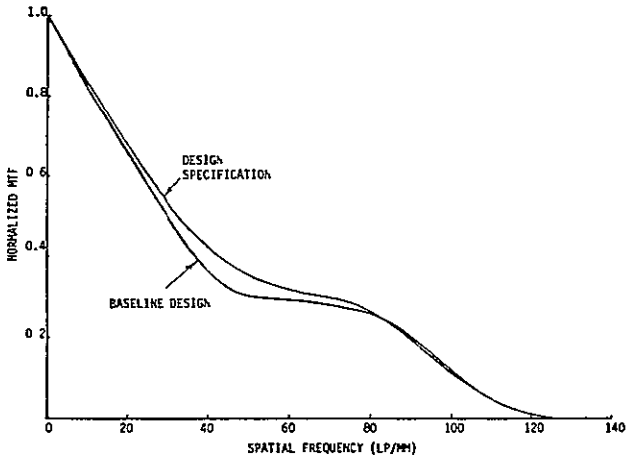

WIDE FIELD CAMERA BASELINE DESIGN
(CENTER OF CCD ARRAY)

Figure 5.2-1

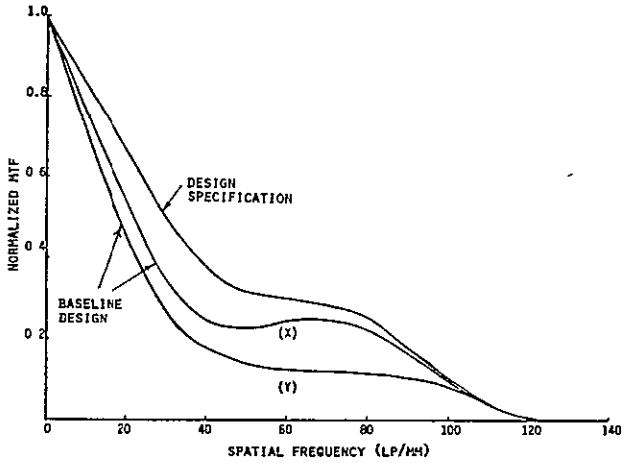

WIDE FIELD CAMERA BASELINE DESIGN
(0.7 FIELD)

Figure 5.2-2

Image quality degraded rapidly, however, for off-axis points on the CCD. The prominent field aberrations were field curvature and astigmatism. Shown in figure 5.2-2 is the actual system MTF at point A^1 on the performance grid (figure 5.2-3). The worst image quality occurred at point A on the grid. Aberration-free MTF for this field point is shown in figure 3.1.5-3 and actual MTF is shown in figure 5.2-4. Comparison of these data at a spatial frequency of 33 cycles/mm shows that field aberrations at point A reduces tangential (X-direction) MTF from a value of 0.35 to a value of 0.16. For radial (Y-direction) MTF, its value is reduced from 0.49 to zero.

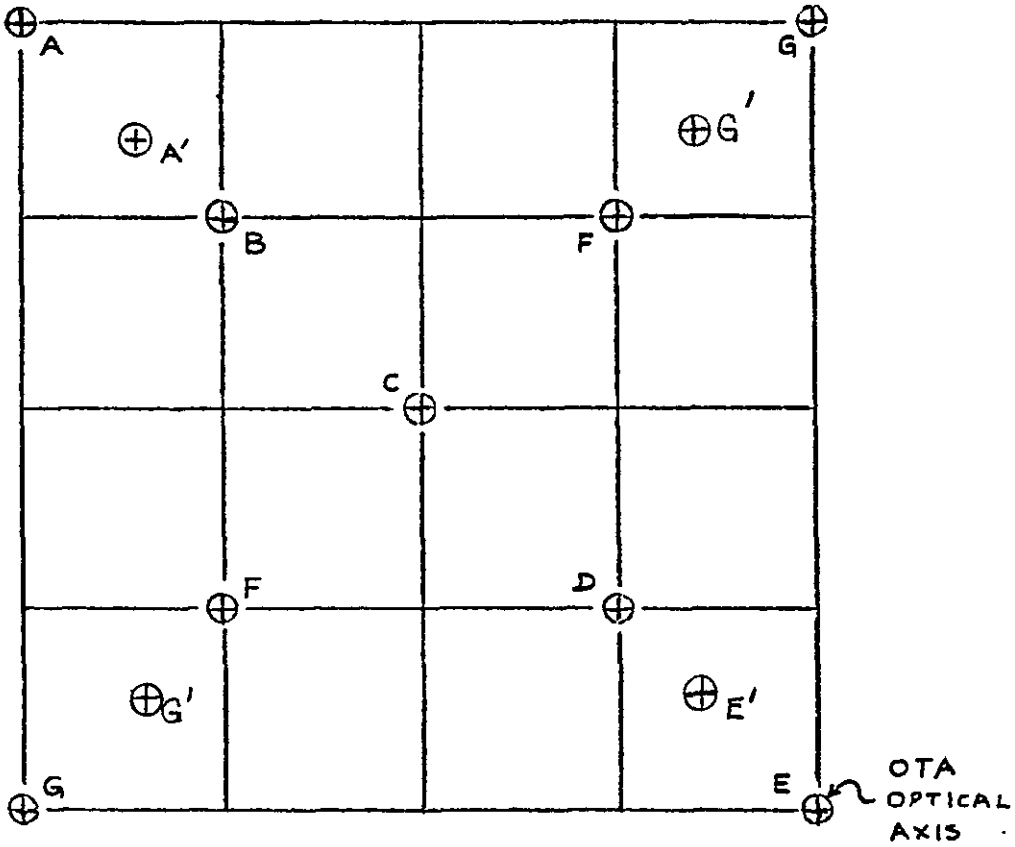

FIELD LOCATION GRID POINTS

Figure 5.2-3

FOLD OUT FOR READY REFERENCE

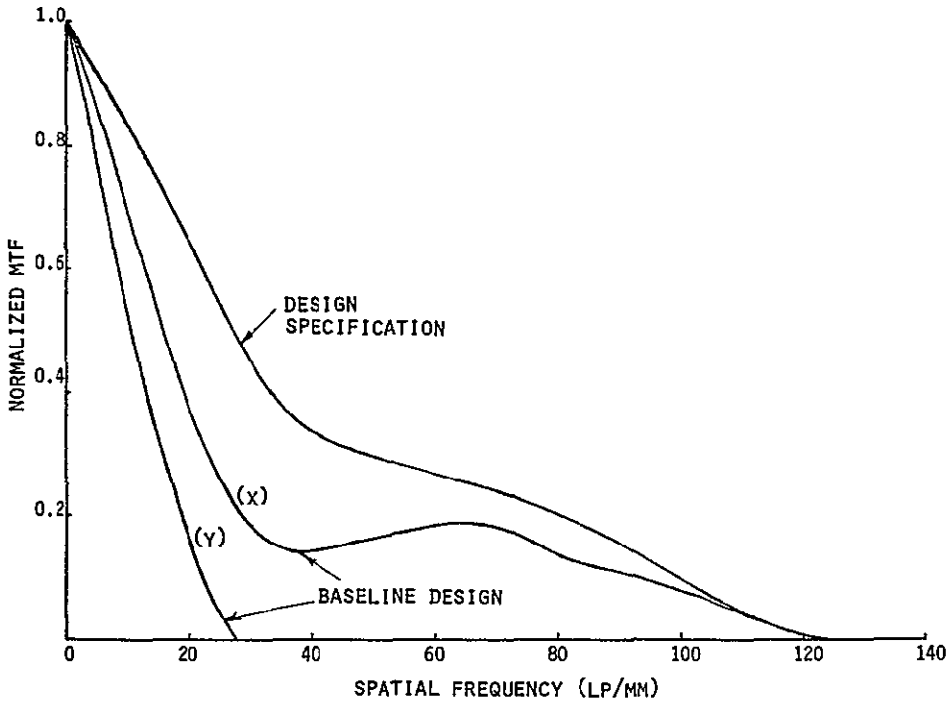

WIDE FIELD CAMERA BASELINE DESIGN
(FULL FIELD)

Figure 5.2-4

MTF at 33 cycles/mm is plotted as a function of relative field angle in figure 5.2-5. The center-point of the CCD detector (grid point C in figure 5.2-3) corresponds to a relative field of 0.0. The outer corner of the CCD, grid point A, corresponds to a relative field of 1.0. The dashed curves depict theoretical aberration-free MTF. Variation of this MTF with field angle is caused by the changing shape and position of the central obscuration in the lens aperture.

The solid curves show the actual MTF for the baseline design. At the center of the CCD, aberration-free performance is achieved. However, MTF falls off rapidly out in the field.

The goal of the optimization is to modify the lens prescription in such a way that off-axis MTF is improved to an acceptable level without degrading on-axis MTF too much. The field aberrations cannot be eliminated. Instead, they are partially cancelled by the introduction of compensating aberrations.

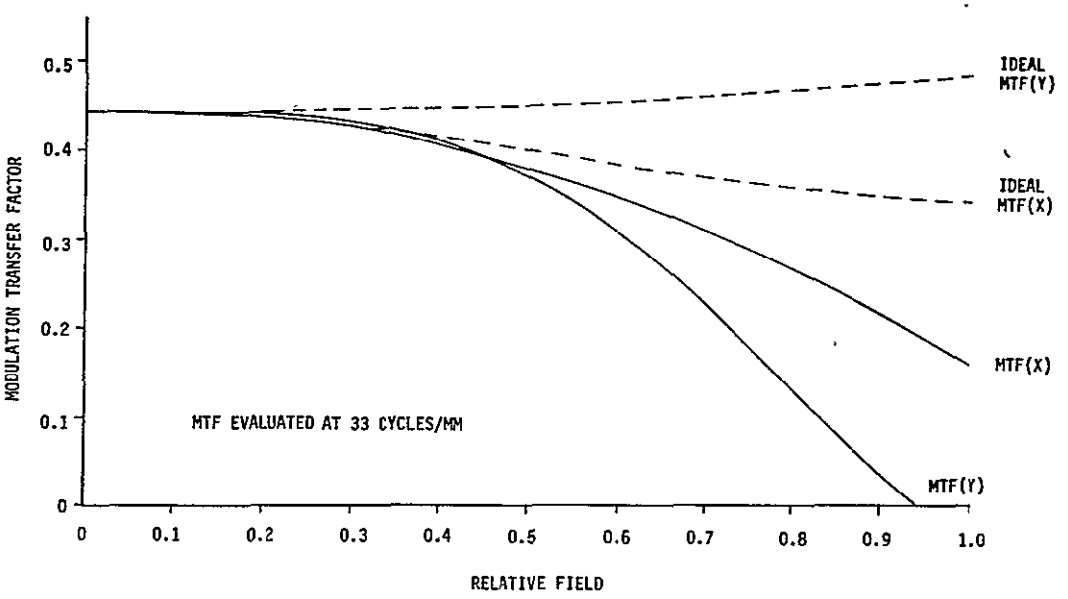

WIDE FIELD CAMERA BASELINE PERFORMANCE

Figure 5.2-5

5.3 PLANETARY CAMERA MATH MODEL

The same procedure was used to construct the BFLT5 math model for the OTA + *f*/30 relay system. For this relay, the chief ray was adjusted until it intercepted the pyramid face at a height of 0.679 cm. The input field angle for this chief ray was 0.0067556 degrees.

The angle of the chief ray between pyramid and folding mirror was 18.61 degrees and its intercept height on the folding mirror was 5.75 cm. The folding mirror was rotated about this intercept point to cause the reflected chief ray to be parallel to the OTA axis. The relay mirrors and cover glass were then centered on this optical axis and these elements were shifted, as a unit, along the optical axis to establish the prescribed back focal distance. The distance between the cover glass and the CCD surface (image plane) was 0.1007 cm.

The pyramid was repositioned along the OTA optical axis, during an earlier step in this modeling procedure, so that the OTA image would be focused at a height of 0.679 cm from the OTA axis. The image locations for the OTA and relay were verified by tracing a set of rays through the system. Finally, the obstructions were added to the math model.

5.4 PLANETARY CAMERA PERFORMANCE PREDICTION

The tilted optical system comprised of the OTA plus baseline *f*/12.88 relay design was evaluated. Shown in figure 5.4-1 through figure 5.4-3 are the actual system MTF calculations at the center of the CCD, 0.7 field, and full field, respectively. Comparison of this data at a spatial frequency of 14 cycles/mm shows that field aberrations at point A reduce tangential (X-direction) MTF from a value of 0.47 to a value of 0.44. For radial (Y-direction) MTF, its value is reduced from 0.47 to 0.41.

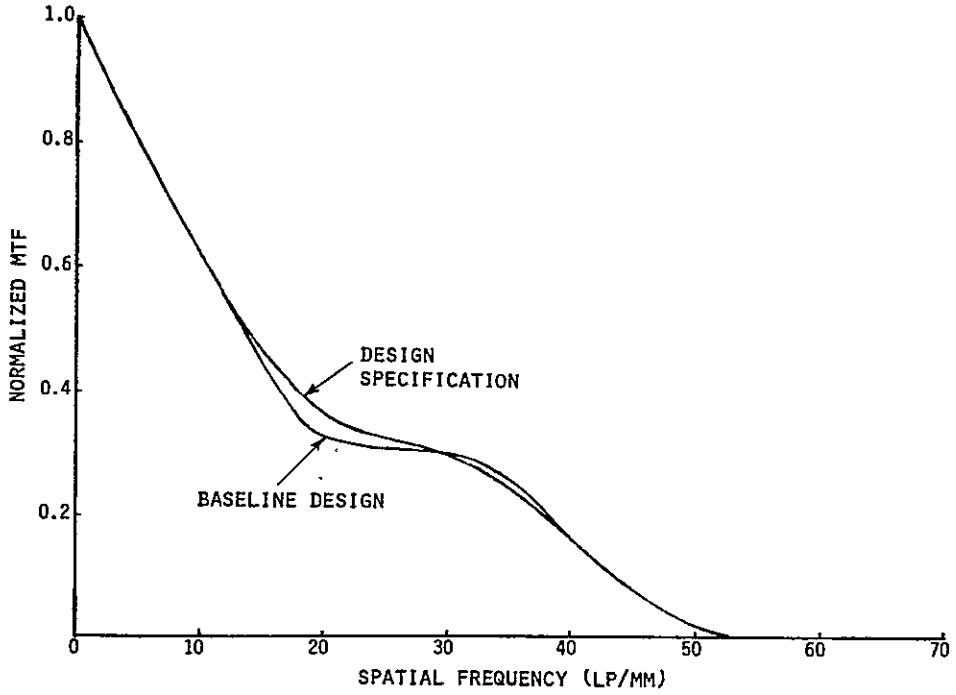

PLANETARY CAMERA BASELINE DESIGN
(CENTER OF CCD)

Figure 5.4-1

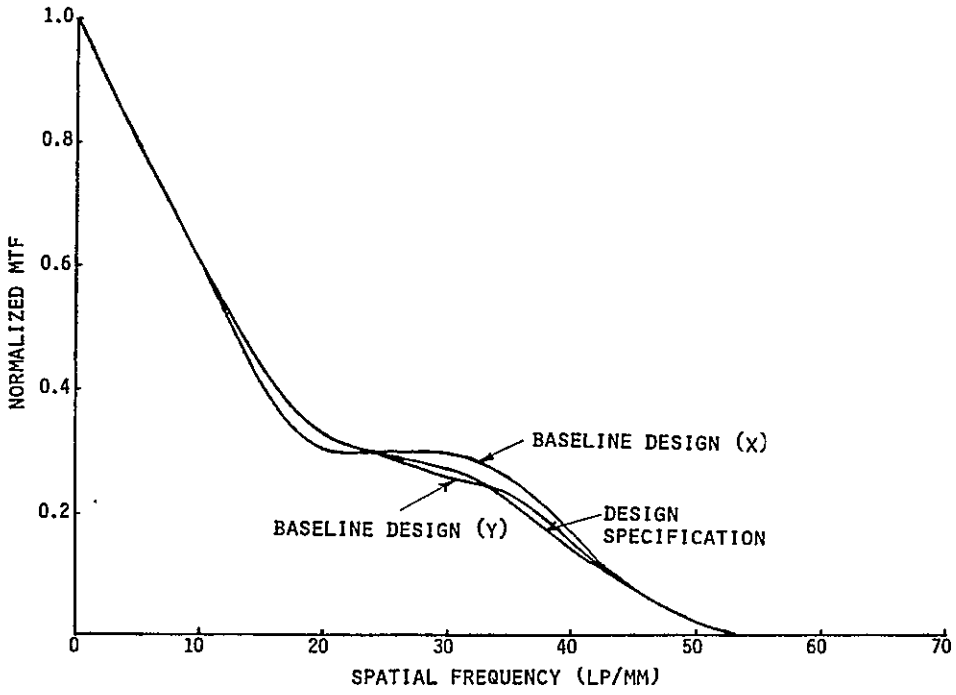

PLANETARY CAMERA BASELINE DESIGN
(0.7 FIELD)

Figure 5.4-2

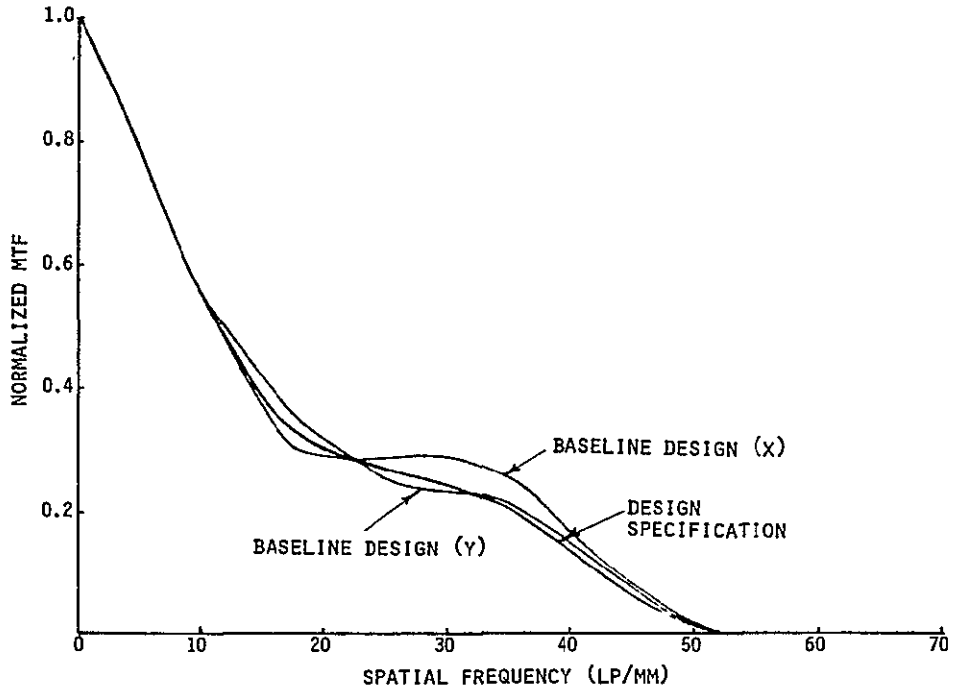

PLANETARY CAMERA BASELINE DESIGN
(FULL FIELD)

Figure 5.4-3

MTF at 14 cycles/mm is plotted as a function of relative field angle in figure 5.4-4. The dashed curves depict theoretical aberration-free MTF. The solid curves show the actual MTF for the baseline design.

Similar to the wide field camera, the planetary camera also has residual astigmatism and field curvature. However, the effect of these aberrations on image quality is negligible because this system operates at a higher f-number and has a smaller angular field. The baseline optical prescription, therefore, needs no modifications.

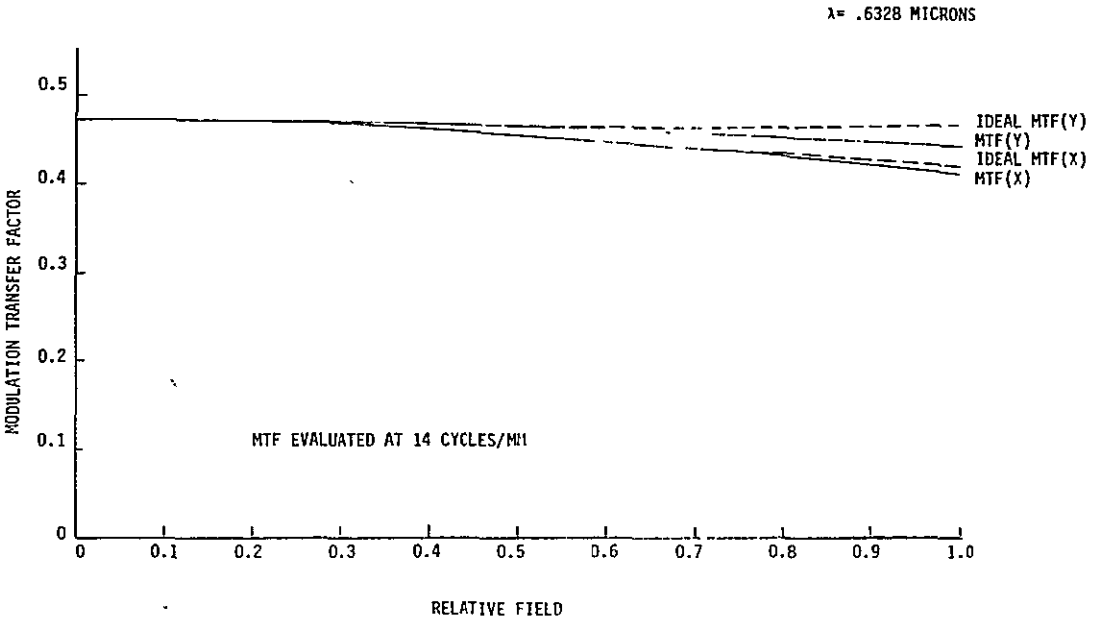

PLANETARY CAMERA BASELINE PERFORMANCE

Figure 5.4-4

ORIGINAL PAGE IS
OF POOR QUALITY

6.0 OPTICAL OPTIMIZATION OF BASELINE DESIGN

6.0 OPTICAL OPTIMIZATION OF BASELINE DESIGN

The goal of the optimization is to modify the lens prescription of the wide field camera in such a way that off-axis MTF is improved to an acceptable level without degrading on-axis MTF too much. In the baseline design, the system has been corrected for third order spherical aberration and coma. The system, however, is degraded by astigmatism and field curvature since these field aberrations are not controlled in the baseline design. The field aberrations cannot be eliminated. Instead, they will be partially cancelled by the introduction of compensating aberrations.

6.1 WIDE FIELD CAMERA OPTIMIZATION

For optical design optimization, the computer program, COOL/GENII, was chosen. COOL/GENII is an automatic lens design program belonging to the Genesee Computer Center, Inc. in Rochester, New York. Kodak has access to this program through an in-plant terminal. The program combines and integrates a wide collection of optical design and evaluation capabilities into a single comprehensive system. As a major component, the COOL/GENII system incorporates the optical design and evaluation capabilities of David Grey Associates programs known collectively as Computer Optics Package (COP). David Grey's optical design program has long been recognized as one of the most powerful tools in the optical design industry. In particular, his orthonormalizaton techniques for optimization are extremely powerful and have been noted for achieving results which were unattainable using other methods. After each optimization run using COOL/GENII, the resultant wavefronts for the tilted system were calculated using the wide field camera math model (see section 5.1). This math model utilizes the Kodak BFLT5 optical evaluation software.

The baseline design consists of two conic mirrors with a plano folding mirror. Not very much can be changed in the lens prescription. The secondary mirror cannot be moved forward toward the pyramid without either increasing the central obscuration or reducing the back focus (axial distance between primary mirror vertex and CCD detector). Moving the secondary mirror back increases the physical length of the system, and this maximum length is restricted.

Aberrations are increased if the primary mirror is moved forward because both the primary mirror and secondary mirror curvatures become stronger. Moving the primary mirror back reduced back focus which is already at its minimum allowable value.

The mirror locations are fixed. Consequently, the mirror radii of curvature are also fixed. Reducing the primary mirror curvature would either increase the central obscuration or increase the system f-number. The system f-number would also increase if the secondary mirror curvature were reduced. Changing the curvature of the pyramid faces would increase the central obscuration.

The only effective degrees of freedom available for optimization are the asphericities of the relay primary and secondary mirrors. For the baseline design, these asphericities have been chosen to yield zero coma and zero aspherical aberration. By changing these asphericities to improve off-axis imagery, the condition of zero spherical aberration is sacrificed. Thus, off-axis performance is improved at the expense of on-axis performance.

The initial plan was to perform a preliminary optimization by using an in-line COOL/GENII model of the OTA plus $f/12.88$ relay system; then, for the final optimization, to use the tilted model. The lens prescription generated by each optimization run would be evaluated by program BFLT5 using the tilted model for all cases.

Lens design program COOL/GENII provides a wide variety of optimization targets such as third-order aberrations, ray intercept deviations at the image surface, astigmatic foci data based on differential ray tracing, and wavefront optical pathlength differences (OPD) in the exit pupil. The procedure is to choose a set of appropriate optimization targets and assign suitable targets and tolerances. A set of targets is specified for each field angle evaluated. The computer program then attempts to bring each target value within its corresponding tolerance by varying the conic constants and asphere coefficients of the relay primary and secondary mirrors.

After some experimentation with various combinations of targets, best results

were obtained by using OPD targets. By specifying OPD goal values and tolerances, the desired wavefront shape at each field angle could be defined. After each optimization run, the resultant wavefronts for the tilted system were calculated with BFLT5, evaluated, and new goal values and tolerances for COOL/GENII were determined. By using these two programs (BFLT5 and COOL/GENII) together in an iterative routine, a final optimized lens prescription was obtained using an in-line model in COOL/GENII and a tilted model in BFLT5. The optimized conic constants (K) and asphere coefficients (A_4 - A_{10}) are:

	Primary Mirror	Secondary Mirror
K	-0.50006	-6.64908
A_4	+0.3914992 E-07	-0.2771794 E-05
A_6	+0.5890965 E-08	-0.2982543 E-05
A_8	+0.6845064 E-09	-0.3224190 E-05
A_{10}	-0.1842629 E-09	-0.3582286 E-05

6.2 WIDE FIELD CAMERA PERFORMANCE PREDICTION

Shown in figures 6.2-1 through 6.2-3 are the optimized system MTF calculations at the center of the CCD, 0.7 field, and full field, respectively. Comparison of this data at a spatial frequency of 33 cycles/mm is shown in figure 6.2-4. The dashed curves depict theoretical aberration-free MTF. The solid curves show the actual MTF for the optimized design. Performance at the center of the CCD has been compromised slightly for a better performance balance across the field. Comparison of this figure with figure 5.2-5 shows how off-axis performance has been improved.

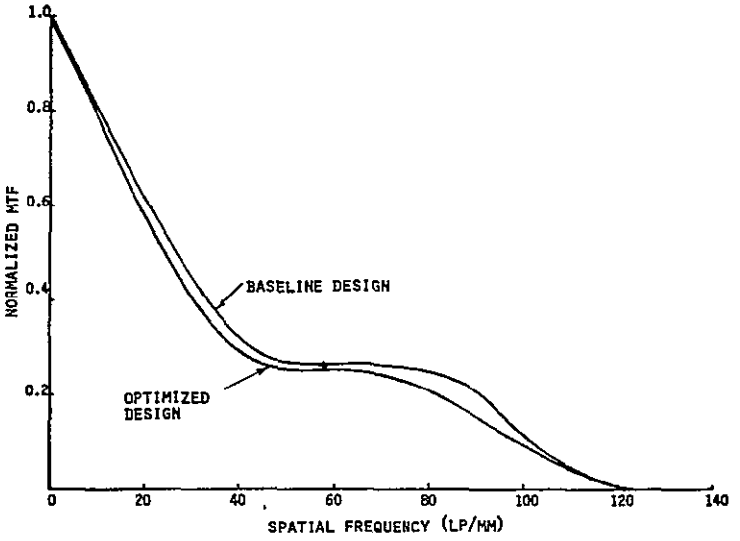

WIDE FIELD CAMERA OPTIMIZATION
(CENTER OF CCD ARRAY)

Figure 6.2-1

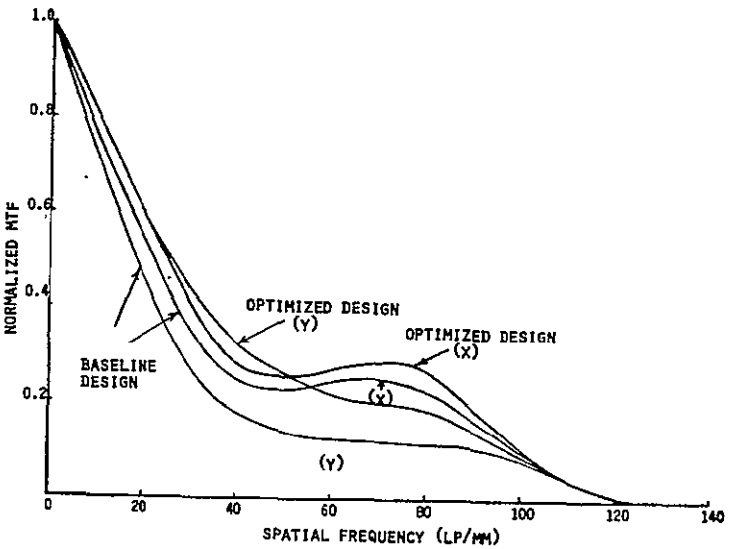

WIDE FIELD CAMERA OPTIMIZATION
(0.7 FIELD)

Figure 6.2-2

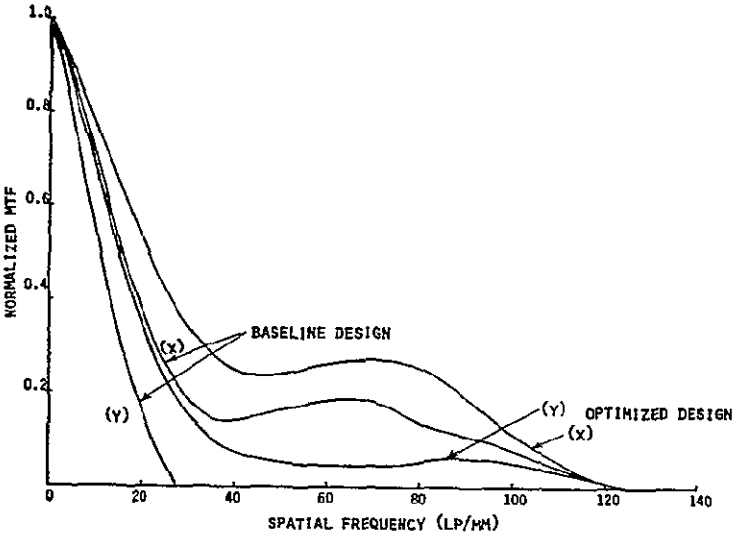

WIDE FIELD CAMERA OPTIMIZATION
(FULL FIELD)

Figure 6.2-3

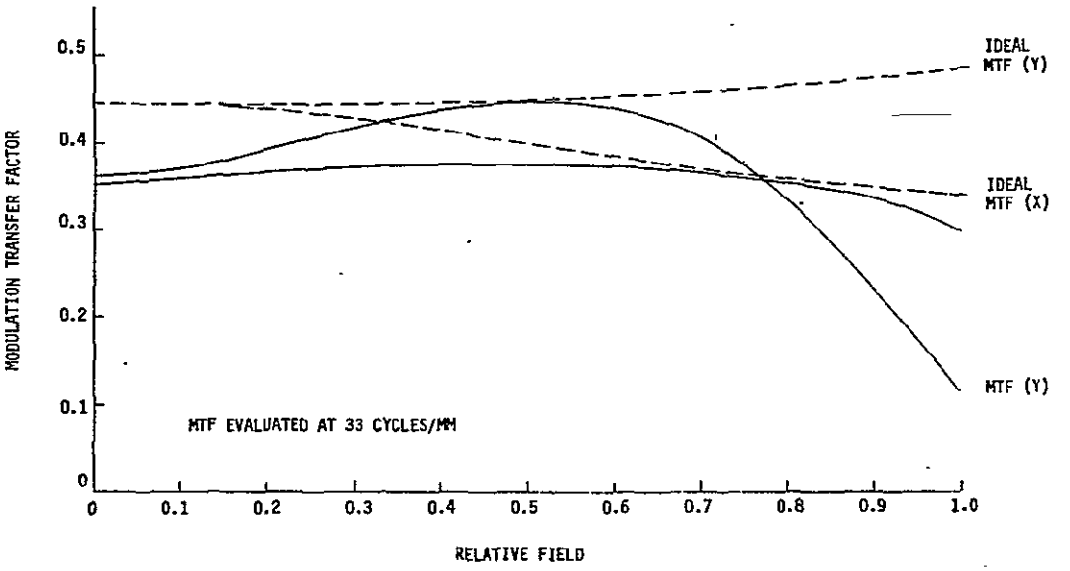

f/12.88 RELAY OPTIMIZED PERFORMANCE
(λ = 0.6328 μm)

Figure 6.2-4

7.0 OPTICAL DESIGN ANALYSIS OF OPTIMIZED DESIGN

7.0 OPTICAL DESIGN ANALYSIS OF OPTIMIZED DESIGN

This section describes the performance of the OTA with WF/PC relay systems in terms of modulation transfer functions (MTF), field curvature, spot diagrams, point spread functions (PSF), encircled energy, geometric distortion, and vignetting. These data relate to monochromatic performance at a spectral wavelength of 0.6328 micron.

Both on-axis and off-axis performance have been calculated. Specific field points are defined on the performance grid shown in figure 5.2-3. Grid point C is the "on-axis" field point with respect to the relay optical axis and is coincident with the center of the 12.2 x 12.2mm CCD (charge coupled device) detector. Due to the tilted optical configuration, however, the OTA is being used off-axis at this grid point. The on-axis image point formed by the OTA is located at the pyramid apex and this point is re-imaged by the relay lens at grid point E.

A line passing through points A-E represents the intersection of the detector surface and the meridional plane of the optical system where the meridional plane is defined as the plane which contains both the OTA and the relay lens optical axes. In the WF/PC optical configuration (figure 3.0-3), the meridional plane is the plane of the paper. Similarly, a line passing through points C-F-G represents the intersection of the detector surface and the sagittal plane, where this plane also contains the relay lens optical axis.

The meridional plane is a plane of symmetry for the optical system. Therefore, except for orientation, performance data at the two grid points denoted F (or G) are identical.

7.1 MODULATION TRANSFER FUNCTION

The $f/12.88$ MTF data was calculated at five focus positions. The back focus values used were nominal, nominal ± 50 microns, and nominal ± 100 microns. At each focus position, average MTF was computed by taking the geometric mean of the radial and tangential MTF values.

Figure 7.1-1 shows geometric mean MTF as a function of relative field at the best-compromise back focus. This curve is the geometric mean of the data given in figure 6.2-4. This best compromise focus position was chosen because it gives uniform performance from on-axis to 0.8 relative field.

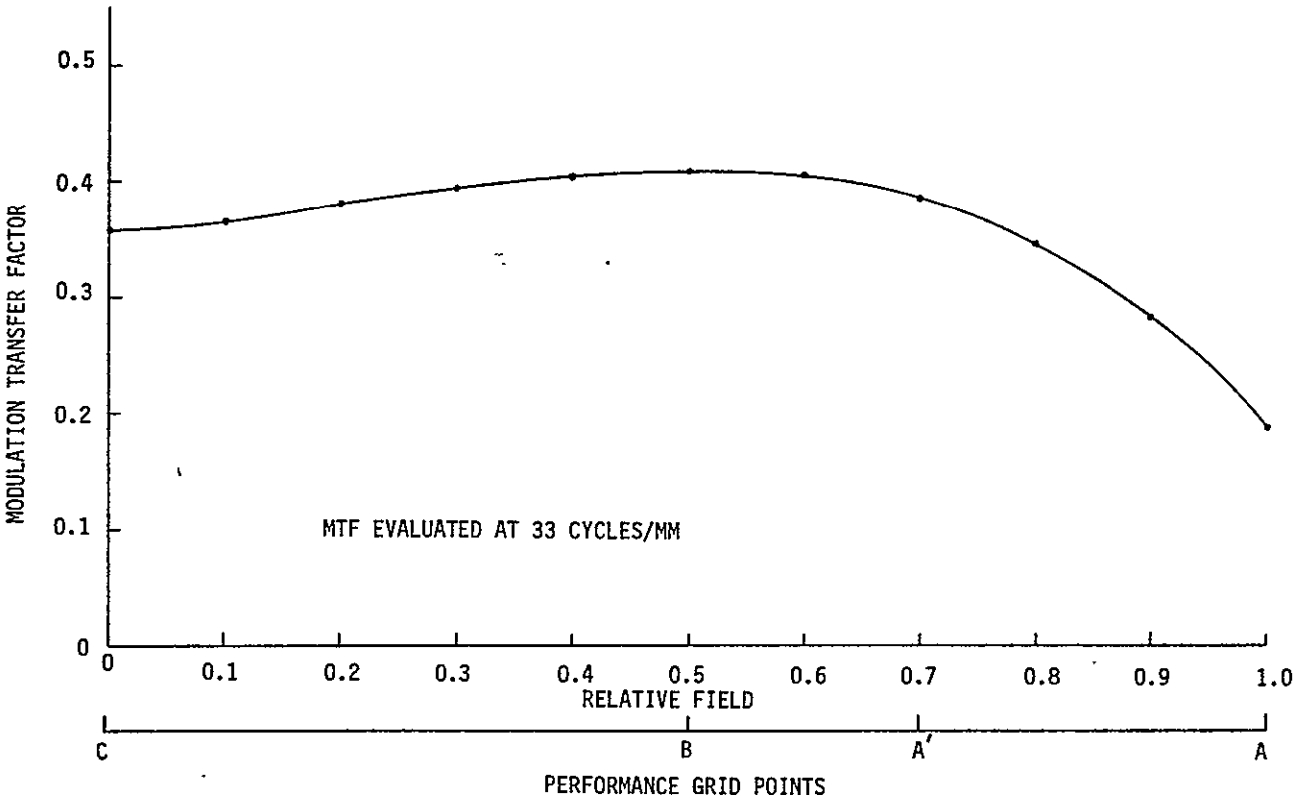

f/12.88 RELAY GEOMETRIC MEAN MTF
AT REFERENCE BACK FOCAL DISTANCE

Figure 7.1-1

Figure 7.1-2 describes MTF performance over the overall image field formed by the four CCD detectors. The outside corners correspond to grid points A. The center of each quadrant is grid point C.

Through-focus MTF over the field of a single detector is shown in figure 7.1-3. By reducing the back focus, MTF at each corner is improved at the expense of MTF at the center.

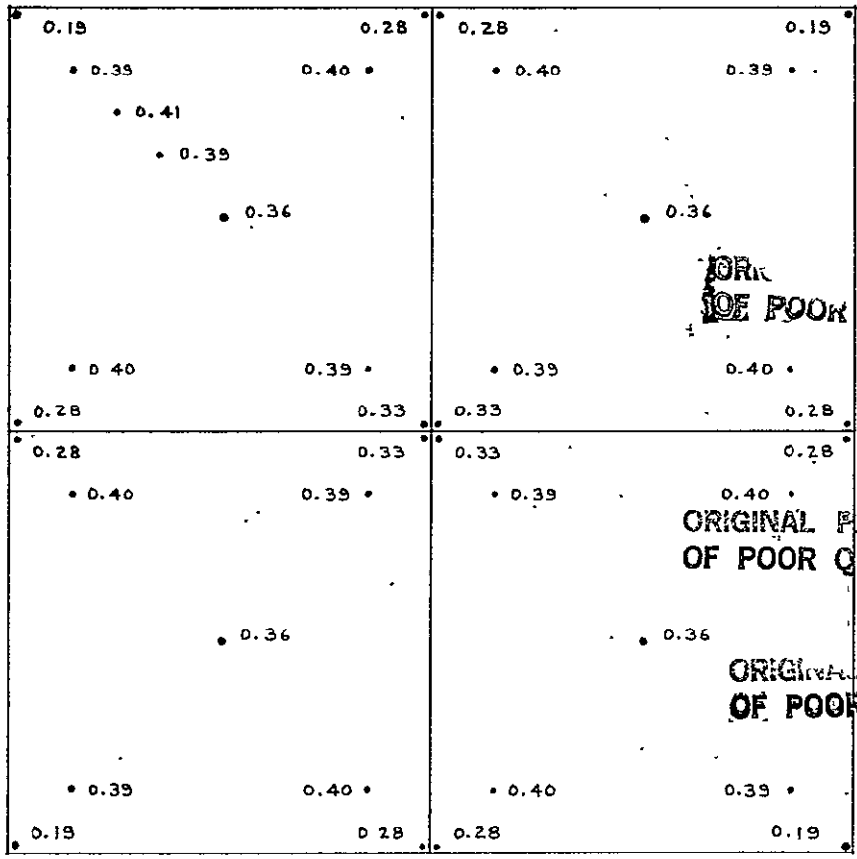

f/12.88 RELAY - OPTIMIZED GEOMETRIC-MEAN MTF
AT VARIOUS FIELD POSITIONS
(SPATIAL FREQUENCY = 33 c/mm, λ = 0.6328 mμ)

Figure 7.1-2

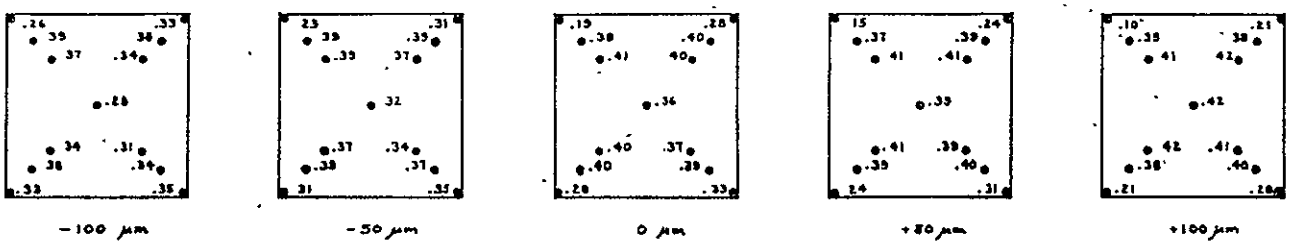

f/12.88 RELAY - THRU-FOCUS MTF OVER DETECTOR FIELD

Figure 7.1-3

In figures 7.1-4 through 7.1-8, relative MTF at the specified grid points are shown as a function of defocus.

MTF is listed as a function of spatial frequency in tables 7.1-1 through 7.1-4. These data correspond to the best-compromise focus position for grid points C, B, A', and A.

The $f/30$ MTF data was calculated at five focus positions. The back focus values used were nominal, nominal ± 100 microns, and nominal ± 200 microns. At each focus position, average MTF was completed by taking the geometric mean of the radial and tangential MTF values.

Figure 7.1-9 shows geometric mean MTF as a function of relative field at the optimum on-axis back focus.

Figure 7.1-10 describes MTF performance over the overall image field formed by the four CCD detectors. The outside corners correspond to grid points A. The center of each quadrant is grid point C.

In figures 7.1-11 through 7.1-14, relative MTF at the specified grid points are shown as a function of defocus.

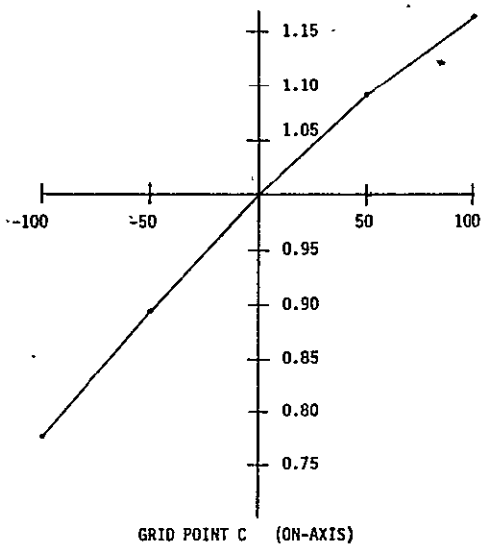

RELATIVE GEOMETRIC MEAN MTF RELATED TO
DEFOCUS AT THE *f*/12.88 RELAY FOCAL PLANE
(DEFOCUS GIVEN IN MICROMETERS)

Figure 7.1-4

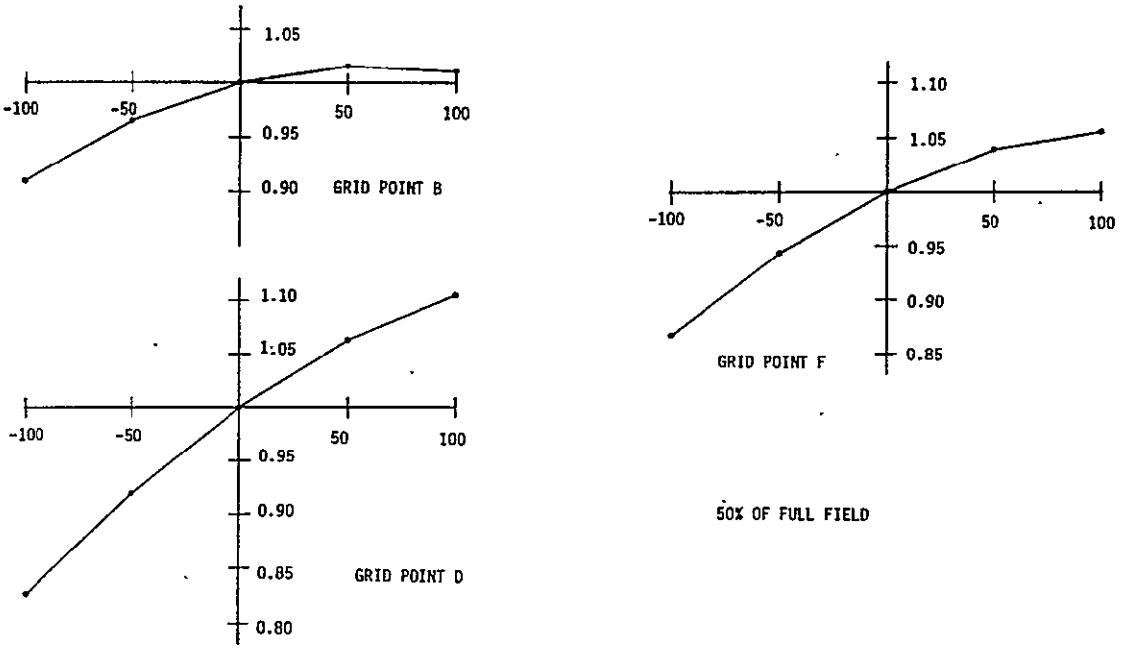

RELATIVE GEOMETRIC MEAN MTF RELATED TO
DEFOCUS AT THE *f*/12.88 RELAY FOCAL PLANE
(DEFOCUS GIVEN IN MICROMETERS)

Figure 7.1-5

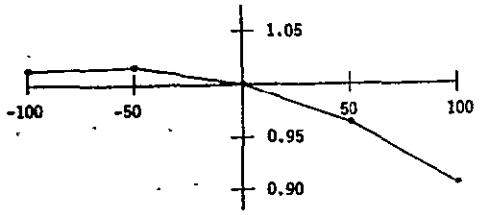

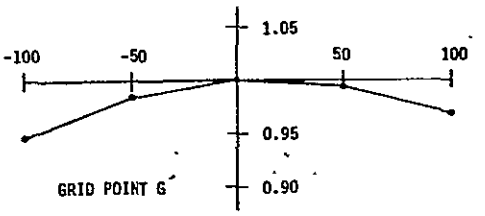

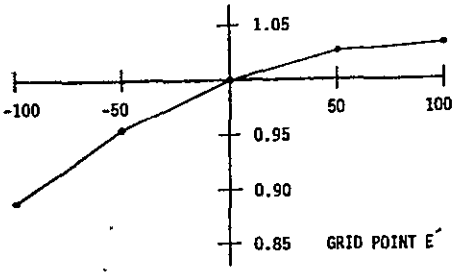

RELATIVE GEOMETRIC MEAN MTF RELATED TO
DEFOCUS AT THE *f*/12.88 RELAY FOCAL PLANE
(DEFOCUS GIVEN IN MICROMETERS)

Figure 7.1-6

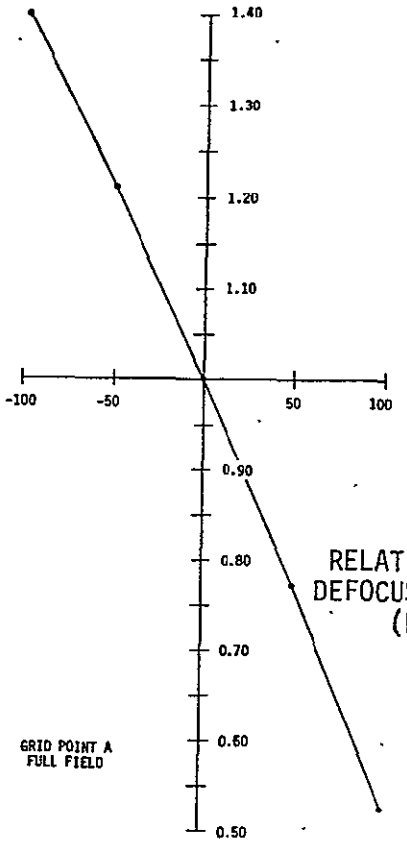

RELATIVE GEOMETRIC MEAN MTF RELATED TO
DEFOCUS AT THE *f*/12.88 RELAY FOCAL PLANE
(DEFOCUS GIVEN IN MICROMETERS)

Figure 7.1-7

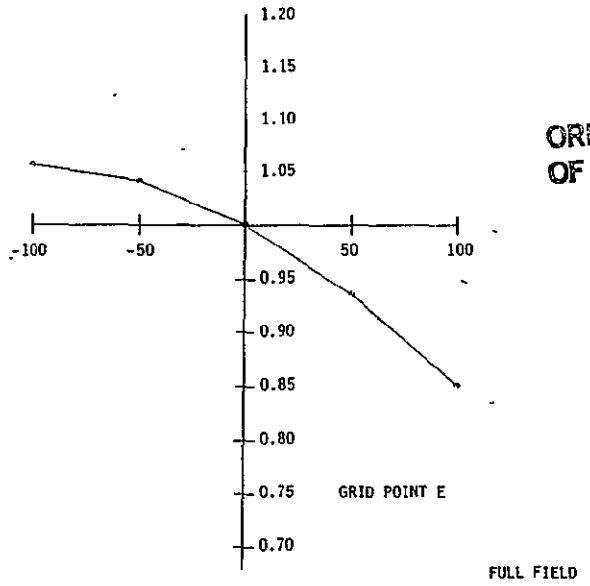

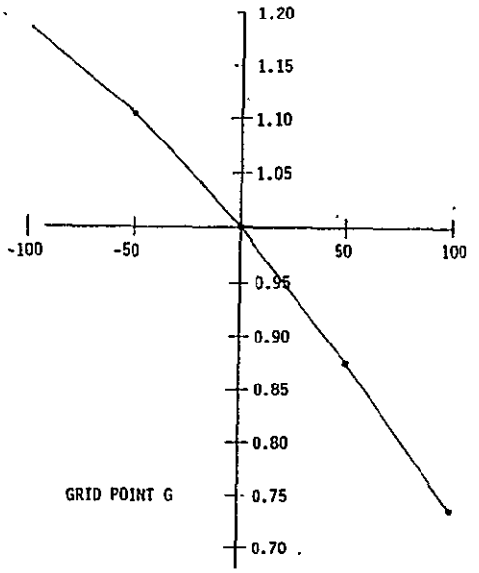

RELATIVE GEOMETRIC MEAN MTF
RELATED TO DEFOCUS

Figure 7.1-8

Table 7.1-1

f/12.88 MTF AT GRID POINT C

DTA= F/12.88 RELAY
THETA= 0.0 DEG. PHI= 0.016 DEG. o Field

GIVEN OR CALCULATED FOCAL PLANE AT 0.23635100D 03 CM.
FOCAL SHIFT= 0.0 CM. RESULTANT FOCAL POSITION= 0.23635100E 03

FREQ	MTF(X)	PHASE(X)	FREQ	MTF(Y)	PHASE(Y)
0.0	1.0000	0.0	0.0	1.0000	0.0
1.749	0.9673	359.9995	1.747	0.9674	0.0015
3.498	0.9311	359.9995	3.494	0.9317	0.0023
5.247	0.8926	359.9995	5.241	0.8939	0.0019
6.996	0.8529	359.9988	6.988	0.8549	0.0004
8.746	0.8126	359.9971	8.735	0.8155	359.9956
10.49	0.7724	359.9963	10.48	0.7761	359.9912
12.24	0.7325	359.9958	12.23	0.7371	359.9871
13.99	0.6933	359.9956	13.98	0.6987	359.9822
15.74	0.6555	359.9956	15.72	0.6616	359.9771
17.49	0.6186	359.9951	17.47	0.6255	359.9719
19.24	0.5827	359.9954	19.22	0.5902	359.9668
20.99	0.5479	359.9951	20.96	0.5559	359.9614
22.74	0.5150	359.9951	22.71	0.5238	359.9563
24.49	0.4833	359.9949	24.46	0.4927	359.9517
26.24	0.4531	359.9951	26.21	0.4627	359.9475
27.99	0.4242	359.9949	27.95	0.4339	359.9436
29.73	0.3975	359.9954	29.70	0.4070	359.9399
31.48	0.3724	359.9951	31.45	0.3817	359.9368
33.23 .3526	0.3496	359.9958	33.19 .3612	0.3587	359.9333
34.98	0.3295	359.9961	34.94	0.3376	359.9297
36.73	0.3130	359.9973	36.69	0.3205	359.9258
38.48	0.2995	359.9965	38.43	0.3063	359.8071
40.23	0.2881	359.9995	40.18	0.2947	359.7917
41.98	0.2782	359.9995	41.93	0.2843	359.7766
43.73	0.2707	359.9995	43.68	0.2758	359.7620
45.48	0.2638	359.9995	45.42	0.2686	359.7463
47.23	0.2592	359.9995	47.17	0.2637	359.7302
48.97	0.2550	359.9995	48.92	0.2593	359.7141
50.72	0.2536	359.9995	50.66	0.2578	359.6965
52.47	0.2522	359.9995	52.41	0.2563	359.6787
54.22	0.2514	359.9995	54.16	0.2555	359.6616
55.97	0.2505	359.9995	55.90	0.2545	359.6443
57.72	0.2495	359.9995	57.65	0.2534	359.6270
59.47	0.2483	359.9995	59.40	0.2521	359.6096
61.22	0.2473	359.9995	61.15	0.2511	359.5928
62.97	0.2459	359.9995	62.89	0.2497	359.5757
64.72	0.2439	359.9995	64.64	0.2476	359.5579
66.47	0.2414	359.9995	66.39	0.2450	359.5398
68.21	0.2389	359.9998	68.13	0.2425	359.5222
69.96	0.2356	359.9995	69.88	0.2392	359.5037
71.71	0.2320	359.9998	71.63	0.2358	359.4858
73.46	0.2275	359.9998	73.37	0.2314	359.4670
75.21	0.2218	359.9998	75.12	0.2259	359.4475
76.96	0.2151	359.9998	76.87	0.2194	359.4275
78.71	0.2079	359.9998	78.62	0.2124	359.4089
80.46	0.1994	359.9998	80.36	0.2041	359.3911
82.21	0.1901	359.9998	82.11	0.1950	359.5564
83.96	0.1798	359.9998	83.86	0.1848	359.5576
85.71	0.1691	359.9998	85.60	0.1740	359.5603
87.46	0.1576	359.9998	87.35	0.1621	359.5623
89.20	0.1469	359.9998	89.10	0.1509	359.5662
90.95	0.1361	359.9998	90.84	0.1397	359.5706
92.70	0.1260	359.9998	92.59	0.1292	359.5769
94.45	0.1159	359.9998	94.34	0.1186	359.5833
96.20	0.1063	359.9998	96.09	0.1087	359.5918
97.95	0.0966	359.9998	97.83	0.0987	359.6001
99.70	0.0881	359.9996	99.58	0.0898	359.6128
101.4	0.0794	0.0000	101.3	0.0808	359.6255
103.2	0.0711	0.0001	103.1	0.0722	359.6404
104.9	0.0625	0.0001	104.8	0.0634	359.6545
106.7	0.0549	0.0002	106.6	0.0555	359.6738
108.4	0.0469	0.0002	108.3	0.0474	359.6921
110.2	0.0398	0.0002	110.1	0.0401	359.7161
111.9	0.0323	0.0005	111.8	0.0325	359.7365
113.7	0.0257	0.0007	113.6	0.0258	359.7671
115.4	0.0186	0.0007	115.3	0.0187	359.7922
117.2	0.0131	0.0006	117.1	0.0131	359.8274
118.9	0.0073	0.0008	118.8	0.0073	359.8567
120.7	0.0037	0.0008	120.5	0.0037	359.9028

Table 7.1-2

f/12.88 MTF AT GRID POINT B

DTA= F/12.86 RELAY
THETA= 0.0 DEG. PHI= .0.024 DEG. 0.5 Field

GIVEN OR CALCULATED FOCAL PLANE AT 0.23635100D 03 CM.
FOCAL SHIFT= 0.0 CM. RESULTANT FOCAL POSITION= 0.23635100E 03

FREQ		MTF(X)	PHASE(X)	FREQ		MTF(Y)	PHASE(Y)
0.0		1.0000	0.0	0.0		1.0000	0.0
1.748		0.9660	359.9995	1.746		0.9682	0.0222
3.497		0.9306	359.9995	3.493		0.9362	0.0402
5.245		0.8945	359.9995	5.239		0.9039	0.0625
6.993		0.8581	359.9995	6.986		0.8716	0.0948
8.742		0.8217	359.9995	8.732		0.8393	0.1401
10.49		0.7855	359.9995	10.48		0.8071	0.2049
12.24		0.7503	359.9995	12.22		0.7751	0.2816
13.99		0.7155	359.9995	13.97		0.7433	0.3764
15.74		0.6811	359.9995	15.72		0.7123	0.4852
17.48		0.6471	359.9995	17.46		0.6814	0.5926
19.23		0.6136	359.9995	19.21		0.6507	0.7077
20.98		0.5804	359.9995	20.96		0.6201	0.8178
22.73		0.5489	359.9995	22.70		0.5902	0.9094
24.48		0.5176	359.9995	24.45		0.5610	0.9822
26.23		0.4870	359.9995	26.20		0.5338	0.9994
27.97		0.4567	359.9995	27.94		0.5098	1.0427
29.72		0.4274	359.9995	29.69		0.4865	1.0651
31.47		0.3986	359.9995	31.43		0.4645	1.0758
33.22	.3745	0.3710	359.9995	33.18	.4458	0.4437	1.0597
34.97		0.3448	359.9995	34.93		0.4229	1.0265
36.72		0.3259	359.9995	36.67		0.4033	0.9676
38.46		0.3061	359.9995	38.42		0.3844	0.9542
40.21		0.2949	359.9995	40.17		0.3661	0.9258
41.96		0.2841	359.9995	41.91		0.3497	0.8953
43.71		0.2760	359.9995	43.66		0.3361	0.8366
45.46		0.2734	359.9995	45.40		0.3224	0.7822
47.21		0.2678	359.9995	47.15		0.3133	0.7194
48.95		0.2656	359.9995	48.90		0.2989	0.6584
50.70		0.2660	359.9995	50.64		0.2951	0.5973
52.45		0.2664	359.9995	52.39		0.2863	0.5440
54.20		0.2674	359.9995	54.14		0.2788	0.5025
55.95		0.2688	359.9995	55.88		0.2732	0.4394
57.70		0.2697	359.9995	57.63		0.2675	0.4082
59.44		0.2705	359.9995	59.38		0.2638	0.3560
61.19		0.2719	359.9995	61.12		0.2607	0.3269
62.94		0.2726	359.9995	62.87		0.2582	0.3279
64.69		0.2727	359.9995	64.61		0.2550	0.3691
66.44		0.2727	359.9995	66.36		0.2519	0.4202
68.19		0.2726	359.9995	68.11		0.2494	0.5110
69.93		0.2713	359.9995	69.85		0.2462	0.6445
71.68		0.2703	359.9995	71.60		0.2438	0.8104
73.43		0.2681	359.9995	73.35		0.2407	1.0121
75.18		0.2646	359.9995	75.09		0.2370	1.2491
76.93		0.2602	359.9995	76.84		0.2326	1.5258
78.68		0.2545	359.9998	78.59		0.2275	1.8298
80.42		0.2482	359.9995	80.33		0.2220	2.1576
82.17		0.2396	359.9998	82.06		0.2151	2.4966
83.92		0.2286	359.9995	83.82		0.2062	2.7625
85.67		0.2146	359.9998	85.57		0.1973	2.9914
87.42		0.1993	359.9998	87.32		0.1878	3.1282
89.17		0.1847	359.9998	89.06		0.1788	3.1301
90.91		0.1702	359.9998	90.81		0.1692	3.0364
92.66		0.1564	359.9998	92.56		0.1596	2.8205
94.41		0.1427	359.9998	94.30		0.1467	2.5415
96.16		0.1297	359.9998	96.05		0.1384	2.0942
97.91		0.1169	359.9998	97.80		0.1263	1.6737
99.66		0.1053	359.9998	99.54		0.1135	1.3331
101.4		0.0938	359.9998	101.3		0.1015	0.9916
103.2		0.0829	359.9998	103.0		0.0887	0.6365
104.9		0.0720	359.9998	104.8		0.0767	0.2937
106.6		0.0623	0.0000	106.5		0.0660	359.9368
108.4		0.0526	0.0000	108.3		0.0554	359.6055
110.1		0.0440	0.0001	110.0		0.0460	359.2864
111.9		0.0352	0.0003	111.8		0.0366	359.0154
113.6		0.0276	0.0004	113.5		0.0284	358.7954
115.4		0.0198	0.0004	115.3		0.0203	358.6416
117.1		0.0138	0.0004	117.0		0.0140	358.5938
118.9		0.0076	0.0004	118.8		0.0076	358.6340
120.6		0.0038	0.0003	120.5		0.0038	358.9026

Table 7.1-3

f/12.88 MTF AT GRID POINT A

OTA+ F/12.88 RELAY
THETA= 0.0 DEG. PHI= 0.027 DEG. T F =+

GIVEN OR CALCULATED FOCAL PLANE AT 0.23635100D 03 CM.
FOCAL SHIFT= 0.0 CM. RESULTANT FOCAL POSITION= 0.23635100E 03

FREQ	MTF(X)	PHASE(X)	FREQ	MTF(Y)	PHASE(Y)
0.0	1.0000	0.0	0.0	1.0000	0.0
1.748	0.9648	359.9995	1.746	0.9673	0.0277
3.496	0.9291	359.9995	3.493	0.9337	0.0645
5.245	0.8932	359.9995	5.239	0.8992	0.1261
6.993	0.8572	359.9995	6.985	0.8639	0.2268
8.741	0.8217	359.9995	8.732	0.8286	0.3774
10.49	0.7865	359.9995	10.48	0.7917	0.5872
12.24	0.7515	359.9995	12.22	0.7553	0.8621
13.99	0.7170	359.9995	13.97	0.7186	1.2107
15.73	0.6827	359.9995	15.72	0.6831	1.6138
17.48	0.6487	359.9995	17.46	0.6478	2.0868
19.23	0.6148	359.9995	19.21	0.6130	2.6265
20.98	0.5811	359.9995	20.96	0.5794	3.1576
22.73	0.5488	359.9995	22.70	0.5510	3.4563
24.47	0.5165	359.9995	24.45	0.5258	3.6485
26.22	0.4847	359.9995	26.19	0.4980	3.8665
27.97	0.4529	359.9995	27.94	0.4732	3.5910
29.72	0.4217	359.9995	29.69	0.4492	3.3995
31.47	0.3905	359.9995	31.43	0.4261	3.0314
33.22	0.3620	359.9995	33.18	0.4042	2.4558
34.96	0.3365	359.9995	34.93	0.3833	1.7256
36.71	0.3195	359.9995	36.67	0.3622	0.8116
38.46	0.3011	359.9995	38.42	0.3449	359.8521
40.21	0.2854	359.9995	40.17	0.3276	358.2671
41.96	0.2747	359.9995	41.91	0.3127	357.[illegible]
43.70	0.2693	359.9995	43.66	0.2984	356.[illegible]
45.45	0.2645	359.9995	45.40	0.2861	355.[illegible]
47.20	0.2626	359.9995	47.15	0.2749	354.[illegible]
48.95	0.2626	359.9995	48.90	0.2652	353.[illegible]
50.70	0.2633	359.9995	50.64	0.2557	352.4736
52.45	0.2646	359.9995	52.39	0.2471	351.4827
54.19	0.2673	359.9995	54.14	0.2393	350.7117
55.94	0.2695	359.9995	55.88	0.2322	349.8191
57.64	0.2724	359.9995	57.63	0.2258	349.0802
59.44	0.2743	359.9995	59.37	0.2195	347.7495
61.19	0.2769	360.0000	61.12	0.2155	346.4158
62.93	0.2794	360.0000	62.87	0.2122	344.9785
64.68	0.2807	0.0000	64.61	0.2099	343.6816
66.43	0.2813	0.0000	66.36	0.2078	342.3754
68.18	0.2826	0.0000	68.11	0.2057	341.2629
69.93	0.2826	0.0000	69.85	0.2035	340.3164
71.67	0.2833	0.0000	71.60	0.2018	339.4258
73.42	0.2826	0.0000	73.35	0.1994	338.7136
75.17	0.2810	0.0000	75.09	0.1965	338.1519
76.92	0.2779	0.0000	76.84	0.1930	337.8625
78.67	0.2742	359.9998	78.58	0.1894	337.7639
80.42	0.2697	359.9998	80.33	0.1857	337.7158
82.16	0.2631	359.9998	82.08	0.1806	338.0635
83.91	0.2506	359.9998	83.82	0.1744	338.9666
85.66	0.2342	359.9998	85.57	0.1684	339.9690
87.41	0.2178	359.9998	87.32	0.1616	340.8630
89.16	0.2020	359.9998	89.06	0.1553	341.6447
90.90	0.1862	359.9998	90.81	0.1482	342.7195
92.65	0.1711	359.9998	92.55	0.1409	343.5024
94.40	0.1560	359.9998	94.30	0.1334	344.3572
96.15	0.1417	359.9998	96.05	0.1258	345.1152
97.90	0.1274	359.9998	97.79	0.1175	345.7791
99.65	0.1145	359.9998	99.54	0.1091	346.1765
101.4	0.1016	359.9998	101.3	0.1005	346.6941
103.1	0.0895	359.9998	103.0	0.0901	346.4960
104.9	0.0774	359.9998	104.8	0.0784	345.9131
106.6	0.0666	0.0000	106.5	0.0678	345.3555
108.4	0.0559	0.0001	108.3	0.0570	344.8[illegible]
110.1	0.0466	0.0002	110.0	0.0474	344.3884
111.9	0.0370	0.0002	111.8	0.0378	344.0134
113.6	0.0288	0.0003	113.5	0.0295	343.7671
115.4	0.0206	0.0003	115.3	0.0214	343.6152
117.1	0.0142	0.0003	117.0	0.0144	343.7129
118.9	0.0078	0.0004	118.7	0.0077	343.9184
120.6	0.0034	0.0004	120.5	0.0034	344.0204

Table 7.1-4

f/12.88 MTF AT GRID POINT A

DIA= F/12.88 RELAY
THETA= 0.0 DEG. PHI= 0.032 DEG. I o F.ld

GIVEN OR CALCULATED FOCAL PLANE AT 0.23635100D 03 CM.
FOCAL SHIFT= 0.0 CM. RESULTANT FOCAL POSITION= 0.23635100E 03

FREQ	MTF(X)	PHASE(X)	FREQ	MTF(Y)	PHASE(Y)
0.0	1.0000	0.0	0.0	1.0000	0.0
1.748	0.9623	0.0002	1.747	0.9601	0.1327
3.496	0.9237	0.0003	3.493	0.9100	0.3374
5.244	0.8842	0.0003	5.240	0.8531	0.6716
6.992	0.8440	0.0004	6.987	0.7912	1.1869
8.740	0.8035	0.0004	8.733	0.7270	1.9308
10.49	0.7620	0.0004	10.48	0.6626	2.9330
12.24	0.7212	0.0004	12.23	0.6009	4.1907
13.98	0.6804	0.0004	13.97	0.5425	5.4682
15.73	0.6397	0.0004	15.72	0.4866	6.4490
17.48	0.5993	0.0004	17.47	0.4332	7.3651
19.23	0.5594	0.0004	19.21	0.3826	8.0634
20.98	0.5203	0.0004	20.96	0.3352	8.5492
22.72	0.4833	0.0004	22.71	0.2921	8.7707
24.47	0.4472	0.0004	24.45	0.2525	8.4429
26.22	0.4125	0.0004	26.20	0.2159	7.5783
27.97	0.3788	0.0004	27.95	0.1836	6.1398
29.72	0.3519	0.0004	29.69	0.1557	4.0047
31.46	0.3262	0.0004	31.44	0.1316	0.8530
33.21	0.3073	0.0004	33.19	0.1122	356.8728
34.96	0.2892	0.0004	34.93	0.0972	352.6616
36.71	0.2732	0.0004	36.68	0.0866	348.1462
38.46	0.2541	0.0004	38.43	0.0791	344.3257
40.20	0.2476	0.0004	40.17	0.0745	341.7864
41.95	0.2396	0.0004	41.92	0.0696	339.8967
43.70	0.2374	0.0003	43.67	0.0658	337.7141
45.45	0.2352	0.0004	45.41	0.0583	335.1453
47.20	0.2357	0.0003	47.16	0.0546	332.2400
48.94	0.2372	0.0004	48.91	0.0506	328.5891
50.69	0.2413	0.0003	50.65	0.0482	324.4707
52.44	0.2447	0.0003	52.40	0.0463	319.4996
54.19	0.2490	0.0003	54.15	0.0446	314.3091
55.94	0.2532	0.0004	55.89	0.0435	308.3958
57.68	0.2565	0.0003	57.64	0.0430	302.8208
59.43	0.2595	0.0004	59.39	0.0428	296.8752
61.18	0.2624	0.0003	61.13	0.0435	292.0083
62.93	0.2650	0.0003	62.88	0.0443	287.1318
64.68	0.2663	0.0003	64.63	0.0459	283.3062
66.42	0.2673	0.0003	66.37	0.0471	280.3662
68.17	0.2682	0.0003	68.12	0.0484	275.5056
69.92	0.2680	0.0003	69.87	0.0498	271.7566
71.67	0.2682	0.0003	71.61	0.0511	266.2190
73.42	0.2674	0.0003	73.36	0.0526	261.7168
75.17	0.2657	0.0003	75.11	0.0536	257.5549
76.91	0.2629	0.0003	76.85	0.0545	254.2692
78.66	0.2601	0.0003	78.60	0.0557	252.4236
80.41	0.2563	0.0003	80.35	0.0561	250.9012
82.16	0.2498	0.0003	82.09	0.0577	251.3526
83.91	0.2373	0.0003	83.84	0.0603	252.9884
85.65	0.2249	0.0003	85.59	0.0625	254.9754
87.40	0.2120	0.0003	87.33	0.0639	256.8098
89.15	0.1993	0.0003	89.08	0.0656	259.0034
90.90	0.1863	0.0003	90.83	0.0663	261.1071
92.65	0.1729	0.0003	92.57	0.0664	263.5693
94.39	0.1594	0.0003	94.32	0.0660	265.9460
96.14	0.1461	0.0002	96.07	0.0650	268.7554
97.89	0.1324	0.0003	97.81	0.0633	271.5443
99.64	0.1194	0.0001	99.56	0.0620	274.3519
101.4	0.1070	359.9998	101.3	0.0593	277.0212
103.1	0.0946	359.9996	103.1	0.0564	281.1187
104.9	0.0826	360.0000	104.8	0.0525	284.5332
106.6	0.0707	0.0000	106.6	0.0487	287.5693
108.4	0.0592	0.0000	108.3	0.0436	291.4121
110.1	0.0482	0.0000	110.0	0.0388	293.7944
111.9	0.0381	0.0000	111.8	0.0335	296.6103
113.6	0.0305	0.0000	113.5	0.0285	298.7742
115.4	0.0216	0.0000	115.3	0.0246	299.4[illegible]
117.1	0.0146	0.0001	117.0	0.0214	299.8977
118.9	0.0081	0.0001	118.8	0.0178	299.8515
120.6	0.0040	0.0000	120.5	0.0040	299.1041

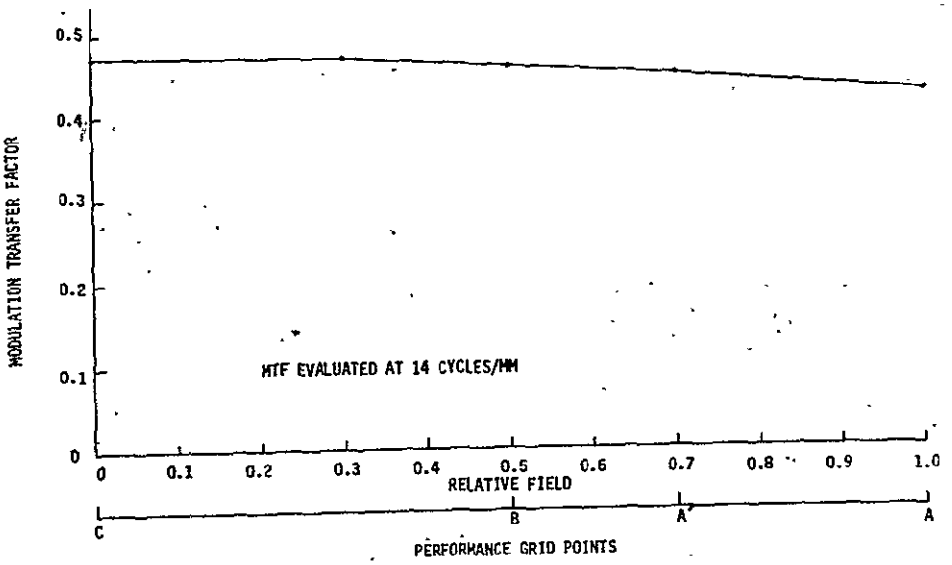

f/30 RELAY GEOMETRIC MEAN MTF
AT REFERENCE BACK FOCAL DISTANCE

Figure 7.1-9

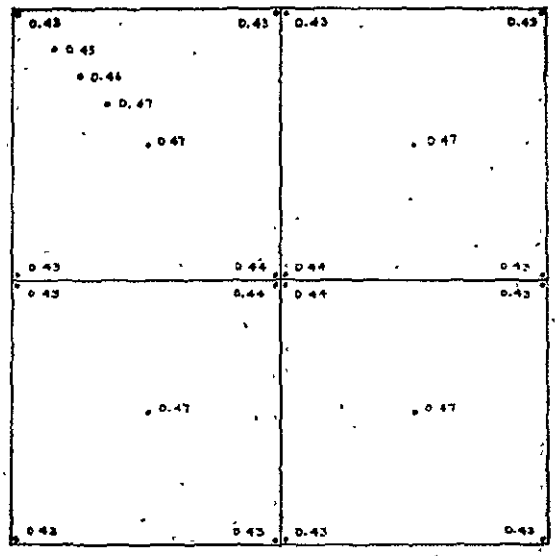

f/30 RELAY - OPTIMIZED GEOMETRIC-MEAN MTF
AT VARIOUS FIELD POSITIONS

Figure 7.1-10

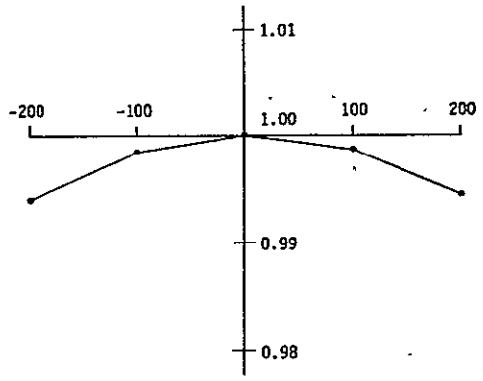

RELATIVE GEOMETRIC MEAN MTF RELATED TO DEFOCUS
AT THE *f*/30 RELAY FOCAL PLANE
(DEFOCUS GIVEN IN MICROMETERS)

Figure 7.1-11

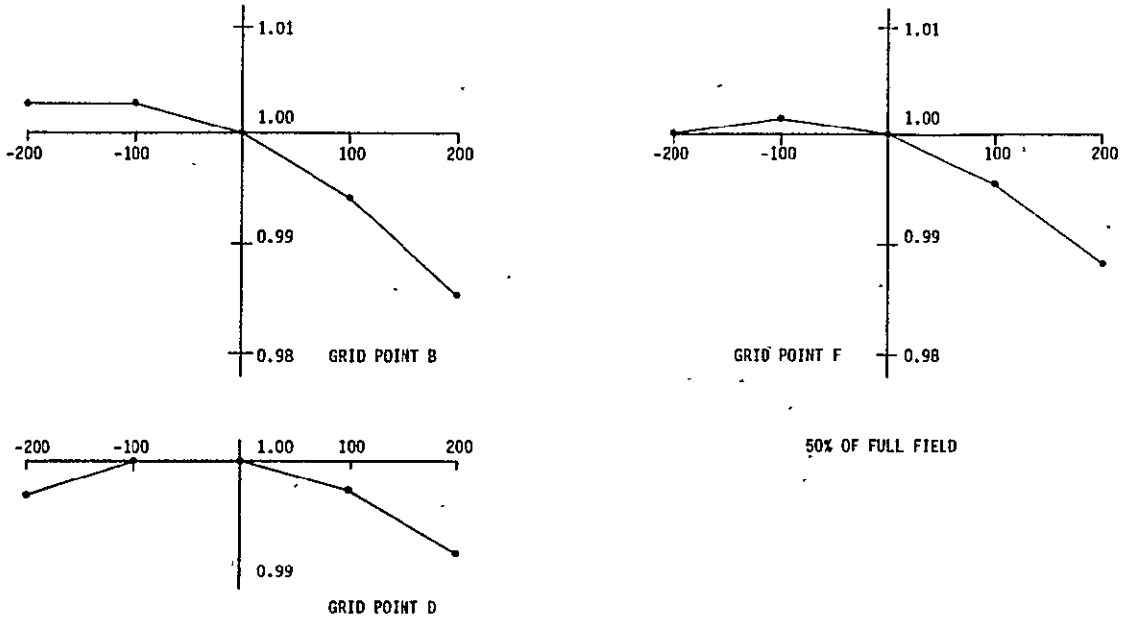

RELATIVE GEOMETRIC MEAN MTF RELATED TO
DEFOCUS AT THE *f*/30 RELAY FOCAL PLANE
(DEFOCUS GIVEN IN MICROMETERS)

Figure 7.1-12

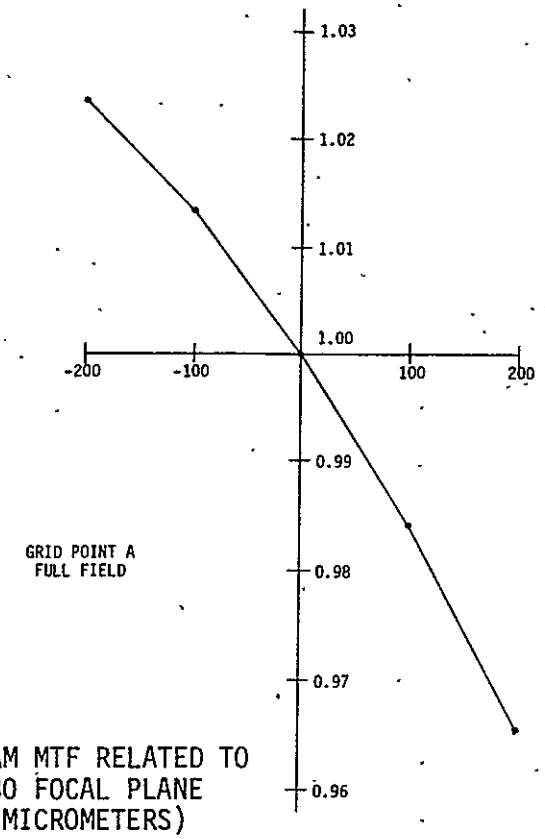

RELATIVE GEOMETRIC BEAM MTF RELATED TO DEFOCUS AT THE $f/30$ FOCAL PLANE (DEFOCUS GIVEN IN MICROMETERS)

Figure 7.1-13

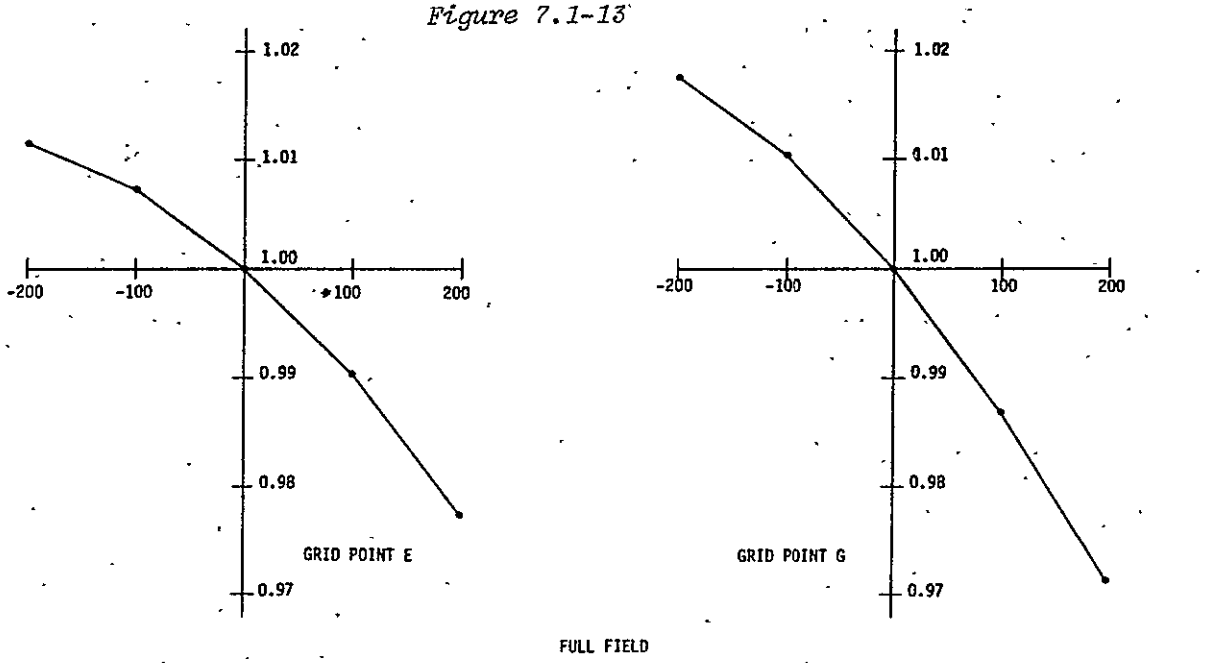

Figure 7.1-14 RELATIVE GEOMETRIC BEAM MTF RELATED TO DEFOCUS AT THE $f/30$ FOCAL PLANE (DEFOCUS GIVEN IN MICROMETERS)

MTF is listed as a function of spatial frequency in tables 7.1-5 through 7.1-8. This data was calculated at the optimum on-axis back focal distance. MTF data at grid points C, B, A', and A are given.

Table 7.1-5

f/30 MTF AT GRID POINT C

OTA + F/30 RELAY
THETA= 0.0 DEG. PHI= 0.007 DEG. 0 FIELD

GIVEN OR CALCULATED FOCAL PLANE AT 0.24509520D 03 CM.
FOCAL SHIFT= 0.0 CM. RESULTANT FOCAL POSITION= 0.24509520E 0.

FREQ	MTF(X)	PHASE(X)	FREQ	MTF(Y)	PHASE(Y)
0.0	1.0000	0.0	0.0	1.0000	0.0
0.7525	0.9708	360.0000	0.7516	0.9709	0.0000
1.505	0.9417	360.0000	1.503	0.9417	359.9998
2.258	0.9125	359.9998	2.255	0.9126	359.9996
3.010	0.8834	359.9998	3.006	0.8835	359.9996
3.763	0.8543	359.9998	3.758	0.8543	359.9998
4.515	0.8252	359.9998	4.510	0.8252	359.9995
5.268	0.7961	359.9998	5.261	0.7961	359.9995
6.020	0.7670	359.9998	6.013	0.7670	359.9993
6.773	0.7382	359.9998	6.764	0.7379	359.9993
7.525	0.7094	359.9998	7.516	0.7088	359.9990
8.278	0.6809	359.9998	8.268	0.6803	359.9990
9.030	0.6524	359.9996	9.019	0.6518	359.9988
9.783	0.6245	359.9996	9.771	0.6239	359.9985
10.54	0.5966	359.9998	10.52	0.5960	359.9983
11.29	0.5693	359.9998	11.27	0.5687	359.9983
12.04	0.5420	359.9996	12.03	0.5415	359.9980
12.79	0.5154	359.9996	12.78	0.5148	359.9976
13.55	0.4887	359.9996	13.53	0.4881	359.9976
14.30	0.4626	359.9996	14.28	0.4620	359.9971
15.05	0.4365	359.9996	15.03	0.4360	359.9966
15.80	0.4117	359.9996	15.78	0.4111	359.9960
16.56	0.3868	359.9998	16.54	0.3862	359.9961
17.31	0.3699	359.9998	17.29	0.3687	359.9958
18.06	0.3553	359.9996	18.04	0.3541	359.9956
18.81	0.3432	359.9998	18.79	0.3420	359.9954
19.57	0.3335	359.9998	19.54	0.3329	359.9949
20.32	0.3258	359.9998	20.29	0.3280	359.9948
21.07	0.3238	359.9998	21.04	0.3232	359.9944
21.82	0.3195	359.9996	21.80	0.3195	359.9941
22.56	0.3159	359.9996	22.55	0.3159	359.9939
23.33	0.3129	359.9996	23.30	0.3129	359.9934
24.08	0.3098	359.9998	24.05	0.3098	359.9932
24.83	0.3068	359.9996	24.80	0.3068	359.9929
25.59	0.3038	359.9996	25.55	0.3038	359.9927
26.34	0.3013	359.9996	26.31	0.3014	359.9924
27.09	0.2989	359.9998	27.06	0.2989	359.9924
27.84	0.2965	359.9998	27.81	0.2965	359.9922
28.60	0.2935	359.9998	28.56	0.2941	359.9919
29.35	0.2904	360.0000	29.31	0.2910	359.9919
30.10	0.2874	359.9996	30.06	0.2880	359.9917
30.85	0.2838	360.0000	30.82	0.2844	359.9917
31.61	0.2789	359.9998	31.57	0.2795	359.9915
32.36	0.2741	360.0000	32.32	0.2747	359.9915
33.11	0.2660	359.9996	33.07	0.2686	359.9912
33.86	0.2613	360.0000	33.82	0.2619	359.9912
34.62	0.2534	359.9998	34.57	0.2541	359.9912
35.37	0.2450	360.0000	35.32	0.2456	359.9912
36.12	0.2353	359.9998	36.08	0.2353	359.9907
36.87	0.2201	360.0000	36.83	0.2201	359.9907
37.63	0.2049	360.0000	37.58	0.2050	359.9907
38.38	0.1904	360.0000	38.33	0.1904	359.9907
39.13	0.1758	360.0000	39.08	0.1759	359.9907
39.88	0.1619	360.0000	39.83	0.1619	359.9910
40.64	0.1479	360.0000	40.59	0.1480	359.9910
41.39	0.1346	360.0000	41.34	0.1346	359.9910
42.14	0.1213	360.0000	42.09	0.1213	359.9912
42.89	0.1091	360.0000	42.84	0.1092	359.9915
43.65	0.0970	360.0000	43.59	0.0970	359.9917
44.40	0.0855	360.0000	44.34	0.0855	359.9919
45.15	0.0740	360.0000	45.10	0.0740	359.9922
45.90	0.0637	360.0000	45.85	0.0637	359.9924
46.66	0.0534	0.0000	46.60	0.0534	359.9927
47.41	0.0443	0.0000	47.35	0.0443	359.9932
48.16	0.0352	0.0000	48.10	0.0352	359.9937
48.91	0.0272	0.0000	48.85	0.0272	359.9941
49.67	0.0194	0.0000	49.61	0.0194	359.9948
50.42	0.0133	0.0000	50.36	0.0133	359.9954
51.17	0.0073	0.0000	51.11	0.0073	359.9961
51.92	0.0036	0.0000	51.86	0.0036	359.9972

Table 7.1-6

f/30 MTF AT GRID POINT B

OTA + F/30 RELAY
THETA= 0.0 DEG. PHI= 0.010 DEG. 0.5 Field

GIVEN OR CALCULATED FOCAL PLANE AT 0.24509520D 03 CM.
FOCAL SHIFT= 0.0 CM. RESULTANT FOCAL POSITION= 0.24509520E 03

FREQ	MTF(X)	PHASE(X)	FREQ.	MTF(Y)	PHASE(Y)
0.0	1.0000	0.0	0.0	1.0000	0.0
0.7525	0.9694	0.0000	0.7515	0.9703	0.0011
1.505	0.9390	0.0000	1.503	0.9408	0.0043
2.257	0.9086	0.0001	2.255	0.9112	0.0096
3.010	0.8781	0.0002	3.006	0.8815	0.0172
3.762	0.8476	0.0003	3.758	0.8519	0.0273
4.515	0.8172	0.0003	4.509	0.8222	0.0404
5.267	0.7873	0.0003	5.261	0.7925	0.0567
6.020	0.7574	0.0003	6.012	0.7628	0.0765
6.772	0.7276	0.0003	6.764	0.7331	0.1004
7.525	0.6977	0.0003	7.515	0.7040	0.1277
8.277	0.6678	0.0003	8.267	0.6749	0.1594
9.030	0.6380	0.0003	9.019	0.6459	0.1973
9.782	0.6093	0.0003	9.770	0.6175	0.2405
10.53	0.5807	0.0003	10.52	0.5897	0.2867
11.29	0.5528	0.0003	11.27	0.5620	0.3441
12.04	0.5248	0.0003	12.02	0.5343	0.4079
12.79	0.4971	0.0003	12.78	0.5067	0.4812
13.54	0.4695	0.0003	13.53	0.4791	0.5658
14.30	0.4425	0.0003	14.28	0.4541	0.6082
15.05	0.4156	0.0003	15.03	0.4314	0.5781
15.80	0.3899	0.0003	15.78	0.4112	0.4910
16.55	0.3654	0.0003	16.53	0.3923	0.3401
17.31	0.3421	0.0003	17.29	0.3740	0.1516
18.06	0.3354	0.0003	18.04	0.3567	359.9888
18.81	0.3213	0.0002	18.79	0.3459	359.8511
19.56	0.3170	0.0003	19.54	0.3349	359.7134
20.32	0.3128	0.0002	20.29	0.3252	359.5830
21.07	0.3047	0.0002	21.04	0.3185	359.4807
21.82	0.3072	0.0002	21.79	0.3118	359.3689
22.57	0.3048	0.0002	22.55	0.3069	359.2371
23.33	0.3036	0.0002	23.30	0.3032	359.1248
24.08	0.3024	0.0002	24.05	0.2996	359.0046
24.83	0.3011	0.0002	24.80	0.2966	358.9067
25.58	0.2999	0.0002	25.55	0.2935	358.8035
26.34	0.2987	0.0002	26.30	0.2905	358.7241
27.09	0.2974	0.0002	27.06	0.2874	358.6414
27.84	0.2956	0.0002	27.81	0.2837	358.5623
28.59	0.2931	0.0002	28.56	0.2801	358.5220
29.35	0.2913	0.0002	29.31	0.2770	358.4826
30.10	0.2882	0.0002	30.06	0.2733	358.4250
30.85	0.2857	0.0002	30.81	0.2702	358.3984
31.60	0.2820	0.0002	31.57	0.2659	358.3664
32.36	0.2777	0.0002	32.32	0.2610	358.3643
33.11	0.2722	0.0002	33.07	0.2549	358.3628
33.86	0.2654	0.0002	33.82	0.2487	358.3977
34.61	0.2586	0.0002	34.57	0.2420	358.4072
35.37	0.2494	0.0002	35.32	0.2340	358.5246
36.12	0.2378	0.0002	36.07	0.2236	358.7273
36.87	0.2215	0.0002	36.83	0.2126	358.8926
37.62	0.2072	0.0001	37.58	0.2011	359.0503
38.38	0.1925	0.0000	38.33	0.1901	359.2371
39.13	0.1776	0.0000	39.08	0.1773	359.3335
39.88	0.1637	0.0000	39.83	0.1633	359.3213
40.63	0.1497	0.0000	40.58	0.1493	359.3091
41.39	0.1362	0.0000	41.34	0.1359	359.2971
42.14	0.1227	0.0000	42.09	0.1224	359.2854
42.89	0.1104	0.0000	42.84	0.1104	359.2734
43.64	0.0982	0.0000	43.59	0.0980	359.2617
44.40	0.0865	0.0000	44.34	0.0864	359.2504
45.15	0.0748	0.0000	45.09	0.0748	359.2387
45.90	0.0643	0.0000	45.84	0.0644	359.2273
46.65	0.0540	0.0000	46.60	0.0540	359.2160
47.40	0.0441	0.0000	47.35	0.0441	359.2043
48.16	0.0346	0.0000	48.10	0.0356	359.1930
48.91	0.0276	360.0000	48.85	0.0276	359.1817
49.66	0.0197	360.0000	49.60	0.0196	359.1703
50.41	0.0135	360.0000	50.36	0.0135	359.1590
51.17	0.0074	360.0000	51.11	0.0074	359.1476
51.92	0.0037	360.0000	51.86	0.0037	359.1363

Table 7.1-7

f/30 MTF AT GRID POINT A

ORIGINAL PAGE IS OF POOR QUALITY

OTA + F/30 RELAY
THETA= 0.0 DEG. PHI= 0.011 DEG.

GIVEN OR CALCULATED FOCAL PLANE AT 0.24509520D 03 CM.
FOCAL SHIFT= 0.0 CM. RESULTANT FOCAL POSITION= 0.24509520E 03

FREQ	MTF(X)	PHASE(X)	FREQ	MTF(Y)	PHASE(Y)
0.0	1.0000	0.0	0.0	1.0000	0.0
0.7525	0.9666	0.0000	0.7516	0.9700	359.9949
1.505	0.9377	0.0002	1.503	0.9400	359.9941
2.257	0.9066	0.0003	2.255	0.9098	359.9980
3.010	0.8754	0.0003	3.006	0.8796	0.0078
3.762	0.8442	0.0003	3.758	0.8492	0.0233
4.515	0.8129	0.0003	4.510	0.8188	0.0454
5.267	0.7820	0.0003	5.261	0.7863	0.0750
6.020	0.7510	0.0004	6.013	0.7579	0.1129
6.772	0.7204	0.0004	6.764	0.7274	0.1600
7.525	0.6897	0.0004	7.516	0.6976	0.2153
8.277	0.6591	0.0004	8.266	0.6679	0.2816
9.030	0.6215	0.0004	9.019	0.6382	0.3603
9.782	0.5992	0.0004	9.771	0.6093	0.4521
10.53	0.5699	0.0004	10.52	0.5805	0.5596
11.29	0.5410	0.0004	11.27	0.5518	0.6849
12.04	0.5121	0.0004	12.03	0.5238	0.8253
12.79	0.4839	0.0004	12.76	0.4961	0.9877
13.54	0.4558	0.0004	13.53	0.4708	1.0595
14.30	0.4282	0.0003	14.28	0.4480	1.0101
15.05	0.4010	0.0004	15.03	0.4264	0.8974
15.80	0.3749	0.0003	15.78	0.4068	0.6744
16.55	0.3519	0.0003	16.54	0.3885	0.3666
17.31	0.3357	0.0003	17.29	0.3703	359.9883
18.06	0.3225	0.0003	18.04	0.3545	359.6516
18.81	0.3136	0.0003	18.79	0.3417	359.3699
19.56	0.3060	0.0003	19.54	0.3301	359.1262
20.32	0.3029	0.0003	20.29	0.3204	358.8677
21.07	0.3011	0.0003	21.04	0.3118	358.6753
21.82	0.2993	0.0003	21.80	0.3046	358.4502
22.57	0.2975	0.0003	22.55	0.2979	358.1960
23.33	0.2969	0.0003	23.30	0.2943	357.9536
24.08	0.2962	0.0003	24.05	0.2907	357.6953
24.83	0.2956	0.0003	24.80	0.2871	357.4211
25.58	0.2950	0.0003	25.55	0.2835	357.2344
26.34	0.2944	0.0003	26.31	0.2805	357.0427
27.09	0.2937	0.0003	27.06	0.2775	356.8430
27.84	0.2925	0.0003	27.81	0.2739	356.6641
28.59	0.2906	0.0003	28.56	0.2702	356.5200
29.35	0.2893	0.0003	29.31	0.2672	356.3555
30.10	0.2866	0.0003	30.06	0.2635	356.2351
30.85	0.2848	0.0003	30.82	0.2604	356.1187
31.60	0.2817	0.0003	31.57	0.2566	356.0557
32.36	0.2773	0.0003	32.32	0.2517	355.9844
33.11	0.2723	0.0003	33.07	0.2461	355.9714
33.86	0.2667	0.0003	33.82	0.2405	356.0254
34.61	0.2598	0.0003	34.57	0.2343	356.0327
35.37	0.2511	0.0003	35.33	0.2264	356.1748
36.12	0.2386	0.0003	36.08	0.2166	356.5293
36.87	0.2235	0.0003	36.83	0.2069	356.8799
37.62	0.2082	0.0003	37.58	0.1966	357.2224
38.38	0.1935	0.0002	38.33	0.1857	357.4932
39.13	0.1786	0.0003	39.08	0.1748	357.8169
39.88	0.1647	0.0002	39.83	0.1632	358.0505
40.63	0.1506	0.0002	40.59	0.1493	358.0149
41.39	0.1370	0.0001	41.34	0.1360	357.9795
42.14	0.1235	0.0000	42.09	0.1227	357.9441
42.89	0.1112	0.0000	42.84	0.1105	357.9089
43.64	0.0989	0.0000	43.59	0.0984	357.8731
44.40	0.0874	0.0000	44.34	0.0866	357.8391
45.15	0.0755	0.0000	45.10	0.0757	357.8040
45.90	0.0650	0.0000	45.85	0.0646	357.7695
46.65	0.0545	0.0000	46.60	0.0543	357.7344
47.41	0.0452	0.0000	47.35	0.0451	357.7007
48.16	0.0359	0.0000	48.10	0.0359	357.660[illegible]
48.91	0.0279	0.0000	[illegible]	0.0273	[illegible]
49.66	0.0196	360.0000	[illegible]	0.0196	[illegible]
50.42	0.0136	360.0000	50.36	0.0136	[illegible]
51.17	0.0074	360.0000	51.11	0.0074	[illegible]
51.92	0.0037	360.0000	51.86	0.0037	357.4495

Table 7.1-8

f/30 MTF AT GRID POINT A

OTA + F/30 RELAY
THETA= 0.0 DEG. PHI= 0.014 DEG. 1.0 Field

GIVEN OR CALCULATED FOCAL PLANE AT 0.24509520D 03 CM.
FOCAL SHIFT= 0.0 CM. RESULTANT FOCAL POSITION= 0.24509520E 02

FREQ	MTF(X)	PHASE(X)	FREQ	MTF(Y)	PHASE(Y)
0.0	1.0000	0.0	0.0	1.0000	0.0
0.7526	0.9676	0.0002	0.7517	0.9693	0.0032
1.505	0.9351	0.0003	1.503	0.9381	0.0182
2.258	0.9024	0.0003	2.255	0.9063	0.0468
3.010	0.8695	0.0004	3.007	0.8742	0.0903
3.763	0.8365	0.0004	3.759	0.8418	0.1506
4.516	0.8035	0.0004	4.510	0.8093	0.2295
5.268	0.7707	0.0004	5.262	0.7766	0.3293
6.021	0.7378	0.0004	6.014	0.7439	0.4522
6.773	0.7050	0.0004	6.766	0.7114	0.6012
7.526	0.6723	0.0004	7.517	0.6790	0.7791
8.279	0.6399	0.0004	8.269	0.6475	0.9013
9.031	0.6076	0.0004	9.021	0.6163	1.2173
9.784	0.5764	0.0004	9.773	0.5862	1.4860
10.54	0.5453	0.0004	10.52	0.5565	1.7994
11.29	0.5151	0.0004	11.26	0.5274	2.1560
12.04	0.4850	0.0004	12.03	0.5017	2.2853
12.79	0.4558	0.0004	12.78	0.4775	2.3064
13.55	0.4266	0.0004	13.53	0.4547	2.2329
14.30	0.3987	0.0004	14.28	0.4333	1.9983
15.05	0.3709	0.0004	15.03	0.4127	1.6307
15.80	0.3464	0.0004	15.79	0.3932	1.1644
16.56	0.3262	0.0004	16.54	0.3751	0.5068
17.31	0.3109	0.0004	17.29	0.3574	359.7239
18.06	0.2991	0.0004	18.04	0.3421	359.0044
18.81	0.2924	0.0003	18.79	0.3289	358.4895
19.57	0.2864	0.0004	19.55	0.3170	357.9651
20.32	0.2847	0.0003	20.30	0.3063	357.4614
21.07	0.2842	0.0004	21.05	0.2973	357.0576
21.83	0.2837	0.0003	21.80	0.2883	356.6150
22.58	0.2831	0.0004	22.55	0.2800	356.1086
23.33	0.2839	0.0003	23.30	0.2735	355.6394
24.08	0.2845	0.0004	24.06	0.2676	355.1626
24.84	0.2851	0.0003	24.81	0.2640	354.6338
25.59	0.2856	0.0004	25.56	0.2602	354.0527
26.34	0.2862	0.0003	26.31	0.2570	353.4473
27.09	0.2867	0.0004	27.06	0.2542	352.9202
27.85	0.2866	0.0003	27.81	0.2509	352.4651
28.60	0.2858	0.0004	28.57	0.2475	351.9919
29.35	0.2850	0.0003	29.32	0.2446	351.5132
30.10	0.2836	0.0004	30.07	0.2412	351.1118
30.86	0.2821	0.0003	30.82	0.2382	350.7141
31.61	0.2794	0.0003	31.57	0.2346	350.4067
32.36	0.2760	0.0003	32.33	0.2303	350.1958
33.11	0.2713	0.0004	33.06	0.2254	350.0694
33.87	0.2661	0.0003	33.83	0.2204	350.1145
34.62	0.2602	0.0004	34.58	0.2148	350.0417
35.37	0.2519	0.0003	35.33	0.2081	350.3423
36.12	0.2385	0.0004	36.08	0.1994	350.9263
36.88	0.2234	0.0003	36.84	0.1907	351.5059
37.63	0.2083	0.0003	37.59	0.1819	352.1833
38.38	0.1938	0.0003	38.34	0.1731	352.8555
39.14	0.1793	0.0003	39.09	0.1637	353.5085
39.89	0.1653	0.0003	39.84	0.1543	354.1536
40.64	0.1513	0.0003	40.59	0.1443	354.7852
41.39	0.1378	0.0002	41.35	0.1342	355.3945
42.15	0.1244	0.0002	42.10	0.1214	355.3132
42.90	0.1121	0.0002	42.85	0.1097	355.2327
43.65	0.0998	0.0002	43.60	0.0979	355.1521
44.40	0.0881	360.0000	44.35	0.0866	355.0720
45.16	0.0763	360.0000	45.10	0.0752	354.9917
45.91	0.0658	360.0000	45.86	0.0650	354.9121
46.66	0.0552	360.0000	46.61	0.0548	354.83[illegible]
47.41	0.0458	360.0000	47.36	0.0455	354.75[illegible]
48.17	0.0364	360.0000	48.11	0.0362	354.674[illegible]
48.92	0.0282	360.0000	48.86	0.0282	354.5947
49.67	0.0201	359.9998	49.62	0.0201	354.5171
50.42	0.0129	359.9995	50.37	0.0131	354.4[illegible]
51.18	0.0076	359.9996	51.12	0.0076	354.3615
51.93	0.0033	359.9996	51.87	0.0036	354.2116

7.2 FIELD CURVATURE

At each grid point in the image field, peak MTF was found by shifting focus. Plotting the focus shift corresponding to peak MTF against field height gave graphs of field curvature.

Field curvature for the *f*/12.88 relay is shown in figure 7.2-1. The values of peak MTF are given along the curved image surface. MTF values along the best-compromise focal plane are also given. The tilted configuration of the OTA + relay caused the image field to be tilted in the meridional plane.

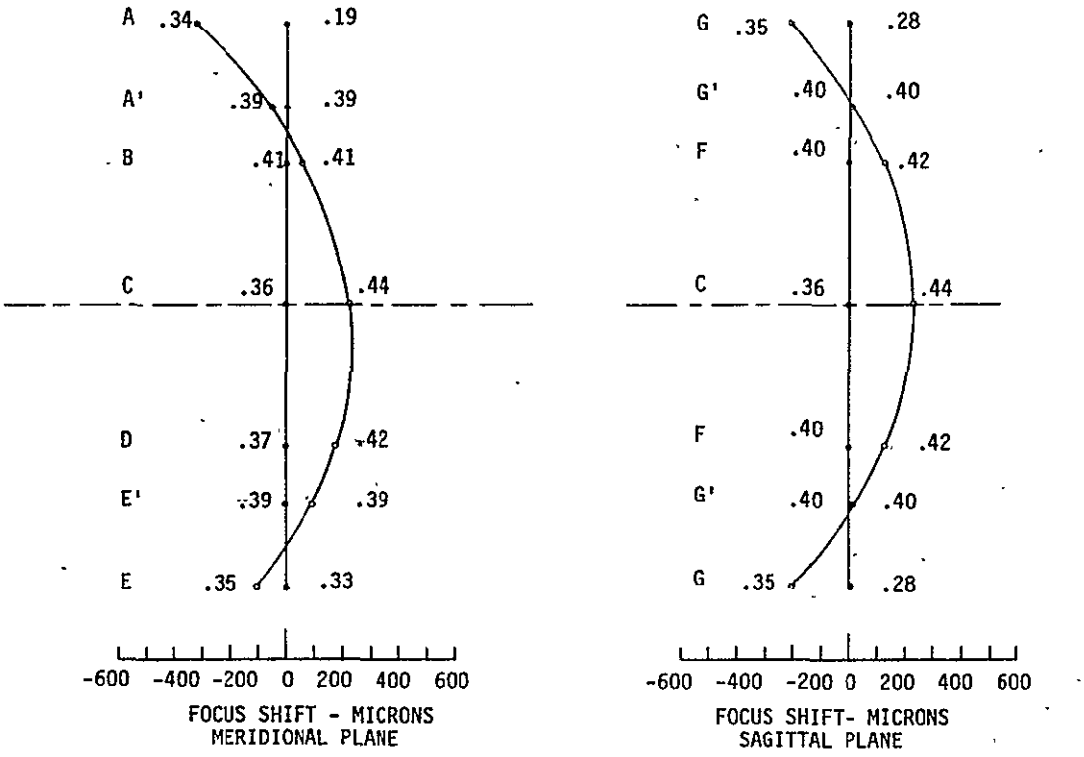

FIELD CURVATURE AND MTF AT POINTS ON THE CURVED IMAGE SURFACE AND ON THE REFERENCE FOCAL PLANE OF *f*/12.88 RELAY

Figure 7.2-1

Figure 7.2-2 shows field curvature for the $f/30$ relay. The magnitude of field curvature for the $f/30$ is about the same as that for the $f/12.88$ relay. However, the MTF loss for the $f/30$ relay is much less because its higher f-number increases the depth of focus.

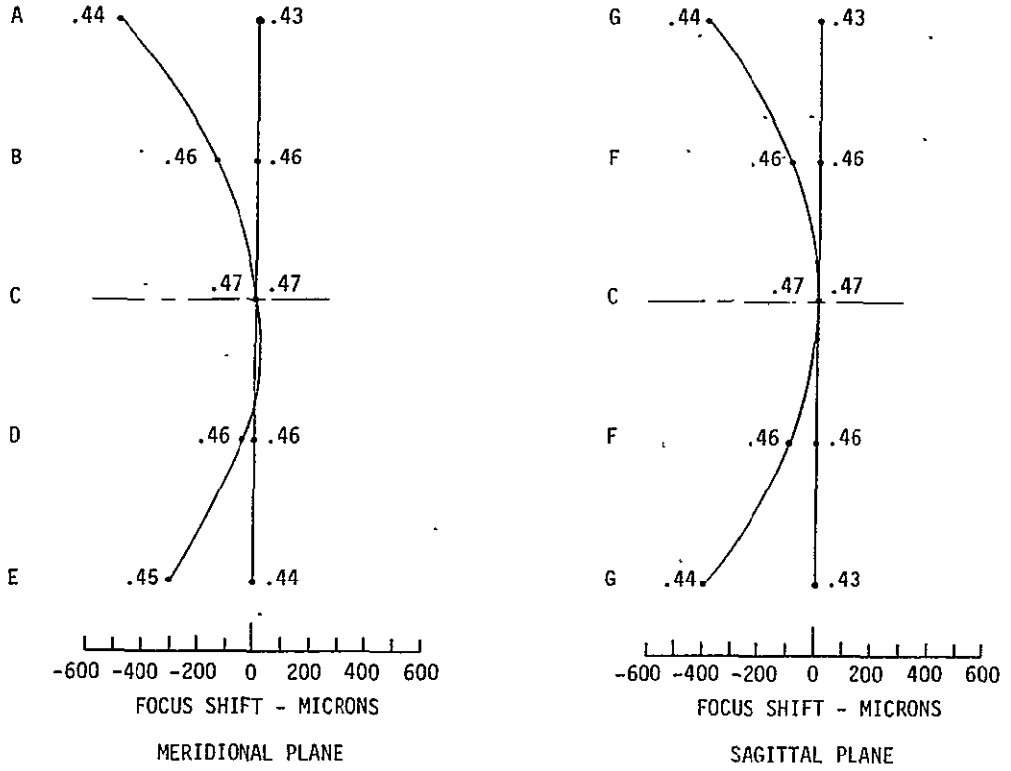

FIELD CURVATURE AND MTF AT POINTS ON THE CURVED IMAGE SURFACE AND ON THE REFERENCE FOCAL PLANE OF $f/30$ RELAY

Figure 7.2-2

7.3 GEOMETRIC SPOT DIAGRAMS

Computer program BFLT5 was used to generate the spot diagrams. A 20 x 20 array of rays entered the lens. The intercepts of these rays at the focal surface (CCD detector) were plotted as individual spots. The entire pattern of spots is the spot diagram. These spot diagrams show the effect of geometric aberrations on image quality, but ignore diffraction effects.

Figures 7.3-1 through 7.3-5 show spot diagrams for the $f/12.88$ relay. For comparison, the core (airy disk) of an aberration-free $f/12.88$ diffraction spread function is also given.

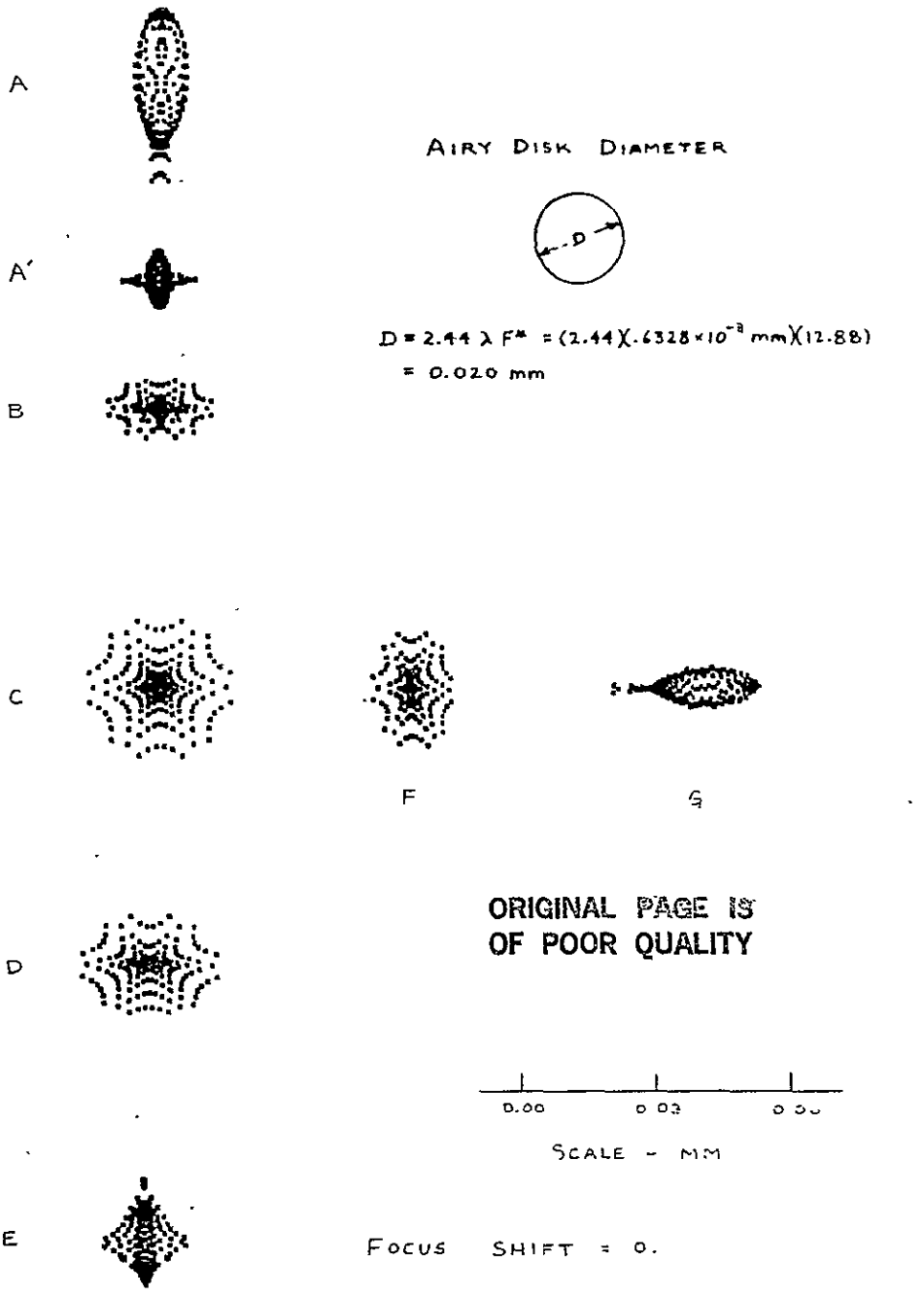

f/12.88 SPOT DIAGRAMS

Figure 7.3-1

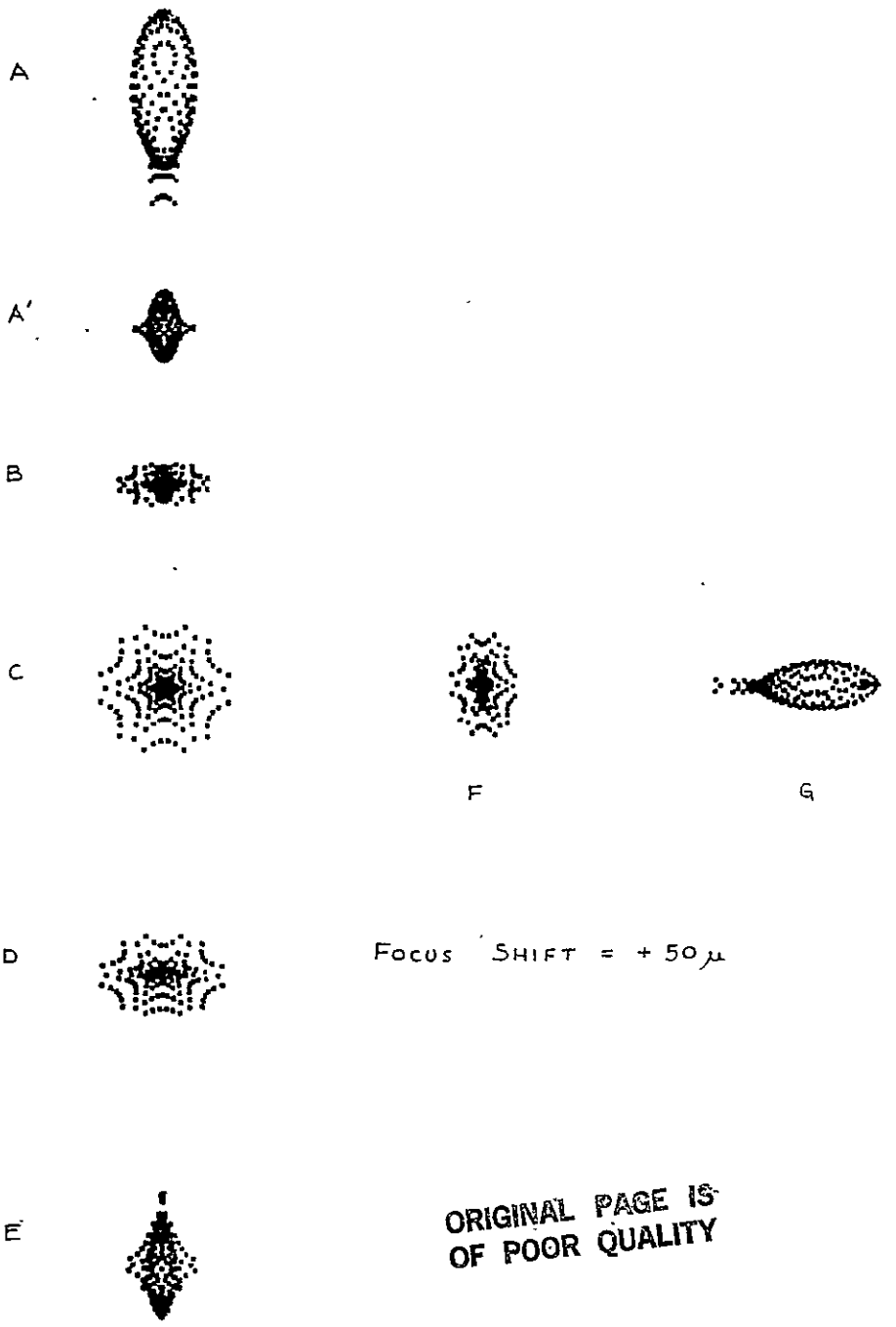

f/12.88 SPOT DIAGRAMS

Figure 7.3-2

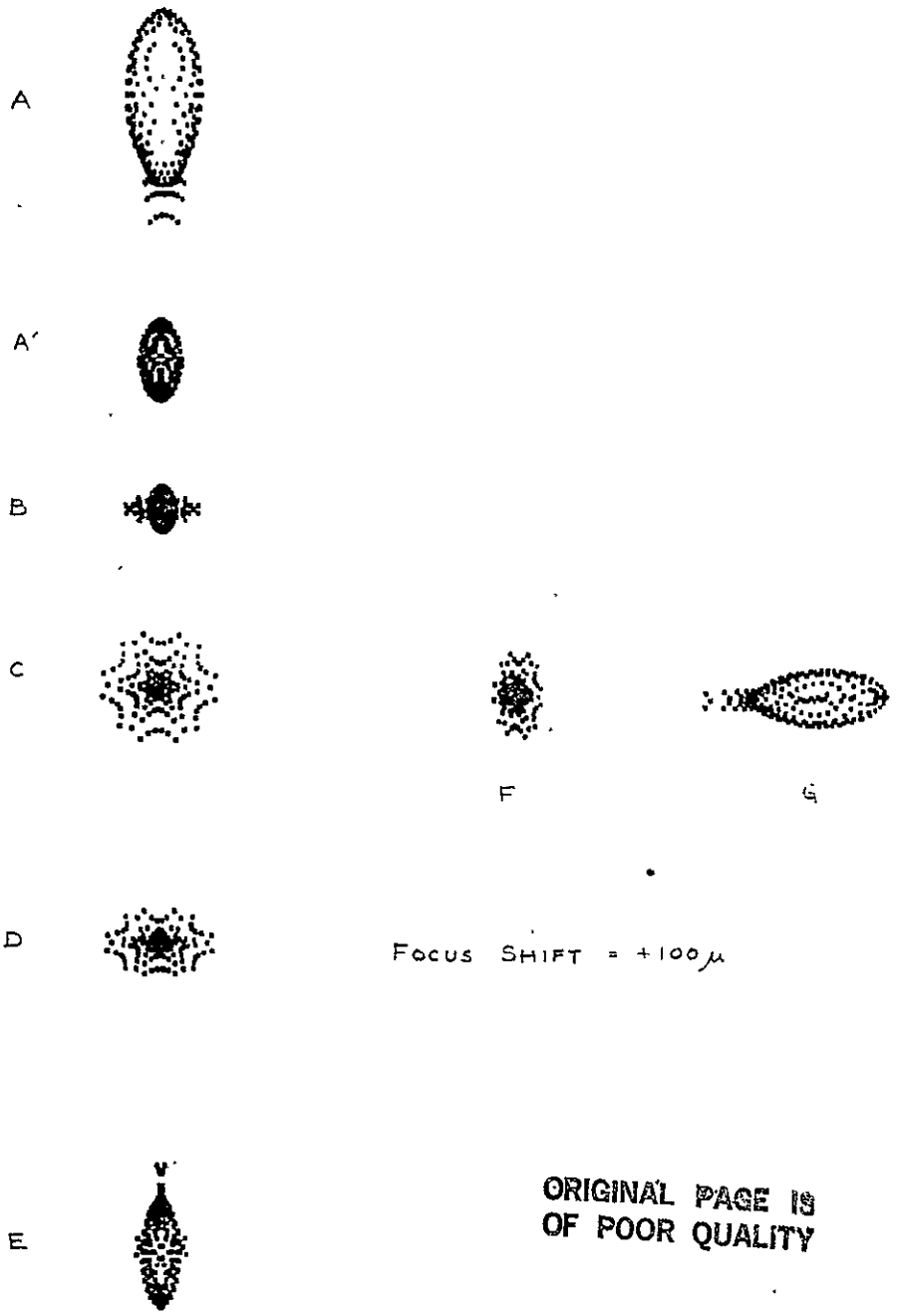

f/12.88 SPOT DIAGRAMS

Figure 7.3-3

C-2

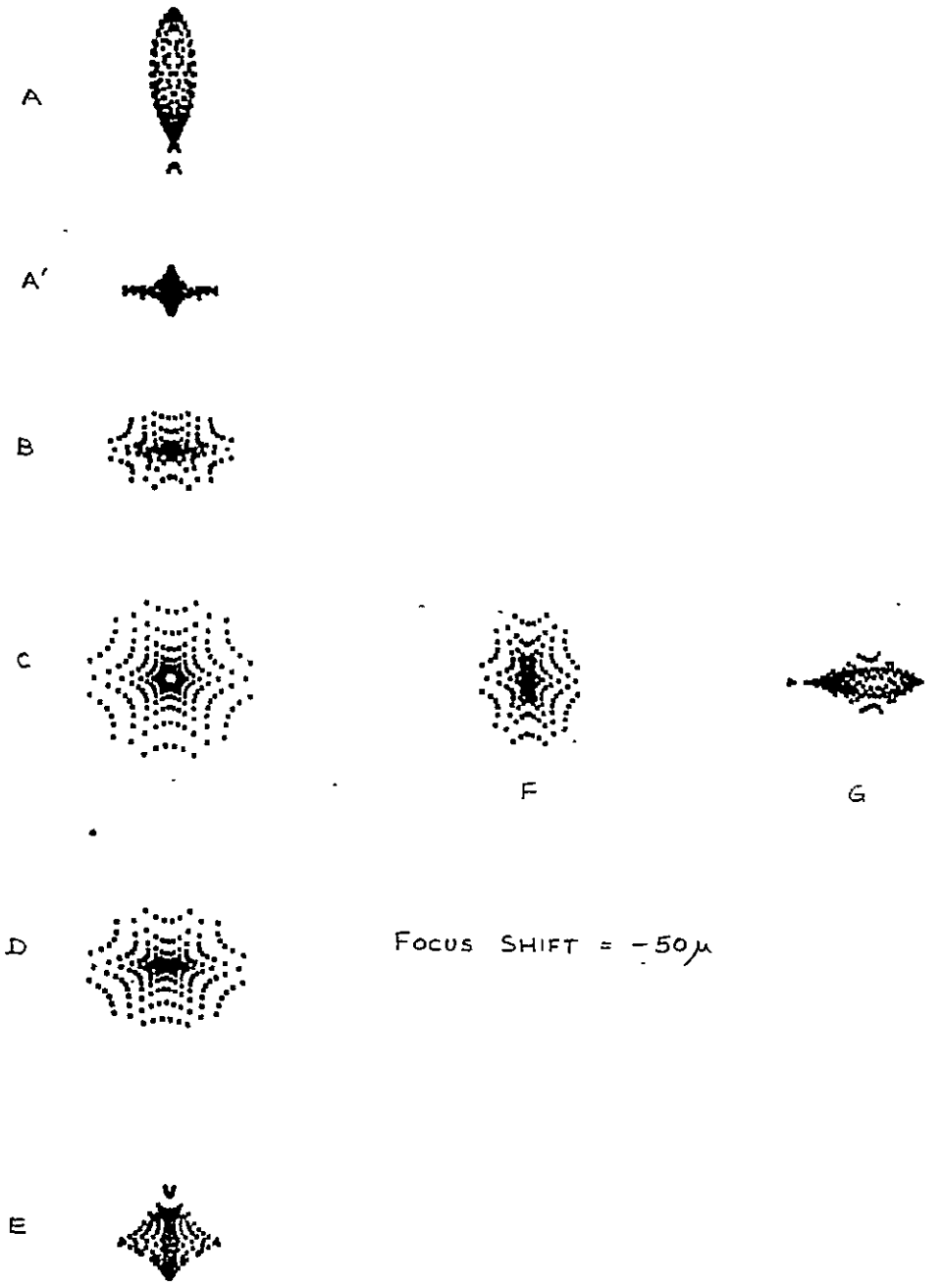

f/12.88 SPOT DIAGRAMS

Figure 7.3-4

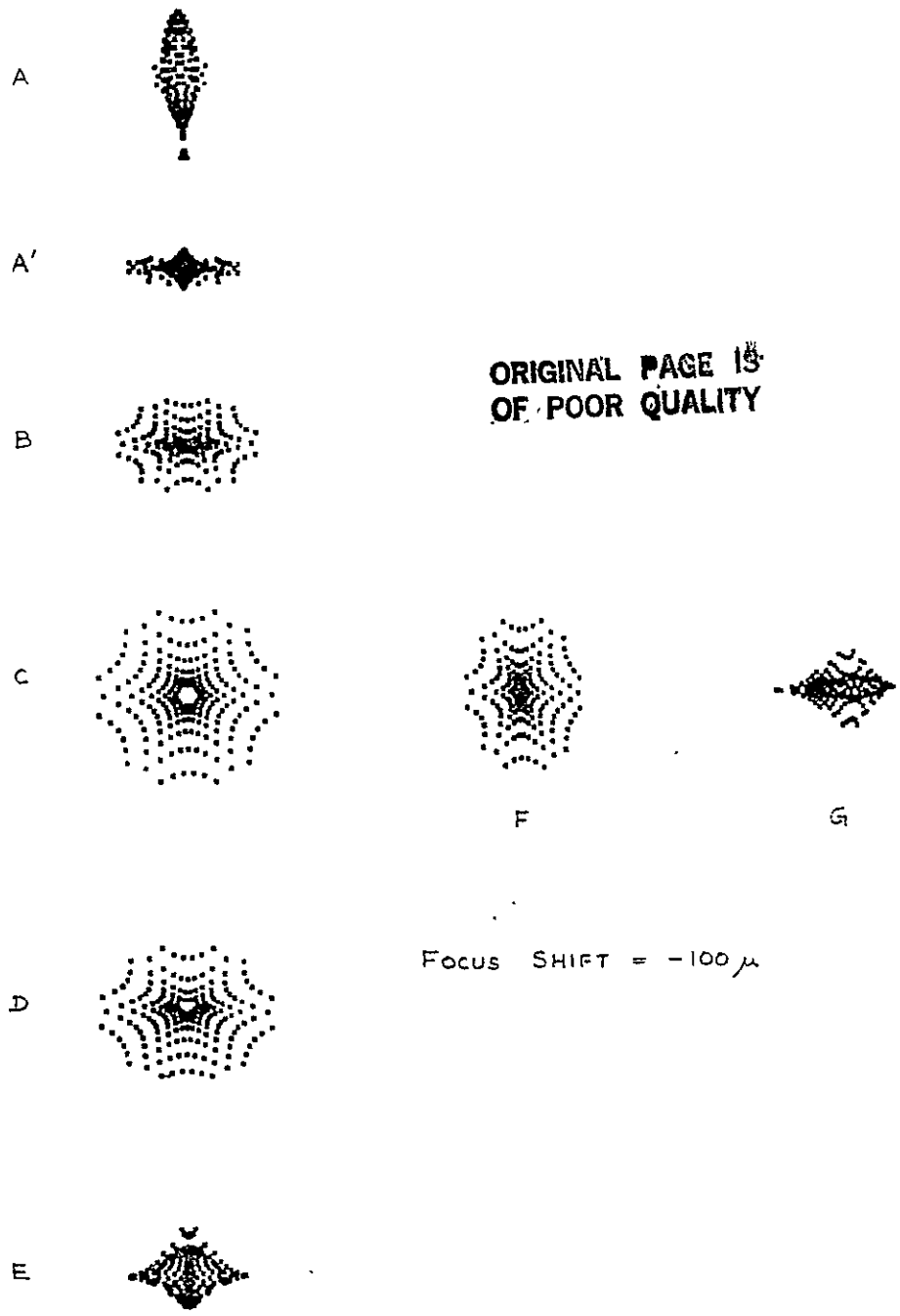

f/12.88 SPOT DIAGRAMS

Figure 7.3-5

Spot diagrams for the *f*/30 relay are shown in figures 7.3-6 through 7.3-10. For this high *f*-number system, the airy disk is much larger than the geometric spot diagrams. This relay, therefore, has near diffraction limited performance.

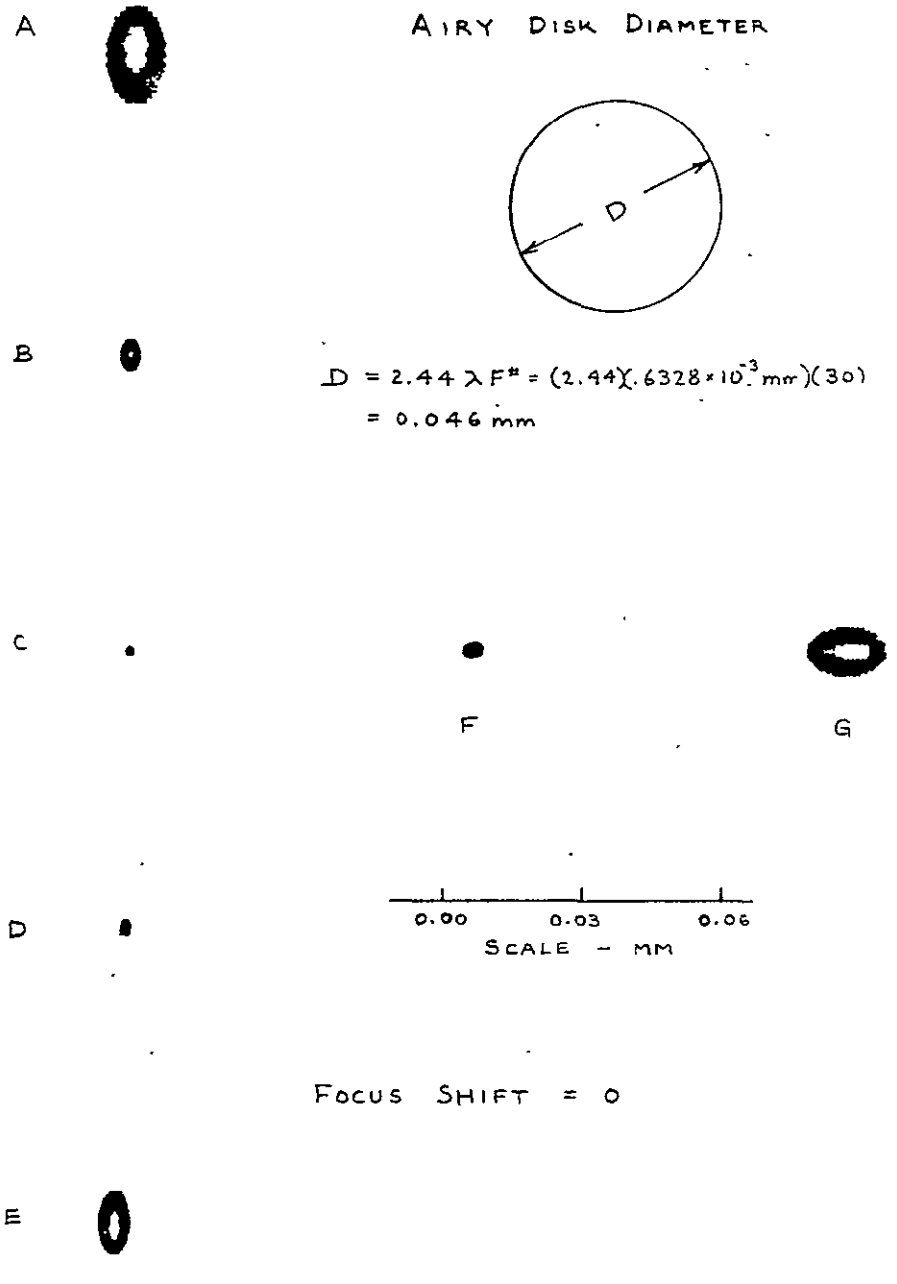

f/30 SPOT DIAGRAMS

Figure 7.3-6

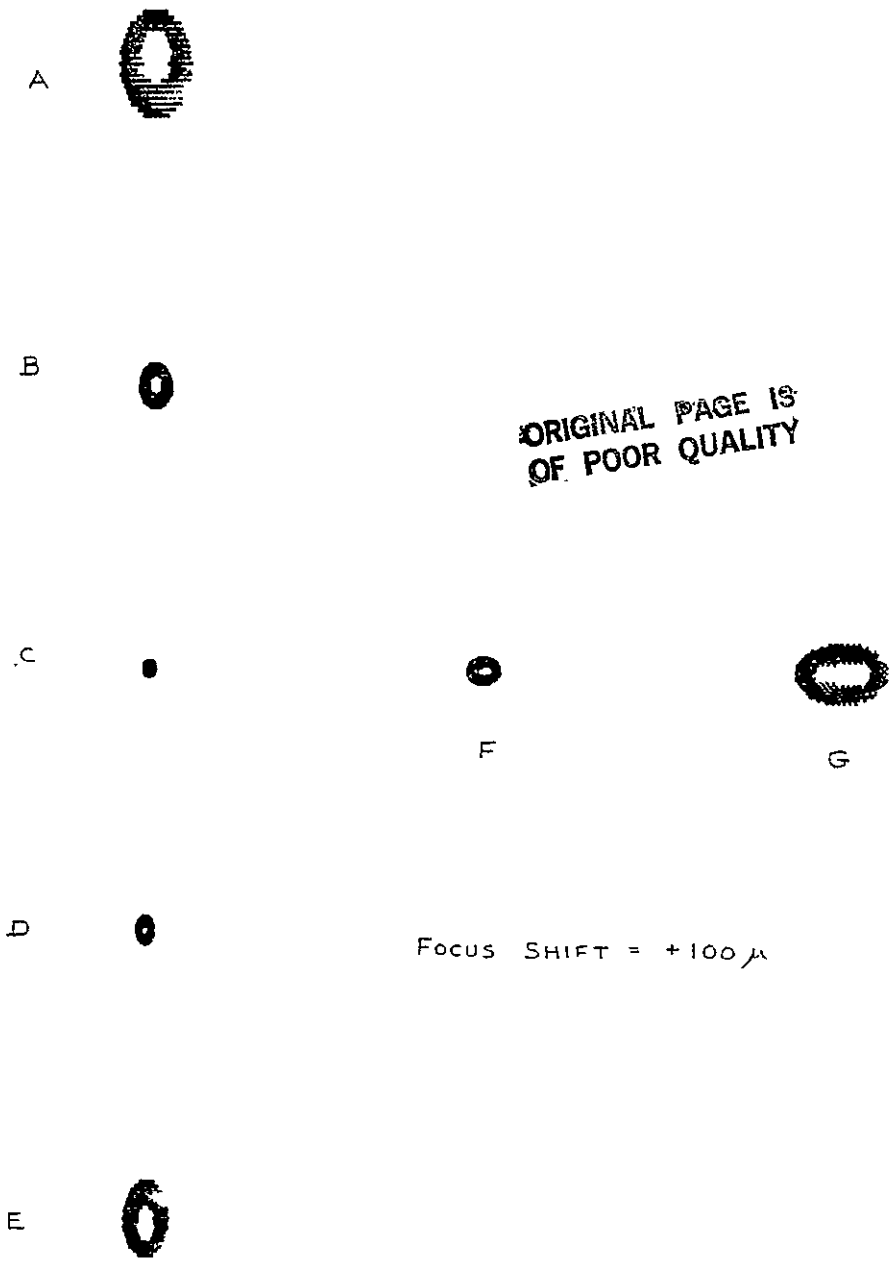

f/30 SPOT DIAGRAMS

Figure 7.3-7

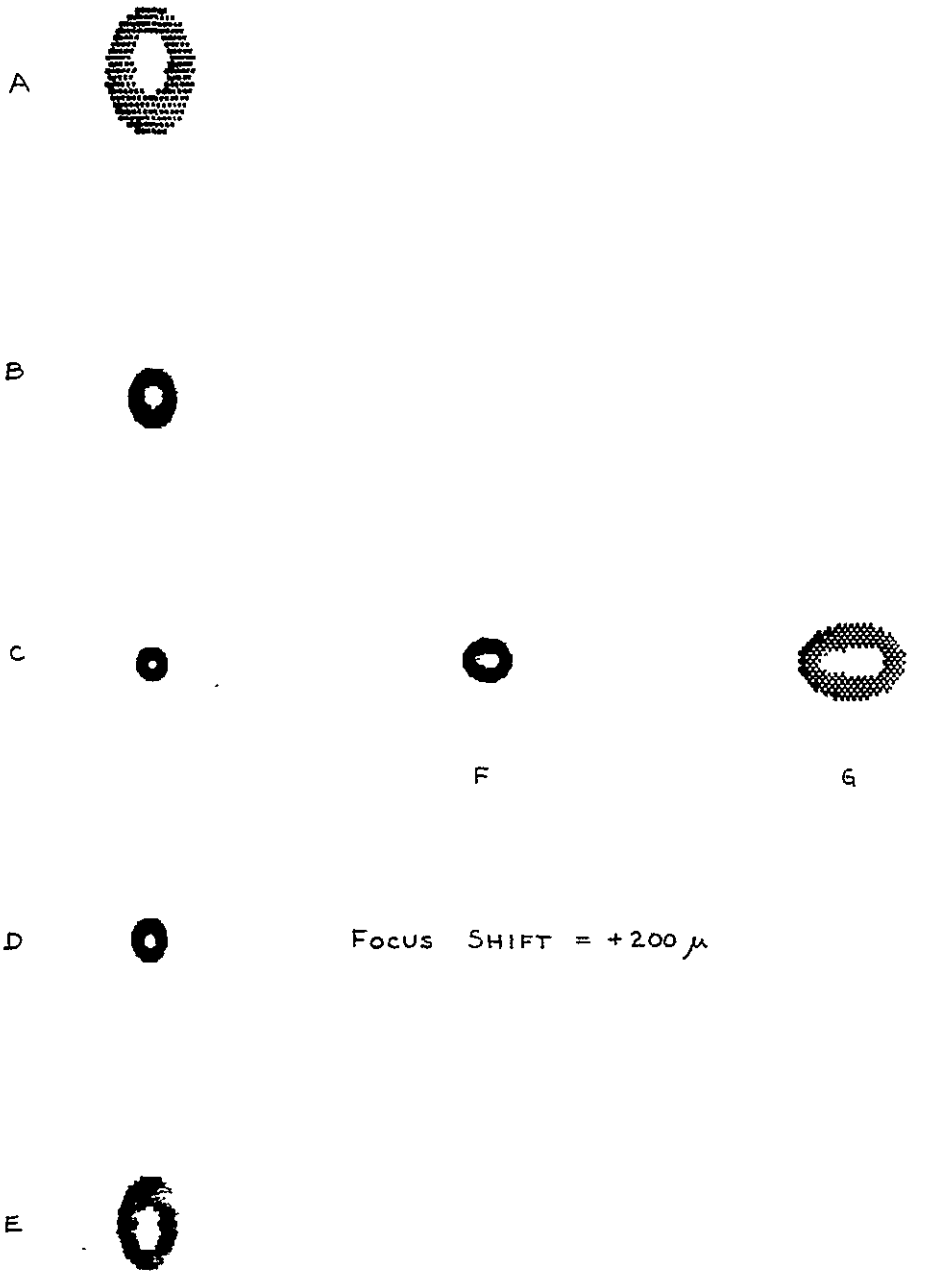

f/30 SPOT DIAGRAMS

Figure 7.3-8

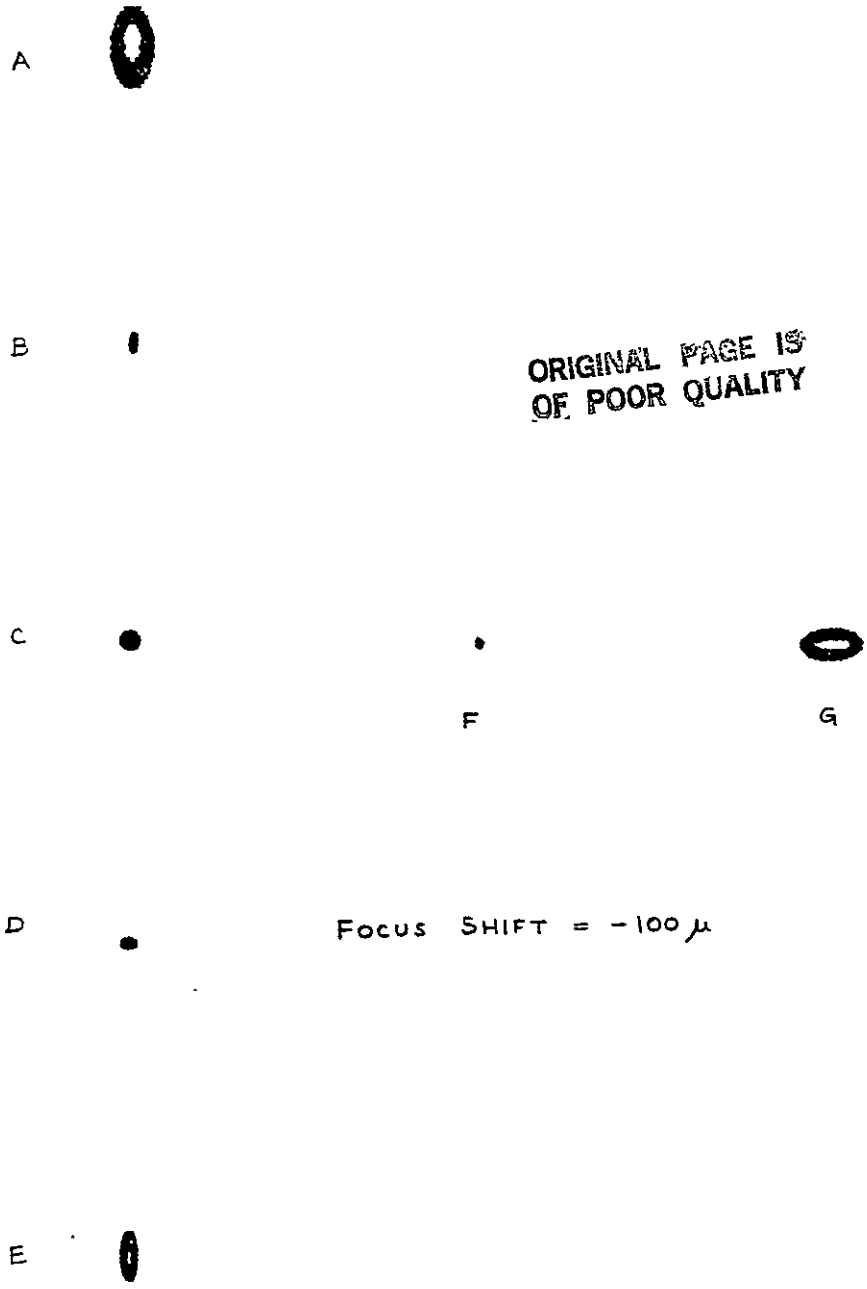

f/30 SPOT DIAGRAMS

Figure 7.3-9

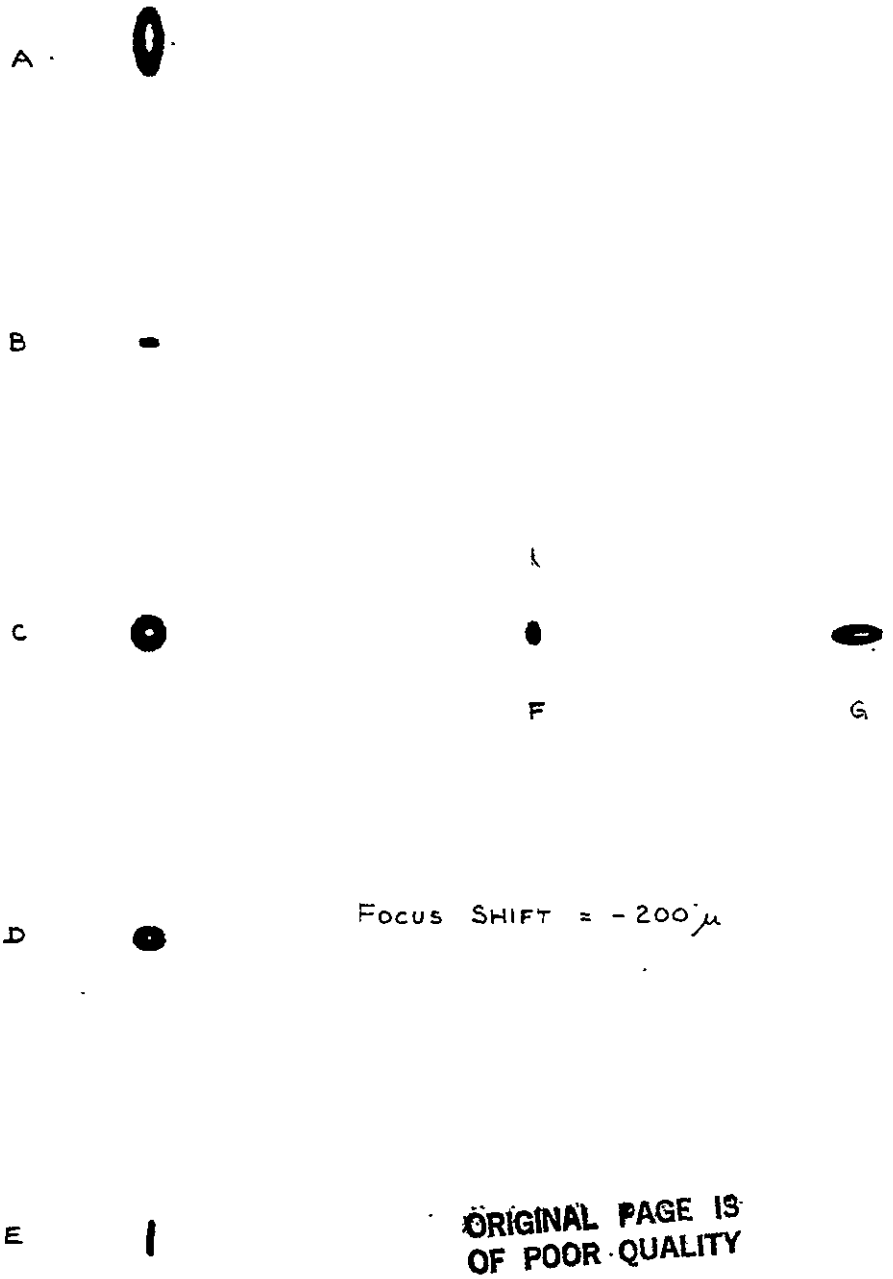

f/30 SPOT DIAGRAMS

Figure 7.3-10

7.4 POINT SPREAD FUNCTIONS

Diffraction-based point spread functions (PSF) were generated by the combination of computer programs BFLT5 and BFLTA. Program BFLT5 ray traced the OTA + relay optical system and produced two data arrays. The "existence array" defines the shape of the diffracting aperture (exit pupil) by assigning the value 1 to each ray that passes through the exit pupil and assigning the value of zero to each blocked ray. The "OPD array" defines the contour of the wavefront in the exit pupil in terms of optical pathlength difference (OPD) along each ray. These two arrays, for each combination of field angle and focus shift, were then recorded on magnetic tape.

After reading the magnetic tape, program BFLTA generated the complex pupil function by combining the existence array and the OPD array. The pupil function, contained in a 32 x 32 array, was then inserted into a larger 256 x 256 "transform array". After performing a Fast Fourier Transform (FFT) of this array and multiplying the result by its complex conjugate, the two-dimensional point spread function was produced.

Point spread functions for the *f*/12.88 relay are shown in figures 7.4-1 through 7.4-10. For grid points A, E, and G, the spread functions are plotted in both the radial and tangential directions because these spread functions are not rotationally symmetric. Each spread function plot also shows the effect of focus shift.

Relative intensity of the spread function peak, if it were aberration free, is also indicated on each plot. The ratio of peak relative intensity of the aberrated spread function to the aberration-free peak is called the Strehl Ratio. This ratio is often used as a figure of merit for optical systems. The Strehl criterion states that an image is near diffraction limited if its Strehl ratio exceeds 0.8.

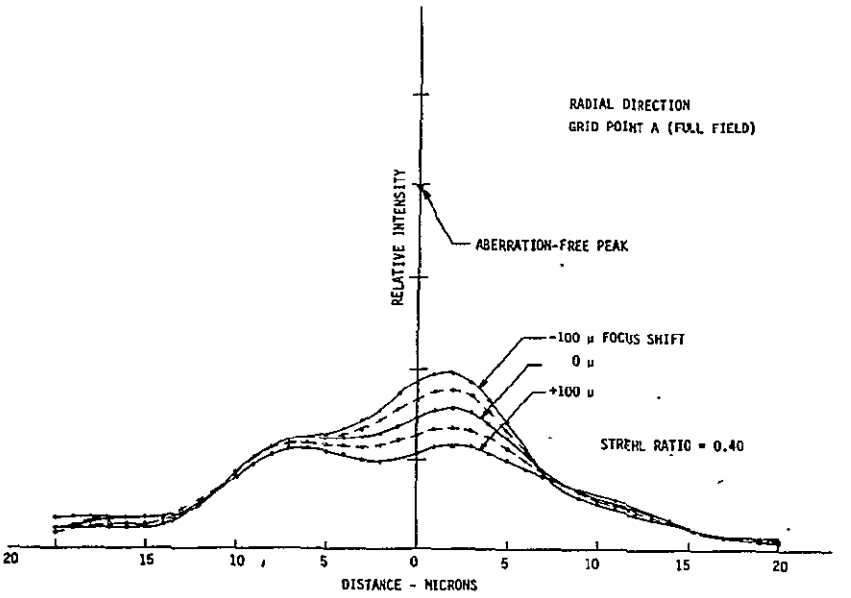

f/12.88 RELAY POINT SPREAD FUNCTION

Figure 7.4-1

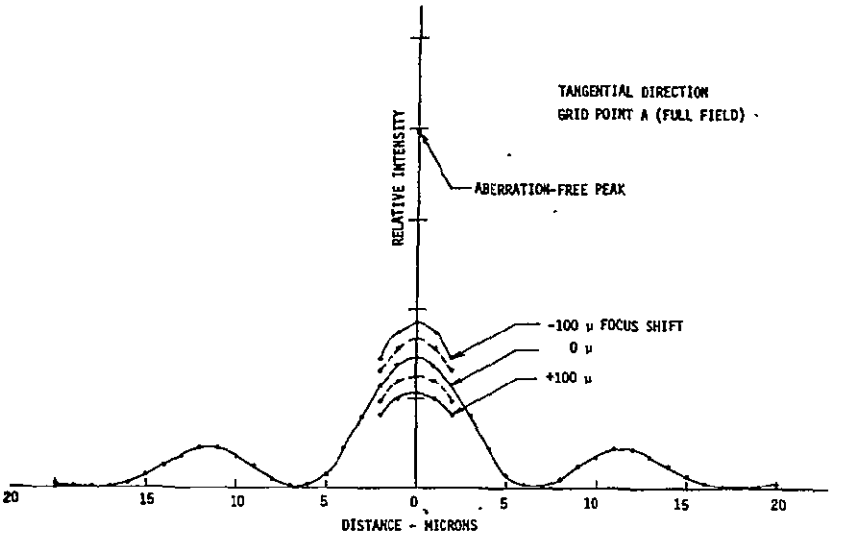

f/12.88 RELAY POINT SPREAD FUNCTION

Figure 7.4-2

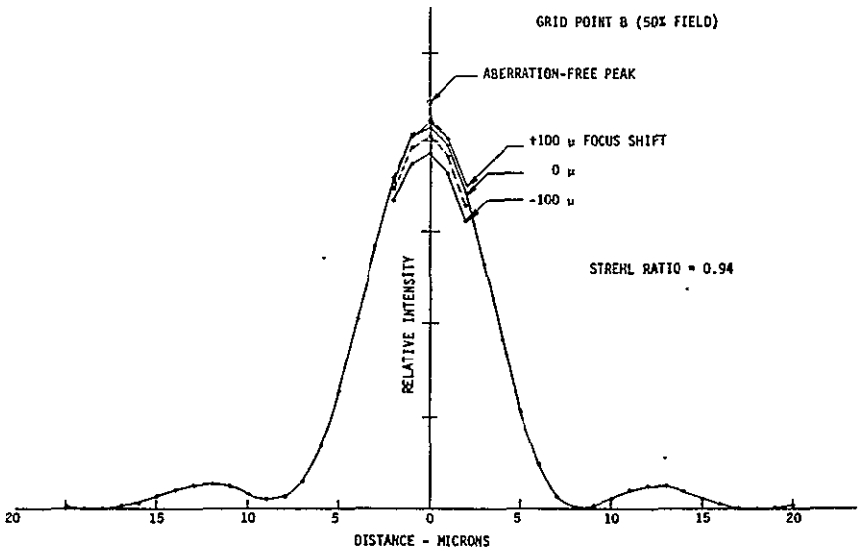

f/12.88 RELAY POINT SPREAD FUNCTION

Figure 7.4-3

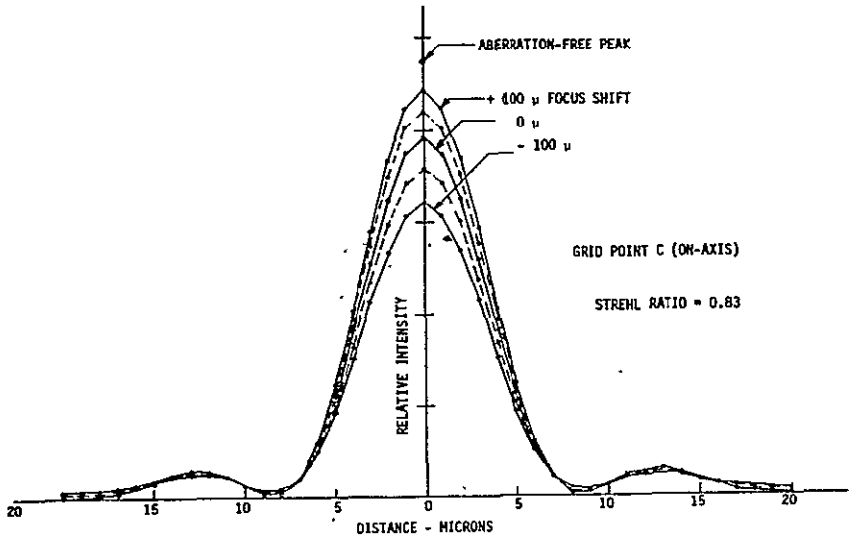

f/12.88 RELAY POINT SPREAD FUNCTION

Figure 7.4-4

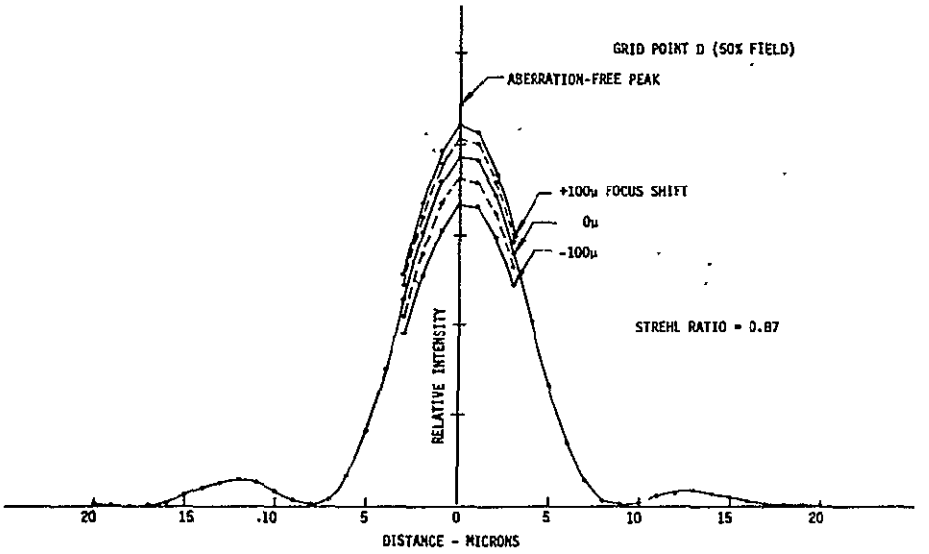

f/12.88 RELAY - POINT SPREAD FUNCTION

Figure 7.4-5

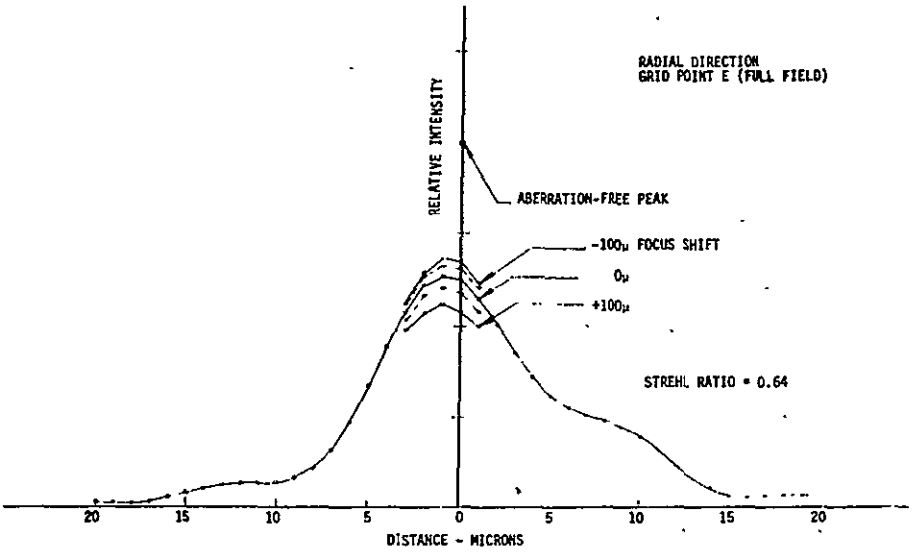

f/12.88 RELAY - POINT SPREAD FUNCTION

Figure 7.4-6

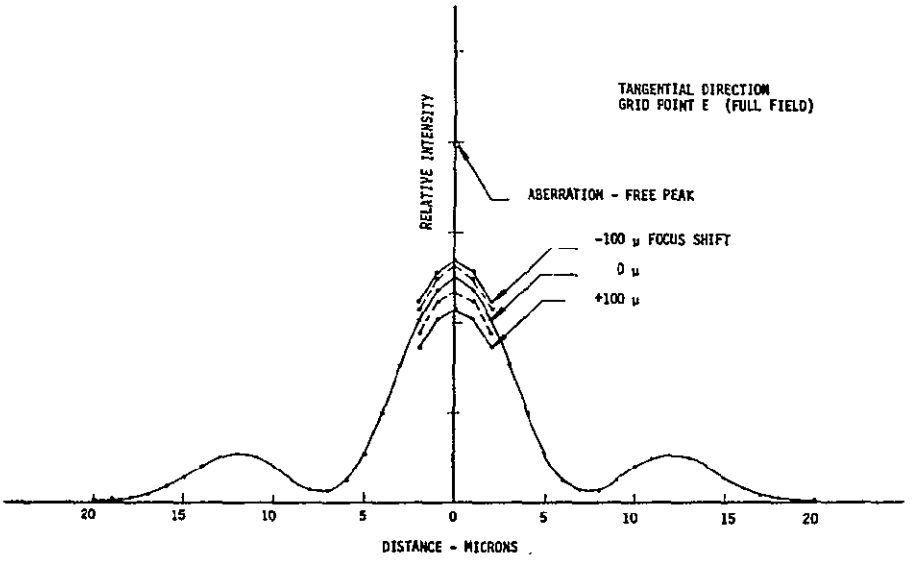

f/12.88 RELAY - POINT SPREAD FUNCTION

Figure 7.4-7

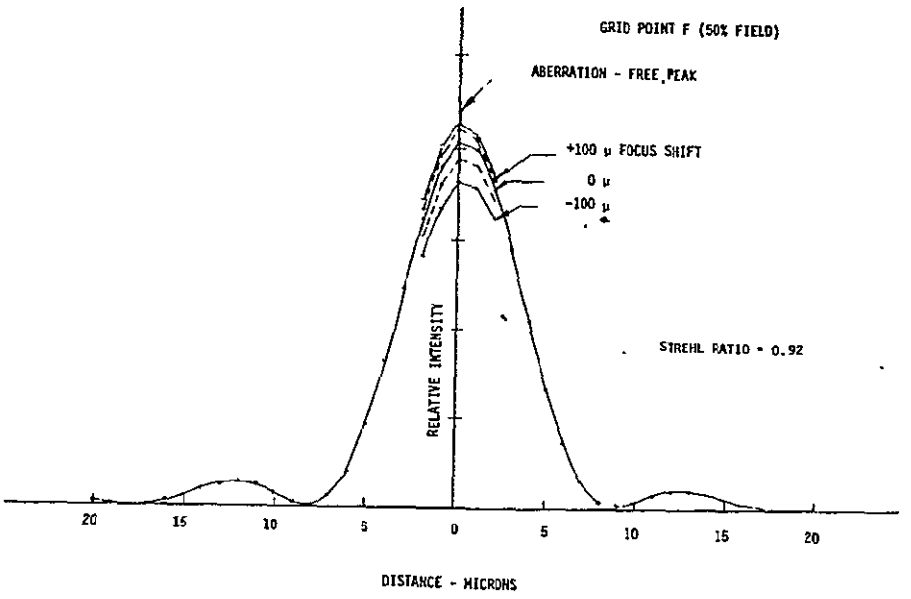

f/12.88 RELAY - POINT SPREAD FUNCTION

Figure 7.4-8

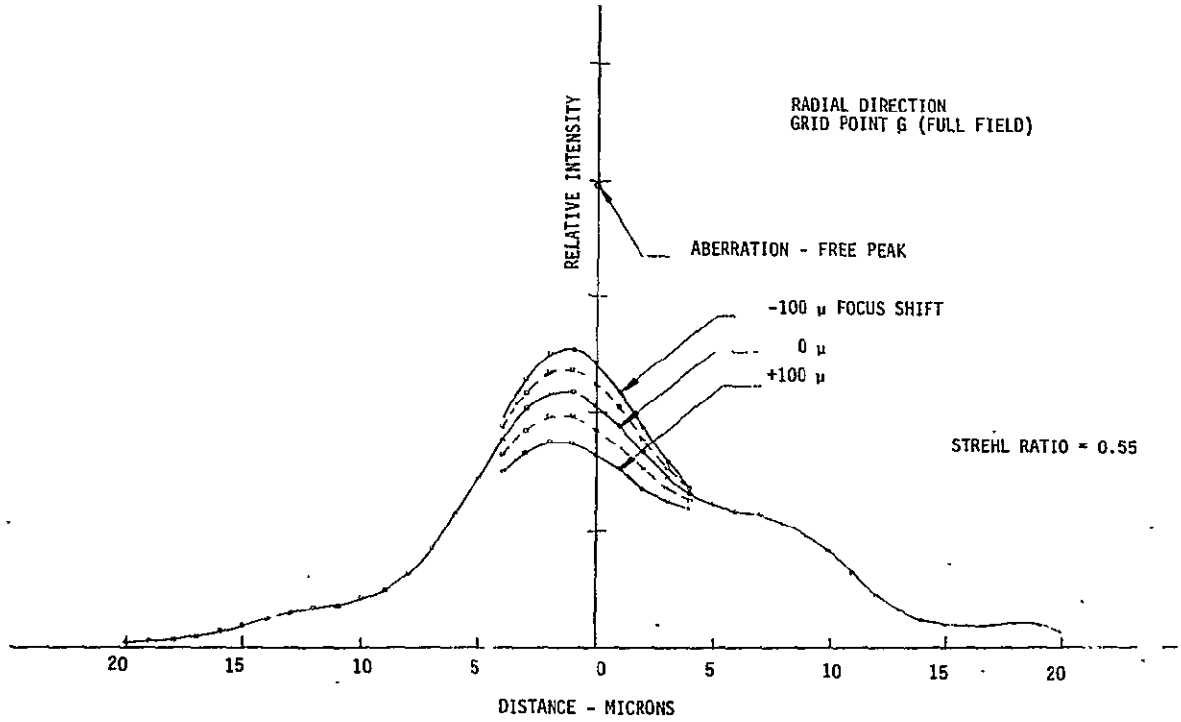

f/12.88 RELAY - POINT SPREAD FUNCTION

Figure 7.4-9

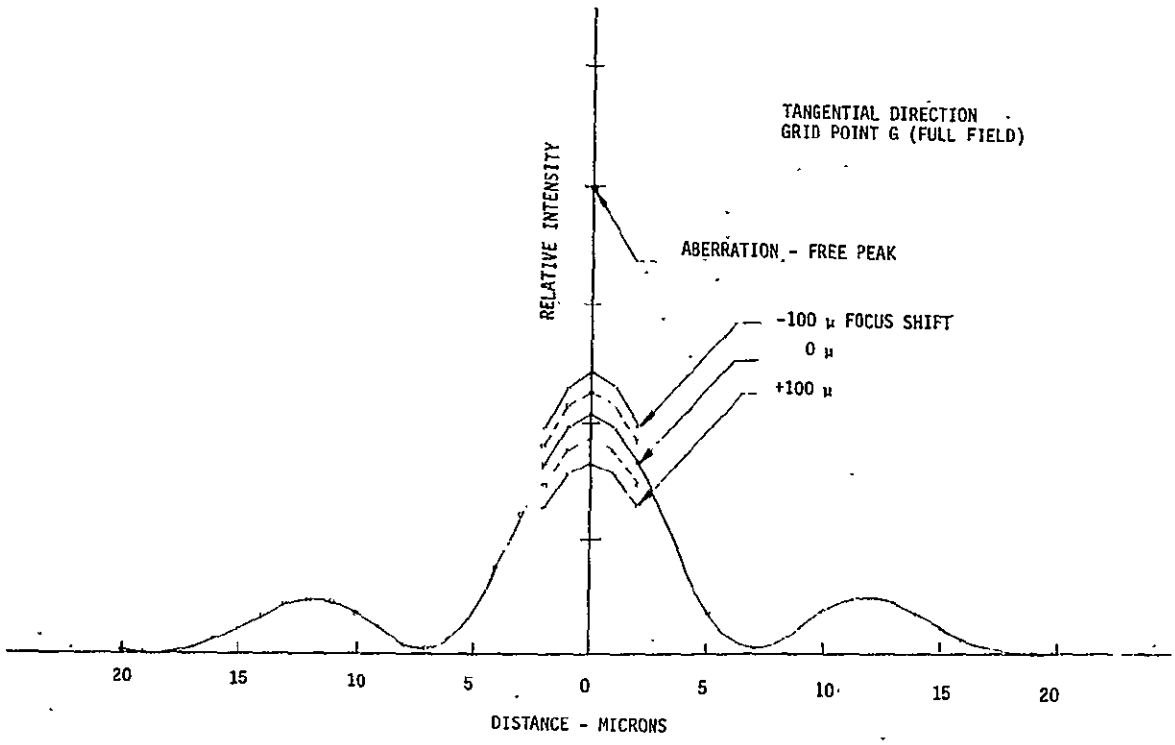

f/12.88 RELAY - POINT SPREAD FUNCTION

Figure 7.4-10

Strehl ratio values (for zero focus shift) are shown on the PSF plots for each performance grid point. These values show that, except for the corners, diffraction limited performance is achieved over the *f*/12.88 relay field. The *f*/30 relay is diffraction limited over its entire field.

The PSF's for the *f*/12.88 relay are given in figures 7.4-1 through 7.4-10 and those for the *f*/30 relay are given in figures 7.4-11 through 7.4-17.

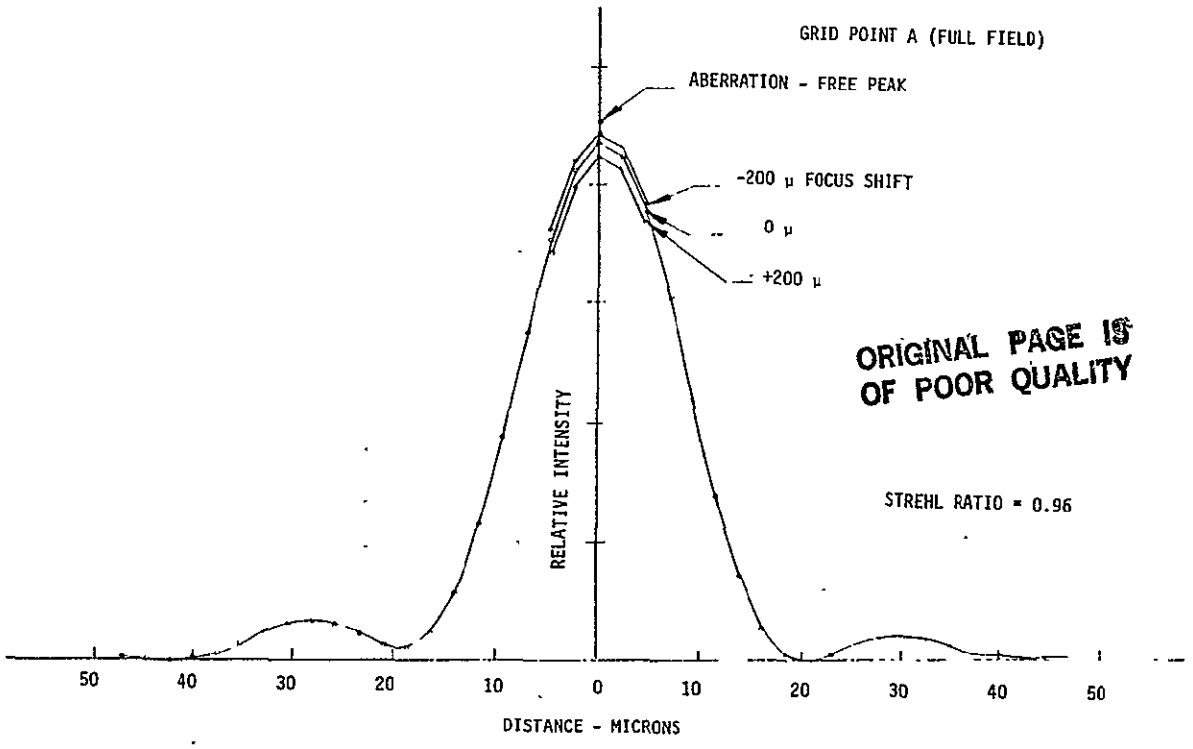

f/30 RELAY - POINT SPREAD FUNCTION

Figure 7.4-11

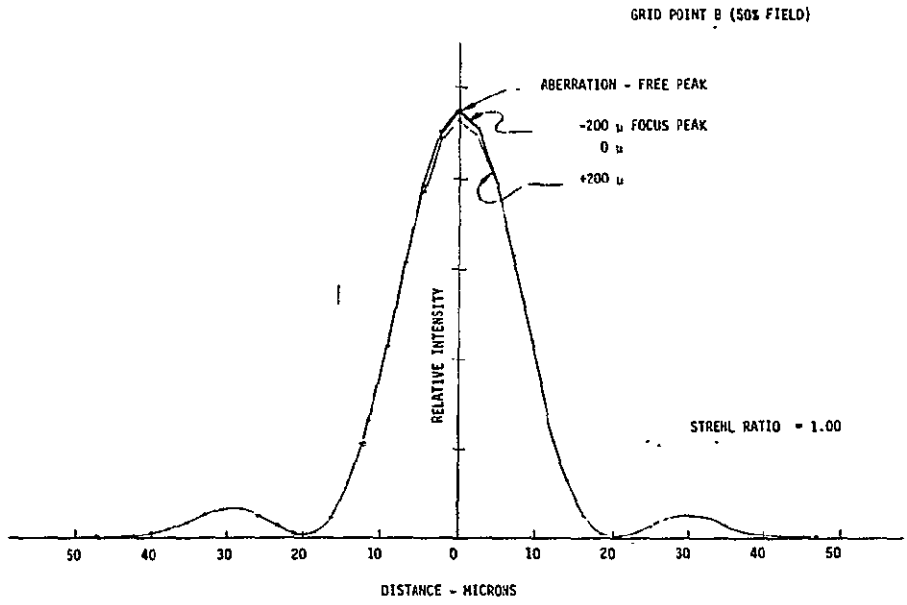

f/30 RELAY - POINT SPREAD FUNCTION

Figure 7.4-12

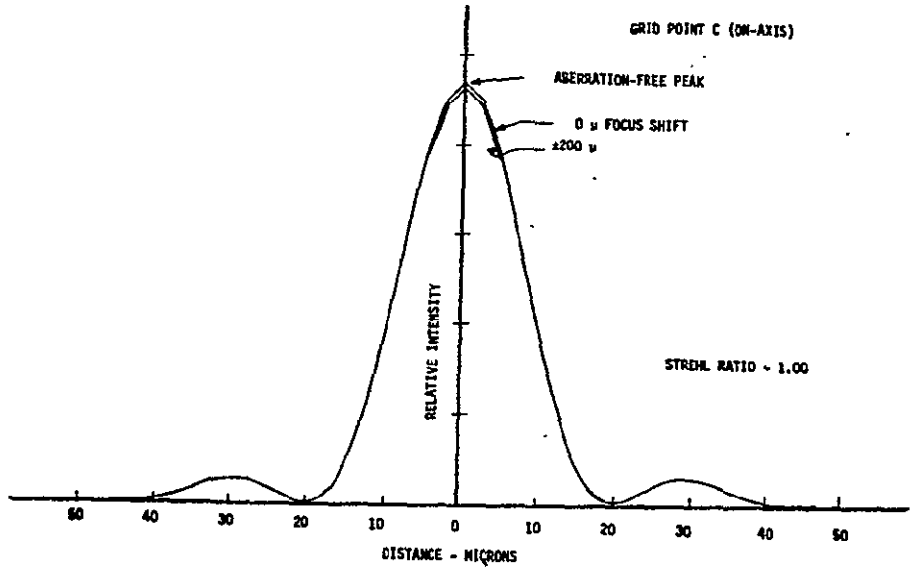

f/30 RELAY - POINT SPREAD FUNCTION

Figure 7.4-13

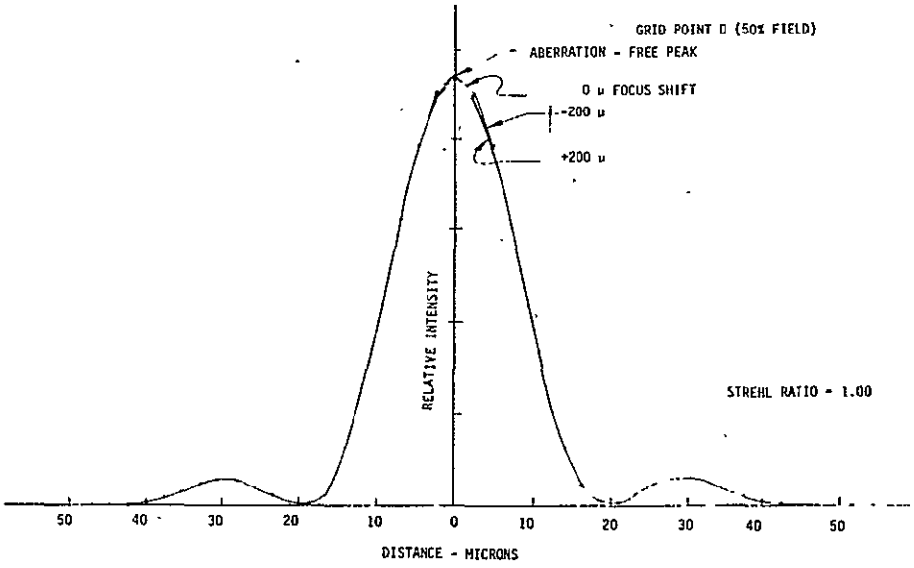

f/30 RELAY - POINT SPREAD FUNCTION

Figure 7.4-14

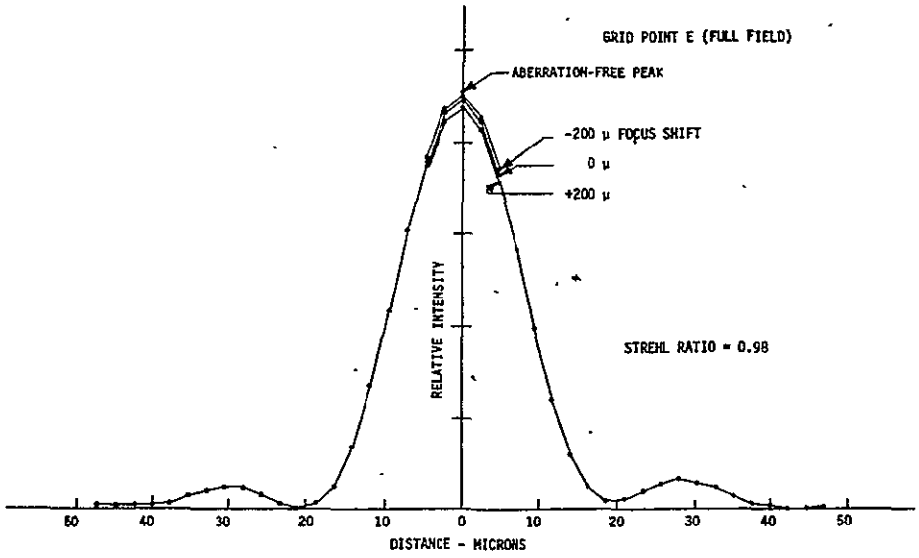

f/30 RELAY - POINT SPREAD FUNCTION

Figure 7.4-15

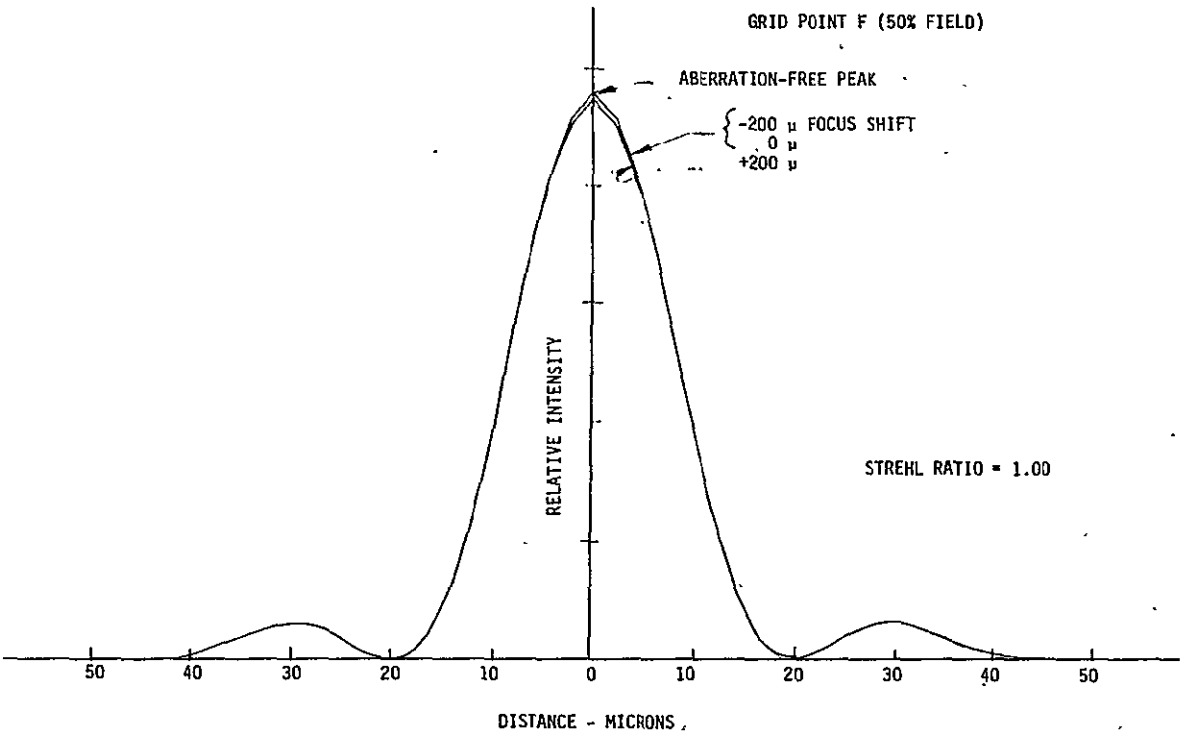

f/30 RELAY - POINT SPREAD FUNCTION

Figure 7.4-16

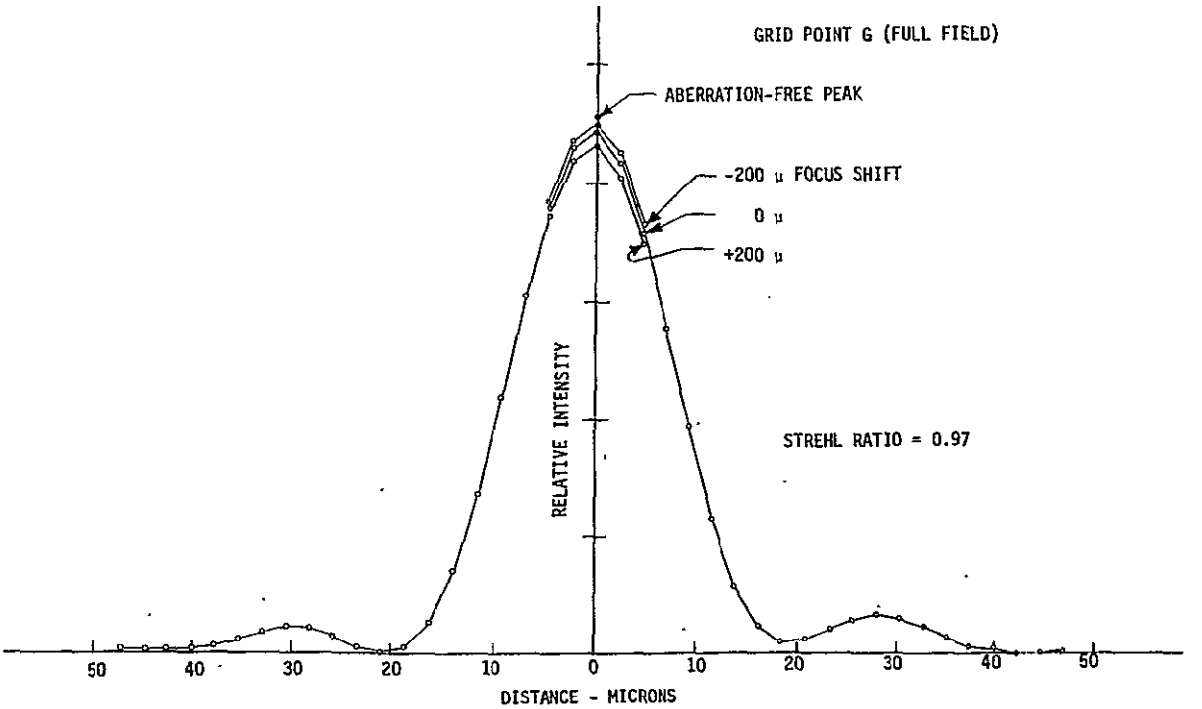

f/30 RELAY - POINT SPREAD FUNCTION

Figure 7.4-17

7.5 ENCIRCLED ENERGY

Encircled energy data were generated by computer program BFLTA. For each specified radius, the integrated energy was found by summing the values of intensity, point by point, over the enclosed portion of the two dimensional point spread function.

The encircled energy diagrams for the *f*/12.88 relay are given in figures 7.5-1 through 7.5-7.

The *f*/30 relay is so well corrected that the encircled energy diagrams for all the grid points are nearly identical. In figure 7.5-8, the plot for grid point C is given. This plot is typical of all the grid points.

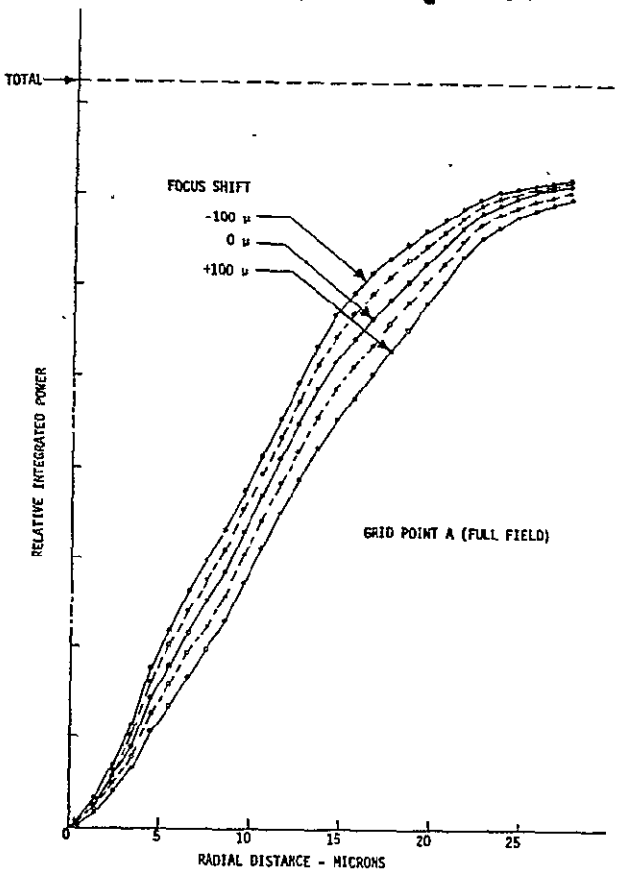

f/12.88 RELAY - ENCIRCLED ENERGY

Figure 7.5-1

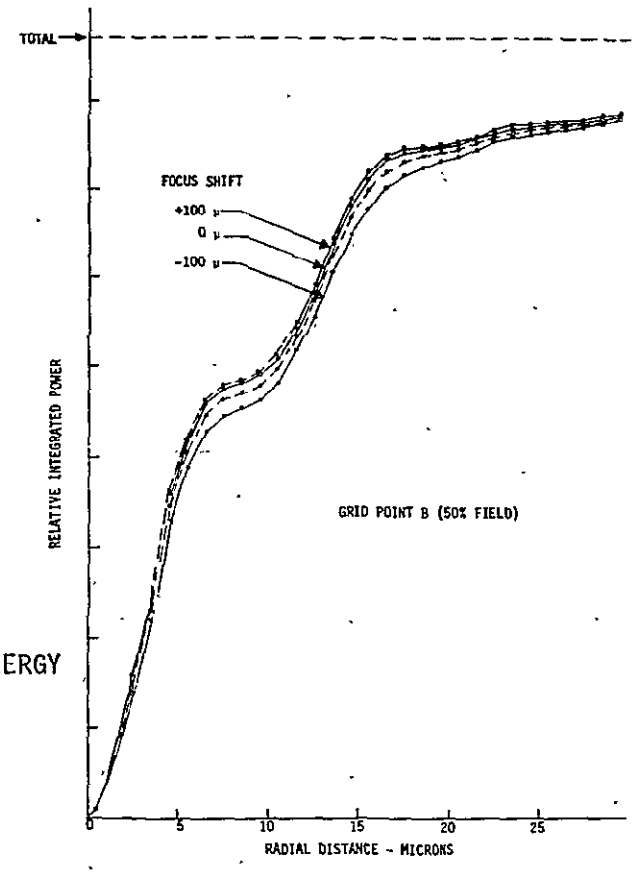

f/12.88 RELAY - ENCIRCLED ENERGY

Figure 7.5-2

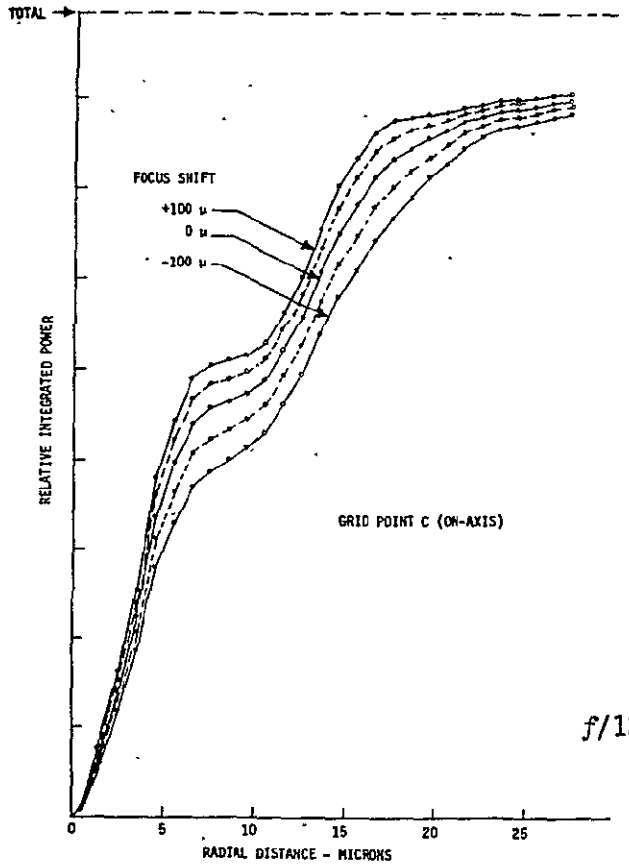

f/12.88 RELAY - ENCIRCLED ENERGY

Figure 7.5-3

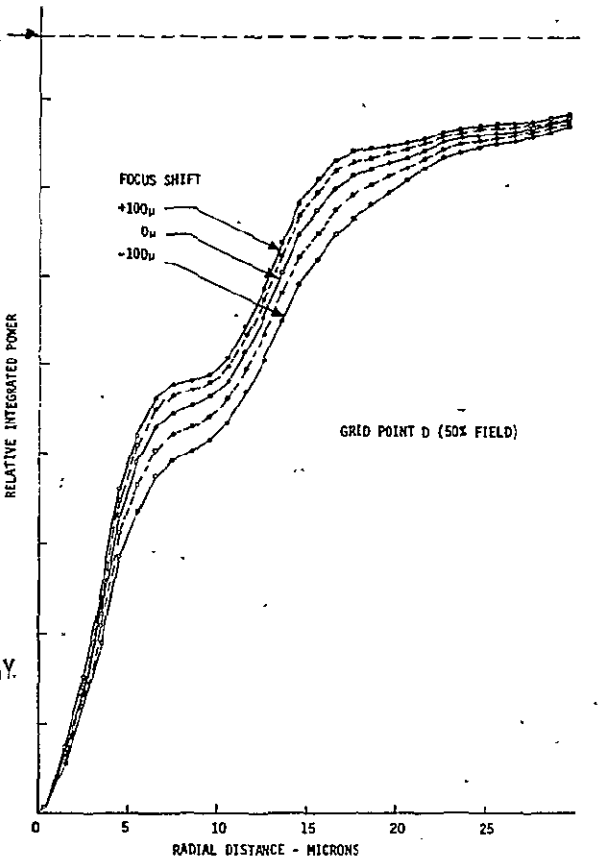

f/12.88 RELAY - ENCIRCLED ENERGY

Figure 7.5-4

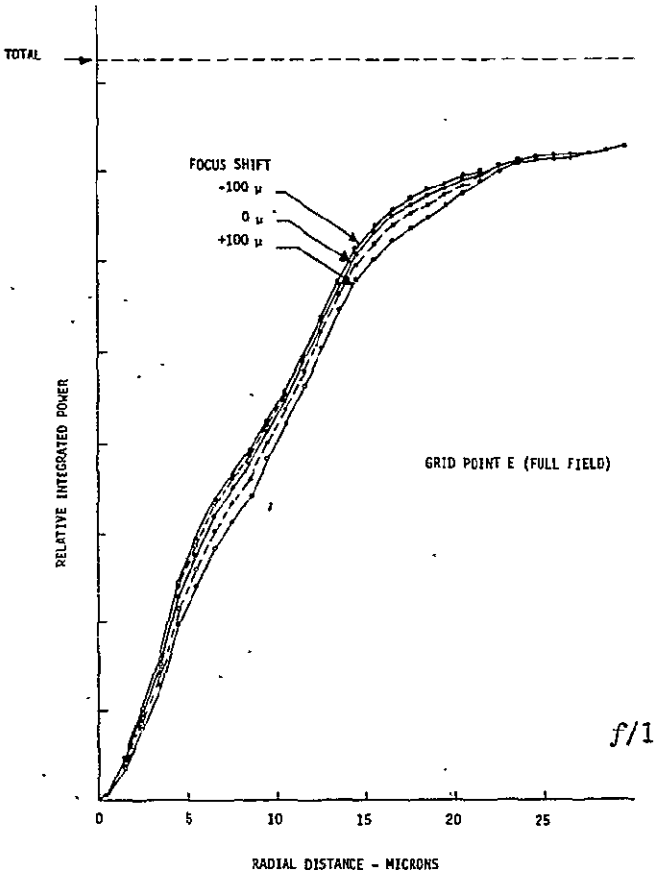

f/12.88 RELAY - ENCIRCLED ENERGY

Figure 7.5-5

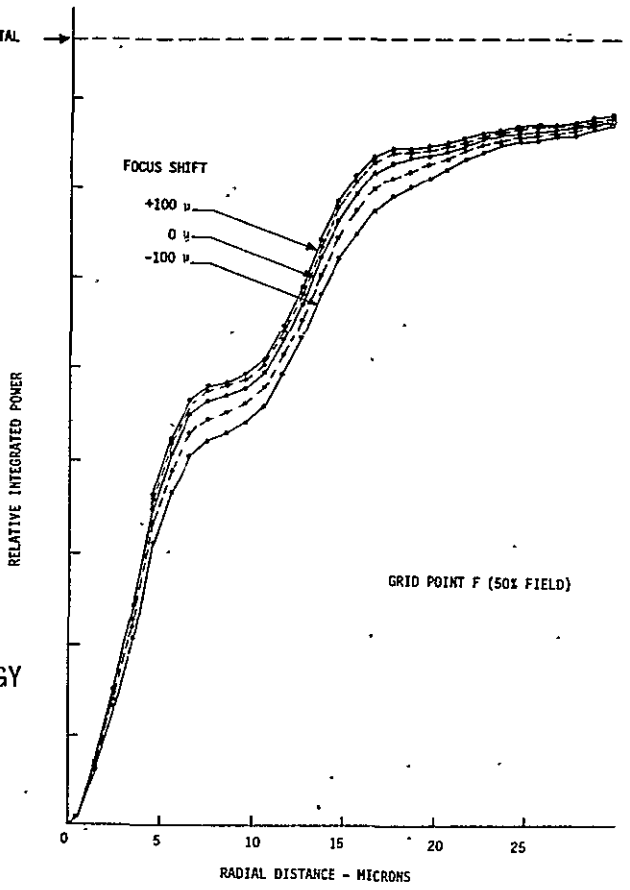

f/12.88 RELAY - ENCIRCLED ENERGY

Figure 7.5-6

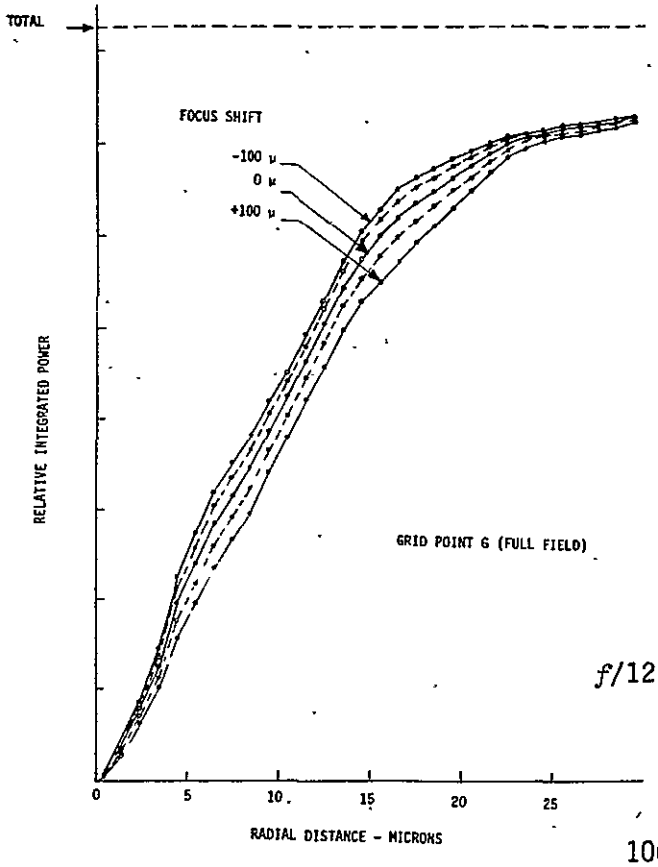

f/12.88 RELAY - ENCIRCLED ENERGY

Figure 7.5-7

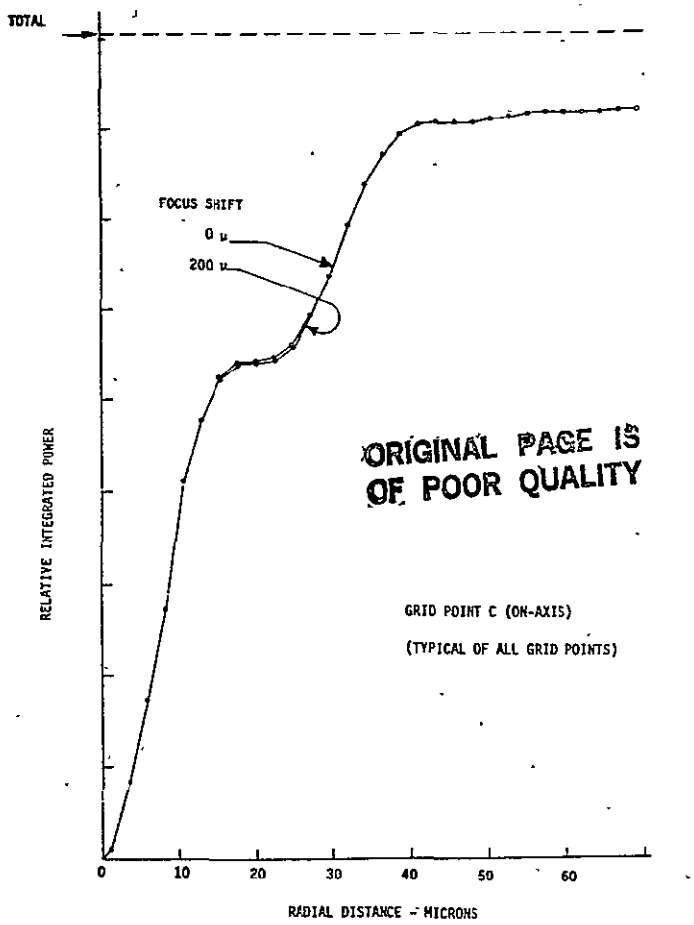

f/30 RELAY - ENCIRCLED ENERGY

Figure 7.5-8

7.6 GEOMETRIC DISTORTION

Computation of geometric distortion has been based upon the expression: % Dst = 100 (Y-y)/y where % Dst is distortion expressed as a percent of the paraxial image height y. This image height is the radial distance between a specified image point on the relay optics focal plane and the on-axis point on that plane. The change in chief ray intercept height, y, is derived by exact trigonometric ray trace. The change in paraxial image height, y, can also be given by the following expression:

$$y = f \tan \emptyset$$

where $\emptyset$ is the change in the input field angle and f is the focal length of the overall system consisting of the OTA optics plus the camera relay optics. This focal length has been calculated by means of a paraxial ray trace of the optical system. It should be noted that the effect of image distortion is angular pointing error. A star at a field angle of θ will appear to be at an angle of $\theta + \Delta\theta$. The angular error can be expressed as follows:

$$\tan(\Delta\theta) = \frac{y}{f}\left(\frac{D}{1+D}\right) .$$

where $D = Dst/100$

The geometric distortion calculations are summarized in tables 7.6-1 and 7.6-2.

Table 7.6-1

GEOMETRIC DISTORTION - f/12.88 RELAY
(f = 3091.0 cm)

Grid Point	ϕ (Degree)	Y (cm)	y (cm)	Dst (%)	$\Delta\theta$ (Arc Second)
A	0.015816	0.854896	0.853244	+0.194	0.110
B	0.007908	0.426959	0.426622	+0.079	0.022
C	0	0	0	-	-
D	0.007908	0.426596	0.426622	-0.006	-0.002
E	0.015816	0.853436	0.853244	+0.023	0.013
F	0.007908	0.426780	0.426622	+0.037	0.010
G	0.015816	0.854191	0.853244	+0.111	0.063

Table 7.6-2

GEOMETRIC DISTORTION - $f/30$ RELAY
(f = 7200.6 cm)

Grid Point	ϕ (Degree)	Y (cm)	y (cm)	Dst (%)	$\Delta\theta$ (Arc Second)
A	0.0067556	0.849387	0.849005	+0.045	0.011
B	0.0033778	0.424548	0.424502	+0.011	0.001
C	0	0	0	-	-
D	0.0033778	0.424392	0.424502	-0.026	-0.003
E	0.0067556	0.848761	0.849005	-0.029	-0.007
F	0.0033778	0.424470	0.424502	-0.008	-0.001
G	0.0067556	0.849078	0.849005	+0.009	0.002

7.7 VIGNETTING

Image irradiance will fall off with increasing distance into the field due to vignetting and the "cosine-fourth power law." Vignetting is determined by tracing an array of rays through the optical system where each ray represents a fraction of the radiant power entering the lens. At each specified field point on the relay lens focal plane, the incident optical power T is related to the input optical power To by the expression:

$$(T/To) = (R/3234)$$

where R is the number of unvignetted rays traced. The relative image irradiance is directly proportional to the relative transmittance and can be found by the expression:

$$(H/Ho) = (T/To)\ \cos^4\theta$$

where $\cos^4\theta$ is the geometric irradiance fall-off factor with θ the slope angle of the chief ray at the relay exit pupil. The vignetting calculations are summarized in tables 7.7-1 and 7.7-2.

Table 7.7-1

RELATIVE IMAGE IRRADIANCE - *f*/12.88 RELAY

Grid Point	R Number	(T/To)	$\cos^4(\theta)$	(H/Ho)
A	2968	0.9177	0.9966	0.9146
A'	3062	0.9468	0.9984	0.9453
B	3132	0.9685	0.9992	0.9677
C	3234	1.0	1.0	1.0
D	3132	0.9685	0.9992	0.9677
E'	3066	0.9481	0.9984	0.9465
E	2968	0.9177	0.9967	0.9147
F	3128	0.9672	0.9991	0.9664
G'	3059	0.9459	0.9984	0.9444
G	2958	0.9147	0.9966	0.9115

Table 7.7-2

RELATIVE IMAGE IRRADIANCE - *f*/30 RELAY

Grid Point	R Number	(T/To)	$\cos^4(\theta)$	(H/Ho)
A	3172	0.9618	0.9991	0.9610
B	3256	0.9873	0.9998	0.9871
C	3298	1.0	1.0	1.0
D	3257	0.9876	0.9998	0.9874
E	3174	0.9624	0.9991	0.9616
F	3256	0.9873	0.9998	0.9871
G	3172	0.9618	0.9991	0.9610

7.8 SENSITIVITY ANALYSIS

This section evaluates the sensitivity of the WF/PC relays to manufacturing variations. The study shows that the back focal distance of the relay is very sensitive to changes in primary mirror and secondary mirror vertex radii of curvature. This potential focus error can be removed, however, by axial adjustments of the CCD detector location, primary-to-secondary mirror spacing, and pyramid positon.

Decenter and tilt of the relay secondary mirror with respect to its primary mirror produces field tilt, coma, and astigmatism. These alignment errors are analyzed in this section in terms of MTF degradation.

7.8.1 Radius of Curvature Tolerances

Focus shift is the consequence of radius of curvature errors. The amount of focus shift is given by the following expression:

$$\Delta BF = r_s \left\{ \frac{r_p\, t_o + (r_p + 2\, t_o)\, t_p}{(r_s - 2\, t_p)(r_p + 2\, t_o) - 2\, r_p\, t_o} \right\}$$

$$- r_s \left\{ \frac{r_p\, t_o + \left(r_p + 2\, t_o\, (1-R_p)\right) t_p}{\left(r_s - 2\, t_p\, (1-R_s)\right)\left(r_p + 2\, t_o\, (1-R_p)\right) - 2\, R_p\, t_o\, (1-R_s)} \right\} \quad (1)$$

where: ΔBF = focus error

r_p = primary mirror radius of curvature

r_s = secondary mirror radius of curvature

t_o = object distance (OTA image - primary mirror)

t_p = primary-secondary mirror spacing

$R_p = (\Delta r_p / r_p)/(1 + \Delta r_p / r_p)$

$R_s = (\Delta r_s / r_s)/(1 + \Delta r_s / r_s)$

$(\Delta r_p/r_p)$ = relative primary mirror radius error

$(\Delta r_s/r_s)$ = relative secondary mirror radius error

A second effect of radius errors is a change in image magnification. Both focus error and magnification error can be compensated during assembly buildup by adjusting the axial location of the CCD detector and the primary mirror to secondary mirror spacing.

The mirror-t_o-mirror spacing adjustment (Δt_p) is:

$$\Delta t_p = \frac{t_p\,(r_p + 2\,t_o) + t_o\,(r_p\,R_s - r_s\,R_p)}{(1-R_s)\,\left(r_p + 2\,t_o\,(1-R_p)\right)} - t_p \qquad (2)$$

And the change (Δt_D) in detector axial position is:

$$\Delta t_D = -\frac{r_s\,\left((r_p + 2\,t_o)\,\Delta\,t_p - 2\,t_o\,(t_p + \Delta t_p)\,R_p\right)}{(r_p + 2\,t_o)\,(r_s - 2\,t_p) - 2\,r_p\,t_o} - \Delta t_p \qquad (3)$$

7.8.1.1 *f*/12.88 Relay Radius of Curvature Tolerances - A tight but reasonable radius of curvature tolerance is ± 0.5 percent. For the primary mirror this yields a radius specification of 40.57 ±0.20 cm. The secondary mirror radius specification is 28.55 ± 0.14 cm.

The back focus variation caused by these radius tolerances is found from equation (1). Evaluating this expression for the *f*/12.88 relay gives:

$$\Delta BF = \frac{149753 - 104950\ (1-R_p)}{\left[32.518\ (1-R_s) + 28.546\right]\left[226.122\ (1-R_p) - 40.5662\right] - 9172.91(1-R_s)} - 20.7626$$

The worst-case condition occurs when the radius errors for the two mirrors have opposite signs.

Let

$$\Delta r_p/r_p = + 0.005 \qquad (+0.5\%)$$

$$\Delta r_s/r_s = - 0.005 \qquad (-0.5\%)$$

Then

$$R_p = + 0.004975$$

$$R_s = - 0.005025$$

And

$$\Delta BF = 1.10 \text{ cm.}$$

Thus, the back focal distance may be anywhere within ± 1.10 cm from its design value when the radius tolerance is ± 0.5 percent.

Focal length and focus can be restored by adjusting the primary-secondary mirror spacing and the axial position of the detector using equations (2) and (3). Evaluating these equations for the *f*/12.88 relay gives:

$$\Delta t_p = \frac{3016.95 - 4586.46\ R_s + 3227.44\ R_p}{(1-R_s)\ 226.122\ (1-R_p) - 40.5662} - 16.2590$$

$$\Delta t_D = 2.99132\ R_p\ (16.2590 + \Delta t_p) - 3.45468\ \Delta t_p$$

The required adjustment ranges are calculated from the above expressions. Based upon the 0.5 percent radius tolerance:

$$\Delta t_p = +0.2284 \text{ cm}$$

$$\Delta t_D = -0.5435 \text{ cm}$$

Thus, the secondary mirror needs an assembly buildup adjustment range of ± 0.23 cm and the detector needs an assembly buildup adjustment range ±0.55 cm.

If vertex radius could be measured perfectly, the radius errors of the manufactured parts would be known exactly, then these exact values could be used in the preceding equations to predict the required amounts of adjustment.

The computer math model was used to verify this analysis. The model was perturbed as follows:

1. The primary mirror radius of curvature was increased from 40.5662 cm to 40.7690 cm (+0.5%).

2. The secondary mirror radius of curvature was decreased from 28.5462 cm to 28.4035 cm (-0.5%).

3. Spacing between primary and secondary mirrors was increased by 0.2284 cm to re-establish the focal length (magnification).

4. The detector was moved 0.5435 cm toward the primary mirror to re-establish focus.

5. MTF of this perturbed system was calculated at three grid points and compared with unperturbed values.

Table 7.8.1-1

RADIUS PERTURBATION COMPARISON

Grid Point	Perturbed MTF	Unperturbed MTF	Image Height Change
A	.181	.188	0.2μ
C	.356	.354	0.0μ
E	.332	.336	0.2μ

The perturbed MTF values are very close to the unperturbed values. The adjustments, therefore, corrected the focus shift caused by the radius errors. Magnification was also compensated by these adjustments as indicated; image height changed by only 0.2 microns.

From a practical standpoint, however, there is always a measurement error where:

$$\frac{\Delta r}{r}\ (\text{actual}) = \frac{\Delta r}{r}(\text{measured}) \pm \frac{\Delta r}{r}\ (\text{error})$$

Thus, the adjustment values calculated from measured data, $\frac{\Delta r}{r}$ (measured), are only approximate. After applying these adjustments, a residual focus error will remain due to the measurement error $\frac{\Delta r}{r}$ (error).

A tight but reasonable accuracy requirement for the radius measurement equipment is ±0.1 percent. Inserting this value ($\Delta r_p/r_p$ = + .001, $\Delta r_s/r_s$=-.001) into equation (1) gives the amount of residual focus error at the detector:

$$\Delta BF = \pm\ 0.2133\ \text{cm}$$

In summary, a vertex radius tolerance of 0.5 percent was specified. This tolerance determined the assembly buildup adjustment ranges. The manufactured mirrors would be measured with equipment having a measurement accuracy of 0.1 percent. Adjustments in the axial positions of the secondary mirror and detector would then be made during assembly buildup, based upon these measured data. Because of measurement error, however, these adjustments are not perfect and a residual focus error, in the range of ±0.22 cm., remains.

This residual focus error can only be removed by an in-process optical test. The WF/PC cannot be assembled to the required accuracy by tight tolerances and mechanical measurements alone. The final focus adjustment must be done optically.

7.8.1.2 *f*/30 Relay Radius of Curvature Tolerances - Evaluation and conclusions for the *f*/30 relay are the same as those described above. In summary, for this relay:

$$\Delta BF = \frac{167084.6 - 130592.9\ (1-R_p)}{(49.294\ (1-R_s) + 23.433)(226.114\ (1-R_p)-51.7800) - 1170818(1-R_s)} - 37.5967$$

$$\Delta t_p = \frac{4296.81 - 5854.09\ R_s + 2649.26\ R_p}{(1-R_s)\ (226.114\ (1-R_p) - 51.7800)} - 24.6470$$

$$\Delta t_D = 5.45899\ R_p\ (24.6470 + \Delta t_p) - 4.20889\ \Delta t_p$$

Based upon a 0.5 percent radius tolerance for the primary and secondary mirrors, the secondary mirror will need a ± 0.29 cm adjustment range and the detector will need a ± 0.51 cm adjustment range.

Also, based upon a radius measurement accuracy of 0.1 percent, the residual focus error at the detector after the adjustments are made will be in the range of ± 0.92 cm.

7.8.1.3 Pyramid Facet Radius of Curvature Tolerance - Each pyramid facet is a concave surface of 306.8400 cm radius. This surface radius was increased 0.5 percent and evaluated. The optical math model showed no significant change in MTF. A radius tolerance of 0.5 percent for this surface, therefore, is appropriate.

7.8.1.4 Primary - Secondary Mirror Spacing Tolerance - A perturbation (Δt_p) in spacing between the relay primary and secondary mirrors causes focus shift (ΔBF) at the detector as given in the expression:

$$\Delta BF = -(M^2 + 1)\ \Delta t_p \qquad (4)$$

where: $$M = r_s (r_p + 2 t_o) / (r_p + 2 t_o)(r_s - 2 t_p) - 2 t_o r_p \quad (5)$$

r_p = primary mirror radius of curvature

r_s = secondary mirror radius of curvature

t_o = object distance (OTA image - primary mirror)

t_p = primary-secondary mirror spacing

Design values for the $f/12.88$ are:

r_p = -40.5662 cm

r_s = -28.5460 cm

t_o = 113.0610 cm

t_p = 16.2590 cm

Evaluating equations (5) and (4) gives:

$$M = 2.454679$$

$$\Delta BF = -7.025449 \, \Delta t_p$$

In the previous section, it was shown that a 0.1 percent error in the knowledge of vertex radii would cause a residual focus error of ±0.22 cm. Inaccuracy (Δt_p) in setting the mirror-to-mirror spacing causes an additional focus error. Since this total residual error is removed later during an optical test, an extremely tight spacing tolerance is not necessary; however, the error caused by this tolerance should be much less than ± 0.22 cm if possible. The above equation shows that a spacing tolerance of ± 0.003 cm produces a focus error of ±0.021 cm. These values seem to be reasonable, so a spacing tolerance of ±0.003 cm is suggested.

As described in the previous section, this tolerance applies to a nominal spacing which is not a fixed value, but depends upon the measured primary and secondary mirror radius of curvature error.

Design values for the $f/30$ relay are:

$$r_p = -51.7800 \text{ cm}$$

$$r_s = -23.4330 \text{ cm}$$

$$t_o = 113.0570 \text{ cm}$$

$$t_p = 24.6470 \text{ cm}$$

Evaluating equations (5) and (4) gives:

$$M = 4.208885$$

$$\Delta BF = -18.714713 \, \Delta t_p$$

Applying the same tolerance (±0.003 cm) as that suggested for the $f/12.88$ relay, the above equation give a resultant focus error of ± 0.056 cm. This error is much smaller than the ± 0.92 cm error caused by uncertainty in the vertex radius measurements. This tolerance of ±0.003 cm, therefore, is suggested for the spacing between the $f/30$ primary and secondary mirrors.

7.8.1.5 Secondary Mirror Decenter and Tilt - The computer math model was used to calculate relative change in MTF caused by secondary mirror misalignment. Figures 7.8.1.5-1 through 7.8.1.5-8 describe the sensitivity of MTF to decenter and tilt of the relay secondary mirror with respect to a fixed primary mirror.

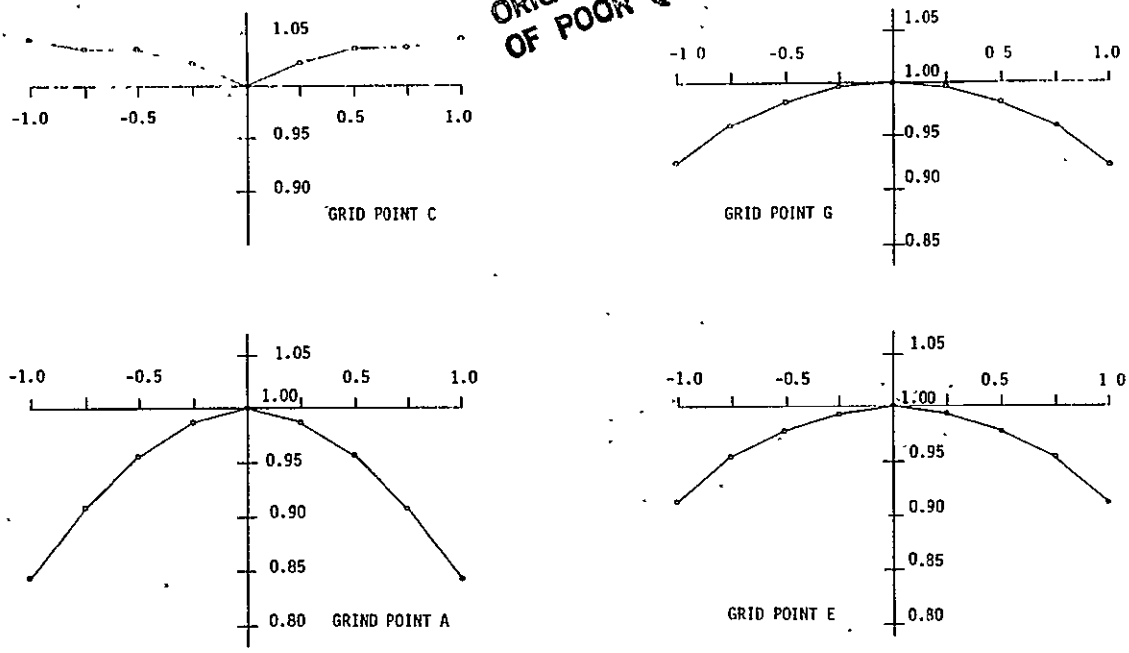

RELATIVE GEOMETRIC MEAN MTF RELATED TO $f/12.88$
RELAY SECONDARY MIRROR DECENTRATION
(DECENTER, IN SAGITTAL PLANE, GIVEN IN MILLIMETERS)

Figure 7.8.1.5-1

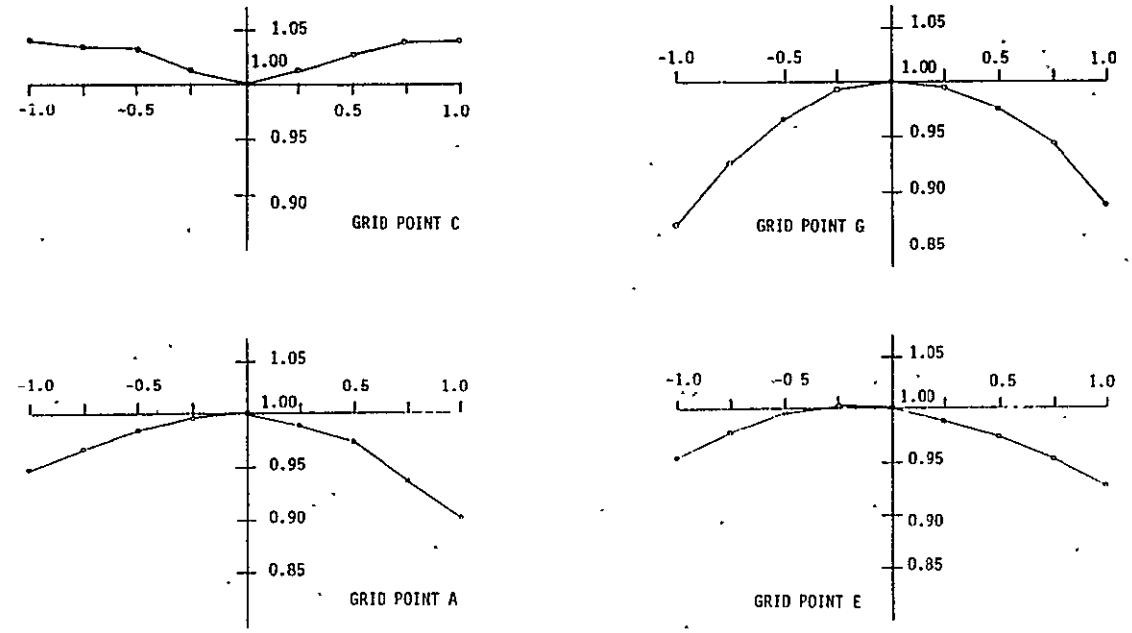

RELATIVE GEOMETRIC MEAN MTF RELATED TO $f/12.88$
RELAY SECONDARY MIRROR DECENTRATION
(DECENTER, IN MERIDIONAL PLANE, GIVEN IN MILLIMETERS)

Figure 7.8.1.5-2

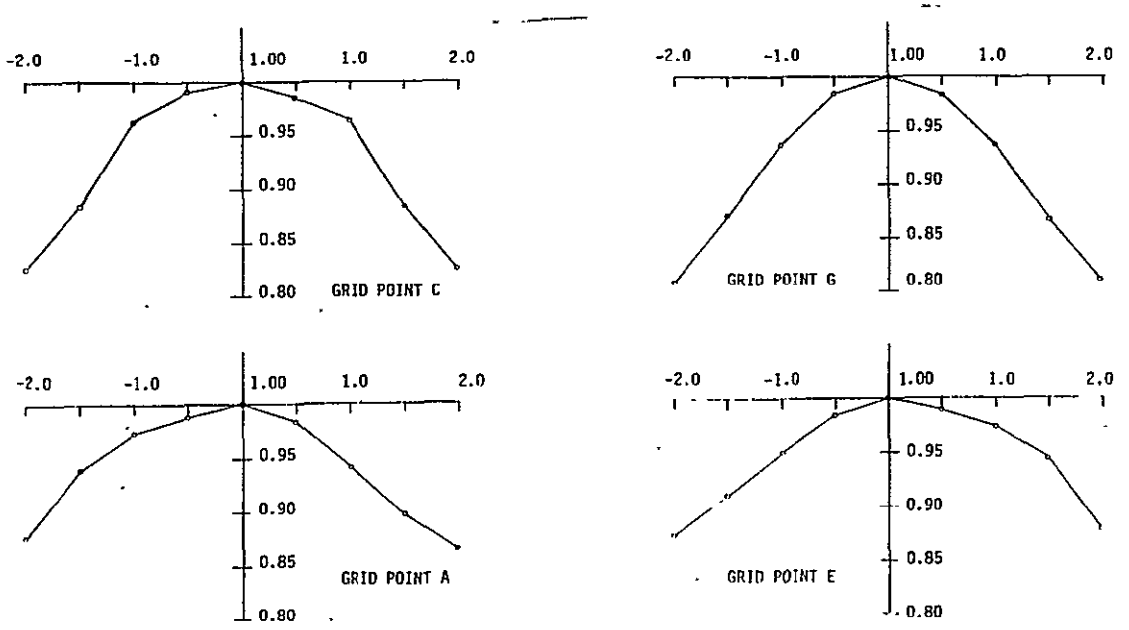

RELATIVE GEOMETRIC MEAN MTF RELATED TO *f*/30
RELAY SECONDARY MIRROR DECENTRATION
(DECENTER, IN MERIDIONAL PLANE, GIVEN IN MILLIMETERS)

Figure 7.8.1.5-3

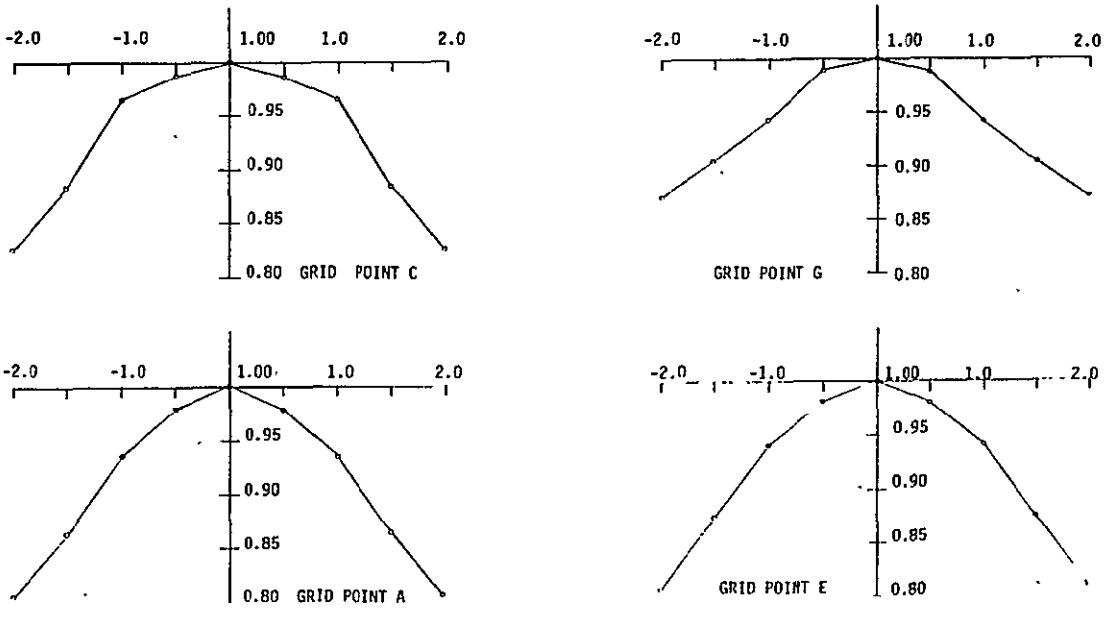

RELATIVE GEOMETRIC MEAN MTF RELATED TO *f*/30
RELAY SECONDARY MIRROR DECENTRATION
(DECENTER, IN SAGITTAL PLANE, GIVEN IN MILLIMETERS)

Figure 7.8.1.5-4

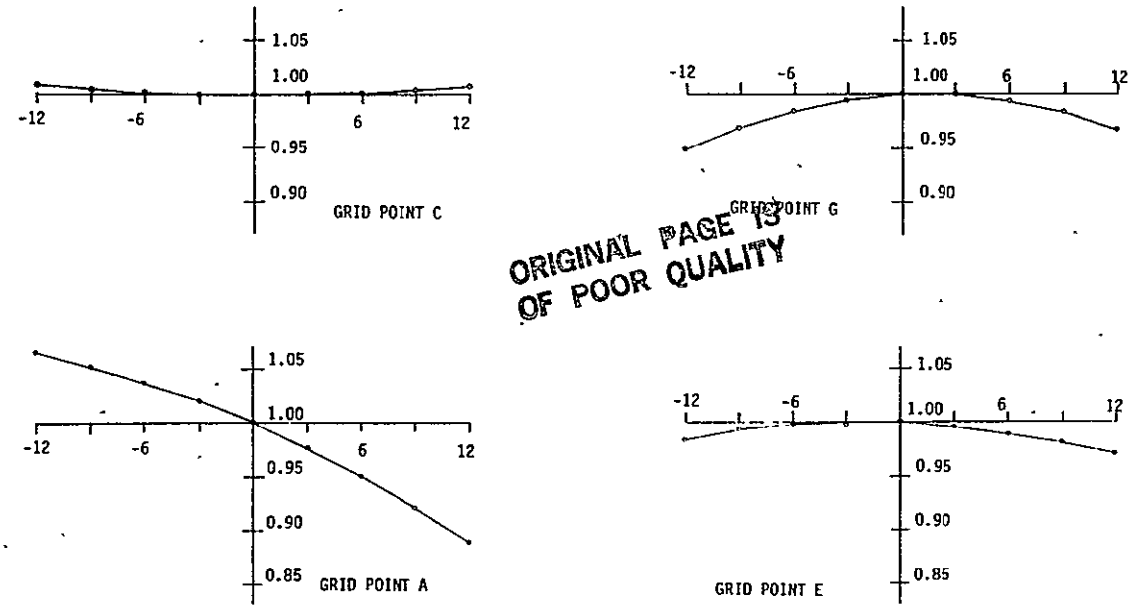

f/12.88 RELAY
RELATIVE GEOMETRIC MEAN MTF RELATED TO SECONDARY MIRROR TILT
(TILT GIVEN IN ARCMINUTES)

(ROTATION AXIS IS NORMAL TO THE MERIDIONAL PLANE
AND TANGENT TO THE MIRROR VERTEX)

Figure 7.8.1.5-5

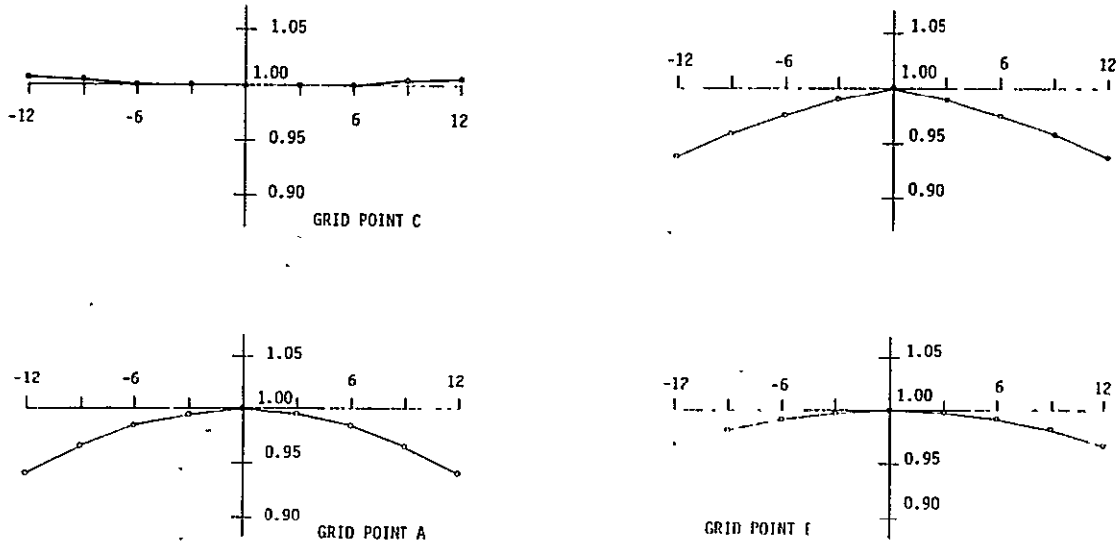

f/12.88 RELAY
RELATIVE GEOMETRIC MEAN MTF RELATED TO SECONDARY MIRROR TILT
(TILT GIVEN IN ARCMINUTES)

(ROTATION AXIS IS NORMAL TO THE SAGITTAL PLANE
AND TANGENT TO THE MIRROR VERTEX)

Figure 7.8.1.5-6

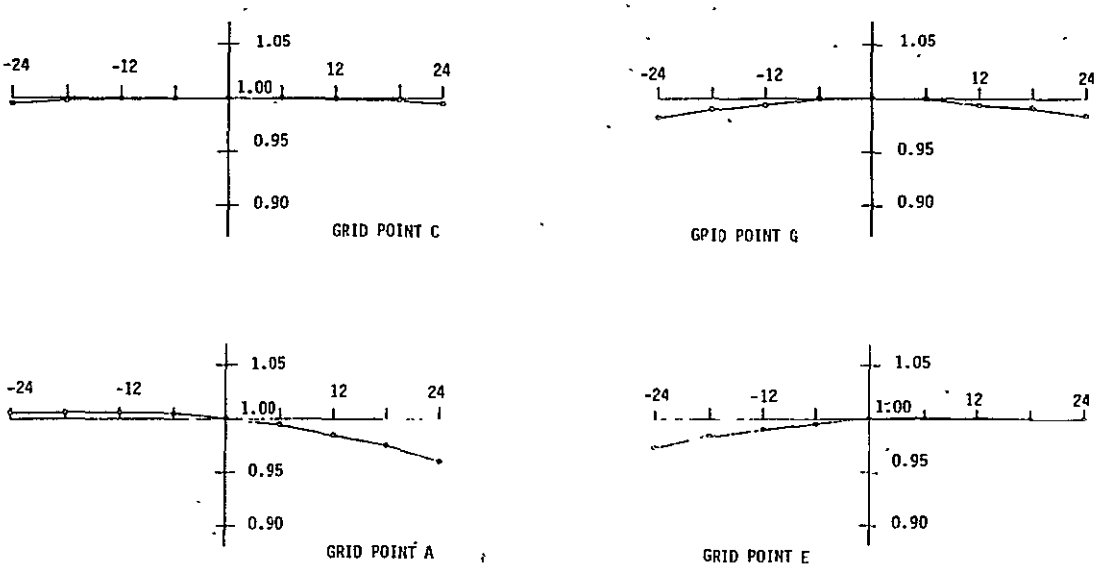

f/30 RELAY
RELATIVE GEOMETRIC MEAN MTF RELATED TO SECONDARY MIRROR TILT
(TILT GIVEN IN ARCMINUTES)

(ROTATION AXIS IS NORMAL TO THE MERIDIONAL PLANE
AND TANGENT TO THE MIRROR VERTEX)

Figure 7.8.1.5-7

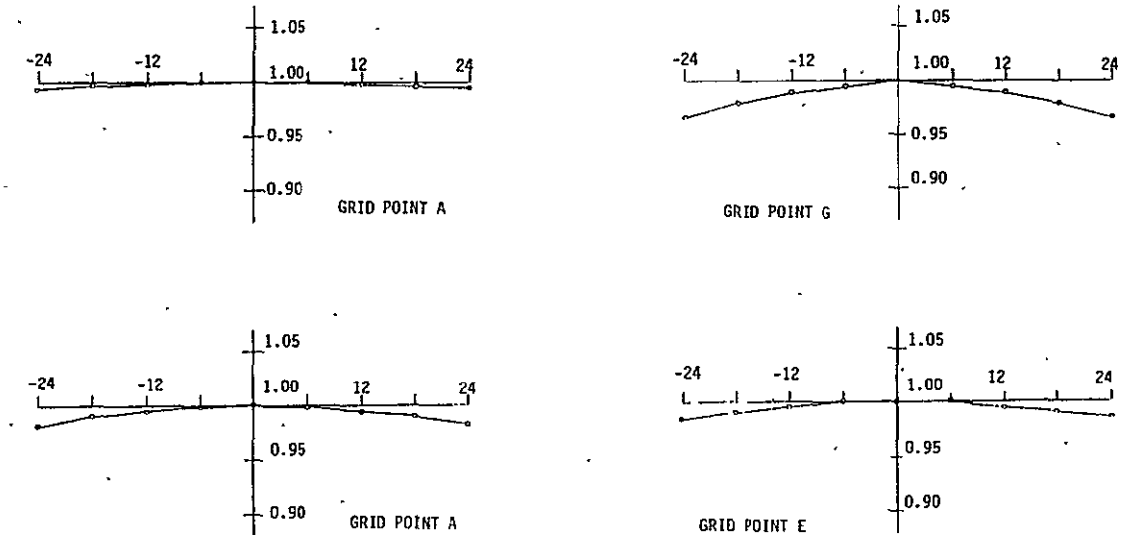

f/30 RELAY
RELATIVE GEOMETRIC MEAN MTF RELATED TO SECONDARY MIRROR TILT
(TILT GIVEN IN ARCMINUTES)

(ROTATION AXIS IS NORMAL TO THE SAGITTAL PLANE
AND TANGENT TO THE MIRROR VERTEX)

Figure 7.8.1.5-8

7.9 BAFFLE REQUIREMENTS

A preliminary baffle requirements study has been performed to assess the need for stray light suppression. Stray light suppression is achieved by first identifying critical surfaces which contribute significant stray light. The amount of stray light contributed by each critical surface can be suppressed by reducing the projected solid angle of this surface as seen by the CCD detectors, reducing the level of incident irradiance on the critical surface, and reducing the bidirectional reflectance distribution function (BRDF) for that surface. The projected solid angle of a critical surface can often be reduced to zero by removing or reorienting the surface, or by blocking the surface with a baffle. The OTA optics are well-baffled so that the source of potential stray light in WF/PC optics is image-forming light at the OTA focal surface. The incident irradiance on critical surfaces can, therefore, be minimized by the use of a well-designed field stop at the focal surface. The BRDF is the ratio of apparent brightness of the critical surface to the incident irradiance. The BRDF of a critical surface can be reduced by the use of matte black paint which absorbs stray light, glossy black paint which reflects the residual stray light into light traps, or vane structures which block the stray light.

Assuming the OTA focal surface is "critically" baffled, no additional baffling is required (WF/PC focal surface is protected for image forming light only over the necessary WF/PC field of view). Assuming the OTA focal surface is not critically baffled, additional effective baffle locations have been determined (figure 7.9-1). In the Wide Field Camera an additional ring baffle could be installed in the Cassegrain relay. Due to the geometry, a baffle is not needed at this location in the Planetary Camera.

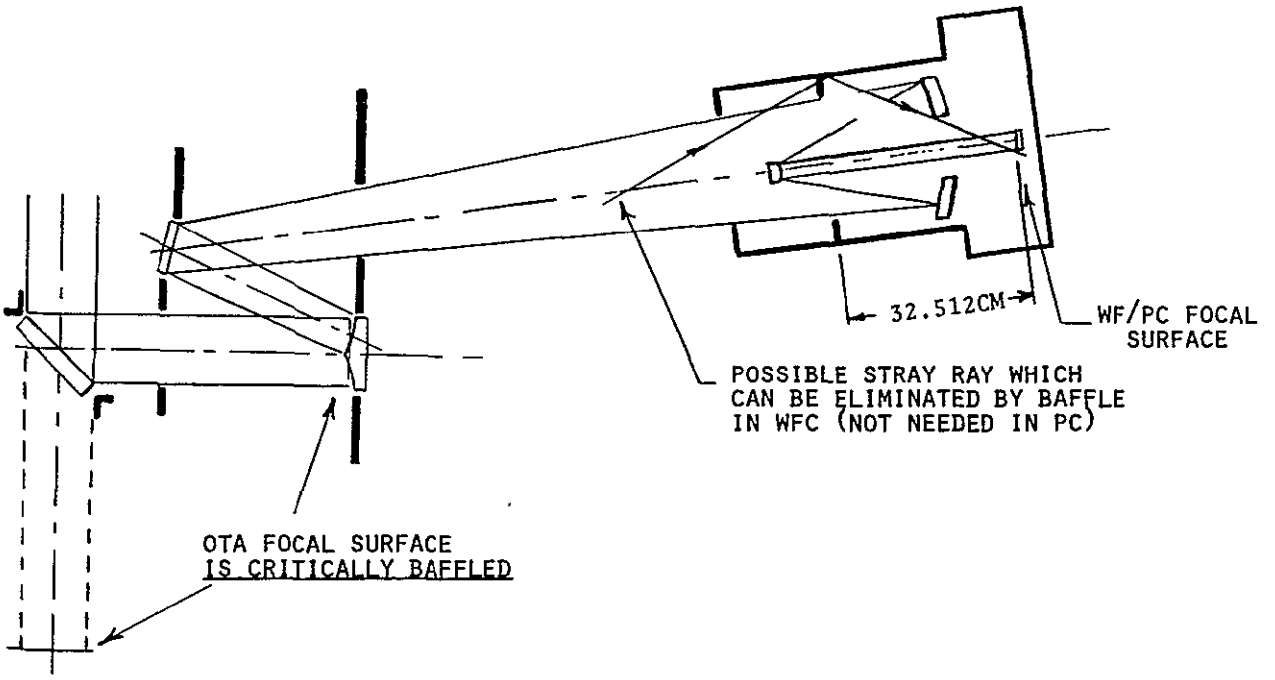

ADDITIONAL EFFECTIVE BAFFLE LOCATIONS

Figure 7.9-1

8.0 OPTICAL MANUFACTURABILITY ANALYSIS OF OPTIMIZED DESIGN

8.0 OPTICAL MANUFACTURABILITY ANALYSIS OF OPTIMIZED DESIGN

8.1 OPTICAL COMPONENT SPECIFICATIONS

The inability of a manufactured optical surface contour to perfectly match the designed surface contour results in degradation of performance (wavefront error and scatter) of an imaging system. These surface deviations result in low spatial frequency figure error and edge roll-off, medium spatial frequency error surface ripple, and high spatial frequency surface roughness. For each optical element, performance levels for each of the three spatial frequency ranges should be specified and quantified. Shown in table 8.1-1 is a summary of the WF/PC optical component specifications.

Table 8.1-1

WF/PC OPTICAL COMPONENT SPECIFICATIONS

Optical Element*	Aspheric Shape	Angle of Incidence	RMS Figure Quality (λ)	Auto-Correlation Length	RMS Surface Roughness (Å)	Scratch/Dig	Radius Fab. (%)	Tolerance Test (%)
WFC PM	General Asphere (≅ Prolate Spheroid)	Normal	0.015	0.125	30	20/5	0.5	0.1
WFC SM	General Asphere (≅ Hyperboloid)	Normal	0.015	0.125	30	20/5	0.5	0.1
PC PM	Prolate Spheroid	Normal	0.015	0.125	30	20/5	0.5	0.1
PC SM	Hyperboloid	Normal	0.015	0.125	30	20/5	0.5	0.1
Pyramid	Spheroid	9.1056°	0.05	-----	15	10/1	0.5	0.2
Reflective Plano Surfaces	Plano	≤ 45°	0.01	-----	30	20/5	---	---
Refractive Plano Surfaces	Plano	Normal	0.01	-----	30	20/5	---	---

8.1.1 Surface Quality

Low spatial frequency information (between 0 and 20 cycles per pupil diameter) can be fully described on a reasonably sized optical pathlength difference (OPD) array (typically 41 by 41 points). The OPD information comes from the interferometric test data of the surface under test (see section 8.4). The output can be topographic maps of the optical surface, wavefront data in terms of peak-to-valley and rms wavefront errors, and optical aberration components

of the wavefront errors (i.e., Zernike circle polynomials). Since a real system must be manufactured to a practical set of fabrication tolerances, a figure of merit must be established which specifies quantitatively system performance satisfying the overall system objectives. For an optical imaging device, the rms wavefront error is an excellent figure of merit (see figure 4.0-3). Once the figure of merit is established it must be used to tolerance individual error contributors. Shown in figure 8.1.1-1 is rms wavefront error versus the angle of incidence for a fixed surface (figure) error (i.e., at normal incidence the wavefront error is twice the figure error). Therefore, a specification on the rms figure error on the surface allows the common denominator of rms wavefront error to be used throughout the optical assembly buildup (unmounted optical component to optical system). For the imaging optics (Cassegrain PM and SM), an rms quality of 0.015 λ has been specified. This value constitutes a starting point for the optical tolerance budgeting (see section 8.5) and is considered state-of-the-art when compared with estimated manufacturing and testing capability.

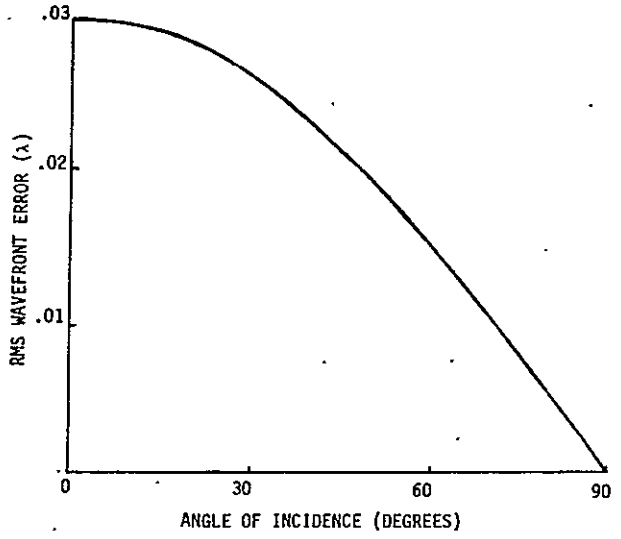

RMS WAVEFRONT ERROR VS ANGLE OF INCIDENCE
(ASSUME SURFACE ERROR = 0.015 λ RMS)

Figure 8.1.1-1

The pyramid mirror is a field lens in the optical system. (Note: If it is placed exactly at the focal point of the OTA, it has no effect on the image forming properties of the system but it bends the ray bundles, which would otherwise miss the two mirror Cassegrain, back toward the axis so that they pass through the Cassegrain.) Shown in figure 8.1.1-1 is the effect on the wavefront degradation due to a variation in the angle of incidence from the normal. This angular deviation is approximately 9 degrees at the pyramid and produces a negligible effect on the rms wavefront error. Since the pyramid mirror does not affect the imaging properties of the system, a relatively loose figure error requirement of 0.05λ rms has been imposed.

The plano surfaces have been specified at a level of 0.01 λ rms. It should be noted that the component test would be at normal incidence; however, the angle of the mirrors is at approximately 45 degrees in end use. Conversion from figure error to wavefront error for budgeting purposes will require the use of figure 8.1.1-1.

8.1.2 Ripple Error

Medium spatial frequency (ripple error) information refers to surface errors with lateral dimensions, ranging from about 1/20 of the aperture to about 1/400 of the aperture. These ripple errors could be caused by the polishing process, by the physical properties of the material being polished and, in some instances, by quilting of the surface due to substrate stiffness variations. For optics in which angles of incidence are near normal and wavelengths are in the visible range, ripple-type errors can usually be ignored if their magnitudes are small compared to the magnitudes of the figure errors. For wavelengths in the ultraviolet, the OTA specification quantifies the medium spatial frequency content by the autocorrelation length ($c \geq 0.125$). The same requirement is used for the imaging optics (primary and secondary mirrors) in the WF/PC optical assembly.

8.1.3 Surface Roughness

The resultant effect of the high spatial frequency content on an optical surface is scattering (veiling glare), figure 8.1.3-1. For optics with wavelengths in the near IR, visible, and UV the scattered light is due to mainly micro-irregularities (large variations in surface roughness). This high frequency microstructure is too fine for a deterministic analysis and must be treated statistically. An rms surface roughness specification is useful.

For the OTA, no scattering or veiling glare requirements are directly imposed. It is expected that to meet the low light level requirements, the veiling glare must be no greater than one percent. This implies a surface roughness on the order of 50 angstroms (rms). Experimental results have shown that good optical polishing practices will yield surface roughness values of this level with a high degree of confidence without measurement verification. For the primary and secondary mirrors a requirement of 30 Å rms has been imposed. (This value is sometimes used as the threshold of superpolishing and would require measurement verification with a device such as a FECO interferometer.)

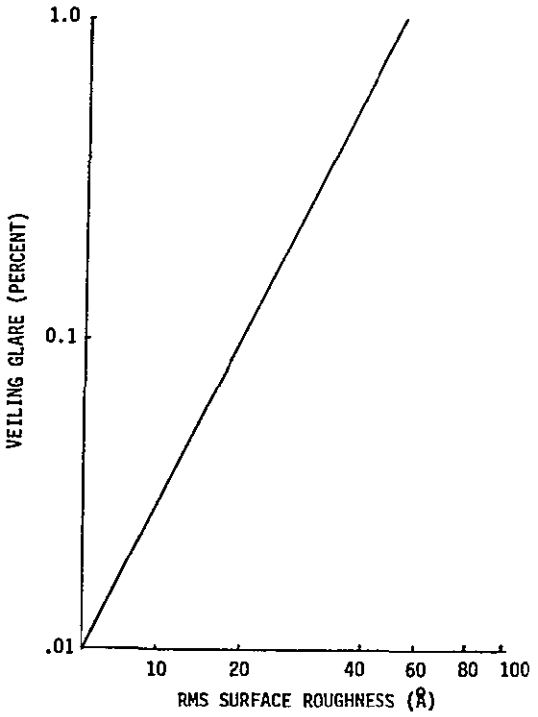

SURFACE SCATTERING

Figure 8.1.3-1

8.1.4 Scratches, Digs and Particulate Contamination

For optics with wavelengths in the far IR, the scattered light is due mainly to large scale macro-irregularities (scratches, digs, pits). In this domain a scratch/dig requirement is useful. Specification for scratch/dig is based on MIL-O-13830A. According to this specification, the scratch number is the maximum allowable width of a scratch in microns. The combined length of the heaviest scratches shouldn't exceed 1/4 the lens diameter. The dig number is one tenth the maximum allowable diameter of a dig in microns. The permissible number of maximum size digs shouldn't be more than one per each 20mm of diameter or fraction thereof on any single optical surface. The sum of the diameters of all digs should not exceed twice the diameter of the maximum size specified.

A scratch/dig specification of 20/5 has been set on the imaging optics. This scratch/dig level is considered extra precise but possible on this size optics.

Since the pyramid mirror acts as a field lens, cosmetic features such as scratches and digs will be imaged directly onto the CCD detector. Assuming the spot image is no greater than one pixel (15 microns) the maximum width of a scratch or dig on the pyramid facet can be no greater than 27.9 microns for the Wide Field Camera and no greater than 12 microns for the Planetary Camera. This implies a worst case scratch/dig requirement of 10/1. This scratch/dig level is at or above reticle quality and has been included as a goal with a scratch/dig level of 10/5 specified as a requirement. Of additional concern on the surface of the pyramid is particulate contamination. Surface particles with diameters greater than 12 microns (under the above resolution assumptions) will be imaged directly onto the CCD. Cleanliness requirements (contamination control) for allowable airborne particles in the room and allowable surface particles during handling will have to be established. A specific detailed cleaning specification must be generated for processing the optics.

8.1.5 Radius Tolerance

The inability of a lens to be manufactured to the designed radius directly affects the lens focal length and can contribute to spherical aberration. For the Cassegrain primary and secondary mirrors, estimated manufacturing and testing capability yields a fabrication tolerance of 0.5 percent with a measurement tolerance of 0.1 percent. Also of importance is the degree of uncertainty in the radius mismatch when the components are combined into the Cassegrain relay (see section 7.8). This would cause a residual focus shift and a resultant wavefront degradation if not compensated for by biasing the CCD detector plane during installation.

For the pyramid mirror, radius changes have "little" effect since the pyramid mirror facet is extremely slow ($f/100$). A fabrication tolerance of 0.5 percent is again assumed with a measurement tolerance of 0.2 percent. The latter value is based on a depth of focus uncertainty of $\lambda/10$.

For the plano surfaces, a tolerance on the radius is of little use. The method usually used is to specify the rms figure error minus the power term and the power term separately in peak-to-valley. For a figure error of 0.01 λ rms, however (as specified in section 8.1.1), the figure error specification is considered sufficient.

8.1.6 Mirror Coating

The mirror coatings have been specified as aluminum with a protective overcoating of magnesium fluoride (same coating as used in OTA optics). For wavelengths longer than 1000A, the intrinsic reflectance of aluminum is higher than that of any other coating material. A good optical polish is necessary since surface scratches can cause variations in the reflectance. This can be especially true in the low UV region around 1200A. Also extremely important are the uniformity and thickness of deposition and the vacuum level of the chamber. Preliminary studies indicate an aluminum layer on the order of 600A should be deposited at a comparatively slow rate of 20A per second at a vacuum level of less than 10^{-6} torr. The high reflectance of aluminum can only be utilized if the formation

of an oxide film can be prevented. This can be done by overcoating the aluminum with a film material of high transparency. Magnesium fluoride is specified which has a cutoff wavelength in the UV at 1150A. To minimize oxidation the protective overcoating would be applied almost simultaneously. Areas of concern are thickness, uniformity, rate and angle of deposition of the overcoating substrate, and vacuum level. The overcoating must be thick enough to prevent oxidation of the aluminum by diffusion of oxygen through the coating. To produce a coating with the highest reflectance at Lyman Alpha, 1215A, the deposition of magnesium would be stopped at a thickness of 250A. The optimum deposition is at a rate of 45A per second at incident angles of 15 degrees or less with a vacuum level of less than 10^{-6} torr. Witness plates would be used to monitor coating thickness, uniformity and reflectivity. The minimum reflectivity of each mirror surface is specified at 70 percent at 1200A and 85 percent at 6328A.

8.1.7 UV Performance Considerations

The wavefront error is defined as an optical path difference between a real wavefront and a reference spherical wavefront. This absolute quantity varies when expressed as a percentage of a wavelength (the shorter the wavelength, the larger the wavefront error). The difference between image quality for the WF/PC is well described by the rms wavefront error expressed in wavelengths of visible light as long as the WF/PC utilizes only the visible region; however, if a UV filter is implemented, the same wavefront error will be larger when expressed in wavelengths of UV light. Thus, it is important that the residual wavefront error be made as small as possible. In the fabrication of the components specifications on ripple error, surface roughness, cleaning and contamination address the parameters to assure the quality that is necessary for UV performance.

During the assembly buildup, wavefront error would be measured at the test wavelength of 6328A. However, optical software exists to perform analyses at any wavelength over the spectral range of interest. (Previous experience has shown that the analytical results agree with test results at other wavelengths.) At the total system level (optical assembly with CCD detector) direct verification of UV performance can be established with the OTA simulator.

8.2 OPTICAL FABRICATION

An assessment has been made of the manufacturability of the optical components comprising the Wide Field Planetary Camera. From a processing viewpoint, the optics fall into three (3) groups:

a. Plano surfaces: folding mirrors, filters and cover plates.
b. Cassegrain relay optics (aspherics).
c. Pyramid reflector.

The processing approaches considered for the optics are described in the following text. Although the tolerances for the various characteristics are not yet completely established, it is apparent that requirements are not at or beyond the state-of-the-art at present in optics manufacturing technology. As is frequently the case, a large part of the limitation in meeting requirements is the exacting demands on testing. Depending on requirements now undefined (such as equality of magnification of the four Cassegrain relay systems), new test techniques and hardware may have to be developed to provide information necessary for processing the elements.

8.2.1 Plano Optical Components

There appear to be no significant problems in manufacturing the parts with plano surfaces, provided the thickness/diameter aspect ratio is sufficiently large to assure mechanical stability of the mirrors. Conventional plano processing and testing techniques now available would be used to manufacture these elements.

8.2.2 Cassegrain Relay Optics

The $f/12.88$ and $f/30$ systems optics are so similar that the same processing approach would be used for both. The fabrication/test cycle is shown in figure 8.2.2-1. Since the aspheric departures from the best fit sphere are fractional wave for all the elements, the best fit sphere would be used as the reference surface from which measurements are made for all the Cassegrain elements. The processing/testing approaches are as follows.

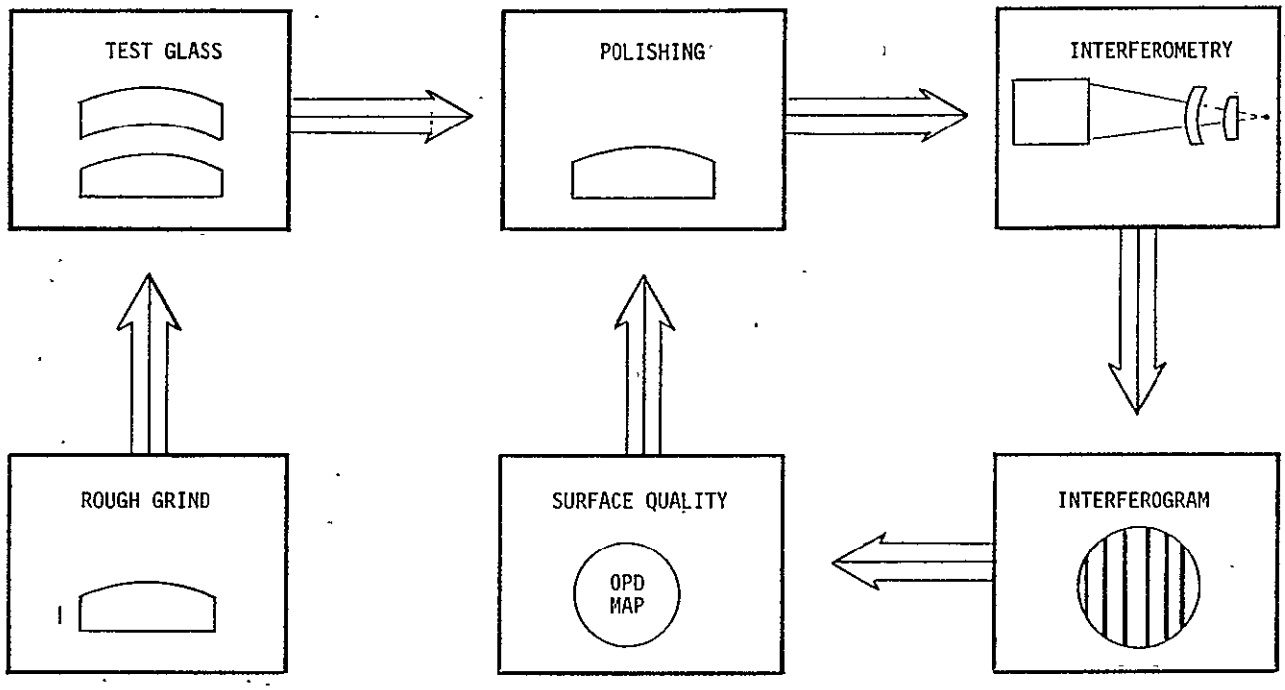

FABRICATION/TEST CYCLE

Figure 8.2.2-1

8.2.2.1 Cassegrain Secondary Mirrors

a. Fabricate test glasses (concave) to the required radii.

b. Calibrate test glasses for both absolute radius and surface accuracy. The absolute radius can be fabricated to 0.5 percent and measured to 0.1 percent or better. The surface sphericity can be defined to 0.005λ rms and any significant residual error in the glass would be backed out of the test data.

c. Fabricate the secondary mirrors to fit the test glass within 0.5λ and smooth for surface contour.

d. Aspherize the surfaces using ACT (area compensated tool) techniques. The area compensated tool minimizes ripple on the surface and can correct both

symmetrical and asymmetrical surface errors. Because the asphericity is small (less than 1λ) relative to the chosen sphere, the exact asphere formula would be entered into the software and then subtracted from the test data during its reduction so that the output would show the difference between the actual and the desired surface. This data would then permit the operator to see where material must be removed. Surface accuracies of about 0.01λ rms can be achieved using this technique. An additional advantage is that all of the four secondaries in a given set of Cassegrain systems will be alike for vertex radius within very narrow limits.

8.2.2.2 Cassegrain Primary Mirrors

a. Fabricate test glasses to the best fit spherical radius.
b. Calibrate test glasses for absolute radius and surface accuracy. The test glasses would not be used to test the surface of the primary mirrors, but would be used to control the radius during the processing steps. They would also be used as set-up masters for an interferometer so that the mirrors are tested at the correct radius of curvature.
c. Fabricate the primary mirrors by conventional techniques to the best fit sphere within 0.5λ. It would be necessary to insert a dummy piece of glass in the hole in the primary during processing so that roll-off of the interior edge is minimized. Care must be taken to prevent strain in this operation that might cause figure change when the dummy glass is removed.
d. Aspherize the optical surface using ACT techniques. Once again, the aspheric departure from the refer-

ence sphere is less than 1λ and the software would be used to generate data showing the departure of the surface as tested from the desired surface. There is one source of error for the primary and that is the positioning of the part being tested at the exact radius of the best fit sphere from the interferometer focal point. This can be accomplished by building a very rigid structure to hold the primary and interferometer at the correct locations. Establishing the mirror position would be done using the test glass in (b) above. Because the position of the primary would vary slightly from test to test, a figure accuracy of between 0.015λ and 0.01λ rms is predicted.

8.2.3 Reflective Pyramid

The most promising approach to the fabrication of this element is to make the four faces of the pyramid separately and identical, and then to cement them to a plate of the same material. Contact blocking the four elements to a base plate does not appear to be as feasible as cementing. New cements are now available that appear to meet environmental requirements. The most difficult requirements to satisfy for the pyramid are the sharpness of the intersections of the faces and the minimizing of the cosmetic defects on the polished surface. It is assumed that the accuracy required for the figure of the spherical surface is no more than a wavelength or two from spherical because it is directly in the focal plane. The processing approach is as follows:

a. Fabricate square blanks of glass to the exact outside dimensions required and oversize for thickness. It may be desirable to polish the edges and taper them slightly to facilitate assembly. Make the sides accurately perpendicular to the base.
b. Surround the blank with pieces of the same material as the blank to form a close fitting dummy that is round, oversize for thickness and having

the blank centered in the assembly. It is important that the dummy parts are tight fitting to the blank edges. Several new cements are available to fill the space between the dummy parts and the blank. These cements will process in a manner similar to glass and make it possible to create a very sharp edge on the finished piece.

c. Make the top and bottom of the assembly accurately parallel.
d. Cement a wedge of glass having the exact 9.105 degree angle at the proper orientation to the base of the assembly.
e. Make the top of the new assembly parallel to the base of the cemented wedge.
f. Grind and polish the spherical surface. Control the angle by maintaining constant edge thickness between the curved surface and the base. Control thickness by maintaining proper thickness of the assembly.
g. Disassemble by removing the cement with suitable solvents. Great care must be taken to avoid chipping the sharp edges of the prism segments.
h. Assemble the pyramid by cementing only the bases of the segments to the base plate. It should be possible to maintain a very narrow joint along the intersections of the four pieces.

By proper control of dimensions during process as noted above, the angular radius and physical dimensions can be held within specification. The sharpness of the face edges can only be estimated at this point, but it is believed that a "blind" area of only a few thousandths of an inch width is achievable. Surface quality of 20/5 can be reached with confidence. Quality of 10/1 may be achievable.

The fabrication/assembly procedure for the four facet pyramid mirror is summarized in figure 8.2.3-1.

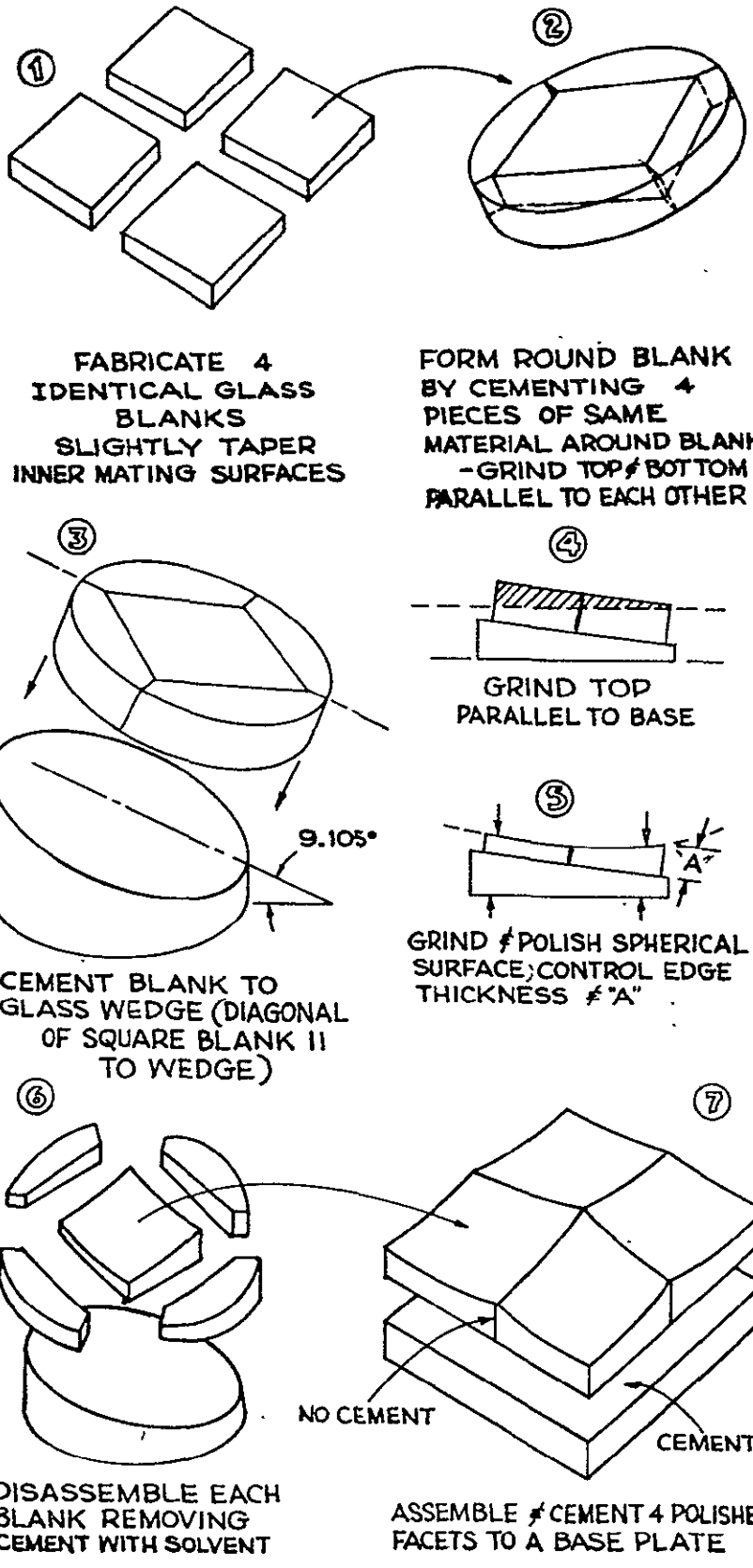

FABRICATION PYRAMID

Figure 8.2.3-1

EASTMAN KODAK COMPANY · 901 ELMGROVE ROAD · ROCHESTER, NEW YORK 14650

8.3 OPTICAL TESTING AND DATA ANALYSIS

Because of Kodak's constant concern for producing high quality products, test capabilities, as part of the quality assurance function, have been developed to very high levels. In addition, the importance of obtaining the minimum possible optical figure errors in optical imaging systems has resulted in development of specialized wavefront data reduction software which is directly

applicable to evaluating the WF/PC at all levels of camera buildup. The wavefront data is obtained interferometrically. The output can be topographic maps of the optical system, wavefront data in terms of peak-to-valley and rms wavefront errors, and optical aberration components of the wavefront errors. Statistical analyses are also available which yield probability values of achieving the measured optical performance.

The general philosophy for optical testing is summarized in table 8.3-1. The size of the optical elements indicate that this philosophy can be utilized in the WF/PC.

Table 8.3-1

OPTICAL TESTING - GENERAL PHILOSOPHY

- Full Aperture
- Full Field
- Zero-G - Simulation
- Operational Temperature
- Noise-Free Environment
- Test Configuration Designed Such That All Reference Test Optics Can Be Readily Calibrated

In the buildup of the WF/PC, five definable test levels can be identified. These five levels are shown in table 8.3-2. It is emphasized that the wavefront quality as dictated in the optical tolerance budgets (section 8.5) can be veri-

fied at each of the first four levels by using interferometric testing techniques and the interferometric evaluation software. At each of these four levels of testing error contributors (such as shown in table 8.3-3) are quantified. A typical test error budget is shown in table 8.3-4. In the example, the test error budget is for a reflective null test of a concave mirror and would be used at either the component or assembly levels.

Table 8.3-2

OPTICAL TESTING LEVELS

Level	
1	Component - Unmounted Optical Element
2	Assembly - Mounted Optical Element Use Same Test Configuration As In Component Test
3	Subsystem - Combine Assemblies For Example, Cassegrain Primary and Secondary Mirror Assemblies
4	System - Combine Subsystems and Assemblies For Example, Two (or Three) Mirror Cassegrain Relays and Pyramid Assembly
5	Camera - Combine System with CCD Detector

Table 8.3-3

TEST ERRORS

Short Term	Medium Term	Long Term
- Turbulence	- Support	- Interferometer
- Noise	- Thermal Distortion	- Calibration Errors
- Software Interpolation	- Alignment	- Alignment Fixture Biases (Spacing Rods, Indicators)

Table 8.3-4

TYPICAL TEST ERROR BUDGET
(REFLECTIVE NULL TEST)

Error Source	Uncertainty, σ_i (λRMS)
Short Term (16 Picture Average)	0.002
Thermal	0.003
Mount	0.005
Alignment	0.002
Interferometer	0.003
Interferometric Data Evaluation System	0.003
Null Residual (After Backout)	0.002
	$\sigma_T = \sqrt{\sum_i \sigma_i^2} = 0.008$

The WF/PC buildup in level four would include the total WF/PC optical assembly without CCD and CCD coverplate. Optical performance at the total camera level (level five) can be verified by evaluating the point spread function directly on the CCD. Performance data, which can be generated mathematically, can include the radial energy distribution, rms blur circle, rms wavefront error and optical aberration components of the wavefront errors. (Note: This test would include a simulated star source from an OTA simulator.)

A summary of the optical test instrumentation which would be used during the entire buildup is shown in table 8.3-5.

Table 8.3-5

OPTICAL TEST INSTRUMENTATION

- Interferometer
  - Wavefront
  - Alignment
  - Focal Length
- Theodolite/Axicon
  - Line of Sight Reference
  - Preliminary Alignment
  - Monitor Reference Optics
  - Initial Test Set-Up
- Focal Surface Reference Fixture (FSRF)
- Point Projecting Microscope

8.4 OPTICAL COMPONENT TESTING

From a testing viewpoint, the unmounted optical components in the WF/PC fall into three groups: plano surfaces (folding mirrors, filters and coverplates), aspherical surfaces (Cassegrain primary and secondary mirrors), and spherical surfaces (pyramid mirror facets).

Two different types of test configurations (in-process and acceptance) have been established for each group. The in-process test configuration would be utilized during the polishing/test cycle ($\leq 0.5\ \lambda$ P-V). (Note: In the early grind stages of fabrication, test instrumentation such as spherometers and test glasses would be used.)

The Fizeau test configuration for a plano surface is shown in figure 8.4-1 and would be used for both the in-process and acceptance test. In this test configuration, the clear aperture of the surface under test has to be less than or equal to the collimating lens diameter. (Note: The largest WF/PC plano surface has a diameter of approximately 5.2 inches.)

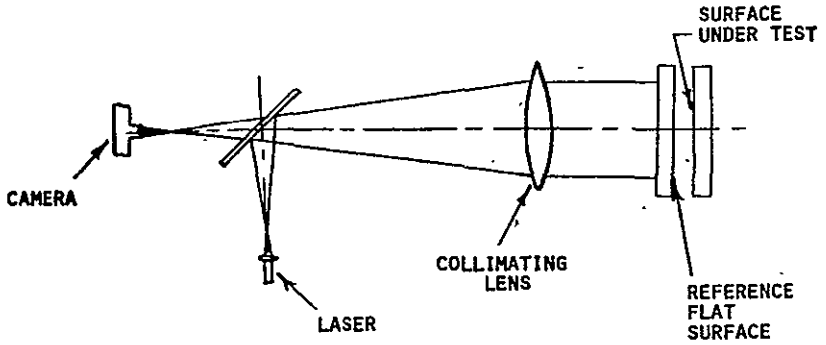

FIZEAU TEST CONFIGURATION
(PLANO SURFACE)

Figure 8.4-1

The testing of aspheric surfaces (either conic aspheric or general aspheric) is usually performed utilizing an additional test optic called a null corrector. The purpose of the null corrector is to introduce a wavefront departing from spherical of a magnitude and sign to cancel effectively (null) the wavefront reflected from the surface being tested. If the surface under test is in error, interference fringes will appear which will describe the departure from the desired asphere. An obvious disadvantage of a null test configuration is the addition of the null corrector which has to be calibrated to the required accuracy (see table 8.3-4). Two different types of null test configurations are shown in figures 8.4-2 and 8.4-3. In the reflective null test configuration, the test has the disadvantage of placing the interferometer between the reflective null and the optic being tested. The test is also very sensitive to inaccuracies in the reflective null calibration since the test wavefront is reflected from the test optic twice. However, since only one test optic surface is used, a relatively low bias (spherical aberration) is introduced. In the refractive null test configuration, the interferometer is placed outside the path of the null corrector and the mirror, thereby minimizing the noise. However, the refractive null is difficult to calibrate and particular attention has to be given to the design fabrication and assembly of the null lens elements. A radially symmetric error (mainly primary spherical aberration) exists which constitutes an uncertainty and cannot be backed out of the test.

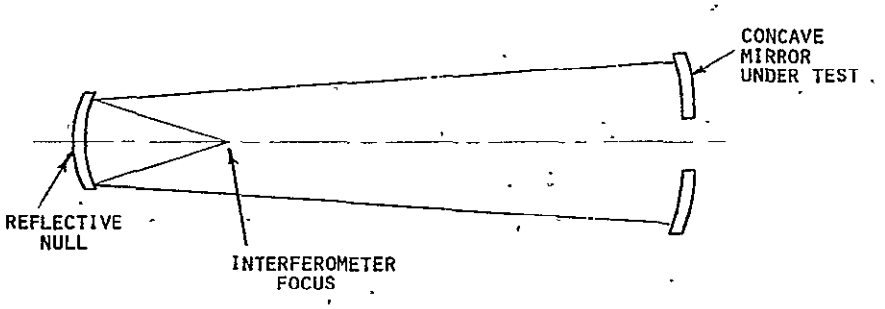

REFLECTIVE NULL TEST CONFIGURATION

Figure 8.4-2

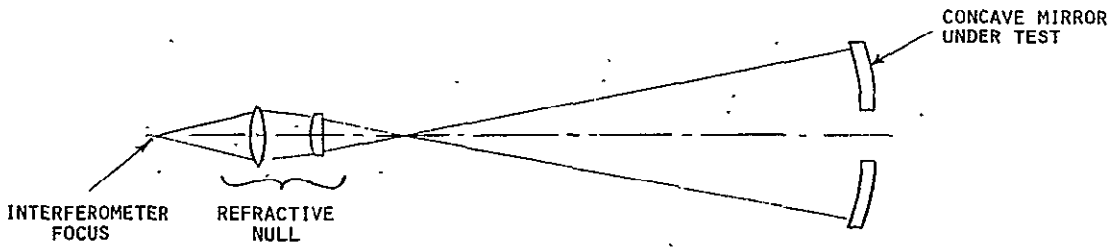

REFRACTIVE NULL TEST CONFIGURATION

Figure 8.4-3

Shown in figure 8.4-4 are the aspheric departures (referenced to the vertex sphere) for the $f/12.88$ and $f/30$ primary mirrors. It should be noted that the maximum aspheric departure is approximately 1.2λ for the $f/12.88$ primary mirror. The difference in asphericity between the optimized general aspheric $f/12.88$ primary mirror and the baseline conic aspheric $f/12.88$ primary mirror is shown in figure 8.4-5. The maximum difference in this case is approximately 0.08λ. Shown in figure 8.4-6 are aspheric departures referenced to other spherical surfaces. This figure indicates that a spherical reference surface (preferred for manufacturing) can be found to reduce the maximum aspheric departure to 0.3λ. These aspheric departure levels will show up on the interferograms as very nearly straight line fringes (closely nulled). This aspheric departure can be handled directly in the interferometric evaluation software and the need for the additional test optic (null corrector) is eliminated. The recommended acceptance test configuration for the primary mirrors is shown in figure 8.4-7. Point ρ is positioned at the radius corresponding to the best fit sphere. The

aspheric departure ($\leq 0.3\lambda$ P/V) would be "backed out" in the computer interferometric evaluation software. An alternate acceptance test configuration is shown in figure 8.4-8. In this test configuration the test utilizes the fact that an ellipsoid (prolate spheroid) has two separated foci on the same side of the mirror under test. The in-process test configuration is shown in figure 8.4-9. In this Fizeau arrangement a convex reference surface is used.

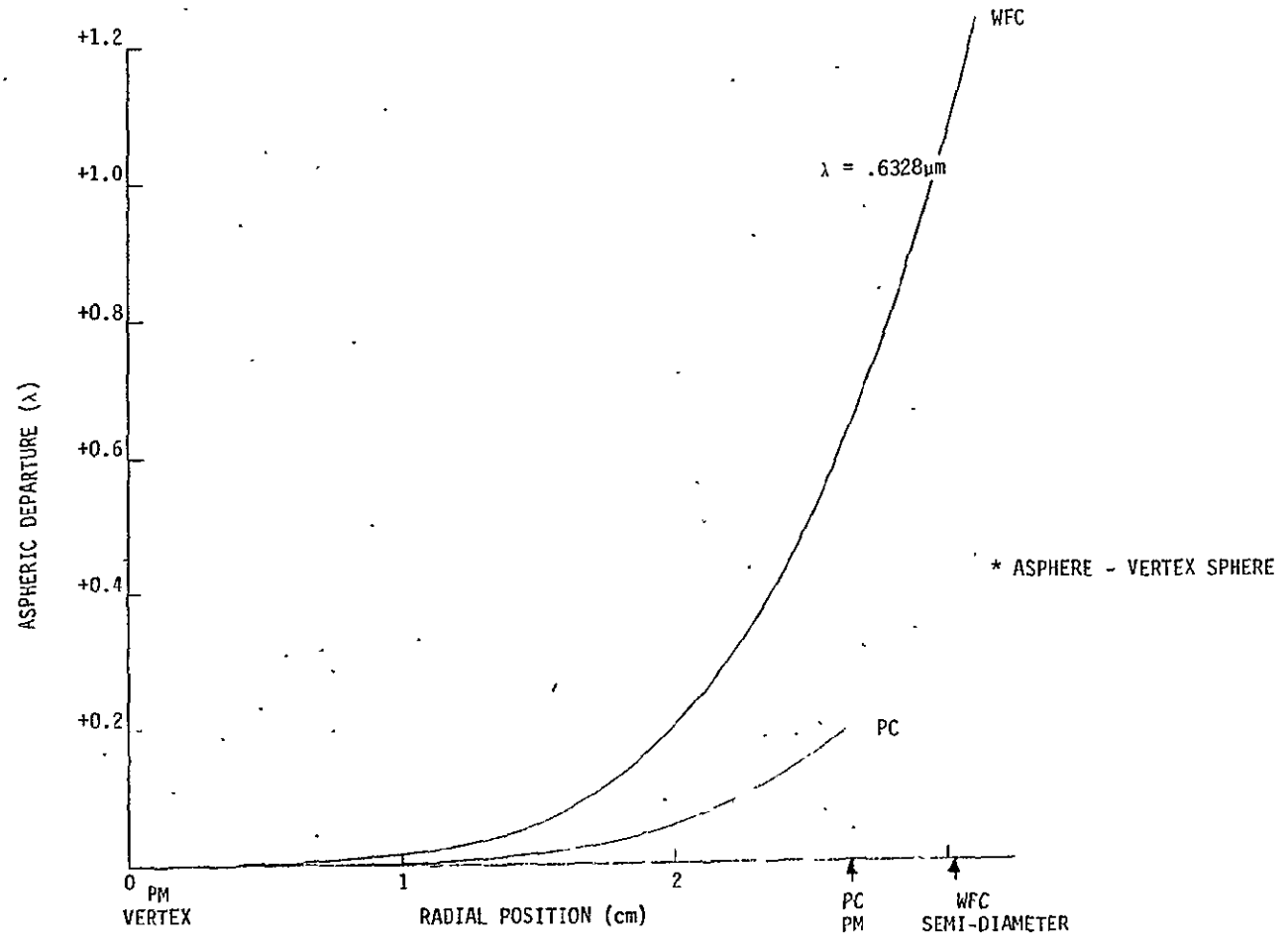

ASPHERIC DEPARTURE*
(PRIMARY MIRROR)

Figure 8.4-4

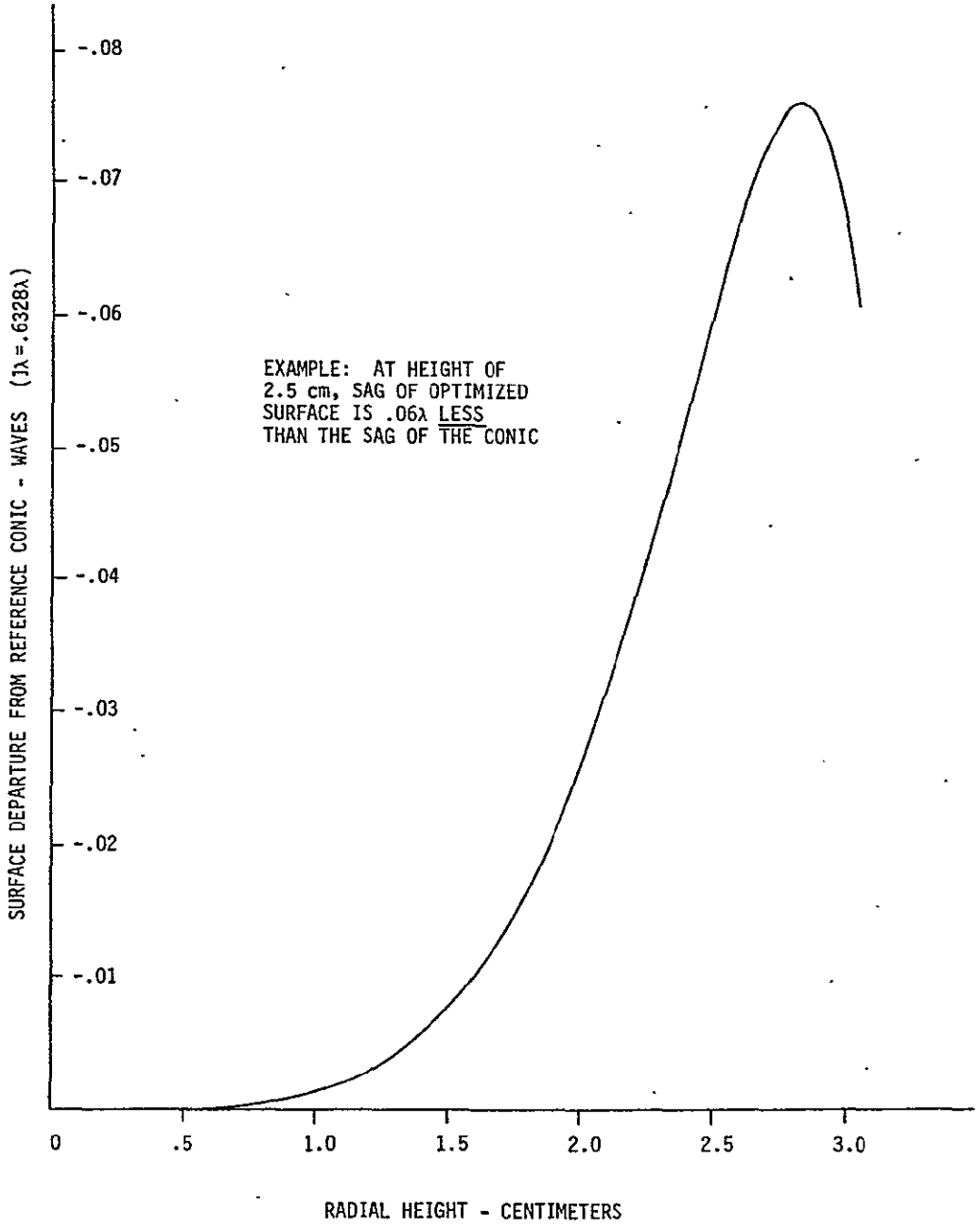

DIFFERENCE IN ASPHERICITY BETWEEN OPTIMIZED *f*/12.88
RELAY PRIMARY MIRROR AND BASELINE CONIC PRIMARY MIRROR

Figure 8.4-5

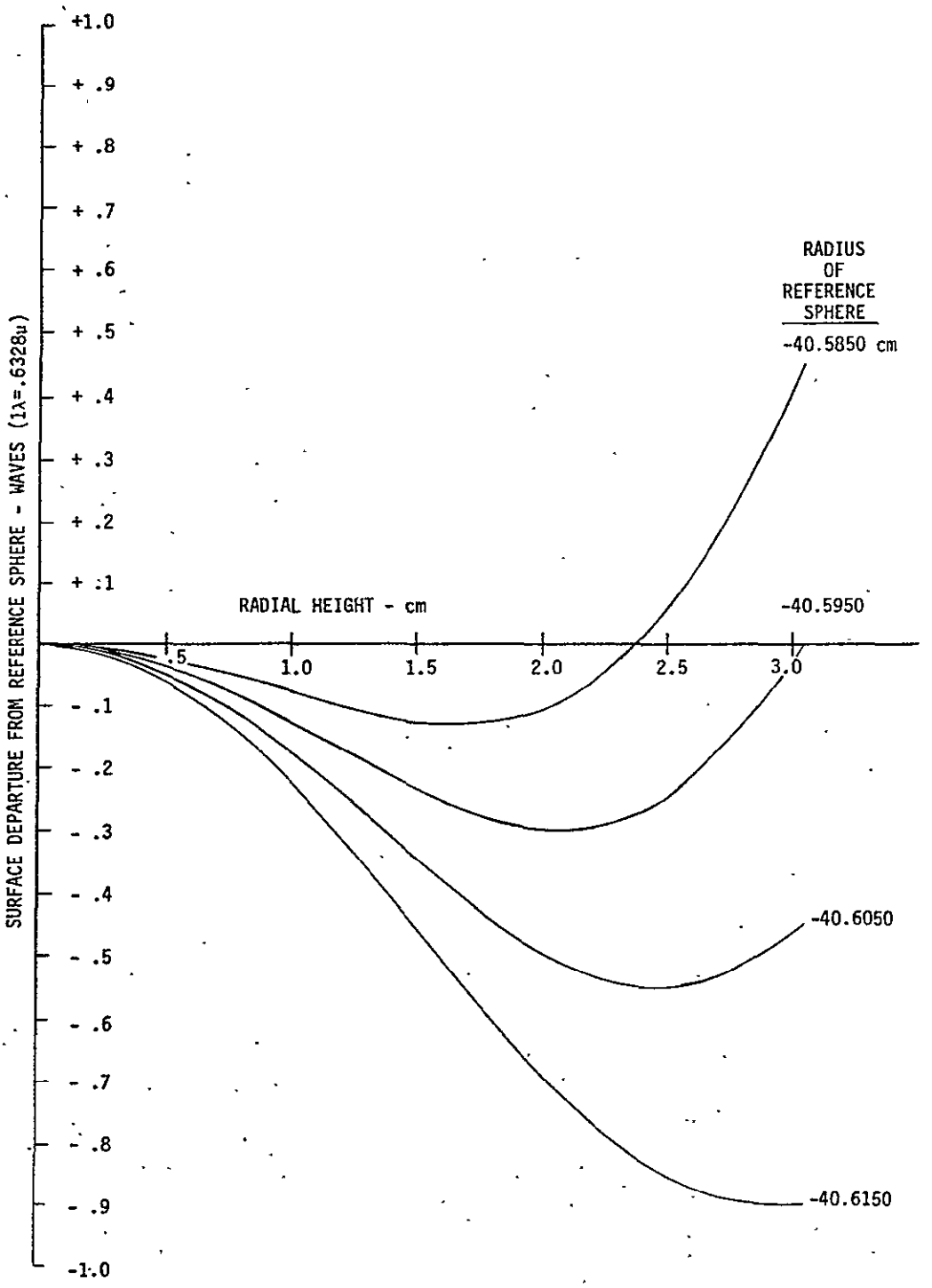

ASPHERIC DEPARTURE OF *f*/12.88 RELAY PRIMARY MIRROR WITH RESPECT TO VARIOUS REFERENCE SPHERES

Figure 8.4-6

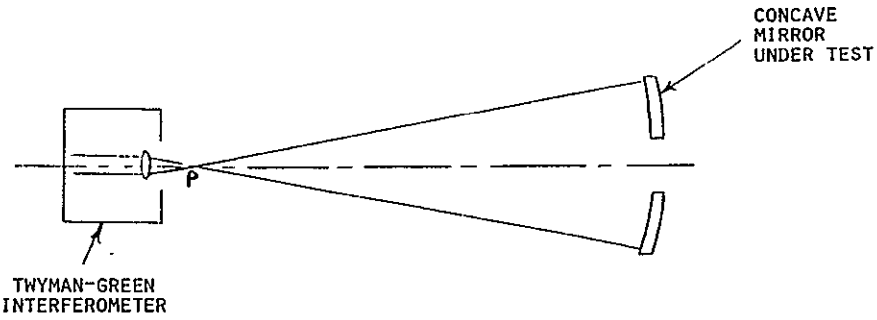

POINT P POSITIONED AT RADIUS CORRESPONDING TO BEST FIT SPHERE (MAXIMUM ASPHERIC DEPARTURE OF 1.2λ "BACKED OUT" IN COMPUTER INTERFEROMETRIC EVALUATION).

TWYMAN-GREEN TEST CONFIGURATION
(ACCEPTANCE)

Figure 8.4-7

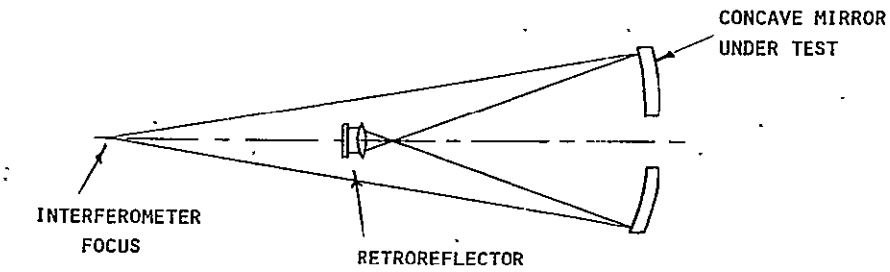

UTILIZES THE FACT THAT AN ELLIPSOID HAS TWO SEPARATED FOCI ON THE SAME SIDE OF THE MIRROR UNDER TEST.

RETROREFLECTOR TEST CONFIGURATION
(ACCEPTANCE)

Figure 8.4-8

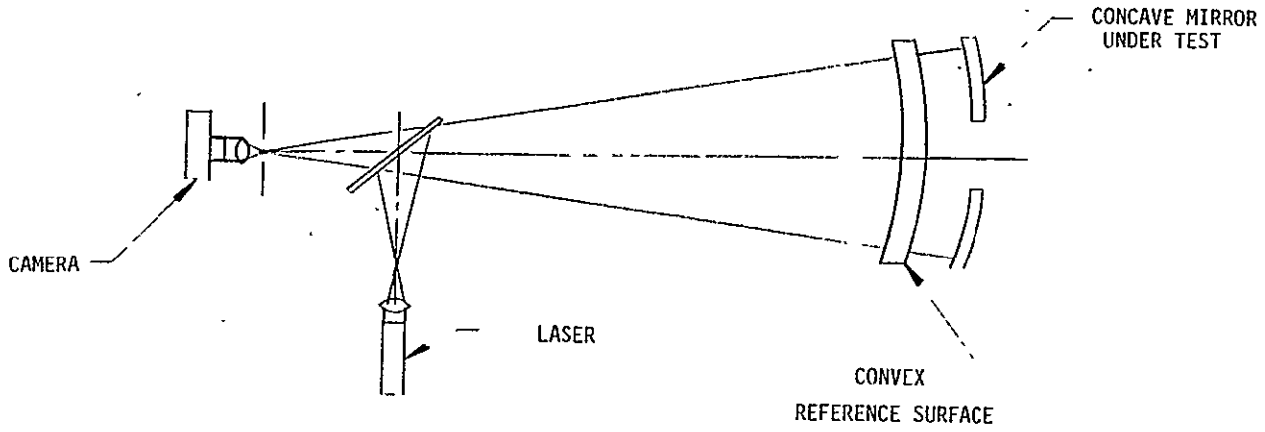

FIZEAU TEST CONFIGURATION
(IN-PROCESS)

Figure 8.4-9

The aspheric departures for the secondary mirrors are shown in figure 8.4-10. It should be noted that the maximum aspheric departure is approximately 0.2 λ for the $f/12.88$ secondary mirror. Shown in figure 8.4-11 is the Fizeau test configuration which would be used for both the in-process and acceptance tests. The aspheric departure ($\leq 0.2\lambda$ P/V) would be "backed out" in the computer interferometric evaluation software. In the acceptance testing, the spherical test glass would be aluminized for 40 to 80 percent reflectance, producing multiple beam fringes with the highly reflective coated convex secondary mirror. An alternate acceptance test configuration is shown in figure 8.4-12. Since the hyperboloid has two foci light rays directed toward the focal point behind the hyperbolic mirror will, after reflection, pass through the other focus. Therefore, the Hindle test provides an exact null test for a perfect hyperboloid with the aid of a larger concave spherical test optic (Hindle sphere).

Shown in figure 8.4-13 is the test configuration to be used for the spherical pyramid mirror facet. This test configuration would be used for both the in-process and acceptance tests. Since the facet is approximately $f/100$, an oversized test plate is needed to measure the radius to within the allowable tolerance (±0.2 percent).

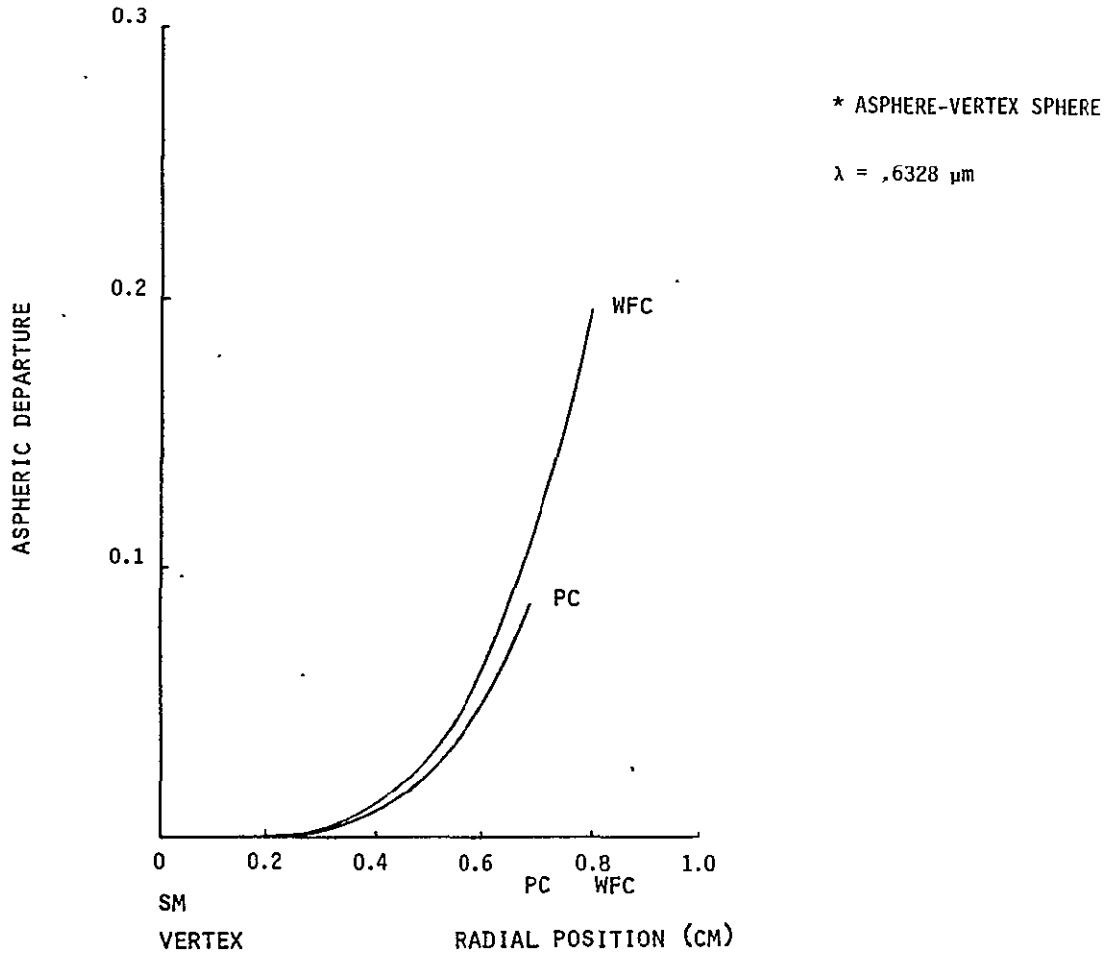

ASPHERIC DEPARTURE* (SECONDARY MIRROR)

Figure 8.4-10

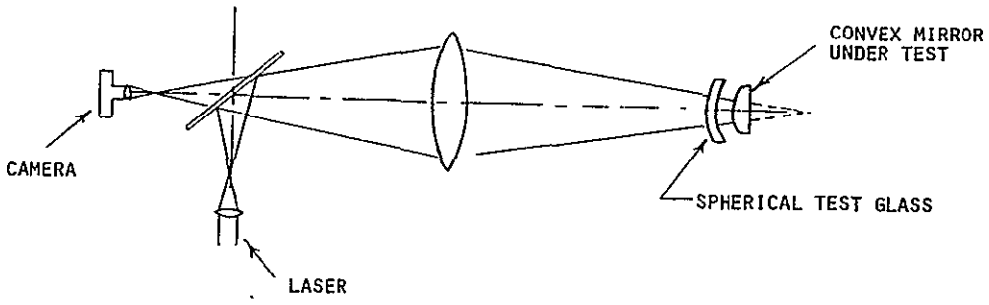

FIZEAU TEST CONFIGURATION

Figure 8.4-11

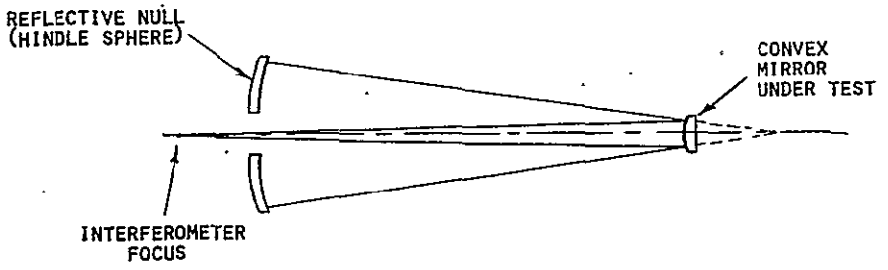

REFLECTIVE NULL TEST CONFIGURATION
("HINDLE" TEST)

Figure 8.4-12

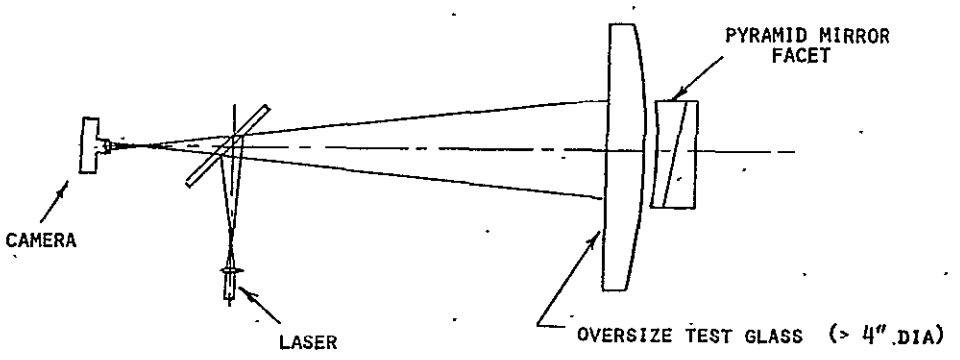

PYRAMID MIRROR TEST CONFIGURATION
(FIZEAU - TEST GLASS)

Figure 8.4-13

In the fabrication approach chosen (see section 8.2), four facets would be fabricated independently and then combined into a four faceted pyramid mirror (figure 8.4-14). The acceptance test configuration for the total mirror is shown in figure 8.4-15. In this test configuration, a point projecting microscope would be installed at four locations on a reference template. A spherical wavefront from the point projecting microscope can only return through the hole if the facet is located in its proper location.

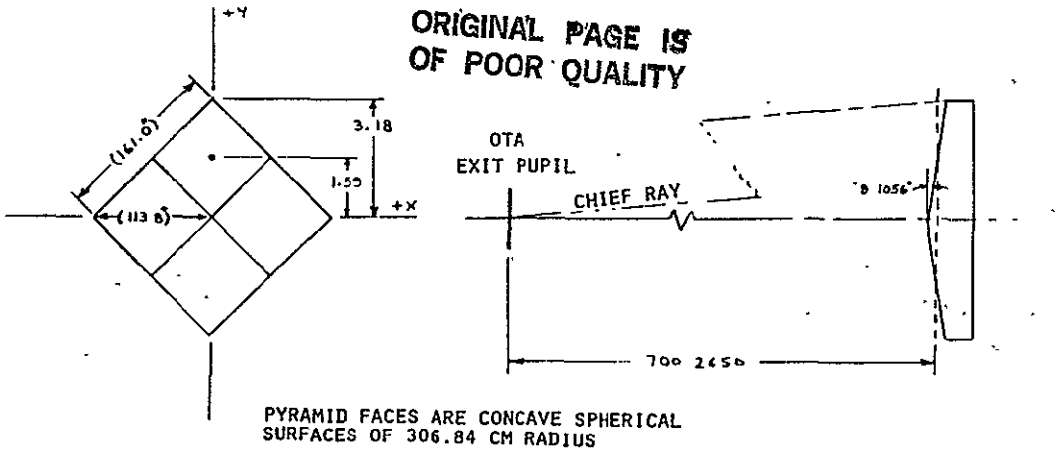

REFLECTING PYRAMID
(PHYSICAL DIMENSIONS AND ANGULAR DIMENSIONS IN OBJECT SPACE)

Figure 8.4-14

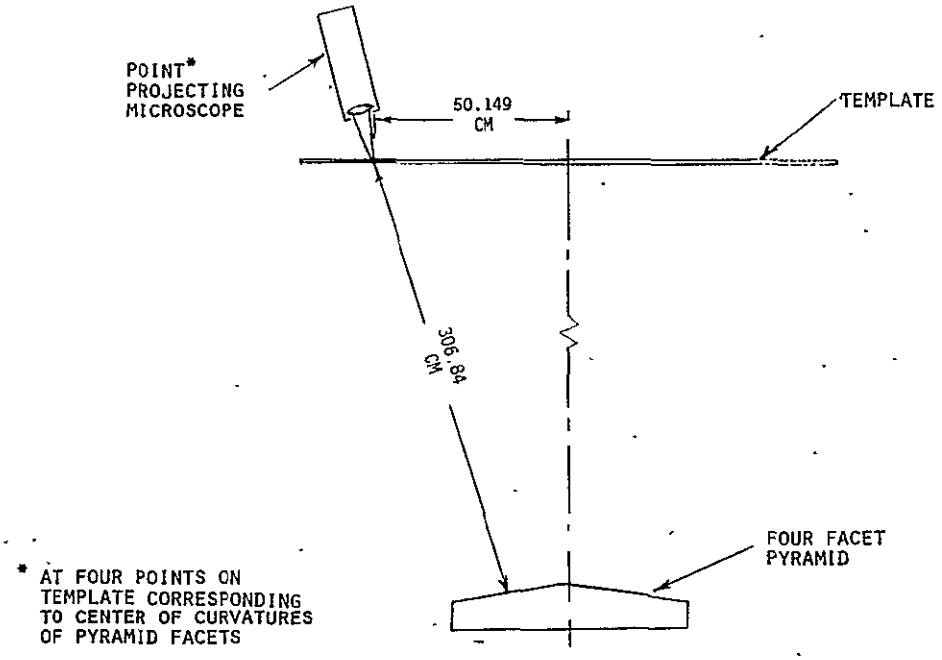

PYRAMID MIRROR ACCEPTANCE TEST CONFIGURATION

Figure 8.4-15

Three spatial frequency domains have been specified for each optical component (see section 8.2). The testing configurations summarized in table 8.4-1 would be used to verify the low spatial frequency figure errors as allocated in the wavefront budgets (see section 8.5) and, the low to mid spatial frequency autocorrelation length requirements. In the high spatial frequency domain, rms surface roughness has been specified. Two techniques are usually used. The first measures the resultant effect of veiling glare directly and calculates the rms roughness (figure 8.1.3-1). The second and preferred method measures the rms surface roughness using a device such as a FECO interferometer.

Table 8.4-1

WF/PC OPTICAL COMPONENT TEST CONFIGURATIONS

	In-Process	Acceptance
WFC Primary Mirror	Fizeau - Convex Reference	Twyman-Green - At Best Fit
PC Primary Mirror	Sphere with Aspheric Backout	Radius with Aspheric Backout Alternate - Retroreflector Test Configuration
WFC Secondary Mirror	Fizeau - Concave Reference	Fizeau - Concave Reference
PC Secondary Mirror	Sphere with Aspheric Backout	Sphere with Aspheric Backout (Multiple Beam Fringes) Alternate - Hindle Test Configuration
Pyramid Mirror	Fizeau - Convex Reference Sphere	Fizeau - Convex Reference Sphere
Plano	Fizeau	Fizeau

Scratch/dig requirements would be verified directly on the optical surface using a measuring microscope with calibrated scale.

8.5 OPTICAL TOLERANCE BUDGETING

Based on the predicted "manufactured" system performance, sensitivity analysis and assembly buildup philosophy, a wavefront error budgeting philosophy is established. Individual error contributors are defined and toleranced. These tolerances are then compared with estimated manufacturing and testing capability, establishing a degree of confidence in the manufacturability of the system.

A real system must be manufactured to a practical set of fabrication tolerances. A figure of merit must be established which can be used to tolerance individual error contributors and serve as a performance indicator for meeting the overall system objectives during assembly buildup. For an optical imaging device, the rms wavefront error is an excellent figure of merit. Shown in figures 8.5-1 and 8.5-2 are the effects of performance degradation on a combined OTA with WF/PC. The designed curves in these cases are the actual MTF calculations as established in sections 5.0 and 6.0. Inherent in the manufacture of a combined OTA with WF/PC is a maximum rms wavefront error of 0.075λ due to the OTA alone. The addition of an independent WF/PC optical system to the OTA must minimize any wavefront error increase to the inherent 0.075λ rms wavefront error.

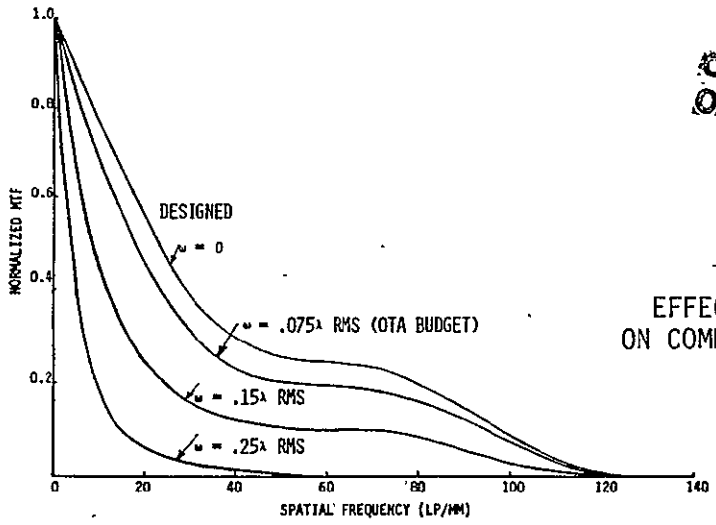

EFFECT OF STATIC WAVEFRONT ERROR
ON COMBINED OTA WITH WIDE FIELD CAMERA

Figure 8.5-1

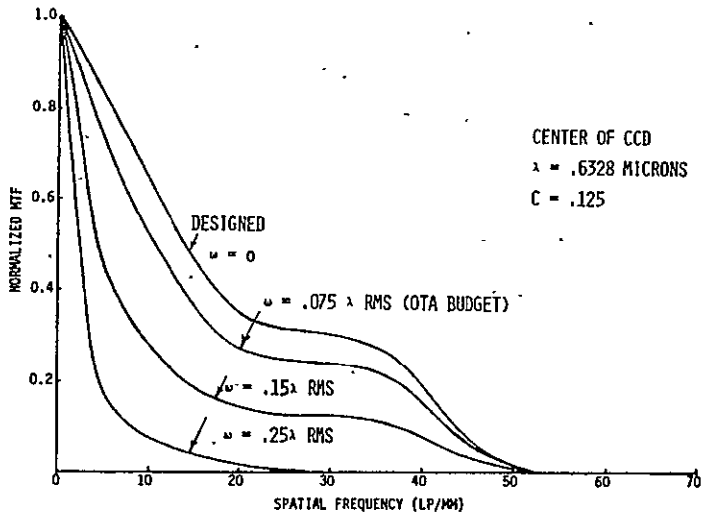

EFFECT OF STATIC WAVEFRONT ERROR
ON COMBINED OTA
WITH PLANETARY CAMERA

Figure 8.5-2

A manufactured optical system will have its wavefront quality (rms wavefront error) degraded by optical element misalignment and focus errors. The sensitivity analysis (section 7.8) establishes the amount of degradation introduced by the misalignment and focus errors. For example, a budgeting philosophy for the two mirror Cassegrain is shown in figure 8.5-3.

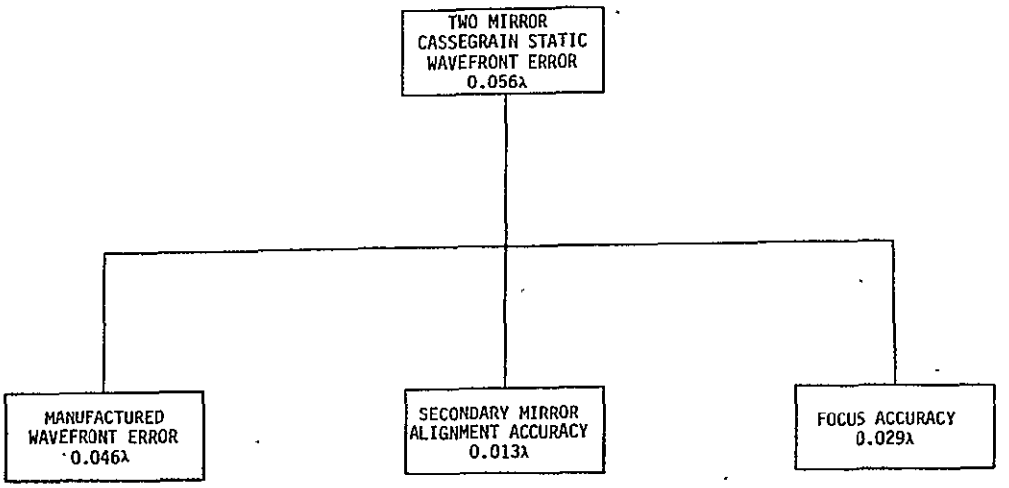

TWO MIRROR CASSEGRAIN WAVEFRONT ERROR
(RMS ERROR AT 0.6328 MICRONS)

Figure 8.5-3

In this philosophy the primary mirror is assumed the fixed reference for the Cassegrain. The manufactured two mirror Cassegrain wavefront quality will be degraded by secondary mirror misalignment and focus errors relative to the primary mirror and misalignments of the focal plane structure relative to the secondary mirror focal surface. In this case the maximum allowable degradation of the manufactured two mirror Cassegrain wavefront quality is the two mirror Cassegrain static wavefront quality. (The manufactured system without misalignment and focus errors would be better than the two mirror Cassegrain static wavefront quality.) With this philosophy the misalignment and focus error values must be retained below the given values. If manufacturing tolerances indicate that passive mounting techniques cannot retain the wavefront error within allowable budget values, active alignment techniques are required to bring the element misalignment and focus errors back within the allowable static wavefront error. (Note: For the OTA, this is the case. An optical

control subsystem is utilized to maintain two tilts, two decenters, and one despace on the secondary mirror within the allocated budgets.)

It should also be emphasized that the Cassegrain primary mirror can only be used as a "fixed" reference for the optical system if the following assumptions are true: (1) primary mirror is dimensionally stable, (2) primary mirror is thermally stable, (3) primary mirror location relative to focal surface is stable, (4) ground testing accuracy is sufficient to establish alignment, and (5) ground testing provides adequate zero 'g' simulation.

Each optical element is allocated separate budgets in the manufactured wavefront budget. A manufactured wavefront budget for the two mirror Cassegrain is shown in figure 8.5-4. In this budget two separate optical assemblies (mirror with mount) are manufactured and then combined to form the final manufactured system. Each optical assembly is further broken down into an allocation for the optical component (without mount) and the mount itself. The contributors should then be compared with estimated manufacturing and testing capability (see section 8.4). Shown in figures 8.5-5 and 8.5-6 are the secondary mirror alignment and focus error budgets. As indicated, if these budgets can be met in the assembly of the Cassegrain, no active alignment techniques will be required to bring the element misalignment and focus errors back within the allowable static wavefront error.

MANUFACTURED WAVEFRONT BUDGET

Figure 8.5-4

PRIMARY MIRROR ASSEMBLY		SECONDARY MIRROR ASSEMBLY	
POLISHING	0.030λ	POLISHING	0.030λ
COATING	0.003λ	COATING	0.003λ
MOUNT STRAIN	0.005λ	MOUNT STRAIN	0.005λ
RSS	0.031λ	RSS	0.031λ

PRIMARY AND SECONDARY MIRROR ASSEMBLIES	0.044λ
ASPHERIC MISMATCH	0.010λ
THERMAL VARIATIONS	0.010λ
TOTAL RSS	0.046λ

CONTRIBUTOR	RMS WAVEFRONT ERROR (@ 0.6328 MICRONS)
INTERFEROMETRIC DETERMINATION OF BEST ALIGNMENT	0.012λ
THERMAL/STRUCTURAL VARIATIONS	0.004λ

SECONDARY MIRROR ALIGNMENT ERROR BUDGET

Figure 8.5-5

CONTRIBUTOR	RMS WAVEFRONT ERROR (@ 0.6328 MICRONS)	2σ FOCUS ERROR (MICRONS)	
		WF	PC
FOCAL SURFACE DEFINITION	.021λ	61.7	334.3
CCD DETECTOR INSTALLATION	.004λ	11.8	65.6
THERMAL STABILITY			
MIRRORS	.008λ	23.5	13.1
METERING STRUCTURE	.018λ	52.9	295.1
CCD SUPPORT STRUCTURE	.004λ	11.8	65.6

FOCUS ERROR BUDGET

Figure 8.5-6

It should be emphasized that three definable levels of testing have been identified in the assembly of the two mirror Cassegrain (see table 8.3-2). Logical test levels are at the component (unmounted optical element), assembly (mounted optical element) and subsystem (combination of primary mirror assembly and secondary mirror assembly).

The overall system requirements (combined OTA with WF/PC optics), as established in section 4.0, specify that the axis static wavefront error must be no more than 0.108 λ rms under orbital operational conditions. Shown in figure 8.5-7 is a preliminary allocation for the Cassegrain relays and the additional WF/PC optics. Further assembly buildup philosophy and tolerance breakdowns are needed in this area.

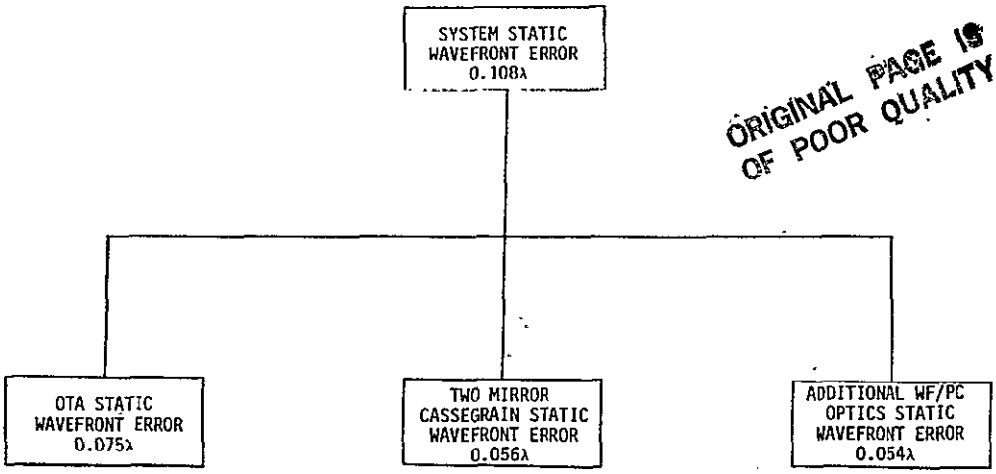

SYSTEM WAVEFRONT ERROR
RMS ERROR AT 0.6328 μm)

Figure 8.5-7

8.6 DEPTH OF FOCUS

Shown in figure 8.6-1 is the relationship between OTA image quality degradation and a focal shift at the OTA focal plane. The focal shift at the OTA focal plane causes a focal shift at the WF/PC focal plane. The relationship between WF/PC image quality degradation and a focal shift at the WF/PC focal plane is shown in figure 8.6-2. The depth of focus corresponds to the longitudinal displacement in the focal plane location as allocated in the wavefront budget. Since a focus accuracy of 0.029 λ rms has been allocated (see figure 8.5-3), a depth of focus for the wide field camera of ± 85 microns and for the planetary camera of ± 475 microns is determined.

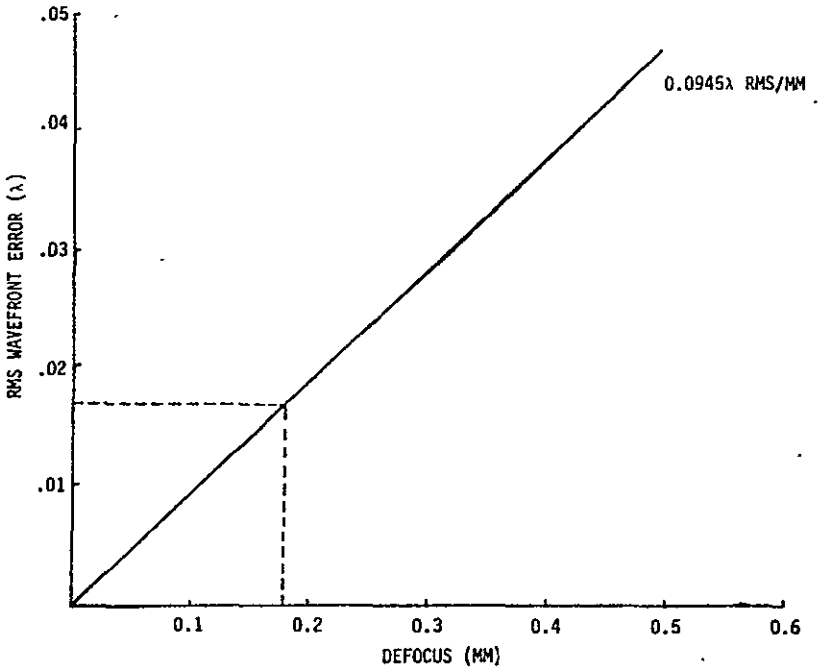

RMS WAVEFRONT ERROR VS DEFOCUS
(OTA FOCAL SURFACE)

Figure 8.6-1

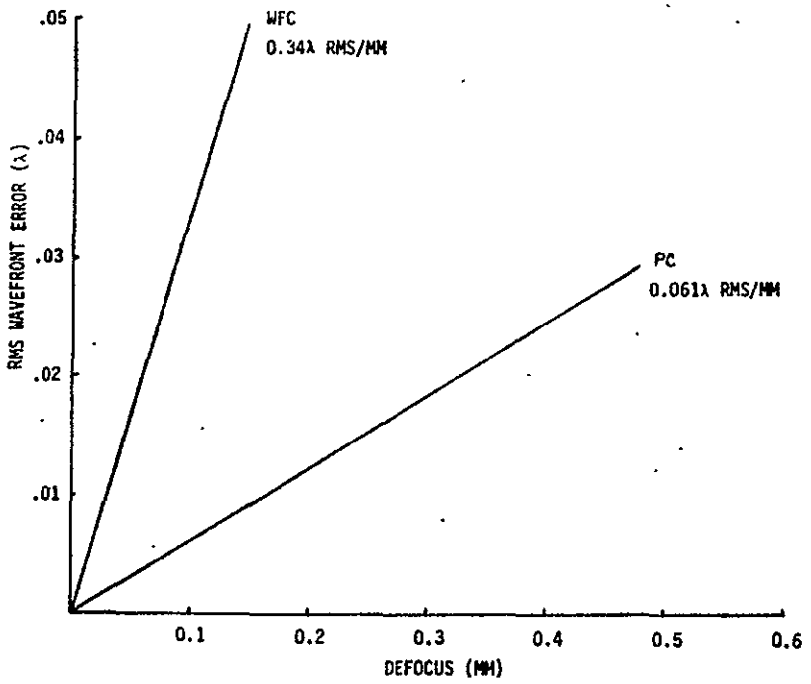

RMS WAVEFRONT ERROR VS DEFOCUS
(WF/PC FOCAL SURFACE)

Figure 8.6-2

8.7 OPTICAL TESTING - TWO MIRROR CASSEGRAIN

The two mirror Cassegrain acceptance test configuration is shown in figure 8.7-1. This configuration is based on the fact that the two mirror Cassegrain is a finite conjugate optical system. On the object side, an interferometer is installed with an $f/24$ objective. On the image side, a retroreflector is installed with an $f/12.9$ objective for the Wide Field Camera and an $f/30$ objective for the Planetary Camera. This retroreflector can be installed at other points in the field mapping out the focal surface contour (focal surface reference fixture -- FSRF). In theory, a spherical wavefront emanating from the interferometer will pass through the Cassegrain twice after reflection from the retroreflector. Deviation in the interferometric pattern from the spherical reference will describe the Cassegrain performance. Shown in figures 8.7-2 and 8.7-3 are the performance predictions (at the center of the CCD) for the WF/PC Cassegrain optics. Based on the optical tolerance budgeting of section 8.5, the OQF at the center of the CCD should be greater than or equal to 88 percent for level 3 testing (table 8.3-2).

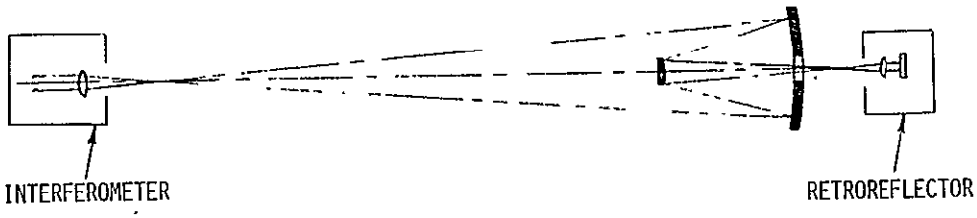

TWO MIRROR CASSEGRAIN ACCEPTANCE TEST CONFIGURATION

Figure 8.7-1

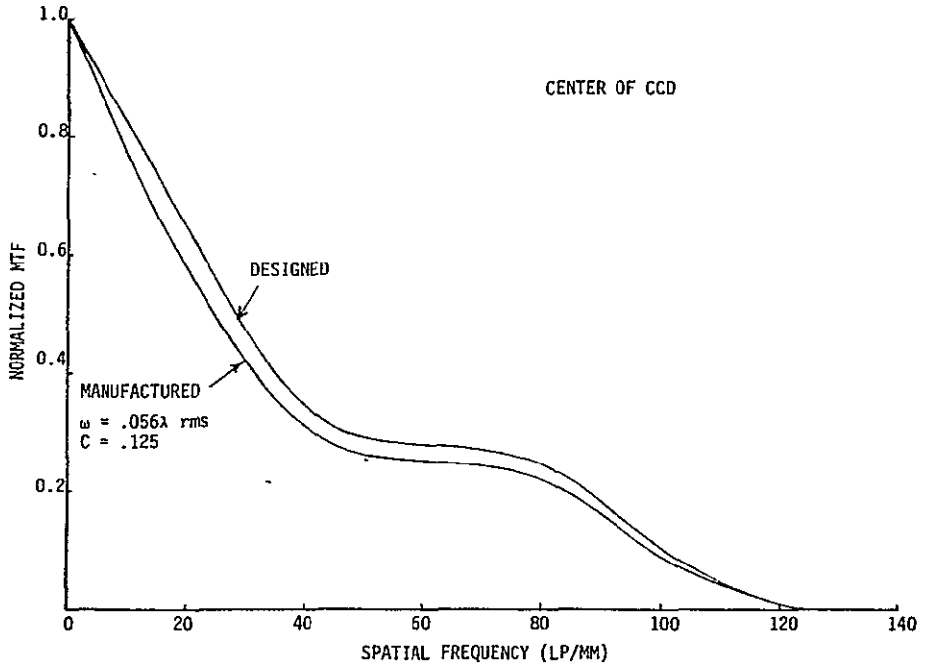

WIDE FIELD CAMERA PERFORMANCE PREDICTION
(TWO MIRROR CASSEGRAIN)

Figure 8.7-2

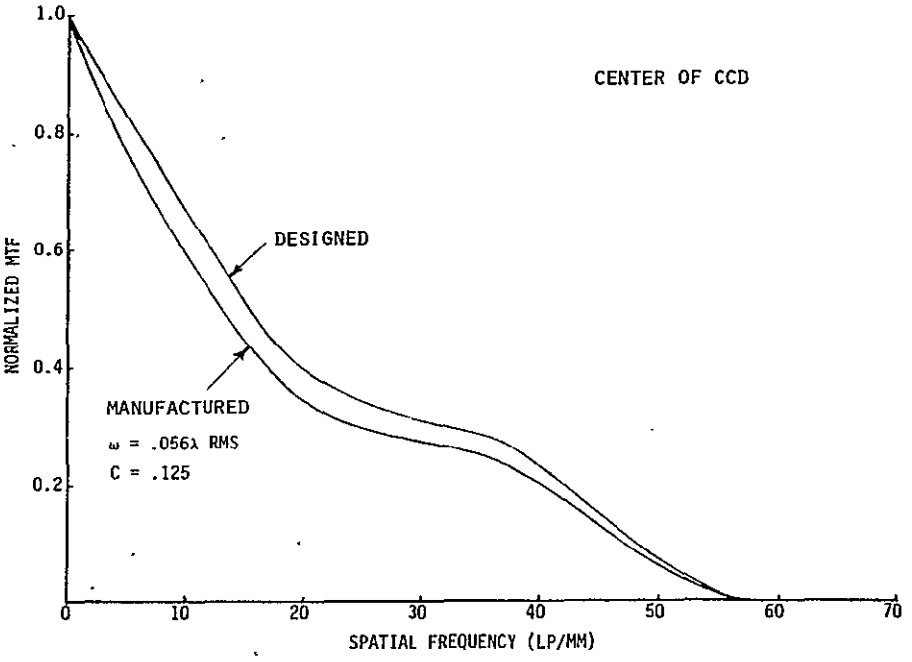

PLANETARY CAMERA PERFORMANCE PREDICTION
(TWO MIRROR CASSEGRAIN)

Figure 8.7-3

Shown in table 8.7-1 is a preliminary assembly buildup sequence for the two-mirror Cassegrain. This sequence is based on interferometric testing for compliance of wavefront quality and secondary mirror alignment. During interferometric alignment, the wavefront error would be measured at four symmetric points in the field. The procedure utilizes the interferometric data evaluation software in which the design residuals are first removed (backout). The wavefront is evaluated for coma and astigmatism.

The equations of table 8.7-2 are then solved using these aberrations. The results are averaged at the four field points, yielding the amount of decenter and tilt to be introduced into the secondary mirror. With this method, an optimum location of the secondary mirror with respect to the "fixed" reference primary mirror would be determined after several iterations.

Table 8.7-1

TWO MIRROR CASSEGRAIN OPTICAL TESTS

1.	Rough alignment	- Align secondary mirror assembly (SMA) to primary mirror reference using theodolite; set primary to secondary airspace using metering rod.
2.	Coarse alignment	- Interferometry; visually minimize coma and astigmatism.
3.	Fine alignment	- Interferometry; four field positions; lock SMA .
4.	Wavefront measurement	- On-axis and selected field points, nominal focus: specified misalignment and defocus (the SMA will be aligned and focused with respect to the primary mirror assembly (PMA) to within the allowable two mirror Cassegrain "static" wavefront error).
5.	Focal surface determination	- Thru-focus interferometry at several field positions; interface mount pads to compensate field tilt; determine focal surface relative to FSRF.
6.	Focal length and back focus determination	- Use selected field point pairs (nodal test).
7.	Set line of sight reference devices	- Theodolites and auxiliary mirrors.
8.	Baffle check	- Auxiliary camera and diffuse light source.
9.	Field size check	- Auxiliary viewing screen and light source.
10.	Final performance check	- Repeat portions of steps 4 and 5.

Table 8.7-2

ALIGNMENT EQUATIONS

$$\text{Decenter}_x = -K_1\ OPD_c\ \text{Sin}\ \phi + K_2\ OPD_a\ \text{Sin}\ (2\theta - \gamma)$$

$$\text{Decenter}_y = K_1\ OPD_c\ \text{Cos}\ \phi - K_2\ OPD_a\ \text{Cos}\ (2\theta - \gamma)$$

$$\text{Tilt}_x = K_4\ OPD_c\ \text{Cos}\ \phi - K_3\ OPD_a\ \text{Cos}\ (2\theta - \gamma)$$

$$\text{Tilt}_y = K_4\ OPD_c\ \text{Sin}\ \phi - K_3\ OPD_a\ \text{Sin}\ (2\theta - \gamma)$$

where:

OPD_c is coma magnitude; ϕ is coma angle

OPD_a is astigmatism magnitude; θ is astigmatism angle

γ is field point azimuth

9.0 FOCUS ANALYSIS

9.0 FOCUS ANALYSIS

Many perturbations in the OTA + WF/PC optical system have a common characteristic: they cause the image at the relay focal plane (CCD detector) to become defocused. This focus error can be removed, if the perturbation is not too large, by a corrective adjustment in the axial position of the pyramid.

A general analysis of pyramid refocusing applies to all these perturbations. They include:

1. Axial displacement of the WF/PC assembly with respect to the OTA image surface.
2. Axial displacement of the OTA image surface with respect to the WF/PC due to perturbations in the OTA such as a change in its primary/secondary mirror spacing.
3. Translation of the WF/PC pickoff mirror with respect to fixed OTA and relay optics.
4. Axial displacement of pyramid with respect to fixed OTA and WF/PC.

The original intent of the focus analysis task was an evaluation of conditions (1) and (2) above. Because the analysis for these conditions could be extended to conditions (3) and (4) for very little extra effort, their evaluation is also included.

The first analysis was to evaluate the MTF of the $f/12.88$ relay after the WF/PC with pickoff mirror is shifted axially with respect to the OTA secondary mirror and the pyramid adjusted axially to remove defocus. The amounts of pickoff mirror perturbation were ± 400 microns and ± 800 microns (condition 1).

The second analysis was to evaluate MTF after the OTA secondary mirror is shifted axially with respect to the OTA primary mirror and the pyramid

adjusted axially to remove defocus. The amounts of secondary mirror perturbations evaluated corresponded with OTA focus shifts of ± 400 microns and ± 800 microns (condition 2).

For both conditions, analysis showed that the perturbations could be completely compensated by axial adjustment of the pyramid. The MTF at all points on the relay focal surface (CCD detector) after the perturbation and pyramid adjustment were restored to their unperturbed values.

Similarly, translation of the pickoff mirror by ± 400 microns and ± 800 microns also were completely compensated by axial adjustment of the pyramid. Directions of pickoff mirror translation evaluated were parallel to the OTA optical axis and normal to the OTA axis in the meridional plane (condition 3).

An error in the axial position of the pyramid will cause a focus error at the relay focal surface. An analytic expression which relates the focus error to the pyramid position error is given.

9.1 PYRAMID FOCUS ADJUSTMENT

The perturbations described as conditions 1, 2, and 3 have a common optical effect. They cause an apparent displacement of the pyramid and relay optics with respect to the OTA image surface. The axial component of this displacement is denoted ΔZ and the lateral (decenter) component is ΔY.

The amount of axial pyramid adjustment needed to restore focus is

$$\Delta z = -\Delta Z/2 \cos^2\alpha$$

where

Δz = axial shift of the pyramid where
+ shift is away from the OTA

α = angle of pyramid facet (9.1056^0)

and evaluation gives:

$$\Delta z = -0.512844\ \Delta Z \qquad (2)$$

The quantity ΔZ depends upon the particular perturbation.

9.2 POINTING ANGLE PERTURBATION

The perturbation and compensating pyramid adjustment changes the system pointing angle. Let the center of the CCD detector correspond to the OTA field angle ϕ before the perturbation. Then, after the perturbation, this field angle becomes $\phi + \Delta\phi$ where

$$\Delta\phi = \tan^{-1}\left[\Delta y/(f-\Delta f) + \tan\phi\ \Delta f/(f-\Delta f)\right] \qquad (3)$$

and f = OTA focal length

Δf = OTA focal length perturbation

$$\Delta y = \Delta Y - \Delta Z\ \tan(\beta-2\alpha) - \Delta z\left[\frac{\sin\beta\cos\alpha}{\cos(\beta-\alpha)} + \tan(\beta-2\alpha)\right]$$

A particular ray, after reflection from the pyramid, will become the optical axis of the relay optics. Between the pyramid and the WF relay folding mirror, the angle of this ray with respect to the OTA axis is denoted β. For the $f/12.88$ design, $\beta=18.34^{o}$. As described previously, $\alpha=9.1056^{o}$. Then, evaluating the above expression,

$$\Delta y = \Delta Y - 0.002248\ \Delta Z - 0.3170\ \Delta z \qquad (4)$$

9.3 EVALUATION OF CONDITION 1

Let the pickoff mirror, pyramid, and relay optics be displaced axially along the OTA axis by distance ΔL. The optical displacement is the same as the physical displacement for the condition, so:

$$\Delta Y = 0$$

$$\Delta Z = \Delta L$$

From equation (2), the amount of axial pyramid adjustment needed to restore focus is:

$$\Delta z = -0.512884\ \Delta L$$

From equation (4), the parameter Δy is:

$$\Delta y = -0.002248\ \Delta L - 0.3170(-0.512844\ \Delta L)$$

$$\Delta y = 0.1603\ \Delta L$$

The OTA focal length (f) is 5760 cm. The OTA is not perturbed, so Δf=0. From equation (3);

$$\Delta\phi = \tan^{-1}\left[\Delta y/f\right]$$

Combining the preceding two equations gives:

$$\Delta\phi = \tan^{-1}\left[2.78\text{x}10^{-5}\ \Delta L\right] \qquad (\Delta L \text{ in cm})$$

The adjustments to the math model for this condition, therefore, are to

a. Shift pyramid and relay optics axially by distance ΔZ.
b. Refocus pyramid by Δz.
c. Adjust OTA input field angles by $\Delta\phi$.

MTF was calculated for the perturbations at grid points A, A', C, and E on the CCD detector surface, as shown in table 9.3-1. Unperturbed MTF and these values of perturbed MTF are given in table 9.3-2.

Table 9.3-1

INPUT PERTURBATIONS

ΔL(μ)	ΔZ(μ)	Δz(μ)	Δφ (degrees)
+800	+800	-410	0.000127
+400	+400	-205	0.000064
-400	-400	+205	-0.000064
-800	-800	+410	-0.000127

Table 9.3-2

MTF AT 33 C/MM

Grid Point	ΔL - Microns				
	+800	+400	0	-400	-800
A	.186	.187	.188	.189	.191
A'	.390	.389	.389	.390	.390
C	.355	.354	.354	.353	.353
E	.336	.336	.336	.336	.335

Table 9.3-2 shows that the effect of axially shifting the pickoff mirror and WF/PC with respect to the OTA image surface is compensated by an axial adjustment of the pyramid. This adjustment restores the MTF to its unperturbed value.

9.4 EVALUATION OF CONDITION 2

The amount of OTA secondary mirror perturbation needed to shift the OTA image surface by $\Delta Z'$ is:

$$\Delta T = -\Delta Z' / (M^2+1)$$

where

ΔT = axial shift of secondary mirror where
+ shift increases the primary-to-secondary mirror spacing

$\Delta Z'$ = axial shift of the OTA image surface where
+ shift is away from the OTA

M = OTA secondary mirror magnification (10.434756)

and evaluation gives:

$$\Delta T = -0.009100\ \Delta Z'$$

The equivalent optical displacement of the relay with respect to the OTA image is

$$\Delta Y = 0$$
$$\Delta Z = -\ \Delta Z'$$

From equation (2), the amount of axial pyramid adjustment needed to restore focus is

$$\Delta z = 0.512884\ \Delta Z'$$

From equation (4), the parameter Δy is

$$\Delta y = +0.002248\ \Delta Z' - 0.3170(0.512844\ \Delta Z')$$

$$\Delta y = -0.1603\ \Delta Z'$$

A change ΔT in OTA secondary mirror location perturbs the OTA focal length as follows:

$$\Delta f = 4f^2\Delta T/(r_p r_s - 4f\Delta T)$$

where

Δf = change in focal length
f = OTA focal length (5760 cm)
r_p = primary mirror radius (-1104.0 cm)
r_s = secondary mirror radius (-135.8 cm)
ΔT = secondary mirror spacing change

From equation 3, the pointing angle is

$$\Delta\phi = \tan^{-1}|\Delta y/(f-\Delta f) + \tan Q\ \Delta f/(f-\Delta f)|$$

The OTA field angle ϕ corresponding to the center-point of the CCD detector is 0.015816 degrees.

The adjustments to the math model for condition 2, therefore, are to

a. Shift OTA secondary mirror position by distance ΔT.
b. Refocus pyramid by Δz.
c. Adjust OTA input field angles by $\Delta\phi$.

MTF, calculated for the perturbations in table 9.4-1, are given in table 9.4-2.

Table 9.4-1

INPUT PERTURBATIONS

$\Delta Z'$ (μ)	ΔT (μ)	Δz (μ)	Δf (cm)	$\Delta\phi$ (degrees)
+800	-7.2804	+410	-0.6444	-0.000129
+400	-3.6402	+205	-0.3222	-0.000065
-400	+3.6402	-205	+0.3222	+0.000065
-800	+7.2804	-410	+0.6444	+0.000129

Table 9.4-2

MTF AT 33 C/MM

Grid Point	$\Delta Z'$ - Microns				
	+800	+400	0	-400	-800
A	.188	.188	.188	.189	.189
A'	.389	.389	.389	.389	.390
C	.355	.355	.354	.353	.352
E	.334	.335	.336	.337	.337

Table 9.4-2 shows that the effect of perturbing the OTA secondary mirror position is compensated by an axial adjustment of the pyramid. This adjustment restores the MTF to its unperturbed value.

9.5 EVALUATION OF CONDITION 3

Let the pickoff mirror be displaced axially along the OTA axis by distance ΔL_Z. Optically, this perturbation causes an apparent displacement of the pyramid and relay optics with respect to the OTA image surface. The axial component of this apparent displacement is ΔZ and the transverse component (decenter) is ΔY. For the ΔL_Z perturbation:

$$\Delta Y = \Delta L_Z \, \text{Sin}\theta$$

$$\Delta Z = \Delta L_Z \, (1 + \text{Cos}\theta)$$

where θ = pickoff mirror angle = 94^o

Similarly, a transverse decentering ΔL_Y of the pickoff mirror with respect to the OTA axis also causes an apparent displacement of the pyramid and relay optics where

$$\Delta Y = \Delta L_Y \, (1 - \cos\theta)$$

$$\Delta Z = \Delta L_Y \, \text{Sin}\theta$$

Evaluating the above expressions:

$$\Delta Y = 0.997564\ \Delta L_Z$$

$$\Delta Z = 0.930244\ \Delta L_Z$$

and

$$\Delta Y = 1.069756\ \Delta L_Y$$

$$\Delta Z = 0.997564\ \Delta L_Y$$

The expressions for ΔL_Y are very nearly equal to those for ΔL_Z. Consequently, only the effects of ΔL_Z need to be analyzed because the conclusions can be applied to ΔL_Y also.

From equation (2), the amount of axial pyramid adjustment needed to restore focus is:

$$\Delta z = -0.512844\ (0.930244\ \Delta L_Z)$$

$$\Delta z = -0.477070\ \Delta L_Z$$

From equation (4), the parameter Δy is:

$$\Delta y = 0.997564\ \Delta L_Z - 0.002248(0.930244\ \Delta L_Z) - 0.3170\ (-0.477070\ \Delta L_Z)$$

$$\Delta y = 1.1467\ \Delta L_Z$$

The OTA focal length (f) is 5760 cm. The OTA is not perturbed, so $\Delta f = 0$. From equation (3);

$$\Delta\phi = \tan^{-1}\ (\Delta y/f)$$

Combining the preceding two equations gives:

$$\Delta\phi = \tan^{-1}\left(1.991\times10^{-4}\ \Delta L_Z\right) \qquad (\Delta L_Z \text{ in cm})$$

The adjustments to the math model for this condition, therefore, are to:

a. Shift pyramid and relay optics axially by distance ΔZ and laterally by distance ΔY. This adjustment is optically equivalent to shifting the pickoff mirror by distance ΔL_Z.
b. Refocus pyramid by Δz.
c. Adjust OTA input field angles by $\Delta\phi$.

MTF was calculated for the perturbations in table 9.5-1 at grid points A, A', C, and E on the CCD detector surface. Unperturbed MTF and these values of perturbed MTF are given in table 9.5-2.

Table 9.5-1

INPUT PERTURBATIONS

ΔL_Z (μ)	ΔY (μ)	ΔZ (μ)	Δz (μ)	ΔQ (degrees)
+800	+798	+744	-382	+0.000913
+400	+399	+372	-191	+0.000456
-400	-399	-372	+191	-0.000456
-800	-798	-744	+382	-0.000913

Table 9.5-2

MTF AT 33 C/MM

Grid Point	ΔL_Z - Microns				
	+800	+400	0	-400	-800
A	.177	.182	.188	.194	.200
A'	.387	.388	.389	.391	.393
C	.358	.356	.354	.352	.350
E	.335	.336	.336	.336	.336

Table 9.5-2 shows that the effect of axially shifting the pickoff mirror is compensated by an axial adjustment of the pyramid. The amount of adjustment Δz was calculated from equation (2) which assumed, in its derivation, that the pyramid facets were plano and that the OTA image surface was flat. These approximations may account for the minor variations in compensated MTF.

Optically, the effect of shifting the pickoff mirror in a direction normal to the OTA axis (in the meridional plane) is nearly the same as the axial shift. Thus, the general conclusion can be made that a ± 800 micron shift of the pickoff mirror in any direction from its nominal position can be fully compensated by an axial adjustment of the pyramid.

9.6 FOCUS ADJUSTMENT AT DETECTOR USING THE PYRAMID

The WF/PC uses the OTA image surface as an "object" and re-images this object onto the CCD detector surface. The back focal distance (BF) between the WF/PC and detector depends upon the distance between the "object" and the WF/PC. An axial shift of the pyramid changes this object distance and, consequently, changes the back focus resulting in a focus error ΔBF at the detector.

Analysis of pyramid refocusing for the perturbations evaluated in this report led to the following two equations for change in object distance Δa:

$$\Delta a' = \Delta Z/\cos(\beta-2\alpha) \qquad (5)$$

$$\Delta a = 2\Delta z \cos^2\alpha/\cos(\beta-2\alpha) \qquad (6)$$

For focus compensation, the change in object distance Δa caused by the pyramid shift Δz must be equal and opposite to the change in object distance $\Delta a'$ caused by the perturbation ΔZ:

$$\Delta a = -\Delta a'$$

Substituting equations (5) and (6) into this expression and solving for Δz gives:

$$\Delta z = -\Delta Z/2\cos^2\alpha$$

and this is equation (1), used in this report for focus compensation.

In the absence of perturbations ($\Delta Z=0$), a shift Δz of the pyramid will cause a change Δa in object distance, thereby producing a focus shift ΔBF at the CCD detector.

By applying the method of finite differences to the paraxial ray trace equations, the following relationship is found:

$$\Delta BF = -\left[\frac{R_p R_s}{(R_p+2T_o)(R_s-2T_p)-2T_o R_p}\right]^2 \left[1-\frac{2(R_s-R_p-2T_p)\Delta a}{(r_p+2T_o)(R_s-2T_p)-2T_o R_p}\right] \Delta a$$

where:

R_p = primary mirror radius (-40.5662 cm)

R_s = secondary mirror radius (-28.5460 cm)

T_o = object distance (113.0610 cm)

T_p = mirror separation (16.2590 cm)

Evaluating the above expression:

$$\Delta BF = -0.28798\ \Delta a + 0.0054717\ (\Delta a)^2$$

Equation (6) is also evaluated, using $\alpha = 9.1056^o$ and $\beta = 18.34^o$:

$$\Delta a = 1.9499\ \Delta z$$

Finally, combining the preceding two expressions:

$$\Delta BF = -0.56154\ \Delta z + 0.020804\ (\Delta z)^2 \qquad (7)$$

This expression relates focus shift ΔBF at the CCD detector to axial translation Δz of the pyramid. The units used in this equation must be centimeters.

The optical system math model is used to verify the focus shift equation as follows:

a. Shift pyramid axially by distance Δz.
b. Move CCD detector axially by ΔBF. If equation (7) is correct, the focus error will be removed.
c. Adjust OTA input field angle using equations (3) and (4) where $\Delta Y = \Delta Z = \Delta f = 0$.

Table 9.6-1

INPUT PERTURBATIONS

Δz (cm)	ΔBF (cm)	$\Delta \phi$ (degrees)
+0.08	-0.0448	-0.000252
-0.08	+0.0451	+0.000252

MTF was calculated for the perturbations, as shown in table 9.6-1, at grid points A, C. and E on the CCD detector surface. Unperturbed MTF and calculated values of perturbed MTF are given in table 9.6-2.

Table 9.6-2

MTF AT 33 C/MM

Grid Point	Δz - Centimeters +.08	0	-.08
A	.191	.188	.186
C	.353	.354	.355
E	.336	.336	.335

Table 9.6-2 shows that focus error is removed when the detector is shifted ΔBF for a pyramid shift of Δz. The math model, therefore, has confirmed the focus shift equation (7).

10.0 SYSTEM PERFORMANCE PREDICTION

10.1 SYSTEM PERFORMANCE PREDICTION (WITHOUT DETECTOR)

Performance predictions for the WF/PC optics without OTA are shown in figures 10.1-1 and 10.1-2. At this level of testing, an OQF of 79 percent is anticipated and can be verified by interferometric testing. Performance predictions for the WF/PC optics with OTA are shown in figures 10.1-3 and 10.1-4. The optimized geometric-mean MTF over the field of the Wide Field Camera at a spatial frequency of 33 cycles/mm is shown in figure 10.1-5. Assuming an anticipated OQF of 63 percent, the predicted manufactured performance is shown in figure 10.1-6. The optimized geometric-mean MTF over the field of the Planetary Camera at a spatial frequency of 14 cycles/mm is shown in figure 10.1-7. Assuming an anticipated OQF of 63 percent, the predicted manufactured performance is shown in figure 10.1-8. (Note: Since a total system test (OTA with WF/PC) is not planned, the predicted OQF cannot be verified by interferometric testing.)

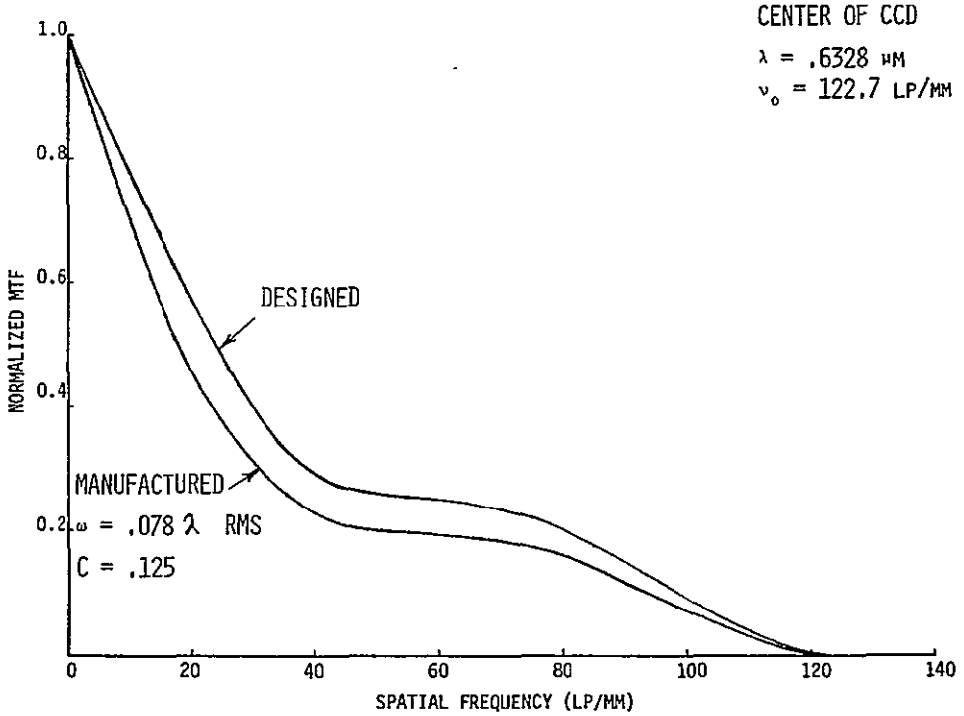

WIDE FIELD CAMERA PERFORMANCE PREDICTION
(WITHOUT OTA)

Figure 10.1-1

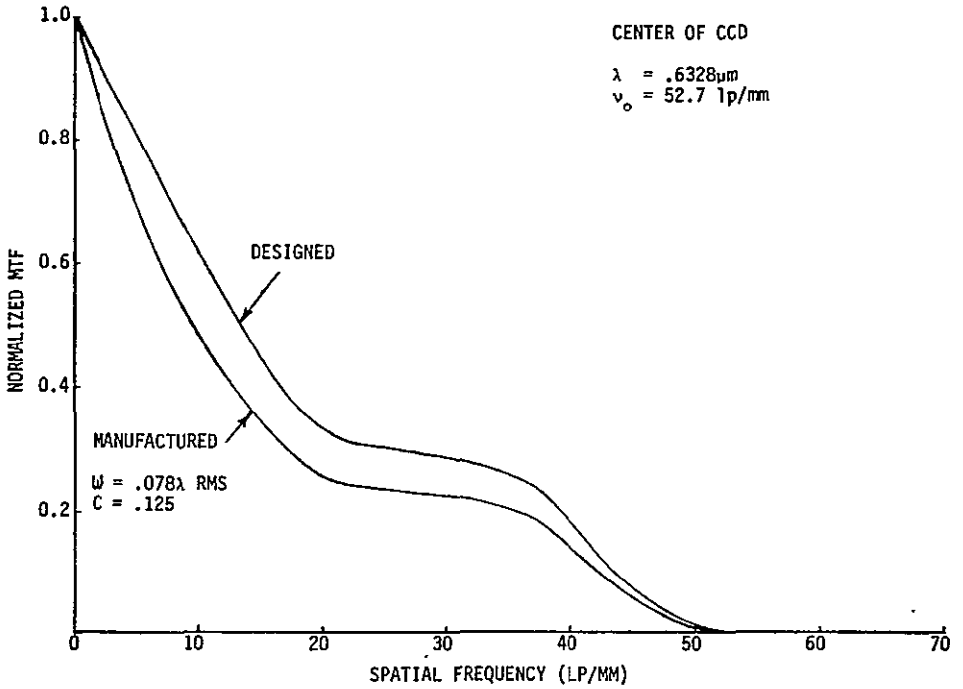

PLANETARY CAMERA PERFORMANCE PREDICTION
(WITHOUT OTA)

Figure 10.1-2

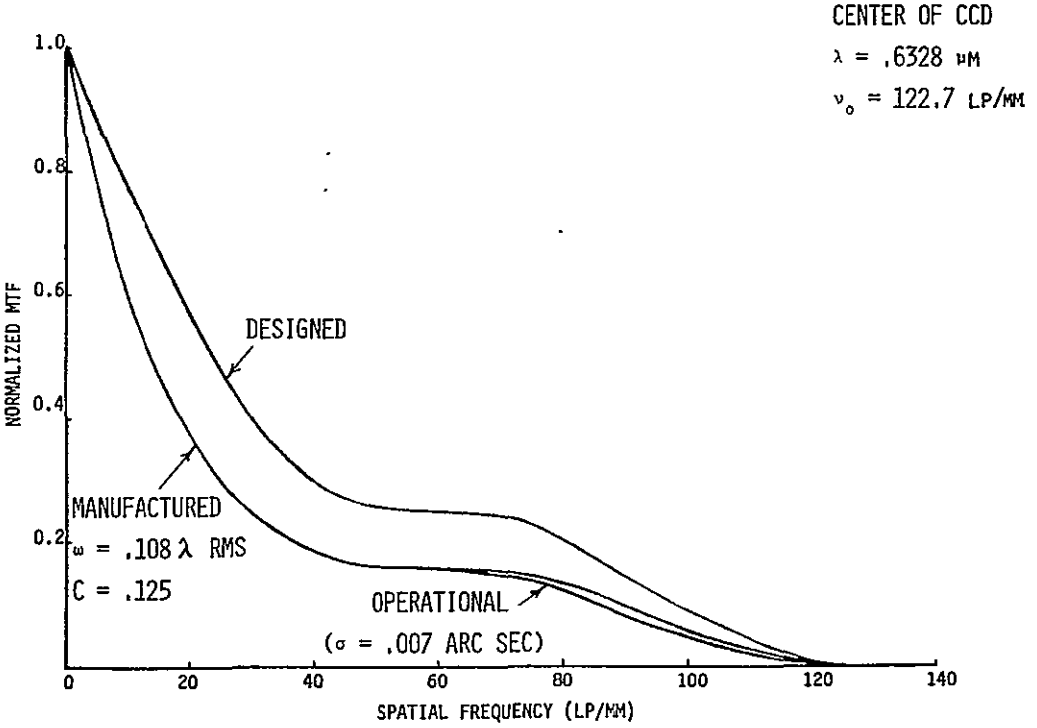

WIDE FIELD CAMERA PERFORMANCE PREDICTION
(WITH OTA)

Figure 10.1-3

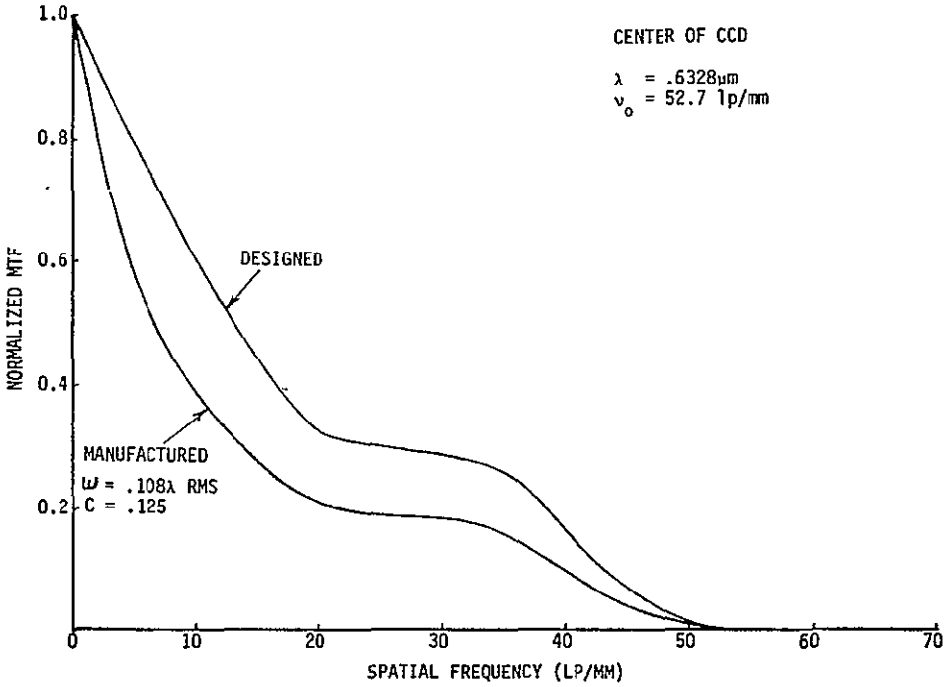

PLANETARY CAMERA PERFORMANCE PREDICTION
(WITH OTA)

Figure 10.1-4

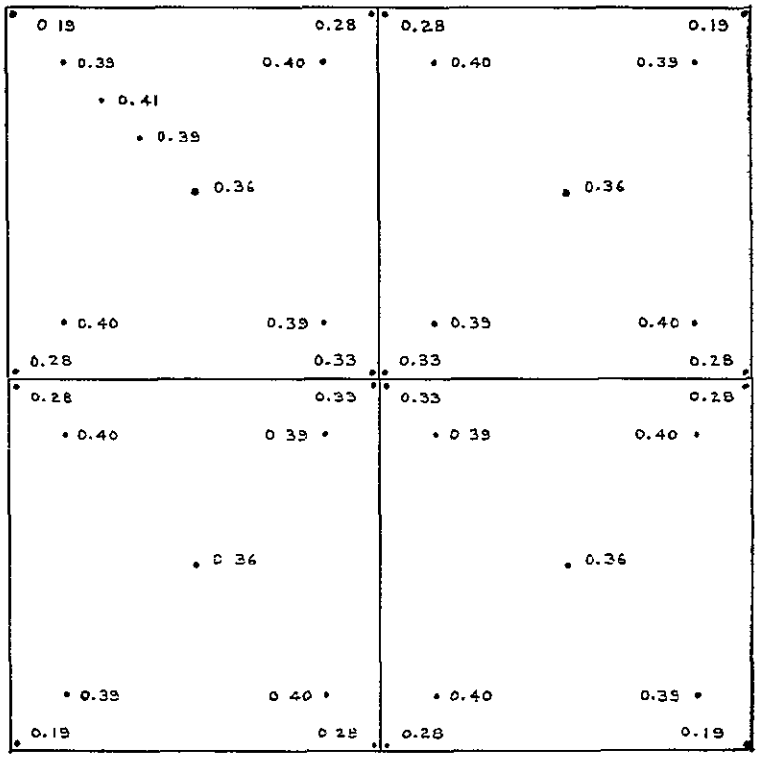

Figure 10.1-5: *f*/12.88 RELAY - OPTIMIZED GEOMETRIC-MEAN MTF
AT VARIOUS FIELD POSITIONS
(SPATIAL FREQUENCY = 33 c/mm, λ = 0.6328 mμ)

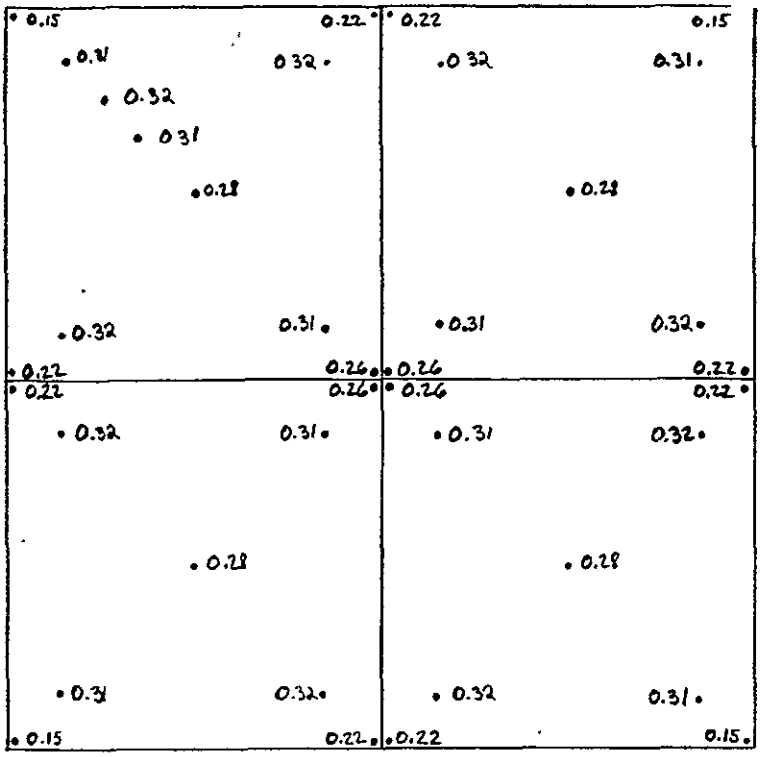

ν = 33 CYCLES/MM
λ = 0.6328 MICRONS

WIDE FIELD CAMERA
(MANUFACTURED MTF AT
VARIOUS FIELD POSITIONS)

Figure 10.1-6

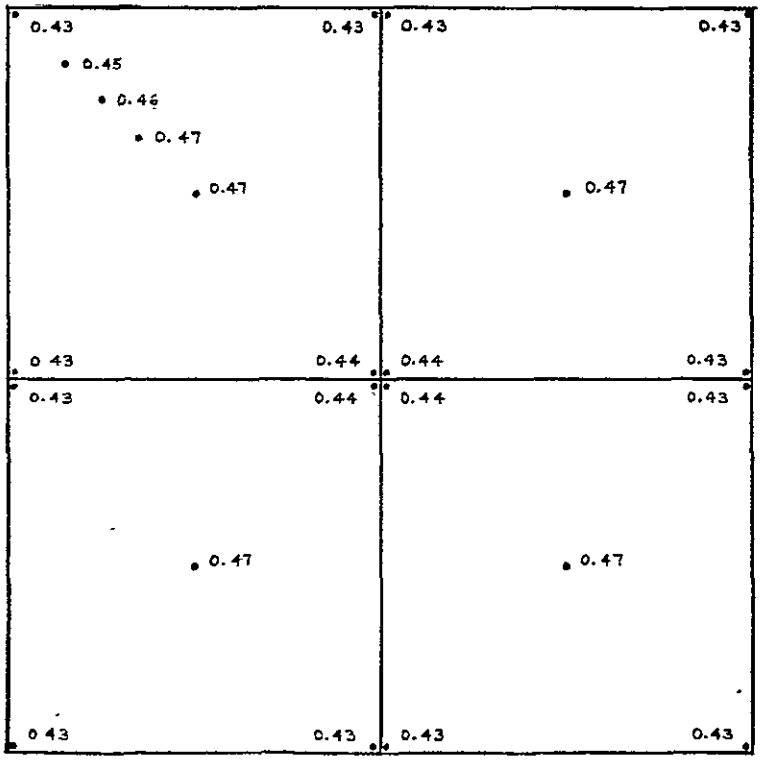

f/30 RELAY - OPTIMIZED
GEOMETRIC-MEAN MTF AT
VARIOUS FIELD POSITIONS
(SPATIAL FREQUENCY = 14 c/mm,
λ = 0.6328 mμ)

Figure 10.1-7

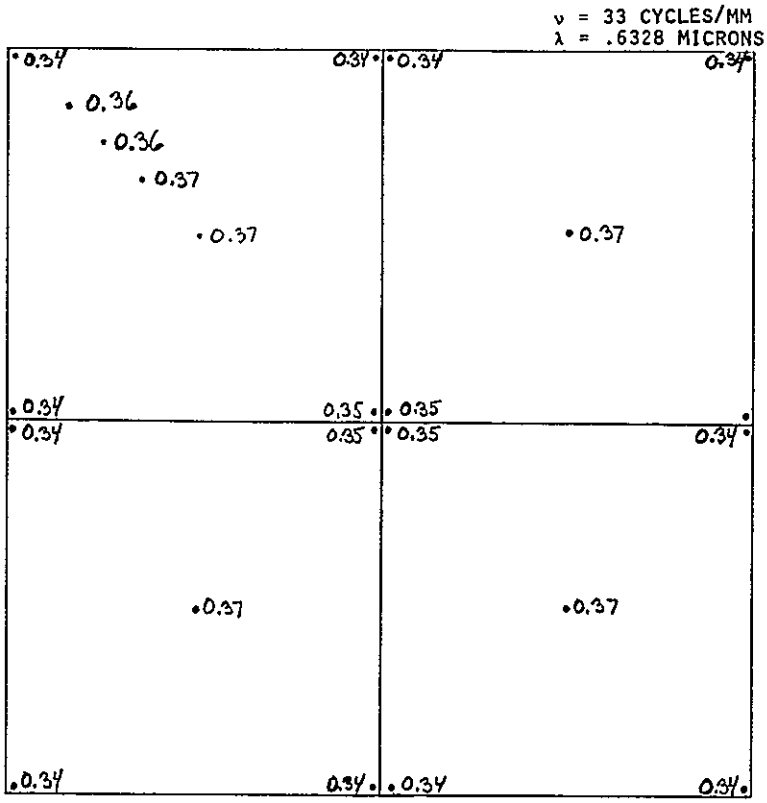

PLANETARY CAMERA
(MANUFACTURED MTF AT VARIOUS FIELD POSITIONS)

Figure 10.1-8

10.2 SYSTEM PERFORMANCE PREDICTION (WITH DETECTOR)

10.2.1 Threshold Modulation Analysis

Threshold modulation (TM) analysis is used to determine, for the human observer, the limiting resolving power of a lens-film combination*. This technique provides a single value indication of system performance and can be applied to a general imaging system as well. In TM analysis, the limiting resolution of a system is determined by the intersection of the (frequency dependent) incident target modulation (ITM) curve†, and the threshold modulation (TM) curve, as illustrated in figure 10.2.1-1.

---

* *T. J. Lauroesch, et al, "Threshold Modulation Curves for Photographic Films", Applied Optics, Vol. 9, No. 4, April 1970, pp. 875-887.*

† *Also known as the aerial image modulation (AIM) curve.*

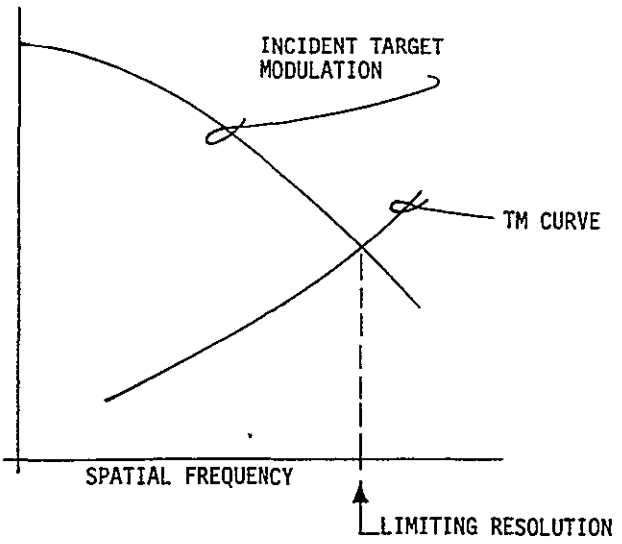

LIMITING RESOLUTION OF A SYSTEM

Figure 10.2.1-1

The incident target modulation represents the modulation *available* at the input to a detector (CCD, film, etc.). ITM is a function of the target contrast, the intervening media between the target and its image on the detector, the modulation transfer function (MTF) and optical quality factor (OQF) of the taking optics, smear, and defocus.

Threshold modulation, on the other hand, represents the *minimum* modulation that is required at the input of the system to perform a given task -- usually detection. Threshold modulation is a function of the MTF's and noise source of all the elements in the image chain from the detector through the user. Threshold modulation is also a function of the signal-to-noise ratio required to perform a particular task with a given performance probability. For example, if the task is to detect a tri-bar pattern with a 50 percent probability of

C-3

detection, the required signal-to-noise ratio (SNR) is 1.5*. If, however, it is necessary to perform target recognition or identification then higher SNR's are required for the same performance probability†.

The following sections contain a formulation of the TM equation, its application to the Wide Field Planetary Camera, and an interpretation of these results.

10.2.2 Threshold Modulation Formulation

The basic formulation of threshold modulation begins with the definitions of modulation and signal-to-noise ratio. Modulation is defined by considering two adjacent resolution elements producing respective signals of S_1 and S_2. Modulation (M) is then defined as

$$M = \frac{|S_1-S_2|}{S_1+S_1} = \frac{\Delta S}{2\bar{S}} ; \qquad (1)$$

and the signal-to-noise ratio (SNR) is given by

$$SNR = \frac{\Delta S}{2\sigma_N} \qquad (2)$$

where,

$\Delta S/2 = |S_1-S_2|/2$, the incremental signal level about the mean

$\bar{S} = (S_1+S_2)/2$, the average signal level

σ_N = the rms noise.

---

* *This calculation assumes a Gaussian process with a 50 percent probability of simultaneously detecting all three bars and two spaces of the tri-bar pattern. The probability of detecting an individual bar or space is* $(0.5)^{1/5} = 0.87$ *and requires a signal-to-noise ratio of* ≥ 1.5 *to achieve this detection probability.*

† *L. M. Biberman, "Perception of Displayed Information", Chapter 5, Plenum Press, New York, 1973.*

By substituting (2) into (1), an expression for modulation in terms of SNR and rms noise results

$$M = \left(\frac{\sigma_N}{\bar{S}}\right) \text{SNR} . \tag{3}$$

It should be noticed that the parenthetical term in (3) has the same form as the definition for modulation shown in (1). Using this similarity, it is convenient to define this term as the "noise modulation" (δ);

$$\delta \equiv \frac{\sigma_N}{\bar{S}} . \tag{4}$$

Using the terminology in (3), the threshold modulation (TM) is that value of modulation which just equals the product of noise modulation and SNR, that is,

$$TM = (SNR)\delta. \tag{5}$$

This equation represents the basic expression for threshold modulation. In general, it is a function of spatial frequency (ν) since the noise modulation is a function of spatial frequency. To illustrate this, consider the noise power spectral density at the *input* to the K-th element in the image chain $\phi_K(\nu)$. The associated rms noise at the *output* of the K-th element can be expressed as

$$\sigma_K^o(\nu) = \left[\gamma_K^2 \, MTF_K^2(\nu) \, \phi_K(\nu)\right]^{1/2}; \tag{6}$$

with the total rms noise given by

$$\sigma_K^o(\nu) = \left[\gamma_K^2 \int_{-\infty}^{\infty} MTF_K^2(\nu) \, \phi_K(\nu) \, d\nu\right]^{1/2}; \tag{7}$$

where

γ_K = gamma of the K-th image chain element

$MTF_K(\nu)$ = modulation tranfer function of K-th image chain element.

Finally, the noise modulation can be written as

$$\delta_K^o(\nu) = \frac{\sigma_K^o(\nu)}{\bar{S}_K} = \left[\frac{\phi_K^o(\nu)}{\bar{S}_K^2}\right]^{1/2}, \tag{8}$$

which illustrates the frequency dependence of the threshold modulation.

Using the previous expressions, the rms noise at the output of an N-element imaging chain is

$$\sigma_o(\nu) = \left[\sum_{j=1}^{N} \phi_j(\nu) \prod_{q=1}^{N} \gamma_q^2 \, MTF_q^2(\nu)\right]^{1/2}, \tag{9}$$

and the resultant expression for threshold modulation at the *output* of this imaging chain is given by

$$TM_o(\nu) = \left[(SNR)^2 \left[\sum_{j=1}^{N} \phi_j(\nu) \prod_{q=1}^{N} MTF_q^2(\nu) + TM_V^2\right]\right]^{1/2}; \tag{10}$$

where TM_V is visual modulation threshold below which a human observer, even under optimum viewing conditions, cannot distinguish the target from its background. TM_V is in the neighborhood of one to five percent modulation*.

From linear system theory, it is known that for a given amount of modulation at the input to the imaging chain (M_I), the resultant modulation at the output (M_O) is given by the product of the input modulation and the cascaded transfer functions, that is

$$M_O(\nu) = M_I(\nu) \prod_{q=1}^{N} \gamma_q \, MTF_q(\nu). \tag{11}$$

---

* *Ibid; Chapter 3*

If the output threshold modulation TM_0 is substituted into (11) and the expression rearranged to solve for the resultant input threshold modulation, the following equation is obtained

$$TM_I(\nu) = \frac{TM_0(\nu)}{\prod_{q=1}^{N} \gamma_q \, MTF_q(\nu)} . \tag{12}$$

This equation illustrates that the threshold modulation required at the input to the imaging chain is simply related to the required output threshold modulation via the system transfer function. The system transfer function is

$$\text{SYSTEM TRANSFER FUNCTION} = \prod_{q=1}^{N} \gamma_q \, MTF_q(\nu).$$

By combining equations (10) and (12), the final expression for the threshold modulation at the *input* to the imaging chain is obtained

$$TM_I(\nu) = \frac{\left[(SNR)^2 \left[\sum_{j=1}^{N} \phi_j(\nu) \prod_{q=1}^{N} \gamma_q^2 \, MTF_q^2(\nu) + TM_V^2\right]\right]^{1/2}}{\prod_{q=1}^{N} \gamma_q \, MTF_q(\nu)} . \tag{13}$$

This expression represents the objective of the preceding analysis. When the TM curve described by (13) is intersected by the incident target modulation curve, the frequency of intersection represents the limiting resolution. At this frequency, the modulation available in the target is just equal to the modulation required at the system's input to achieve the desired system performance.

In the following section a TM equation for the Wide Field/Planetary Camera is developed. This equation is based on CCD sensor characteristics described in a document entitled, Technical Proposal, Investigation Definition Team, Wide Field/Planetary Camera for Space Telescope, submitted by the California Institute of Technology, James A. Westphal, Principal Investigator.

10.2.3 WF/PC Threshold Modulation Equation

In this section a first order expression for the threshold modulation equation for the WF/PC is derived. This expression utilizes the CCD characteristics described in the aforementioned document, and assumes that all elements in the WFC and PC imaging chains between the output of the CCD sensor and the reconstructed images contribute *no* degradation to the reconstructed images. This assumption is necessary due to the lack of specific information on these image chain elements. As a result, the first order expression for the TM equation will be optimistic in that the TM curve will be too low and the predicted limiting resolution too high.

From the WF/PC reference document, the CCD is characterized as being photon noise limited (for nominal exposures) with 10 to 20 rms electrons and an MTF as illustrated in figure 10.2.3-1*. As a consequence of this characterization and the previous assumption, the TM equation reduces to a rather simple expression consisting of one noise term, one MTF term, the visual threshold modulation (TM_V) term, and the signal-to-noise ratio.

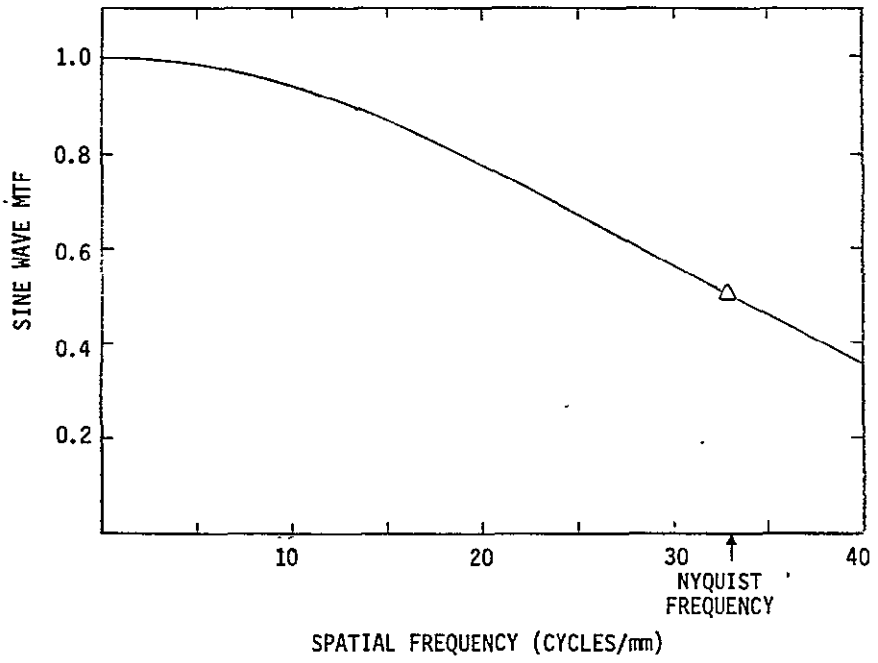

SINE WAVE MTF
Figure 10.2.3-1

* *This MTF has been reproduced from the WF/PC reference document.*

10.2.3.1 Photon Noise Modulation - Using the definition of noise modulation from (4) and the fact that the rms photon noise (σ_p) is equal to the square root of the average signal level,

$$\sigma_p = \sqrt{\bar{s}}$$

the photon noise modulation can be expressed as

$$\delta = \frac{1}{\sigma_p} \tag{14}$$

The photon noise, expressed in mean-squared electrons, is given by

$$\sigma_p^2 = \left(\frac{ER}{q}\right) A \text{ , MS-electrons;} \tag{15}$$

where

E = exposure, joules/M^2

R = CCD responsivity, amps/watt

A = CCD area, M^2

q = electronic charge, 1.6×10^{-19} coulombs/electron.

Using 20 rms electrons for the photon noise and a sensor area of 15μx15μ, the term in parenthesis in (15) can be evaluated as follows:

$$\frac{ER}{q} = \frac{400}{2.25 \times 10^{-10}} = 1.78 \times 10^{12} \text{ MS-electrons/M}^2. \tag{16}$$

If this term is represented by the constant (K) and if the sensor area (A) is rewritten in terms of spatial frequency:

$$A = \frac{10^{-6}}{4\nu^2} \text{ , M}^2; \tag{17}$$

where ν represents spatial frequency in cycles per millimeter; then the equation for the photon noise can be rewritten as

$$\sigma_p^2(\nu) = \frac{K \times 10^{-6}}{4\nu^2} \quad , \quad 0 \leq \nu \leq \nu_c \; ; \tag{18}$$

where

$K = 1.78 \times 10^{12}$ MS-electrons/M^2

ν = spatial frequency (c/mm)

ν_c = Nyquist frequency, 33.3 c/mm.

By substituting (18) into (14), an expression for the photon noise modulation results

$$\delta(\nu) = 1.5 \; \nu \times 10^{-3}. \tag{19}$$

10.2.3.2 The TM Equation - The threshold modulation at the output of the WF/PC can now be written as

$$TM_o(\nu) = \left[SNR^2 \delta^2(\nu) + TM_v^2 \right]^{\frac{1}{2}} \tag{20}$$

or

$$TM_o(\nu) = 10^{-2} \left[2.25 \cdot SNR^2 \cdot \nu^2 \times 10^{-2} + 9 \right]^{\frac{1}{2}}, \tag{21}$$

where 3 percent visual threshold modulation has been arbitrarily assumed*. Finally, the threshold modulation required at the input to the CCD is given by

---

* *Equations (19) and (20) do not contain the CCD transfer function, namely $\gamma \cdot MTF(\nu)$, since the photon noise is specified at the output of the CCD, rather than at its input.*

$$TM_I(\nu) = \frac{10^{-2}\left[2.25.SNR^2.\nu^2 x 10^{-2} + 9\right]^{\frac{1}{2}}}{\gamma.MTF(\nu)}, \qquad (22)$$

where

γ = CCD gamma = 1.0

MTF(ν) = CCD MTF illustrated in figure 10.2.3-1.

When the signal-to-noise ratio required to perform a given task, such as detection, recognition, or identification, is substituted into the above equation, and the resultant curve intersected by the incident target modulation curves for the Wide Field and Planetary Cameras, the frequencies of intersection will represent the first order limits of resolution for these systems. These limits are identified in the following section.

10.2.4 Resolution Limits

To determine the resolution limits for the WFC and PC, signal-to-noise ratios of 1:1, 5:1, and 10:1 were selected to establish the first order performance bounds for these two systems. In addition, two values of target contrast (C), ∞:1 and 2:1, were selected. The target contrast affects the modulation in the target M_T through the following relation

$$M_T = \frac{C-1}{C+1} \; ; \; 1 \leq C \leq \infty. \qquad (23)$$

For the selected values of target contrast, the corresponding values of target modulation are 100 percent and 33 percent, respectively. The target modulation is used to scale (multiply) the MTF of the taking optics; this scaled MTF represents the *incident target modulation curve* which is intersected with the TM curve to determine the limiting resolution. Occasionally, it is convenient to scale (divide) the TM curve by the target modulation, rather than scaling the taking optics MTF. Using this approach, the scaled TM curve is then intersected with the MTF of the taking optics to determine the limiting

resolution of the system. Following this approach, (22) can be rewritten as

$$TM_I'(\nu) = \frac{10^{-2}\left[2.25.SNR^2.\nu^2 x 10^{-2} + 9\right]^{\frac{1}{2}}}{M_T.\gamma.MTF(\nu)} \qquad (24)$$

This TM curve and the operational MTF's for the Wide Field and Planetary Cameras are illustrated in figures 10.2.4-1 and 10.2.4-2, respectively. These figures show that for SNR=10:1, and a contrast of 2:1, the lower limits of resolution are 11 lp/mm and 9.5 lp/mm, respectively. From these figures it can be seen that the upper resolution limit, for alias free operation, is set by the Nyquist frequency (33 lp/mm) rather than the CCD noise.

An interpretation of the resolution bounds for the Planetary camera is shown in figures 10.2.4-3 and 10.2.4-4. These figures are based on the following relationship between resolvable distance (RD) and limiting resolution:

$$RD = \frac{H}{f\nu} \quad , \qquad (25)$$

where H is the distance to the planet, f is the system focal length, and ν is the spatial frequency at the intersection of the TM curve with the MTF curve of the optics. Since the spatial frequency cutoff of the optics determines the limiting resolution of the Space Telescope independent of the detector, a minimum resolvable distance can be defined as follows:

$$MRD = \frac{H}{f\nu_o} = \frac{H\lambda f\#}{f} = \frac{H\lambda}{D} \quad ,$$

where $f\#$ is the system f-number, D is the diameter of the entrance pupil of the optics (2.4 meters), and λ is a nominal wavelength at 0.6 microns.

As illustrated in figures 10.2.4-3 and 10.2.4-4, the minimum resolved distance on Venus would be approximately 10^{-3} x Venus diameter. Theoretically, this is the best that can be obtained, based on the diameter of the Space Telescope and the distance to Venus.

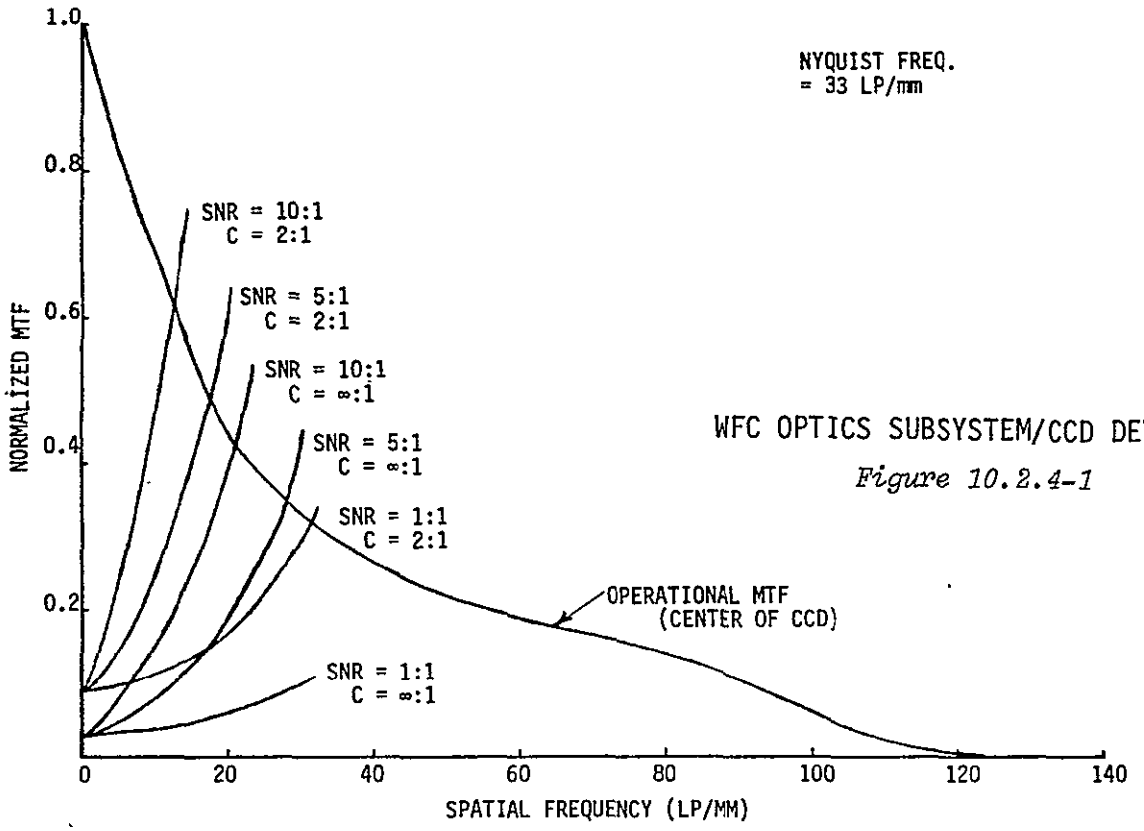

WFC OPTICS SUBSYSTEM/CCD DETECTOR

Figure 10.2.4-1

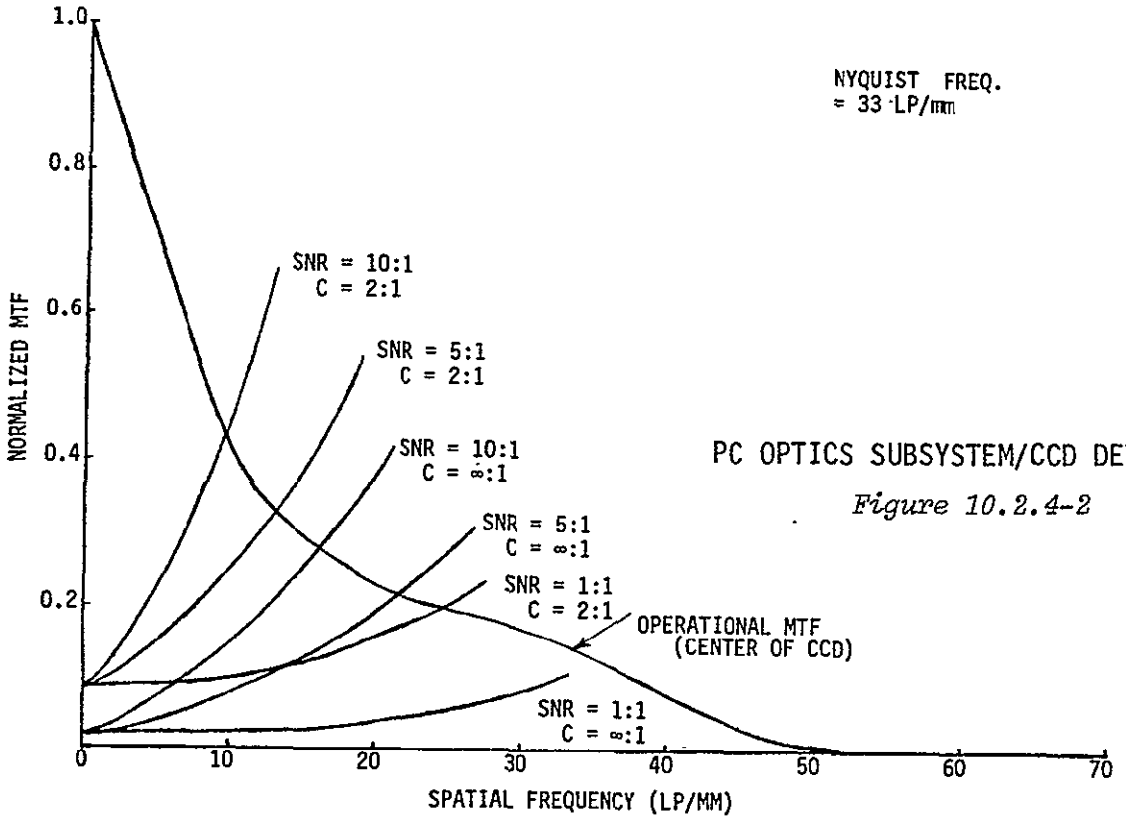

PC OPTICS SUBSYSTEM/CCD DETECTOR

Figure 10.2.4-2

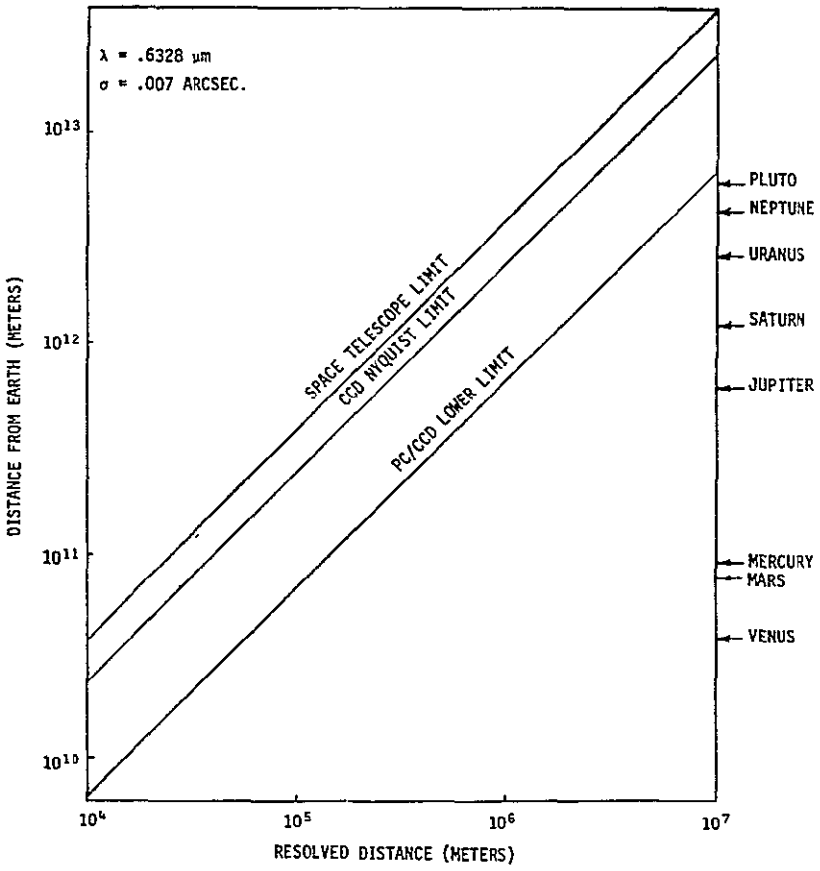

PLANETARY RESOLUTION

Figure 10.2.4-3

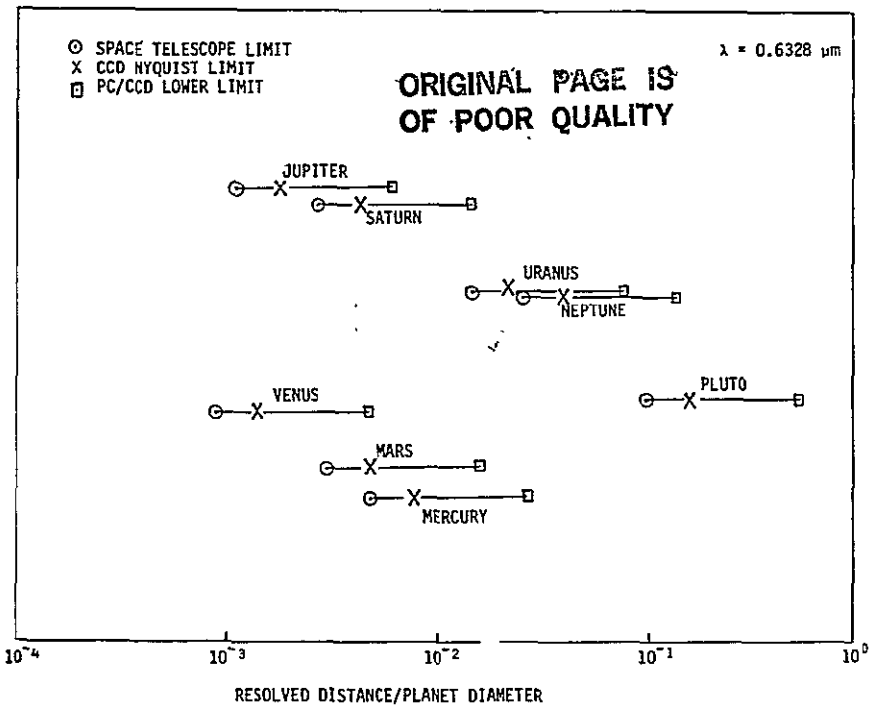

RATIO OF RESOLVED DISTANCE TO PLANET DIAMETER

Figure 10.2.4-4

Utilizing the CCD detector, however, the resolved distance of Venus would more realistically be $5x10^{-3}$ x Venus diameter (5X theoretical minimum).

10.2.5 Pointing Stability Errors

As shown in section 4.0, a pointing stability error will decrease the operational MTF of the optics. (In the change from a static manufacturing environment to a dynamic operational environment, the imaging performance is degraded by image motion.) Shown in figure 10.2.5-1 is the effect of pointing stability errors on a combined OTA with Planetary Camera. It should be noted that small pointing stability errors (based on the model in section 4.0) affect mainly the higher spatial frequencies. Since the TM curve intersects the MTF curves below the Nyquist Frequency, relatively small pointing stability errors have little effect on planetary resolved distance. (It is emphasized that the Space Telescope is designed for a pointing stability error less than 0.007 arcseconds.) The effect of the pointing stability error on the resolved distance on Mars and Venus is shown in figure 10.2.5-2. Assuming a pointing stability error of 0.021 arcseconds (3X Space Telescope limit), the resolved distance on Venus would be increased to 28 kilometers from a resolved distance of 22 kilometers with no pointing stability error.

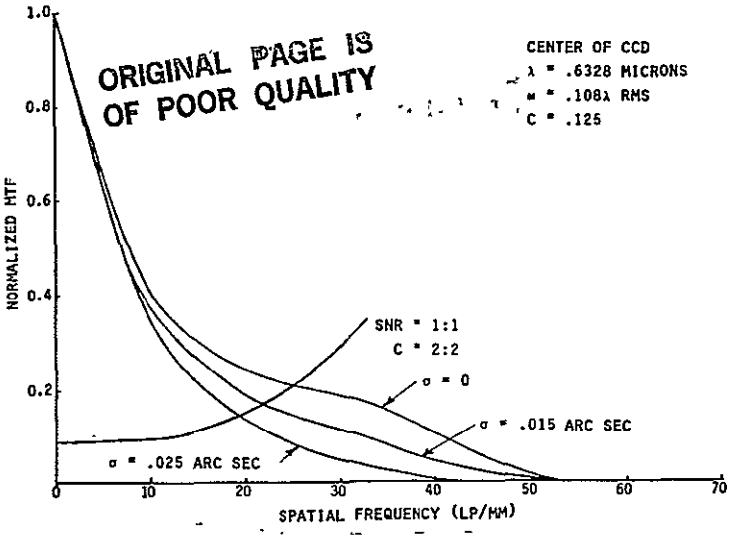

EFFECT OF POINTING STABILITY ERRORS ON A COMBINED OTA WITH PLANETARY CAMERA

Figure 10.2.5-1

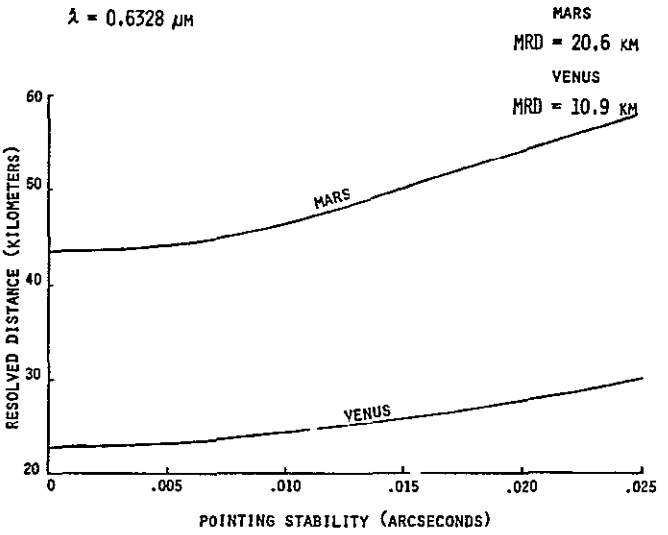

RESOLVED DISTANCE

Figure 10.2.5-2

11.0 CONCLUSIONS

11.0 CONCLUSIONS

Utilizing the Kodak optical design evaluation software, it was shown for the wide field camera baseline design that the optical performance at the center of each CCD array is diffraction-limited. Image quality degrades rapidly, however, for off-axis points on the CCD. The prominent field aberrations are field curvature and astigmatism. The field aberrations cannot be eliminated. Instead, they are partially cancelled by the introduction of compensating aberrations. The only effective degrees of freedom available for optimization are the asphericities of the relay primary and secondary mirrors. For the baseline design, these asphericities have been chosen to yield zero coma and zero spherical aberration. By changing these asphericities (conic aspheres to general aspheres) to improve off-axis and imagery, the condition of zero spherical aberration is sacrificed. Thus, off-axis performance is improved at a slight expense of on-axis performance. Similar to the Wide Field Camera, the Planetary Camera also has residual astigmatism and field curvature. However, the effect of these aberrations on image quality is negligible because this system operates at a higher f-number and has a smaller angular field. The baseline optical prescription, therefore, needs no modifications.

From a manufacturing standpoint, the unmounted optics fall into three groups: plano surfaces, spherical pyramid, and aspherics. Based on the established system budgeting philosophy, there appear to be no significant problems in manufacturing the unmounted plano surfaces using conventional Kodak plano processing and testing techniques. A procedure for assembly of an unmounted, four-faceted, pyramid mirror has been configured. Two areas of concern remain in its manufacturability. The first is the tolerance on the "sharpness" of the edges which affects the total field coverage, and the second is the scratch/dig cosmetic requirements. A tolerance on the edge sharpness should be established in the near future and compared with state-of-the-art manufacturing capability. Since the pyramid acts as a field lens, dust and dirt -- as well as scratches and digs on the surface -- will be imaged directly onto the CCD. Specifications on the size and number of particles and surface defects should also be established in the near future and compared with state-of-the-art manufacturing capability. The Cassegrain primary and secondary mirrors

utilize conic and general aspheric surfaces. It is extremely important that these designed aspheric terms be incorporated into the manufactured surface. (The effect of nonconformance is a drastic loss in image quality in the field.) The approach chosen (Kodak area compensating tooling procedure) appears to be applicable. In this approach, the symmetric and asymmetric errors are determined interferometrically in a clean, "noise-free" environment. The symmetric and asymmetric errors are then addressed separately, with different tools. It should be noted that the deviation of the manufactured surface contour from the designed surface contour cannot exceed 3×10^{-7} inches at the edge of the 2-inch diameter WFC primary mirror. Similar tolerances are needed on the ½-inch convex secondary mirrors, and analyses indicate that these unmounted components will be the most difficult of the optical elements in the WF/PC to manufacture. For these reasons, it is engineering judgement that the aspheric surfaces are within manufacturing state-of-the-art; however, a development program will be required to substantiate this finding.

The Wide Field/Planetary Camera Optics Study has addressed manufacturability of unmounted optical components *only*. It is a basic assumption that these optical components will be mounted properly to within the allowable tolerances as allocated in the WF/PC wavefront budget. (Deflection induced in the manufactured unmounted WFC primary mirror, due to mount strain, cannot exceed 6×10^{-8} inches.) Acceptance tests configured for the unmounted mirrors (based on interferometric testing with the interferometric data evaluation software) in a clean, "noise-free" environment should also be used "after mounting", and the results compared with the WF/PC wavefront budget for conformance of the optical mount. It should also be noted that the optical coating is in place. Contamination and improper handling during installation of the mount can destroy the coating.

An acceptance test configuration has been established for the Cassegrain relay. The relay consists of two assemblies (mirrors with mounts). The configuration is based on interferometric alignment of the secondary mirror to the primary mirror. Again, testing would utilize the interferometric evaluation software in a clean, "noise-free" environment. Two properties of the Cassegrain would be obtained. The first describes the image quality over the field of view

and the second describes the location and contour of the focal surface. A special device called a focal surface reference fixture (FSRF) would be used in conjunction with the interferometry. It is emphasized that a quantitative determination of image quality and a focal surface "map" require interferometric data evaluation techniques. The "classic" qualitative star test, utilizing a point source microscope, does *not* have the required accuracy.

The Wide Field/Planetary Camera Optics Study established overall optical system requirements for a combined OTA with WF/PC. These performance requirements dictate interferometric testing (wavefront quality, alignment, and focus) during manufacture of the unmounted mirrors, during buildup, and at the total WF/PC level.

APPENDIX A - OPTICAL TOLERANCE MATRIX

APPENDIX A

OPTICAL TOLERANCE MATRIX

The optical tolerance matrix has been filled out based on several assumptions. The "firm" values have been obtained from section 8.5, Optical Tolerance Budgeting. As emphasized in this section, the budgeting philosophy is based on the Cassegrain primary mirror being the fixed reference for the system. Resultant perturbation analyses are based on this assumption. Also assumed is that this budgeting philosophy will be used and continued throughout the buildup (component level to camera level).

The "firm" values were obtained from a direct comparison of data from the Kodak optical evaluation software and closed form equation solutions. The "preliminary" values have not been obtained through this depth of analysis and, in most cases, are based on engineering judgement. The "to be determined" values are based on the fact that not enough thermal/mechanical design information is available to perform an adequate analysis or to make an engineering judgement. This data is especially necessary in determining operational (dynamic) tolerances.

It should be noted that radius tolerances on the plano surfaces have not been defined in the matrix. For surface quality levels of 0.01 wave, a figure error requirement with a test configuration will completely specify the plano surface (see section 8.1).

WF/PC OPTICAL SYSTEM

OPTICAL ELEMENT MANUFACTURING REQUIREMENTS

ELEMENT	SURFACE	RADIUS OR ASPHERIC COEFFICIENTS	SURFACE ACCURACY		THICKNESS PLUS TOLERANCE	MINIMUM CLEAR APERTURE	PYRAMID ANGLE PLUS TOLERANCE
			RADIUS	SURFACE ERROR (λRMS)			
1. Pick off Mirror	1	PLANO	N/A	0.01	N/A	13.72* DIAG.	N/A
2. Filter	1 2	PLANO PLANO	N/A N/A	0.01 0.01	0.50±0.02* (EQUIVALENT THICKNESS OF FUSED SILICA)	**	N/A
3. Pyramid	1	306.84	1.53	0.05	N/A	*f*/12.9: 3.22 *f*/30: 1.38	50.149 ±0.020 (see DWG. D231-123)
4. *f*/12.9 Fold Mirror	1	PLANO	N/A	0.015	N/A	4.45*	N/A
5. *f*/12.9 Primary Mirror	1	R_V 40.5662 κ -.50006 A_4 + 3914992E-07 A_6 +.5B90965E-08 A_8 +.6845064E-09 A_{10} - 1842629E-09	0.20	0.015	N/A	6.08	N/A

* *Preliminary value*
** *To be determined*
N/A Not applicable

ELEMENT	SURFACE	RADIUS OR ASPHERIC COEFFICIENTS	SURFACE ACCURACY		THICKNESS PLUS TOLERANCE	CLEAR APERTURE	PYRAMID ANGLE PLUS TOLERANCE
			RADIUS	SURFACE ERROR (λ RMS)			
6. *f*/12.9 Secondary Mirror	1	R_v 26.5462 κ - 6.64908 A_4 - 2771794E-05 A_6 - 2982543E-06 A_8 - .3224190E-05 A_{10} - .3582286E-05	0.14	0.015	N/A	1.62	N/A
7. *f*/30 Fold Mirror	1	PLANO	N/A	0.01	N/A	2.26*	N/A
8. *f*/30 Primary Mirror	1	R_v 51.7800 κ -.284 $A_4 - A_{10}$ 0	0.26	0.015	N/A	5.30	N/A
9. *f*/30 Secondary Mirror	1	R_v 23.4330 κ -2.420 $A_4 - A_{10}$ 0	0.12	0.015	N/A	1.40	N/A
10. CCD Window	1 2	PLANO PLANO	N/A N/A	0.01 0.01	0.25 ±0.02*	*f*/12.9: $\frac{1}{2}$ 1.72 *f*/30: $\frac{1}{2}$ 1.72	N/A
11. CCD	1	PLANO	**	N/A	N/A	*f*/12.9: 1.72 *f*/30: 1.72	N/A

* *Preliminary value*
** *To be determined*
N/A Not applicable

WF/PC OPTICAL SYSTEM

ALLOWABLE OPTICAL ELEMENT POSITIONING TOLERANCES

ELEMENT	AIR-SPACE	POSITIONING & LONG-TERM STABILITY TOLERANCE			STABILITY TOLERANCE DURING AN EXPOSURE		
		AIRSPACE ± Δ Z (min)	DE-CENTER ± Δ x/y(min)	TILT ± Δθ x/y(min)	AIRSPACE ± Δ Z (μ)	DE-CENTER ± Δ x/y (μ)	TILT ± Δθ x/y (sec)
WF/PC Interface with the SSM	---	0.1	0.5	.16	0.5	0.5	0.003
Pick-Off Mirror	---	---	0.5*	10*			
Filter	17.5276	0.2*	1.0*	5*			
Pyramid	18.7579	0.2*	0.5*	2*			
f/12.9 Fold Mirror	16.0462	0.1*	2.0*	2*			
f/12.9 Relay Optics Subassembly	To *f*/12.9 Primary 96.9957	0.1*	0.5*	5*			
	---	---					

* *Preliminary value*
** *To be determined*
N/A Not applicable

EASTMAN KODAK COMPANY • 901 ELMGROVE ROAD • ROCHESTER, NEW YORK 14650

ELEMENT	AIR-SPACE	POSITIONING & LONG-TERM STABILITY TOLERANCE			STABILITY TOLERANCE DURING AN EXPOSURE		
		AIRSPACE ± Δ Z (mm)	DE-CENTER ± Δ x/y(mm)	TILT ± Δθ x/y(min)	AIRSPACE ± Δ Z	DE-CENTER ± Δ x/y	TILT ± Δθ x/y
f/12.9 Primary Mirror	---	---	0.0 REF.	0.0 REF.			
	16.2590	0.03					
f/12.9 Secondary Mirror			0.2	3			
	20.7315	0.02					
CCD Window (BACK SURFACE)			2.0*	1*			
	0.1011	0.02*					
CCD			2.0*	1*			

* *Preliminary value*
** *To be determined*
N/A Not applicable

ELEMENT	AIR-SPACE	POSITIONING & LONG-TERM STABILITY TOLERANCE			STABILITY TOLERANCE DURING AN EXPOSURE		
		AIRSPACE ± Δ Z (mm)	DE-CENTER ± Δ x/y(mm)	TILT ± Δθ x/y(min)	AIRSPACE ± Δ Z	DE-CENTER ± Δ x/y	TILT ± Δθ x/y
---	---	---	0.5*	2*			
	From Pyramid						
f/30 Fold Mirror	15.9102	0.1*	2.0*	2*			
	To *f*/30 Primary						
f/30 Relay Optics Subassembly	97.1469	0.1*	0.5*	5*			
f/30 Primary Mirror			0.0 REF.	0.0 REF.			
	24.6470	0.03					
f/30 Secondary Mirror			0.4	3			
	37.5603	0.02					
			2.0*	1*			
CCD Window (BACK SURFACE)	---	---					

* *Preliminary value*
** *To be determined*
N/A Not applicable

ELEMENT	AIR-SPACE	POSITIONING & LONG-TERM STABILITY TOLERANCE			STABILITY TOLERANCE DURING AN EXPOSURE		
		AIRSPACE ± Δ Z (mm)	DE-CENTER ± Δ x/y(mm)	TILT ± Δθ x/y(min)	AIRSPACE ± Δ Z	DE-CENTER ± Δ x/y	TILT ± Δθ x/y
CCD	0.1011	0.02*	2.0*	1*			

* *Preliminary value*
** *To be determined*
N/A Not applicable

APPENDIX B - OPTICAL COMPONENT DRAWINGS

NO D231-115

NOTES:

1. MATERIAL:

1.1 THE MATERIAL USED SHALL BE CORNING® FUSED SILICA, NO 7940

1.2 THE α OF ALL THE MATERIAL USED TO FABRICATE ANY MIRROR BLANK SHALL BE $0.05 \pm 0.02 \times 10^{-6}$ IN/IN/°C OVER A TEMPERATURE RANGE OF -20° TO 20°C WITH A 95% CONFIDENCE LEVEL.

2. GLASS QUALITY.

2.1 INCLUSIONS SUCH AS BUBBLES AND SEEDS WITHIN THE .04 CENTIMETER THICK "CRITICAL ZONE" SHOWN ON THE DRAWING SHALL NOT EXCEED 0.051 CENTIMETERS IN MEAN DIAMETER. THERE SHALL BE NO MORE THAN AN AVERAGE OF 0.02 PER CUBIC CENTIMETER. AVERAGE SIZE OF SUCH INCLUSIONS SHALL BE NO GREATER THAN 0.031 CENTIMETERS IN MEAN DIAMETER

2.2 OPAQUE INCLUSIONS WITHIN THE 0.4 CENTIMETER THICK "CRITICAL ZONE" SHOWN ON THE DRAWING SHALL NOT EXCEED 0.051 CENTIMETERS IN MEAN DIAMETER. THERE SHALL BE NO MORE THAN AN AVERAGE OF 0.01 PER CUBIC CENTIMETER

3 ANNEAL

3.1 BIREFRINGENCE MEASUREMENTS SHALL BE MADE PERPENDICULAR TO THE 6.36 CENTIMETER SURFACE. THE RELATIVE RETARDATION RESULTING FROM PERMANENT STRAIN SHALL BE NO MORE THAN 20 Mμ PER CENTIMETER OF LIGHT PATH

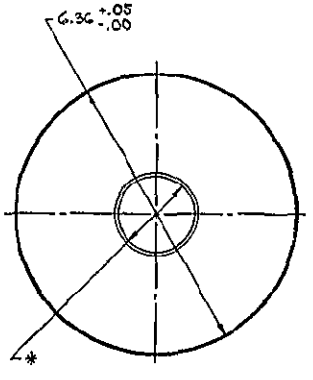

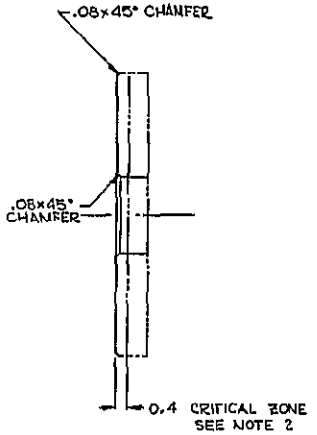

* = TO BE DETERMINED

UNLESS OTHERWISE SPECIFIED: LINEAR TOLERANCE ± .025 CM; ANGULAR TOLERANCE ±; DIMENSIONS ARE IN CENTIMETERS; DIMENSIONS APPLY AFTER FINISH UNLESS TOTAL TOLERANCE IS .001 (.025 MM) OR LESS AND ON ALL SURFACE EXCEPT PLACES DIMENSIONS APPLY BEFORE FINISH; KAD PRODUCT DESIGN STANDARDS APPLY; THIRD ANGLE PROJECTION	MATERIAL: SEE NOTE 1 FINISH SCALE OF ORIG DWG. 2/1	EASTMAN KODAK CO. KODAK APPARATUS DIVISION ROCHESTER, N.Y.	FIRST USED ON NAME BLANK, PRIMARY MIRROR WIDE FIELD CAMERA WF/PC SKETCH NO. SIZE D NO D231-115

NO	ZIP NO. DATE PTD.	REVISIONS	DR. BY APP'D

205

NO D231-116

NOTES:

1. SURFACE 1 SHALL BE A FIGURE OF REVOLUTION AND SHALL CONFORM TO THE ASPHERIC EQUATION

$$X = \frac{CY^2}{1+\sqrt{1-(K+1)C^2Y^2}} + EY^4 + FY^6 + GY^8 + HY^{10}$$

WHERE:

X = SAG IN CENTIMETERS OF THE ASPHERIC SURFACE RELATIVE TO A PLANE LOCATED AT THE VERTEX AND NORMAL TO THE OPTICAL AXIS

$$C = \frac{1}{40.5662}$$

1.1 THE NOMINAL VERTEX RADIUS OF THE ASPHERIC SURFACE SHALL BE 40.5662 ±0.20 CENTIMETERS

1.2 SURFACE 1 SHALL NOT DEVIATE FROM THE ASPHERIC CURVATURE BY MORE THAN 0.015 WAVELENGTH (RMS) (ROOT MEAN SQUARE) AFTER REFLECTIVE COATING. (WAVELENGTH REFERENCE IS 0.6328 MICRONS) AS MEASURED WITH THE TEST SET-UP SHOWN IN D23126. THE GRID SPACING OF THE SAMPLE POINTS ON THE MIRROR SURFACE SHALL NOT EXCEED 0.15 CENTIMETERS.

1.3 THE ASPHERIC TABLE OF COEFFICIENTS SHOWN BELOW IS BASED ON THE NOMINAL VALUE OF THE VERTEX RADIUS.

K = −0.50006 E = +0.3914992 E-07 F = +0.5890965E-08
G = +0.6845064E-09 H = −0.1842629E-09

2. CLEAR APERTURE:
   2.1 SURFACE-1 SHALL HAVE A CLEAR APERTURE BOUNDED ON THE OUTSIDE BY A DIAMETER OF 6.048 CENTIMETERS MINIMUM AND ON THE INSIDE BY A DIAMETER OF 1.676 CENTIMETERS MAXIMUM.
   2.2 FOR ALL MIRROR TESTS BEFORE COATING, SURFACE-1 SHALL HAVE AN UNCOATED CLEAR APERTURE BOUNDED ON THE OUTSIDE BY A DIAMETER OF 6.048 CENTIMETERS MINIMUM AND ON THE INSIDE BY A CIRCLE OF 1.676 CENTIMETERS MAXIMUM.
3. SURFACES MARKED "P" POLISHED, ALL OTHERS GROUND TO A FINISH EQUIVALENT TO 120 GRIT OR BETTER AND FELT POLISHED.
4. REFLECTIVE COATING:
   4.1 SURFACE-1 SHALL CONFORM TO NOTE 1.2 AFTER COATING.
   4.2 SURFACE-1 SHALL BE COATED WITH 800 ANGSTROMS OF ALUMINUM WITH 250 ANGSTROMS OF MAGNESIUM FLUORIDE AS A PROTECTIVE COATING.
   4.3 SURFACE-1 SHALL HAVE A MINIMUM REFLECTANCE OF 70% AT A WAVELENGTH OF 0.1200 MICRONS AND A MINIMUM REFLECTANCE OF 85% AT 0.6328 MICRONS WHEN MEASURED AT NORMAL INCIDENCE
   4.4 SURFACE CLEANING SHALL BE IN ACCORDANCE WITH ✳.
5. THE OPTICAL VERTEX SHALL BE WITHIN ✳ CENTIMETERS RADIALLY OF THE MECHANICAL VERTEX.
6. SYSTEM AXES:
   6.1 ANGULAR ORIENTATION OF THE Y AXIS SHALL CONSIDER OPTIMIZATION OF THE ASSEMBLED SYSTEM WAVEFRONT BY ROTATIONAL MATCHING OF THE PRIMARY AND SECONDARY MIRRORS.
   6.2 THE Y AXIS SHALL BE IDENTIFIED BY A 0.013 CENTIMETER WIDE LINE ON SURFACE 2. IDENTIFYING CHARACTER AND LINE SHALL BE DRAWN PER ✳.
   COLOR: FLAT BLACK MAT'L REQ'D.
7. THE AUTOCORRELATION LENGTH OF THE SYSTEM WAVEFRONT ERROR SHALL BE 0.125 OR LONGER WHEN MODELED AS A GAUSSIAN FUNCTION OVER THE SPATIAL FREQUENCIES FROM 0-20 CYCLES PER PUPIL DIAMETER.
8. SURFACE QUALITY 20-5, MIL-O-13830A
9. THE MAXIMUM SURFACE ROUGHNESS SHALL BE 30 ANGSTROMS RMS.

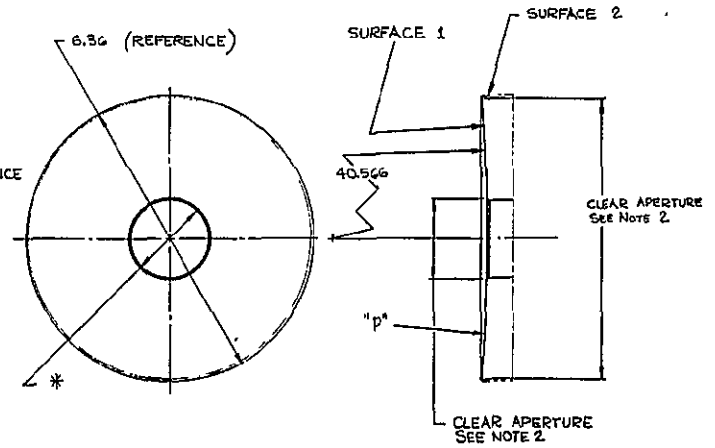

✳ = TO BE DETERMINED

REVISIONS		
CHG NO / DATE REL	REVISIONS	DR BY / APPD
NO		

UNLESS OTHERWISE SPECIFIED
LINEAR TOLERANCE ± .025 CM
ANGULAR TOLERANCE ±
DIMENSIONS ARE IN CENTIMETERS
DIMENSIONS APPLY AFTER FINISH. MARKED TOTAL TOLERANCE IS .001 (.025MM) ON .686 AND ON ALL THREADS. IN ALL OTHER PLACES DIMENSIONS APPLY BEFORE FINISH
KAD PRODUCT DESIGN STANDARDS APPLY
THIRD ANGLE PROJECTION

MATERIAL: MAKE FROM D231-115
FINISH
SCALE OF ORIG. DWG 2/1

EASTMAN KODAK CO.
KODAK APPARATUS DIVISION
ROCHESTER, N.Y.
DR T.NEWETT DATE 11/15/78
CH. DES. P.A. JONES
DFTG. APPD
ENG
ORIG. CHG NO
RELEASED

FIRST USED ON
NAME PRIMARY MIRROR, WIDE FIELD CAMERA WF/PC
SKETCH NO
SIZE D
NO D231-116

206

NOTES :

1.0 TWO ALTERNATE TEST CONFIGURATIONS HAVE BEEN ESTABLISHED.

2.0 AN ACCEPTABLE TEST INTERFEROGRAM MAY CONTAIN A MAX OF * WAVE COMA. THE COMA CORRESPONDS TO A DECENTERING OF THE VERTEX OF THE PRIMARY MIRROR RELATIVE TO THE TEST AXIS OF * CM. COMA IS DEFINED IN THE FOLLOWING FIGURE :

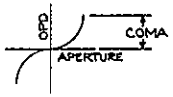

3.0 IN CONFIGURATION #1 THE PRIMARY MIRROR SURFACE ERROR IS CALCULATED BY THE EQUATION : $E(X,Y) = \frac{1}{2}\,OPD(X,Y) + BO(X,Y)$ WHERE $E(X,Y)$ IS EQUAL TO THE PRIMARY MIRROR SURFACE ERROR AT POINT X,Y ON THE SURFACE DEFINED AS THE SAG OF THE ACTUAL SURFACE MINUS THE SAG OF THE DESIRED SURFACE. (HENCE, A HILL ON THE ACTUAL SURFACE IS A POSITIVE SURFACE ERROR). $OPD(X,Y)$ = THE MEASURED WAVEFRONT OPTICAL PATH LENGTH DIFFERENCE CORRESPONDING TO POINT X,Y ON THE PRIMARY MIRROR SURFACE. THE OPD SIGN CONVENTION IS THAT A POSITIVE OPD VALUE CORRESPONDS TO A LEADING WAVEFRONT SUCH AS WOULD BE PRODUCED BY A HILL ON THE PRIMARY MIRROR SURFACE. $BO(X,Y)$ IS EQUAL TO THE BACKOUT EQUATION FOR TEST RESIDUALS. THE VALUE OF THE BACKOUT EQUATION AT POINT X,Y IS TO BE ADDED TO THE VALUE OF SURFACE OPD AT POINT X,Y AS STATED IN THE PRECEDING EQUATION. THE BACKOUT EQUATION FOR THE PRIMARY MIRROR SURFACE CONTOUR IS A RADIALLY SYMMETRIC FUNCTION EXPRESSED IN UNITS OF CENTIMETERS :

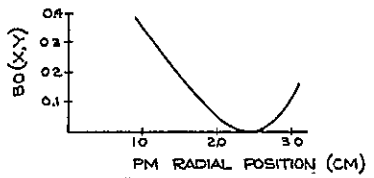

4.0 IN CONFIGURATION #2, THE PRIMARY MIRROR SURFACE ERROR IS CALCULATED BY THE EQUATION : $E(X,Y) = \frac{1}{4}\,OPD(X,Y) - \frac{1}{4}\,R(X,Y) + BO(X,Y)$ WHERE $E(X,Y)$, $OPD(X,Y)$ AND $BO(X,Y)$ ARE DEFINED IN NOTE 3.0. $R(X,Y)$ = THE RETROREFLECTOR WAVEFRONT ERROR AS DETERMINED FROM DIRECT CALIBRATION WITH AN INTERFEROMETER

$BO(X,Y)$:

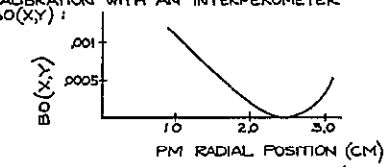

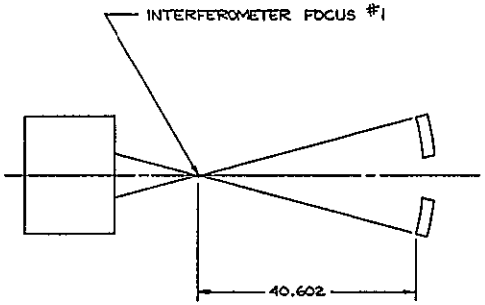

CONFIGURATION #1
(DIRECT TWYMAN - GREEN)

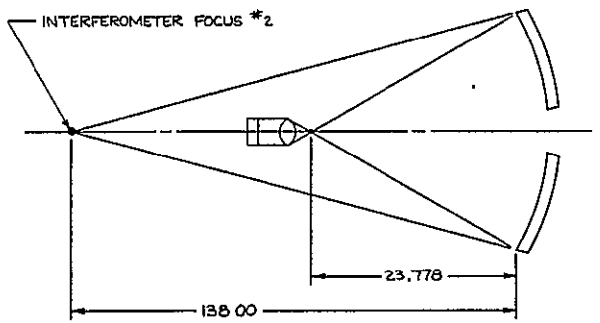

CONFIGURATION #2
(RETROREFLECTOR)

NO	ORIG. NO. DATE REL.	REVISIONS	DR. BY APPR.

UNLESS OTHERWISE SPECIFIED LINEAR TOLERANCE ± ANGULAR TOLERANCE ± DIMENSIONS ARE IN DIMENSIONS APPLY AFTER FINISH WHERE TOTAL TOLERANCE IS .001 (.03MM) OR LESS AND ON ALL THREADS IN ALL OTHER PLACES DIMENSIONS APPLY BEFORE FINISH. KAD PRODUCT DESIGN STANDARDS APPLY THIRD ANGLE PROJECTION	MATERIAL FINISH SCALE OF ORIG. DWG. NONE	EASTMAN KODAK CO. KODAK APPARATUS DIVISION ROCHESTER, N.Y.	PRINT MADE ON NAME WIDE FIELD CAMERA PRIMARY MIRROR ACCEPTANCE TEST CONFIGURATION, WF/PC SKETCH NO. CODE IDENT D NO D231-117
		DR. P. SPANGENBERG DATE 2-19-79 CK. DES. ENG. P. A. JONES DATE MFG. ENG. ORIG. DWG. NO. RELEASED	

207

NO. D231-118

NOTES:

1. MATERIAL:
   1.1 THE MATERIAL USED SHALL BE CORNING® FUSED SILICA, NO 7940

   1.2 COEFFICIENT OF THERMAL EXPANSION (α)
   1.2.1 THE α OF ALL THE MATERIAL USED TO FABRICATE ANY MIRROR BLANK SHALL BE $0.00 \pm .03 \times 10^{-6}$ IN/IN/°C OVER A TEMPERATURE RANGE OF -20°C TO 20°C WITH A 95% CONFIDENCE LEVEL.

2. GLASS QUALITY:
   2.1 INCLUSIONS SUCH AS BUBBLES AND SEEDS WITHIN THE 0.4 CENTIMETER THICK "CRITICAL ZONE" SHOWN ON THE DRAWING SHALL NOT EXCEED 0.051 CENTIMETERS IN MEAN DIAMETER. THERE SHALL BE NO MORE THAN AN AVERAGE OF 0.02 PER CUBIC CENTIMETER. AVERAGE SIZE OF SUCH INCLUSIONS SHALL BE NO GREATER THAN .0030 CENTIMETERS IN MEAN DIAMETER.

   2.2 OPAQUE INCLUSIONS WITHIN THE 0.4 CENTIMETER THICK "CRITICAL ZONE" SHOWN ON THE DRAWING SHALL NOT EXCEED 0.051 CENTIMETERS IN MEAN DIAMETER. THERE SHALL BE NO MORE THAN AN AVERAGE OF 0.01 PER CUBIC CENTIMETER.

3. ANNEAL:
   3.1 BIREFRINGENCE MEASUREMENTS SHALL BE MADE PERPENDICULAR TO THE 1.93 CENTIMETER SURFACE. THE RELATIVE RETARDATION RESULTING FROM PERMANENT STRAIN SHALL BE NO MORE THAN 20 mμ PER CENTIMETER OF LIGHT PATH.

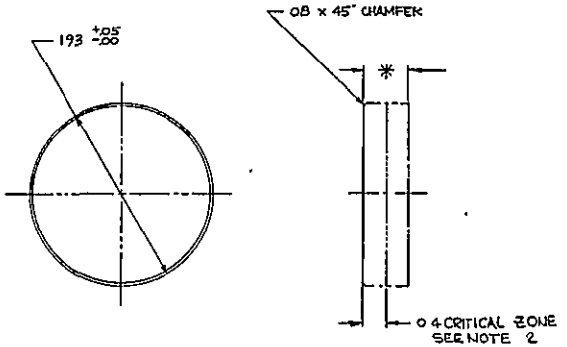

* = TO BE DETERMINED

NO.	REVISIONS	DR. BY APP'D
ORG. NO. DATE REL.		

UNLESS OTHERWISE SPECIFIED
LINEAR TOLERANCE ± .025 CM
ANGULAR TOLERANCE ±
DIMENSIONS ARE IN CENTIMETERS
DIMENSIONS APPLY AFTER FINISH WHERE TOTAL TOLERANCE IS .001 (.025MM) OR LESS AND ON ALL THREADS IN ALL OTHER PLACES DIMENSIONS APPLY BEFORE FINISH
KAD PRODUCT DESIGN STANDARDS APPLY
THIRD ANGLE PROJECTION

MATERIAL: SEE NOTE 1
FINISH:
SCALE OF ORIG. DWG. 4/1

EASTMAN KODAK CO.
KODAK APPARATUS DIVISION
ROCHESTER N.Y.

DR. T. Hewitt DATE 11/17/78
CK. P.A JONES
OPTG
ORIG. CHG. NO
RELEASED

FIRST USED ON
NAME BLANK, SECONDARY MIRROR WIDE FIELD CAMERA WF/PC
SKETCH NO
ORIG. SIZE D
NO D231-118

208

NOTES:

1. SURFACE 1 SHALL BE A FIGURE OF REVOLUTION AND SHALL CONFORM TO THE ASPHERIC EQUATION

$$X = \frac{CY^2}{1+\sqrt{1-(k+1)C^2Y^2}} + EY^4 + FY^6 + GY^8 + HY^{10}$$

WHERE:
X = SAG IN CENTIMETERS OF THE ASPHERIC SURFACE RELATIVE TO A PLANE LOCATED AT THE VERTEX AND NORMAL TO THE OPTICAL AXIS

$$C = \frac{1}{28.5462}$$

1.1 THE NOMINAL VERTEX RADIUS OF THE ASPHERIC SURFACE SHALL BE 28.5462 ± .014 CENTIMETERS.
1.2 SURFACE 1 SHALL NOT DEVIATE FROM THE ASPHERIC CURVATURE BY MORE THAN 0.015 WAVELENGTH (RMS) (ROOT MEAN SQUARE) AFTER REFLECTIVE COATING. (WAVELENGTH REFERENCE IS 0.6328 MICRONS) AS MEASURED WITH THE TEST SET-UP SHOWN IN D231-120. THE GRID SPACING OF THE SAMPLE POINTS ON THE MIRROR SURFACE SHALL NOT EXCEED 0.05 CENTIMETERS.
1.3 THE ASPHERIC TABLE OF COEFFICIENTS SHOWN BELOW IS BASED ON THE NOMINAL VALUE OF THE VERTEX RADIUS.

K = -6.64908 E = -.2777946E-05 F = -.2982543E-05
G = -.3224190E-05 H = -.3582286E-05

2. CLEAR APERTURE:
2.1 SURFACE-1 SHALL HAVE A CLEAR APERTURE OF 1.62 +0.00 -0.05 CENTIMETERS DIAMETER.
2.2 FOR ALL MIRROR TESTS BEFORE COATING, SURFACE-1 SHALL HAVE AN UNCOATED CLEAR APERTURE OF 1.66 +0.00 -0.05 CENTIMETERS DIAMETER.

3. SURFACES MARKED "P" POLISHED, ALL OTHERS GROUND TO A FINISH EQUIVALENT TO 120 GRIT OR BETTER AND FELT POLISHED.

4. REFLECTIVE COATING:
4.1 SURFACE-1 SHALL CONFORM TO NOTE 1.2 AFTER COATING.
4.2 SURFACE-1 SHALL BE COATED WITH 800 ANGSTROMS OF ALUMINUM WITH 250 ANGSTROMS OF MAGNESIUM FLUORIDE AS A PROTECTIVE COATING.
4.3 SURFACE-1 SHALL HAVE A MINIMUM REFLECTANCE OF 70% AT A WAVELENGTH OF 0.1200 MICRONS AND A MINIMUM REFLECTANCE OF 85% AT 0.6328 MICRONS, WHEN MEASURED AT NORMAL INCIDENCE.
4.4 SURFACE CLEANING SHALL BE IN ACCORDANCE WITH PROCEDURE *.

5. THE OPTICAL VERTEX SHALL BE WITHIN .002 CENTIMETERS RADIALLY OF THE MECHANICAL VERTEX.

6. SYSTEM AXES:
6.1 ANGULAR ORIENTATION OF THE Y AXIS SHALL CONSIDER OPTIMIZATION OF THE ASSEMBLED SYSTEM WAVEFRONT BY ROTATIONAL MATCHING OF THE PRIMARY AND SECONDARY MIRRORS.
6.2 THE Y AXIS SHALL BE IDENTIFIED BY A 0.013 CENTIMETER WIDE LINE ON SURFACE 2. IDENTIFYING CHARACTER AND LINE SHALL BE DRAWN PER *.
COLOR: FLAT BLACK MAT'L REQ'D.

7. THE AUTOCORRELATION LENGTH OF THE SYSTEM WAVEFRONT ERROR SHALL BE 0.125 OR LONGER WHEN MODELED AS A GAUSSIAN FUNCTION OVER THE SPATIAL FREQUENCIES FROM 0-20 CYCLES PER PUPIL DIAMETER.

8. SURFACE QUALITY 20-5, MIL-G-13830A.

9. THE MAXIMUM SURFACE ROUGHNESS SHALL BE 30 ANGSTROMS RMS.

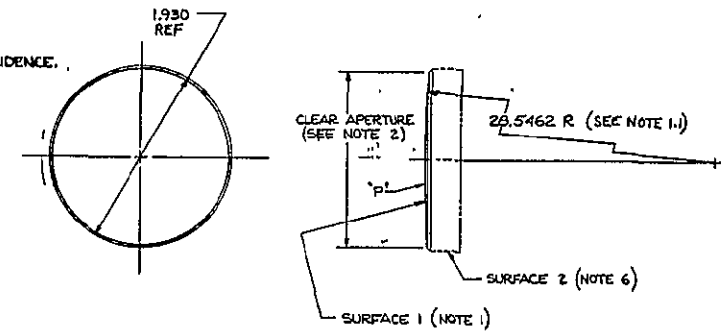

* = TO BE DETERMINED

D231-119

209

NO.	REVISIONS	BY APPR.
CHG. NO. DATE REL.		

UNLESS OTHERWISE SPECIFIED
LINEAR TOLERANCE ± .025 CM
ANGULAR TOLERANCE ±
DIMENSIONS ARE IN CENTIMETERS
DIMENSIONS APPLY AFTER FINISH WHERE TOTAL TOLERANCE IS .001 (0.0254MM) OR LESS AND ON ALL THREADS. IN ALL OTHER PLACES DIMENSIONS APPLY BEFORE FINISH.
EAD PRODUCT DESIGN STANDARDS APPLY
THIRD ANGLE PROJECTION

MATERIAL: MAKE FROM D231-118
FINISH
SCALE OF ORIG. DWG. 4/1

EASTMAN KODAK CO.
KODAK APPARATUS DIVISION
ROCHESTER, N.Y.

DR. Thewett	DATE 11/20/78		
CK.		DES. ENG. P.A JONES	
DATE		MFG. ENG.	
ORIG. CHG. NO.			
RELEASED			

FIRST USED ON
NAME SECONDARY MIRROR
WIDE FIELD CAMERA
WF/PC
SKETCH NO.
SIZE D
NO. D231-119

NOTES:

1.0 TWO ALTERNATE TEST CONFIGURATIONS HAVE BEEN ESTABLISHED

2.0 AN ACCEPTABLE TEST INTERFEROGRAM MAY CONTAIN A MAX OF * WAVE COMA. THIS COMA CORRESPONDS TO A DECENTERING OF THE VERTEX OF THE SECONDARY MIRROR RELATIVE TO THE TEST AXIS OF * Cm. COMA IS DEFINED IN THE FOLLOWING FIGURE:

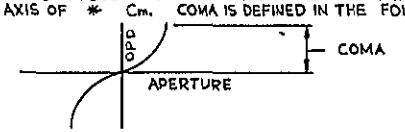

3.0 IN CONFIGURATION #1, THE SECONDARY MIRROR SURFACE ERROR IS CALCULATED BY THE EQUATION. $E(X,Y) = 1/4\ OPD(X,Y) - 1/2\ N(X,Y) + BO(X,Y)$ WHERE $E(X,Y)$ IS EQUAL TO THE SECONDARY MIRROR SURFACE ERROR AT POINT X,Y ON THE SURFACE DEFINED AS THE SAG OF THE ACTUAL SURFACE MINUS THE SAG OF THE DESIRED SURFACE. (HENCE, A "HILL" ON THE ACTUAL SURFACE IS A POSITIVE SURFACE ERROR). $OPD(X,Y)$ = THE MEASURED WAVEFRONT OPTICAL PATH LENGTH DIFFERENCE CORRESPONDING TO POINT X,Y ON THE SECONDARY MIRROR SURFACE. THE OPD SIGN CONVENTION IS THAT A POSITIVE OPD VALUE CORRESPONDS TO A LEADING WAVEFRONT SUCH AS WOULD BE PRODUCED BY A "HILL" ON THE SECONDARY MIRROR SURFACE. $BO(X,Y)$ IS EQUAL TO THE BACKOUT EQUATION FOR TEST RESIDUALS. THE VALUE OF THE BACKOUT EQUATION AT POINT X,Y IS TO BE ADDED TO THE VALUE OF SURFACE OPD AT POINT X,Y AS STATED IN THE PRECEDING EQUATION. THE BACKOUT EQUATION FOR THE SECONDARY MIRROR SURFACE CONTOUR IS A RADIALLY SYMMETRIC FUNCTION EXPRESSED IN UNITS OF CENTIMETERS: $BO(X,Y) = *$. $N(X,Y)$ - THE HINDLE SPHERE SURFACE ERROR AS DETERMINED FROM DIRECT INTERFEROMETRIC CALIBRATION

4.0 SURFACE 2 SHALL BE SPHERICAL WITHIN 0.02 WAVELENGTH RMS OVER THE CLEAR APERTURE WHEN REFERENCED TO 0.6328 MICRON LIGHT

4.1 THE CLEAR APERTURE OF SURFACE 2 SHALL BE 3.707 CM MIN O.D AND 0.689 MAX I.D

4.2 SURFACE 2 IS TO BE POLISHED. ALL OTHER HINDLE SPHERE SURFACES ARE TO BE GROUND TO A FINISH EQUIVALENT TO A 120 GRIT OR BETTER AND FELT POLISHED.

4.3 SURFACE QUALITY - 50/30, IN ACCORDANCE WITH MIL-O-13830A.

4.4 SURFACE 2 SHALL CONFORM TO NOTE 4.0 AFTER COATING. SURFACE 2 SHALL HAVE A HIGH REFLECTANCE COATING APPLIED. THE MINIMUM AVERAGE REFLECTANCE OF THE SURFACE 2 COATING SHALL BE 95% OR GREATER AT THE SPECTRAL WAVELENGTH OF 0.6328 MICRONS WHEN MEASURED NORMAL TO THE SURFACE.

4.5 SURFACE CLEANING SHALL BE IN ACCORDANCE WITH PROCEDURE *.

4.6 SURFACE 2 SHALL BE A SPHERICAL FIGURE OF REVOLUTION WITH A SPHERICAL VERTEX RADIUS OF 18.331± * CENTIMETERS.

$$C = \frac{1}{18.331} \qquad K \cdot E \cdot F \cdot G \cdot H \cdot O$$

5.0 A LINE THROUGH INTERFEROMETER FOCI POINTS 1 & 2 MUST PASS THROUGH THE SECONDARY MIRROR SURFACE WITHIN * OF THE MECHANICAL CENTER.

6.0 IN CONFIGURATION #2 THE SECONDARY SURFACE ERROR IS CALCULATED BY THE EQUATION. $E(X,Y) = 1/2\ OPD(X,Y) - [S(X,Y) - OPD_T(X,Y)] + BO(X,Y)$ WHERE $E(X,Y)$, $OPD(X,Y) \neq BO(X,Y)$ ARE DEFINED IN NOTE 3.0

$S(X,Y)$ = THE MEASURED SURFACE ERROR CORRESPONDING TO POINT X,Y ON THE TEST GLASS

$OPD_T(X,Y)$ = THE MEASURED TRANSMITTED WAVEFRONT OPTICAL PATH LENGTH DIFFERENCE CORRESPONDING TO POINT X,Y ON THE TEST GLASS

7.0 SURFACES 3 AND 4 SHALL BE SPHERICAL WITHIN 0.02 WAVELENGTH RMS OVER THE CLEAR APERTURE WHEN REFERENCED TO 0.6328 MICRON LIGHT

7.1 THE CLEAR APERTURE OF SURFACES 3 AND 4 SHALL BE *

7.2 SURFACES 3 AND 4 TO BE POLISHED ALL OTHER SURFACES ARE TO BE GROUND TO A FINISH EQUIVALENT TO A 120 GRIT OR BETTER AND FELT POLISHED.

7.3 SURFACE QUALITY - 50/30 IN ACCORDANCE WITH MIL-O-13830A

7.4 SURFACE 3 SHALL CONFORM TO NOTE 7.0 AFTER COATING. SURFACE 3 SHALL HAVE A REFLECTANCE COATING APPLIED. THE MINIMUM AVERAGE REFLECTANCE OF THE SURFACE 3 COATING SHALL BE 60% AT THE SPECTRAL WAVELENGTH OF 0.6328 MICRONS WHEN MEASURED NORMAL TO THE SURFACE.

7.5 SURFACES 3 AND 4 CLEANING SHALL BE IN ACCORDANCE WITH PROCEDURE *

7.6 SURFACES 3 AND 4 SHALL BE SPHERICAL FIGURES OF REVOLUTION WITH NOMINAL SPHERICAL VERTEX RADII OF 28.5462 ±*

8.0 A LINE THROUGH INTERFEROMETER FOCI POINT #3 AND THE MECHANICAL CENTER OF SURFACE 3 MUST PASS THROUGH THE SECONDARY MIRROR SURFACE WITHIN * OF THE MECHANICAL CENTER.

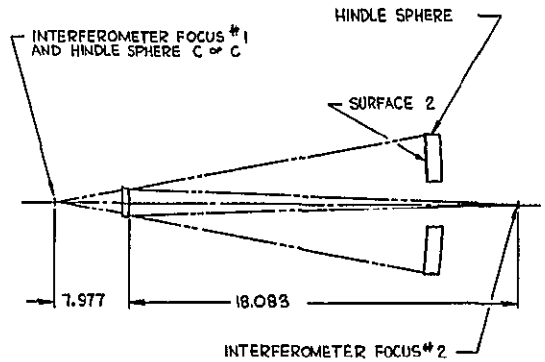

CONFIGURATION #1 (HINDLE)

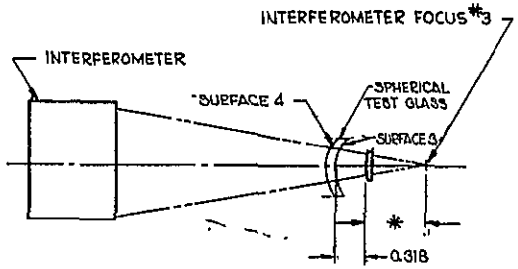

CONFIGURATION #2 (FIZEAU)

ORIGINAL PAGE IS OF POOR QUALITY

NO.	REVISIONS	BY APVD

UNLESS OTHERWISE SPECIFIED: LINEAR TOLERANCE ±; ANGULAR TOLERANCE ±; DIMENSIONS ARE IN CENTIMETERS; DIMENSIONS APPLY AFTER FINISH WHERE TOTAL TOLERANCE IS .001 (.0025M) OR LESS AND ON ALL THREADS, IN ALL OTHER PLACES DIMENSIONS APPLY BEFORE FINISH; KAD PRODUCT DESIGN STANDARDS APPLY; THIRD ANGLE PROJECTION

MATERIAL

FINISH

SCALE OF DRG. DWG. NONE

EASTMAN KODAK CO.
KODAK APPARATUS DIVISION
ROCHESTER, N.Y.

DR. Titcutt DATE 1/2/79

CH. DES. ENG. P.A TOVES

DATE INFO. ENG.

DRWG. CHG. NO. RELEASED

PART WHERE USED

NAME WIDE FIELD CAMERA SECONDARY MIRROR ACCEPTANCE TEST CONFIGURATION, WF/PC

SKETCH NO. REV. D

NO. D 231-120

210

NOTES:

1. MATERIAL
   1.1 THE MATERIAL USED SHALL BE CORNING® FUSED SILICA, NO 7940

   1.2 THE α OF ALL THE MATERIAL USED TO FABRICATE ANY MIRROR BLANK SHALL BE $0.50 \pm 0.02 \times 10^{-6}$ IN/IN/°C OVER A TEMPERATURE RANGE OF -20° TO 20°C WITH A 95% CONFIDENCE LEVEL

2. GLASS QUALITY
   2.1 INCLUSIONS SUCH AS BUBBLES AND SEEDS WITHIN THE 0.8 CENTIMETER THICK "CRITICAL ZONE" SHOWN ON THE DRAWING SHALL NOT EXCEED 0.051 CENTIMETERS IN MEAN DIAMETER. THERE SHALL BE NO MORE THAN AN AVERAGE OF 0.02 PER CUBIC CENTIMETER. AVERAGE SIZE OF SUCH INCLUSIONS SHALL BE NO GREATER THAN 0.030 CENTIMETERS IN MEAN DIAMETER.

   2.2 OPAQUE INCLUSIONS WITHIN THE 0.4 CENTIMETER THICK "CRITICAL ZONE" SHOWN ON THE DRAWING SHALL NOT EXCEED 0.051 CENTIMETERS IN MEAN DIAMETER. THERE SHALL BE NO MORE THAN AN AVERAGE OF 0.01 PER CUBIC CENTIMETER.

3. ANNEAL
   3.1 BIREFRINGENCE MEASUREMENTS SHALL BE MADE PERPENDICULAR TO THE 2.32 CENTIMETER SURFACE. THE RELATIVE RETARDATION RESULTING FROM PERMANENT STRAIN SHALL BE NO MORE THAN 20 nm PER CENTIMETER OF LIGHT PATH

4. THE TAPER SIDES SHALL BE IDENTIFIED BY A 0.013 CENTIMETER WIDE LINE. IDENTIFYING CHARACTER AND LINE, SHALL BE DRAWN PER * COLOR: FLAT BLACK MATERIAL REQUIRED

211

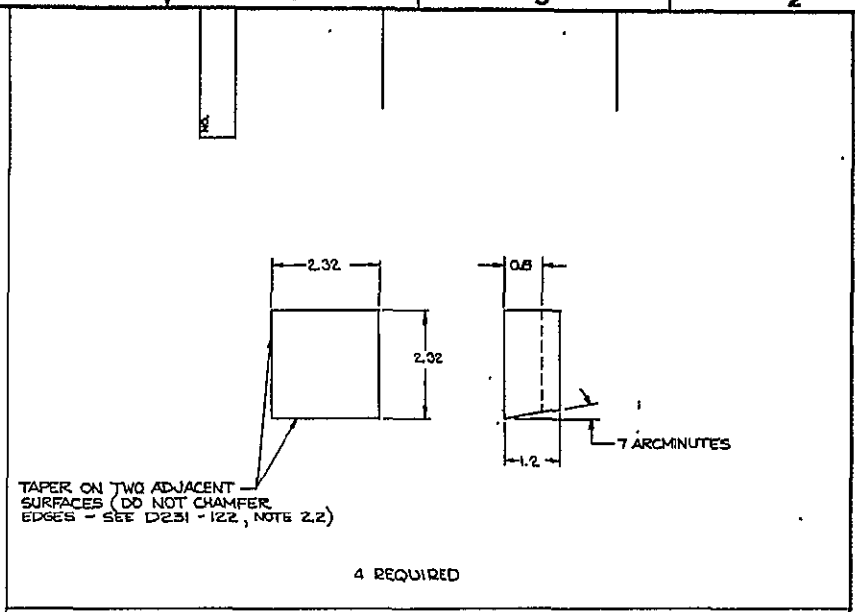

4 REQUIRED

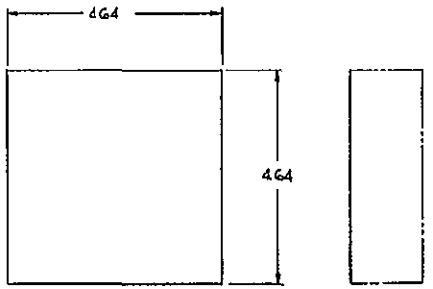

1 REQUIRED

NO.	REVISIONS	BY APPR.

UNLESS OTHERWISE SPECIFIED
LINEAR TOLERANCE ± .025 CM
ANGULAR TOLERANCE ±
DIMENSIONS ARE IN CENTIMETERS
DIMENSIONS APPLY AFTER FINISH WHERE TOTAL TOLERANCE IS .001 (.0127MM) OR LESS AND ON ALL THREADS, IN ALL OTHER PLACES DIMENSIONS APPLY BEFORE FINISH.
READ PRODUCT DRAWING STANDARDS APPLY
THIRD ANGLE PROJECTION

MATERIAL

FINISH

SCALE OF ORIG. DRG.

EASTMAN KODAK CO.
ROCHESTER, N.Y.
DR. DH Hyde DATE 13 FEB 79
CK. DES. ENG. P.A. JONES
APPD. ENG.
ORIG. ENG. REL.
RELEASED

NAME BLANK, PYRAMID MIRROR WF/PC
SIZE D
NO. D231-121

NOTES:

1. SURFACES 1 THROUGH 4 SHALL BE SPHERICAL FIGURES OF REVOLUTION. THE NOMINAL VERTEX RADIUS SHALL BE 306.84 ± 1.53 CENTIMETERS.
   1.1. SURFACES 1 THROUGH 4 SHALL NOT DEVIATE FROM THE SPHERICAL CURVATURE BY MORE THAN 0.05 WAVELENGTH (RMS) (ROOT MEAN SQUARE) AFTER REFLECTIVE COATING (WAVELENGTH REFERENCE IS 0.6328 MICRONS) AS MEASURED WITH THE TEST SET-UP SHOWN IN D231-123. THE GRID SPACING OF THE SAMPLE POINTS ON THE MIRROR SURFACE SHALL NOT EXCEED 0.06 CENTIMETERS.

2. CLEAR APERTURE
   2.1 SURFACES 1 THROUGH 4 SHALL HAVE A CLEAR APERTURE BOUNDED ON THE OUTSIDE BY A DIAMETER OF * CENTIMETERS.
   2.2 FOR ALL MIRROR TESTS BEFORE COATING, SURFACES 1 THROUGH 4 SHALL HAVE AN UNCOATED CLEAR APERTURE BOUNDED ON THE OUTSIDE BY A DIAMETER OF * CENTIMETERS MINIMUM.

3. SURFACES MARKED "P" POLISHED, ALL OTHERS GROUND TO A FINISH EQUIVALENT TO 120 GRIT OR BETTER AND FELT POLISHED.

4. REFLECTIVE COATING
   4.1 SURFACES 1 THROUGH 4 SHALL CONFORM TO NOTE 1.1 AFTER COATING.
   4.2 SURFACES 1 THROUGH 4 SHALL BE COATED WITH 800 ANGSTROMS OF ALUMINUM WITH 250 ANGSTROMS OF MAGNESIUM FLUORIDE AS A PROTECTIVE COATING.
   4.3 SURFACES 1 THROUGH 4 SHALL HAVE A MINIMUM REFLECTANCE OF 70% AT A WAVELENGTH OF 0.1200 MICRONS AND A MINIMUM REFLECTANCE OF 85% AT 0.6328 MICRONS WHEN MEASURED AT NORMAL INCIDENCE.
   4.4 SURFACE CLEANING SHALL BE IN ACCORDANCE WITH *.

5. THE LOCATIONS OF THE CENTER OF CURVATURES OF SURFACES 1 THROUGH 4 AFTER REFLECTIVE COATING SHALL BE MEASURED WITH TEST SET-UP SHOWN IN D231-123.
   5.1 THE LOCATIONS OF THE CENTER OF CURVATURES ON THE REFERENCE TEMPLATE SHOWN IN D231-123 SHALL BE 50.149 ± * CENTIMETERS.
   5.2 THE OPTICAL VERTEX ON SURFACES 1 THROUGH 4 SHALL BE WITHIN * CENTIMETERS RADIALLY OF THE MECHANICAL VERTEX.
   5.3 SURFACES LABELED WITH THE IDENTIFICATION LINE ON D231-121 SHALL BE INSIDE SURFACES WHEN INSTALLED ON SURFACE 5.

6. SURFACE BONDING SHALL BE IN ACCORDANCE WITH *.

7. A SURFACE QUALITY OF 10-1 SHALL BE GOAL WITH A SURFACE QUALITY OF 10-5 A REQUIREMENT; MIL-O-13830A

8. THE MAXIMUM SURFACE ROUGHNESS SHALL BE 15 ANGSTROMS RMS.

212

NO. D231-122

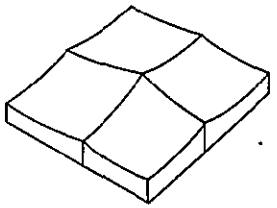

ASSEMBLY - 4 POLISHED FACETS

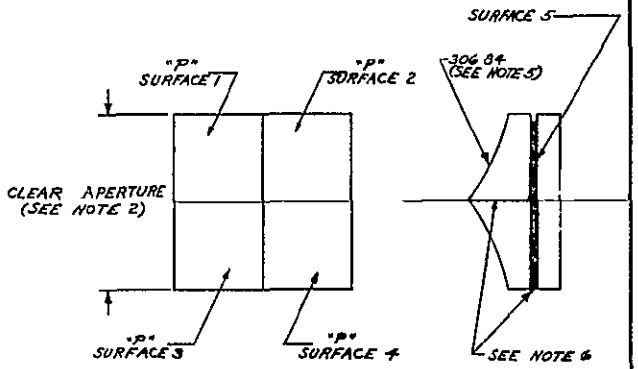

NO.	REVISIONS	BY APPR.

UNLESS OTHERWISE SPECIFIED: LINEAR TOLERANCE ±; ANGULAR TOLERANCE ±; DIMENSIONS ARE IN; DIMENSIONS APPLY AFTER FINISH WHERE TOTAL TOLERANCE IS .001 (.0254mm) OR LESS AND ON ALL THREADS. IN ALL OTHER PLACES DIMENSIONS APPLY BEFORE FINISH. KAD PRODUCT DESIGN STANDARDS APPLY. THIRD ANGLE PROJECTION	MATERIAL: MAKE FROM D231 - 121	EASTMAN KODAK CO. KODAK APPARATUS DIVISION ROCHESTER, N.Y.
	FINISH	MFR. PLB DATE 2-14-79
		DES. ENG. P. A. JONES
	SCALE OF ORIG. DWG.	MFG. ENG.
		ORIG. CYG. NO. RELEASED

FIRST USED ON

NAME PYRAMID MIRROR, WF/PC

SIZE D

SKETCH NO.

NO. D231-122

NOTES:

1.0 AN ACCEPTABLE TEST INTERFEROGRAM MAY CONTAIN A MAX OF * WAVE COMA. THIS COMA CORRESPONDS TO A DECENTERING OF THE VERTEX OF THE PYRAMID MIRROR FACET RELATIVE TO THE TEST AXIS OF * Cm. COMA IS DEFINED IN THE FOLLOWING FIGURE:

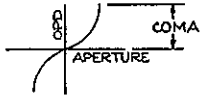

2.0 IN CONFIGURATION *1 THE PYRAMID MIRROR FACET SURFACE ERROR IS CALCULATED BY THE EQUATION:

$$E(X,Y) = \tfrac{1}{2}\,OPD(X,Y) - [S(X,Y) + OPD_T(X,Y)] + BO(X,Y)$$

WHERE E(X,Y) IS EQUAL TO THE PYRAMID MIRROR SURFACE ERROR AT POINT X,Y ON THE SURFACE DEFINED AS THE SAG OF THE ACTUAL SURFACE MINUS THE SAG OF THE DESIRED SURFACE. (HENCE, A 'HILL' ON THE ACTUAL SURFACE IS A POSITIVE SURFACE ERROR). OPD (X,Y) = THE MEASURED WAVEFRONT OPTICAL PATH LENGTH DIFFERENCE CORRESPONDING TO POINT X,Y ON THE PYRAMID MIRROR FACET SURFACE. THE OPD SIGN CONVENTION IS THAT A POSITIVE OPD VALUE CORRESPONDS TO A LEADING WAVEFRONT SUCH AS WOULD BE PRODUCED BY A 'HILL' ON THE PYRAMID MIRROR FACET SURFACE. BO (X,Y) IS EQUAL TO THE BACKOUT EQUATION FOR TEST RESIDUALS. THE VALUE OF THE BACKOUT EQUATION AT POINT X,Y IS TO BE ADDED TO THE VALUE OF SURFACE OPD AT POINT X,Y AS STATED IN THE PRECEDING EQUATION. THE BACKOUT EQUATION FOR THE PYRAMID MIRROR FACET SURFACE CONTOUR IS A RADIALLY SYMMETRIC FUNCTION EXPRESSED IN UNITS OF CENTIMETERS: BO(X,Y) = *. S(X,Y) = THE MEASURED SURFACE ERROR CORRESPONDING TO POINT X,Y ON THE TEST GLASS. $OPD_T(X,Y)$ = THE MEASURED TRANSMITTED WAVEFRONT OPTICAL PATHLENGTH DIFFERENCE CORRESPONDING TO POINT X,Y ON THE TEST GLASS.

3.0 SURFACE 1 SHALL BE PLANO AND SURFACE 2 SHALL BE SPHERICAL WITHIN 0.02 WAVELENGTH RMS OVER THE CLEAR APERTURE WHEN REFERENCED TO 0.6328 MICRON LIGHT.

3.1 THE CLEAR APERTURE OF SURFACES 1 AND 2 SHALL BE 110 CENTIMETERS MINIMUM IN DIAMETER.

3.2 SURFACES 1 AND 2 TO BE POLISHED. ALL OTHER SURFACES ARE TO BE GROUND TO A FINISH EQUIVALENT TO A 120 GRIT OR BETTER AND FELT POLISHED.

3.3 SURFACE QUALITY - 50/30 IN ACCORDANCE WITH MIL-O-13830A.

3.4 SURFACE 2 SHALL CONFORM TO NOTE 3.0 AFTER COATING. SURFACE 2 SHALL HAVE A REFLECTANCE COATING APPLIED. THE MINIMUM AVERAGE REFLECTANCE OF THE SURFACE 2 COATING SHALL BE 60% AT THE SPECTRAL WAVELENGTH OF 0.6328 MICRONS WHEN MEASURED NORMAL TO THE SURFACE.

3.5 SURFACES 1 AND 2 CLEANING SHALL BE IN ACCORDANCE WITH PROCEDURE *.

3.6 SURFACE 2 SHALL BE A SPHERICAL FIGURE OF REVOLUTION WITH NOMINAL SPHERICAL VERTEX RADIUS OF 306.84 ± *.

4.0 A LINE THROUGH THE INTERFEROMETER FOCUS AND THE MECHANICAL CENTER OF SURFACE 2 MUST PASS THROUGH THE PYRAMID MIRROR FACET SURFACE WITHIN * OF THE MECHANICAL CENTER.

5.0 IN CONFIGURATION *2 THE FOUR PYRAMID MIRROR FACETS (SEE D231-122) ARE COMBINED INTO ONE PYRAMID MIRROR.

6.0 THE POINT PROJECTED BY THE MICROSCOPE SHALL BE LESS THAN 2 MICRONS IN DIAMETER.

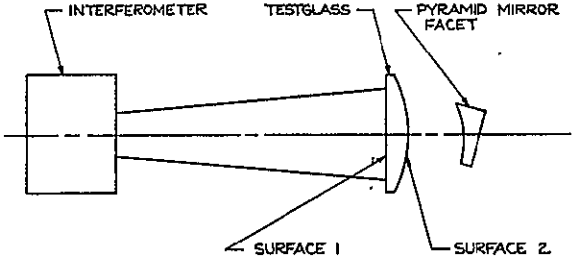

CONFIGURATION *1
(FIZEAU - TEST GLASS)

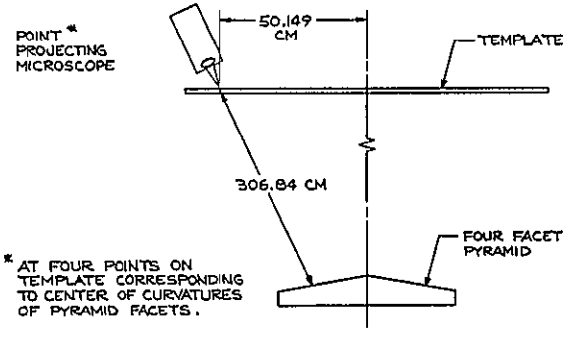

* AT FOUR POINTS ON TEMPLATE CORRESPONDING TO CENTER OF CURVATURES OF PYRAMID FACETS.

CONFIGURATION *2

213

NO.	REVISIONS	BY

UNLESS OTHERWISE SPECIFIED
LINEAR TOLERANCE ±
ANGULAR TOLERANCE ±
DIMENSIONS ARE IN
DIMENSIONS APPLY AFTER FINISH WHERE TOTAL TOLERANCE IS .001 (.025MM) OR LESS AND ON ALL THREADS. IN ALL OTHER PLACES DIMENSIONS APPLY BEFORE FINISH.
READ PRODUCT DESIGN STANDARDS APPLY
THIRD ANGLE PROJECTION

MATERIAL
FINISH
SCALE OF ORIG. DRG. NONE

EASTMAN KODAK CO.
KODAK AMATEUR DIVISION
ROCHESTER, N.Y.
DR. DATE 2-14-79
CK. P.A. JONES
APPR. MFG. ENG.
ORIG. ENG. NO.
RELEASED

NAME PYRAMID MIRROR ACCEPTANCE TEST CONFIGURATION WF/PC
SIZE D
NO. D231-123

NO. D231-124

NOTES:

1. MATERIAL:
   - 1.1 THE MATERIAL USED SHALL BE CORNING® FUSED SILICA, NO 7940
   - 1.2.1 THE α OF ALL THE MATERIAL USED TO FABRICATE ANY MIRROR BLANK SHALL BE $0.50^{\pm}\ 0.02 \times 10^{-6}$ IN/IN/°C OVER A TEMPERATURE RANGE OF -20° TO 20°C WITH A 95 % CONFIDENCE LEVEL.
2. GLASS QUALITY:
   - 2.1 INCLUSIONS SUCH AS BUBBLES AND SEEDS WITHIN THE 0.4 CENTIMETER THICK "CRITICAL ZONE" SHOWN ON THE DRAWING SHALL NOT EXCEED 0.051 CENTIMETERS IN MEAN DIAMETER. THERE SHALL BE NO MORE THAN AN AVERAGE OF 0.02 PER CUBIC CENTIMETER. AVERAGE SIZE OF SUCH INCLUSIONS SHALL BE NO GREATER THAN 0.030 CENTIMETERS IN MEAN DIAMETER.
   - 2.2 OPAQUE INCLUSIONS WITHIN THE 0.4 CENTIMETER THICK "CRITICAL ZONE" SHOWN ON THE DRAWING SHALL NOT EXCEED 0.051 CENTIMETERS IN MEAN DIAMETER. THERE SHALL BE NO MORE THAN AN AVERAGE OF 0.01 PER CUBIC CENTIMETER
3. ANNEAL
   BIREFRINGENCE MEASUREMENTS SHALL BE MADE PERPENDICULAR TO THE 5.60 CENTIMETER SURFACE. THE RELATIVE RETARDATION RESULTING FROM PERMANENT STRAIN SHALL BE NO MORE THAN 20 $\mu\mu$ PER CENTIMETER OF LIGHT PATH.

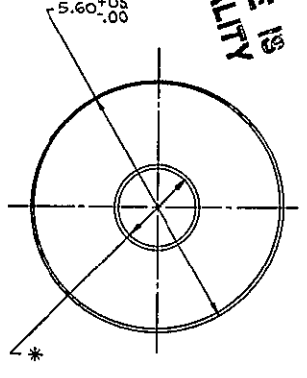

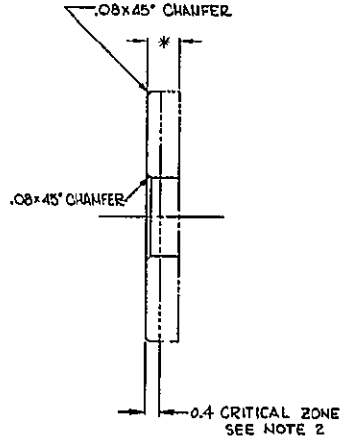

* = TO BE DETERMINED

UNLESS OTHERWISE SPECIFIED LINEAR TOLERANCE ± .025 CM ANGULAR TOLERANCE ± DIMENSIONS ARE IN CENTIMETERS DIMENSIONS APPLY AFTER FINISH WHERE TOTAL TOLERANCE IS .001 (.025MM) OR LESS AND ON ALL THREADS. IN ALL OTHER PLACES DIMENSIONS APPLY BEFORE FINISH KAD PRODUCT DESIGN STANDARDS APPLY THIRD ANGLE PROJECTION	MATERIAL SEE NOTE 1 FINISH SCALE OF ORIG. DWG 2/1	EASTMAN KODAK CO. KODAK APPARATUS DIVISION ROCHESTER N.Y DR THEWETT DATE 11/17/78 CK DES ENG P. A JONES DPTO. MFG ENG. ORIG. DWG. NO RELEASED	FIRST USED ON NAME BLANK, PRIMARY MIRROR PLANETARY CAMERA WF/PC SKETCH NO DWG SIZE D NO D231-124

NO.	ENG NO DATE REL	REVISIONS	DR. BY APP'D

214

NO. D231 - 125

NOTES:

1. SURFACE 1 SHALL BE A FIGURE OF REVOLUTION AND SHALL CONFORM TO THE ASPHERIC EQUATION

$$X = \frac{CY^2}{1+\sqrt{1-(K+1)C^2Y^2}} + EY^4 + FY^6 + GY^8 + HY^{10}$$

WHERE:

X = SAG IN CENTIMETERS OF THE ASPHERIC SURFACE RELATIVE TO A PLANE LOCATED AT THE VERTEX AND NORMAL TO THE OPTICAL AXIS

$$C = \frac{1}{51.7800}$$

1.1 THE NOMINAL VERTEX RADIUS OF THE ASPHERIC SURFACE SHALL BE 51.7800 ±.026 CENTIMETERS

1.2 SURFACE 1 SHALL NOT DEVIATE FROM THE ASPHERIC CURVATURE BY MORE THAN .0015 WAVELENGTH (RMS) (ROOT MEAN SQUARE) AFTER REFLECTIVE COATING. (WAVELENGTH REFERENCE IS 0.6328 MICRONS) AS MEASURED WITH THE TEST SET-UP SHOWN IN D231-126. THE GRID SPACING OF THE SAMPLE POINTS ON THE MIRROR SURFACE SHALL NOT EXCEED 0.15 CENTIMETERS.

1.3 THE ASPHERIC TABLE OF COEFFICIENTS SHOWN BELOW IS BASED ON THE NOMINAL VALUE OF THE VERTEX RADIUS.

K = -0.284 E = 0.0 F = 0.0
G = 0.0 H = 0.0

2. CLEAR APERTURE:
   2.1 SURFACE-1 SHALL HAVE A CLEAR APERTURE BOUNDED ON THE OUTSIDE BY A DIAMETER OF 5.285 CENTIMETERS MINIMUM AND ON THE INSIDE BY A DIAMETER OF 1.570 CENTIMETERS MAXIMUM.
   2.2 FOR ALL MIRROR TESTS BEFORE COATING, SURFACE-1 SHALL HAVE AN UNCOATED CLEAR APERTURE BOUNDED ON THE OUTSIDE BY A DIAMETER OF 5.285 CENTIMETERS MINIMUM AND ON THE INSIDE BY A CIRCLE OF 1.570 CENTIMETERS MAXIMUM.
3. SURFACES MARKED "P" POLISHED, ALL OTHERS GROUND TO A FINISH EQUIVALENT TO 120 GRIT OR BETTER AND FELT POLISHED.
4. REFLECTIVE COATING:
   4.1 SURFACE-1 SHALL CONFORM TO NOTE 1.2 AFTER COATING.
   4.2 SURFACE-1 SHALL BE COATED WITH 800 ANGSTROMS OF ALUMINUM WITH 250 ANGSTROMS OF MAGNESIUM FLUORIDE AS A PROTECTIVE COATING.
   4.3 SURFACE-1 SHALL HAVE A MINIMUM REFLECTANCE OF 70% AT A WAVELENGTH OF 0.1200 MICRONS AND A MINIMUM REFLECTANCE OF 85% AT 0.6328 MICRONS WHEN MEASURED AT NORMAL INCIDENCE.
   4.4 SURFACE CLEANING SHALL BE IN ACCORDANCE WITH *.
5. THE OPTICAL VERTEX SHALL BE WITHIN * CENTIMETERS RADIALLY OF THE MECHANICAL VERTEX.
6. SYSTEM AXES:
   6.1 ANGULAR ORIENTATION OF THE Y AXIS SHALL CONSIDER OPTIMIZATION OF THE ASSEMBLED SYSTEM WAVEFRONT BY ROTATIONAL MATCHING OF THE PRIMARY AND SECONDARY MIRRORS.
   6.2 THE Y AXIS SHALL BE IDENTIFIED BY A 0.013 CENTIMETER WIDE LINE ON SURFACE 2. IDENTIFYING CHARACTER AND LINE SHALL BE DRAWN PER *.
   COLOR: FLAT BLACK MAT'L REQ'D.
7. THE AUTOCORRELATION LENGTH OF THE SYSTEM WAVEFRONT ERROR SHALL BE 0.125 OR LONGER WHEN MODELED AS A GAUSSIAN FUNCTION OVER THE SPATIAL FREQUENCIES FROM 0-20 CYCLES PER PUPIL DIAMETER.
8. SURFACE QUALITY 20-5, MIL-O-13830A.
9. THE MAXIMUM SURFACE ROUGHNESS SHALL BE 30 ANGSTROMS RMS.

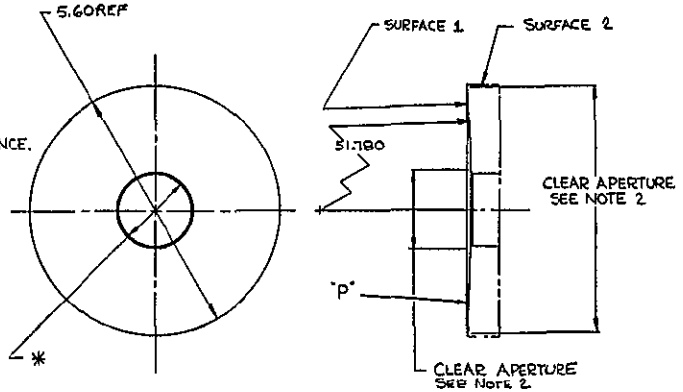

* = TO BE DETERMINED

NO.	CHG. NO. DATE REL.	REVISIONS	BY APP'D

UNLESS OTHERWISE SPECIFIED
LINEAR TOLERANCE ± .025 CM
ANGULAR TOLERANCE ±
DIMENSIONS ARE IN CENTIMETERS
DIMENSIONS APPLY AFTER FINISH WHERE TOTAL TOLERANCE IS .001 (.025MM) OR LESS AND ON ALL THREADS. SCALE DIMENSIONS PLACES DIMENSIONS APPLY BEFORE FINISH.
R&D PRODUCT DESIGN STANDARDS APPLY
THIRD ANGLE PROJECTION

MATERIAL: MAKE FROM D231-124
FINISH
SCALE OF ORIG. DWG. 2/1

EASTMAN KODAK CO.
KODAK APPARATUS DIVISION
ROCHESTER, N.Y.
DR. THEWES DATE 11/10/78
CK. ORIG ENG P A JONES
DFTG. APPD ENG
ORIG. CHG NO
RELEASED

FIRST USED ON
NAME PRIMARY MIRROR, PLANETARY CAMERA WF/PC
SKETCH NO SIZE D
NO. D231-125

215

NOTES:

1.0 TWO ALTERNATE TEST CONFIGURATIONS HAVE BEEN ESTABLISHED

2.0 AN ACCEPTABLE TEST INTERFEROGRAM MAY CONTAIN A MAX OF * WAVE COMA. THE COMA CORRESPONDS TO A DECENTERING OF THE VERTEX OF THE PRIMARY MIRROR RELATIVE TO THE TEST AXIS OF * CM. COMA IS DEFINED IN THE FOLLOWING FIGURE:

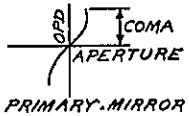

3.0 IN CONFIGURATION #1 THE PRIMARY MIRROR SURFACE ERROR IS CALCULATED BY THE EQUATION:
$E(X,Y) = \frac{1}{2}\,OPD(X,Y) + BO(X,Y)$ WHERE $E(X,Y)$ IS EQUAL TO THE PRIMARY MIRROR SURFACE ERROR AT POINT X,Y ON THE SURFACE DEFINED AS THE SAG OF THE ACTUAL SURFACE MINUS THE SAG OF THE DESIRED SURFACE. HENCE, A "HILL" ON THE ACTUAL SURFACE IS A POSITIVE SURFACE ERROR. $OPD(X,Y)$ = THE MEASURED WAVEFRONT OPTICAL PATH LENGTH DIFFERENCE CORRESPONDING TO POINT X,Y ON THE PRIMARY MIRROR SURFACE. THE OPD SIGN CONVENTION IS THAT A POSITIVE OPD VALUE CORRESPONDS TO A LEADING WAVEFRONT SUCH AS WOULD BE PRODUCED BY A "HILL" ON THE PRIMARY MIRROR SURFACE. $BO(X,Y)$ IS EQUAL TO THE BACKOUT EQUATION FOR TEST RESIDUALS. THE VALUE OF THE BACKOUT EQUATION AT POINT X,Y IS TO BE ADDED TO THE VALUE OF SURFACE OPD AT POINT X,Y AS STATED IN THE PRECEDING EQUATION. THE BACKOUT EQUATION FOR THE PRIMARY MIRROR SURFACE CONTOUR IS A RADIALLY SYMMETRIC FUNCTION EXPRESSED IN UNITS OF CENTIMETERS: $BO(X,Y) = *$.

4.0 IN CONFIGURATION #2 THE PRIMARY MIRROR SURFACE ERROR IS CALCULATED BY THE EQUATION:
$E(X,Y) = \frac{1}{2}\,OPD(X,Y) - \frac{1}{2}R(X,Y) + BO(X,Y)$ WHERE $E(X,Y)$, $OPD(X,Y)$ AND $BO(X,Y)$ ARE DEFINED IN NOTE 3.0. $R(X,Y)$ = THE RETROREFLECTOR WAVEFRONT ERROR AS DETERMINED FROM DIRECT CALIBRATION WITH AN INTERFEROMETER. $BO(X,Y) = *$.

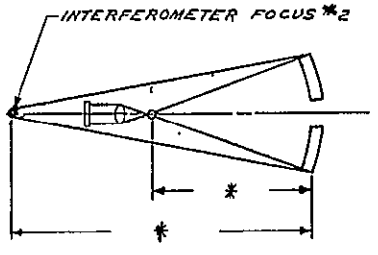

CONFIGURATION #2 (RETROREFLECTOR)

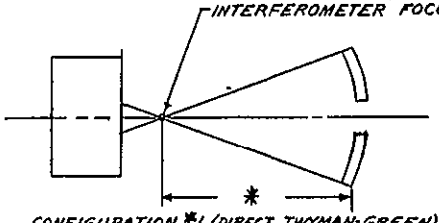

CONFIGURATION #1 (DIRECT TWYMAN-GREEN)

NO D231-126

CHG. NO. DATE REL.	REVISIONS	DR BY APPR.

UNLESS OTHERWISE SPECIFIED
LINEAR TOLERANCE ±
ANGULAR TOLERANCE ±
DIMENSIONS ARE IN
DIMENSIONS APPLY AFTER FINISH WHERE TOTAL TOLERANCE IS .001 (.025MM) OR LESS AND ON ALL THREADS IN ALL OTHER PLACES DIMENSIONS APPLY BEFORE FINISH.
KAD PRODUCT DESIGN STANDARDS APPLY
THIRD ANGLE PROJECTION

MATERIAL
FINISH
SCALE OF DRIG. DWG. 5

EASTMAN KODAK CO.
KODAK APPARATUS DIVISION
ROCHESTER, N.Y.
DR. PLB DATE 2-15-79
CK. DES. ENG. P.A JONES
DFTG. MFG. ENG.
CHG. ORD. NO.
RELEASED

PRINT UNDER
NAME PLANETARY CAMERA PRIMARY MIRROR ACCEPTANCE TEST CONFIGURATION, WF/PC
SKETCH NO. DWG. SIZE D
NO D231-126

216

NO. D231-127

NOTES:

1. MATERIAL:

1.1 THE MATERIAL USED SHALL BE CORNING® FUSED SILICA, NO 7940.

1.2 THE α OF ALL THE MATERIAL USED TO FABRICATE ANY MIRROR BLANK SHALL BE $0.50 \pm 0.02 \times 10^{-6}$ IN/IN/°C OVER A TEMPERATURE RANGE OF -20° TO 20°C WITH A 95% CONFIDENCE LEVEL.

2. GLASS QUALITY:

2.1 INCLUSIONS SUCH AS BUBBLES AND SEEDS WITHIN THE 0.4 CENTIMETER THICK "CRITICAL ZONE" SHOWN ON THE DRAWING SHALL NOT EXCEED 0.051 CENTIMETERS IN MEAN DIAMETER. THERE SHALL BE NO MORE THAN AN AVERAGE OF 0.02 PER CUBIC CENTIMETER. AVERAGE SIZE OF SUCH INCLUSIONS SHALL BE NO GREATER THAN 0.030 CENTIMETERS IN MEAN DIAMETER

2.2 OPAQUE INCLUSIONS WITHIN THE 0.4 CENTIMETER THICK "CRITICAL ZONE" SHOWN ON THE DRAWING, SHALL NOT EXCEED 0.051 CENTIMETERS IN MEAN DIAMETER. THERE SHALL BE NO MORE THAN AN AVERAGE OF 0.01 PER CUBIC CENTIMETER.

3. ANNEAL

3.1 BIREFRINGENCE MEASUREMENTS SHALL BE MADE PERPENDICULAR TO THE 17.1 CENTIMETER SURFACE. THE RELATIVE RETARDATION RESULTING FROM PERMANENT STRAIN SHALL BE NO MORE THAN 20 Mμ PER CENTIMETER OF LIGHT PATH.

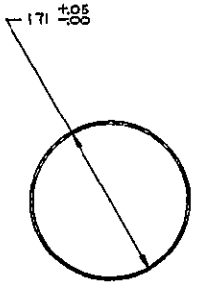

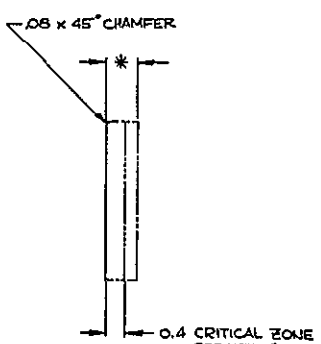

* = TO BE DETERMINED

UNLESS OTHERWISE SPECIFIED: LINEAR TOLERANCE ± .02 CM; ANGULAR TOLERANCE ±; DIMENSIONS ARE IN CENTIMETERS; DIMENSIONS APPLY AFTER FINISH. WHERE TOTAL TOLERANCE IS .001 OR LESS AND ON ALL TAPERS OR ALL OTHER PLACES DIMENSIONS APPLY BEFORE PLATING; KAD PRODUCT DESIGN STANDARDS APPLY; THIRD ANGLE PROJECTION	MATERIAL: SEE NOTE 1 FINISH	EASTMAN KODAK CO. KODAK APPARATUS DIVISION ROCHESTER, N.Y.	FIRST USED ON
		DR T. Hewett DATE 11/17/78	NAME BLANK, SECONDARY MIRROR, PLANETARY CAMERA WF/PC
		CK	DES ENG P. TOMES
		APVD	MFG ENG.
	SCALE OF ORIG. DWG 4/1	ORIG CHG. NO RELEASED	SKETCH NO. SIZE D
			NO. D231-127

CHG NO DATE REL.	REVISIONS	DR. BY APVD
NO		

217

NO. D231-128

NOTES:

1. SURFACE 1 SHALL BE A FIGURE OF REVOLUTION AND SHALL CONFORM TO THE ASPHERIC EQUATION

$$X = \frac{CY^2}{1+\sqrt{1-(K+1)C^2Y^2}} + EY^4 + FY^6 + GY^8 + HY^{10}$$

WHERE:

X = SAG IN CENTIMETERS OF THE ASPHERIC SURFACE RELATIVE TO A PLANE LOCATED AT THE VERTEX AND NORMAL TO THE OPTICAL AXIS.

$C = \frac{1}{23.4330}$

1.1 THE NOMINAL VERTEX RADIUS OF THE ASPHERIC SURFACE SHALL BE 23.4330 ± 0.12 CENTIMETERS.

1.2 SURFACE 1 SHALL NOT DEVIATE FROM THE ASPHERIC CURVATURE BY MORE THAN 0.015 WAVELENGTH (RMS) (ROOT MEAN SQUARE) AFTER REFLECTIVE COATING. (WAVELENGTH REFERENCE IS 0.6328 MICRONS) AS MEASURED WITH THE TEST SET-UP SHOWN IN D231-129. THE GRID SPACING OF THE SAMPLE POINTS ON THE MIRROR SURFACE SHALL NOT EXCEED 0.05 CENTIMETERS.

1.3 THE ASPHERIC TABLE OF COEFFICIENTS SHOWN BELOW IS BASED ON THE NOMINAL VALUE OF THE VERTEX RADIUS.

K = 0.0 E = 0.0 F = 0.0
G = 0.0 H = 0.0

2. CLEAR APERTURE:
   2.1 SURFACE-1 SHALL HAVE A CLEAR APERTURE OF 1.397 ± * CENTIMETERS DIAMETER.
   2.2 FOR ALL MIRROR TESTS BEFORE COATING, SURFACE 1 SHALL HAVE AN UNCOATED CLEAR APERTURE OF 1.397 ± * CENTIMETERS DIAMETER.

3. SURFACES MARKED "P" POLISHED, ALL OTHERS GROUND TO A FINISH EQUIVALENT TO 120 GRIT OR BETTER AND FELT POLISHED.

4. REFLECTIVE COATING:
   4.1 SURFACE -1 SHALL CONFORM TO NOTE 1.2 AFTER COATING.
   4.2 SURFACE -1 SHALL BE COATED WITH 800 ANGSTROMS OF ALUMINUM WITH 250 ANGSTROMS OF MAGNESIUM FLUORIDE AS A PROTECTIVE COATING.
   4.3 SURFACE-1 SHALL HAVE A MINIMUM REFLECTANCE OF 70% AT A WAVELENGTH OF 0.1200 MICRONS AND A MINIMUM REFLECTANCE OF 85% AT 0.6328 MICRONS. WHEN MEASURED AT NORMAL INCIDENCE.
   4.4 SURFACE CLEANING SHALL BE IN ACCORDANCE WITH PROCEDURE *

5. THE OPTICAL VERTEX SHALL BE WITHIN * CENTIMETERS RADIALLY OF THE MECHANICAL VERTEX.

6. SYSTEM AXES:
   6.1 ANGULAR ORIENTATION OF THE Y AXIS SHALL CONSIDER OPTIMIZATION OF THE ASSEMBLED SYSTEM WAVEFRONT BY ROTATIONAL MATCHING OF THE PRIMARY AND SECONDARY MIRRORS.
   6.2 THE Y AXIS SHALL BE IDENTIFIED BY A 0.013 CENTIMETER WIDE LINE ON SURFACE 2. IDENTIFYING CHARACTER AND LINE SHALL BE DRAWN PER *.
   COLOR: FLAT BLACK MAT'L REQ'D.

7. THE AUTOCORRELATION LENGTH OF THE SYSTEM WAVEFRONT ERROR SHALL BE 0.125 DR LONGER WHEN MODELED AS A GAUSSIAN FUNCTION OVER THE SPATIAL FREQUENCIES FROM 0-20 CYCLES PER PUPIL DIAMETER.

8. SURFACE QUALITY 20-5: MIL-O-13830A.

9. THE MAXIMUM SURFACE ROUGHNESS SHALL BE 30 ANGSTROMS RMS.

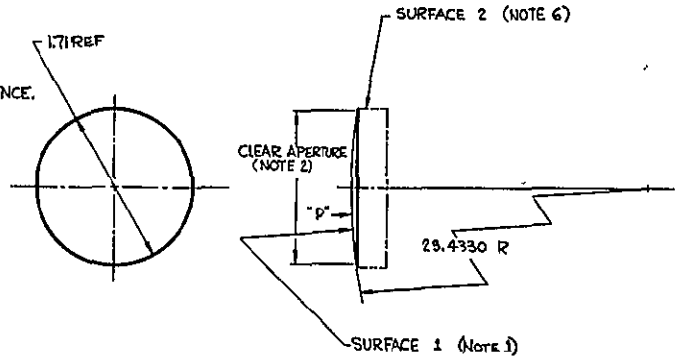

* = TO BE DETERMINED

UNLESS OTHERWISE SPECIFIED: LINEAR TOLERANCE ± .025 CM; ANGULAR TOLERANCE ±; DIMENSIONS ARE IN CENTIMETERS; DIMENSIONS APPLY AFTER FINISH WHERE TOTAL TOLERANCE IS .001 (.0254MM) OR LESS AND ON ALL THREADS, IN ALL OTHER PLACES DIMENSIONS APPLY BEFORE FINISH; READ PRODUCT DESIGN STANDARDS APPLY; THIRD ANGLE PROJECTION	MATERIAL: MAKE FROM D231-127; FINISH; SCALE OF DRG. DIM. 4/1	EASTMAN KODAK CO. ROCHESTER, N.Y.	NAME: SECONDARY MIRROR PLANETARY CAMERA WF/PC; NO. D231-128; SIZE D

NO.	REVISIONS	BY

NOTES:

1.0 TWO ALTERNATE TEST CONFIGURATIONS HAVE BEEN ESTABLISHED.

2.0 AN ACCEPTABLE TEST INTERFEROGRAM MAY CONTAIN A MAX OF * WAVE COMA. THIS COMA CORRESPONDS TO A DECENTERING OF THE VERTEX OF THE SECONDARY RELATIVE TO THE TEST AXIS OF * Cm. COMA IS DEFINED IN THE FOLLOWING FIGURE:

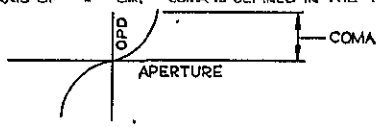

3.0 IN CONFIGURATION #1, THE SECONDARY MIRROR SURFACE ERROR IS CALCULATED BY THE EQUATION: $E(X,Y) = 1/4\ OPD(X,Y) - 1/2\ N(X,Y) + BO(X,Y)$ WHERE $E(X,Y)$ IS EQUAL TO THE SECONDARY MIRROR SURFACE ERROR AT POINT X,Y ON THE SURFACE DEFINED AS THE SAG OF THE ACTUAL SURFACE MINUS THE SAG OF THE DESIRED SURFACE. (HENCE, A "HILL" ON THE ACTUAL SURFACE IS A POSITIVE SURFACE ERROR). $OPD(X,Y)$ = THE MEASURED WAVEFRONT OPTICAL PATH LENGTH DIFFERENCE CORRESPONDING TO POINT X,Y ON THE SECONDARY MIRROR SURFACE. THE OPD SIGN CONVENTION IS THAT A POSITIVE OPD VALUE CORRESPONDS TO A LEADING WAVEFRONT SUCH AS WOULD BE PRODUCED BY A "HILL" ON THE SECONDARY MIRROR SURFACE. $BO(X,Y)$ IS EQUAL TO THE BACKOUT EQUATION FOR TEST RESIDUALS. THE VALUE OF THE BACKOUT EQUATION AT POINT X,Y IS TO BE ADDED TO THE VALUE OF SURFACE OPD AT POINT X,Y AS STATED IN THE PRECEDING EQUATION. THE BACKOUT EQUATION FOR THE SECONDARY MIRROR SURFACE CONTOUR IS A RADIALLY SYMMETRIC FUNCTION EXPRESSED IN UNITS OF CENTIMETERS. $BO(X,Y) = *$. $N(X,Y)$ = THE HINDLE SPHERE SURFACE ERROR AS DETERMINED FROM DIRECT INTERFEROMETER CALIBRATION.

4.0 SURFACE 2 SHALL BE SPHERICAL WITHIN 0.02 WAVELENGTH RMS OVER THE CLEAR APERTURE WHEN REFERENCED TO 0.6328 MICRON LIGHT.

4.1 SURFACE 2 IS TO BE POLISHED. ALL OTHER HINDLE SPHERE SURFACES ARE TO BE GROUND TO A FINISH EQUIVALENT TO A 120 GRIT OR BETTER AND FELT POLISHED.

4.2 SURFACE QUALITY - 50/30, IN ACCORDANCE WITH MIL-O-13830A.

4.3 SURFACE 2 SHALL CONFORM TO NOTE 4.0 AFTER COATING. SURFACE 2 SHALL HAVE A HIGH REFLECTANCE COATING APPLIED. THE MINIMUM AVERAGE REFLECTANCE OF THE SURFACE 2 COATING SHALL BE 95% OR GREATER AT THE SPECTRAL WAVELENGTH OF 0.6328 MICRONS WHEN MEASURED NORMAL TO THE SURFACE.

4.4 SURFACE CLEANING SHALL BE IN ACCORDANCE WITH PROCEDURE *

4.5 SURFACE 2 SHALL BE A SPHERICAL FIGURE OF REVOLUTION WITH A NOMINAL VERTEX RADIUS OF 25.8298 ± * CENTIMETERS.

4.6 THE CLEAR APERTURE OF SURFACE 2 SHALL BE 3.935 Cm MIN O.D. AND 0.845 Cm MAX I.D.

5.0 A LINE THROUGH INTERFEROMETER FOCI POINTS 1 & 2 MUST PASS THROUGH THE SECONDARY MIRROR SURFACE WITHIN * OF THE MECHANICAL CENTER.

6.0 IN CONFIGURATION #2, THE SECONDARY MIRROR SURFACE ERROR IS CALCULATED BY THE EQUATION:

$$E(X,Y) = \tfrac{1}{2}\, OPD(X,Y) - \left[S(X,Y) + OPD_T(X,Y)\right] + BO(X,Y)$$

WHERE $E(X,Y)$, $OPD(X,Y)$, $BO(X,Y)$ ARE DEFINED IN NOTE 3.0
$S(X,Y)$ = THE MEASURED SURFACE ERROR CORRESPONDING TO POINT X,Y ON THE TEST GLASS.
$OPD_T(X,Y)$ = THE MEASURED TRANSMITTED WAVEFRONT OPTICAL PATHLENGTH DIFFERENCE CORRESPONDING TO POINT X,Y ON THE TEST GLASS.

7.0 SURFACE 3 & 4 SHALL BE SPHERICAL WITHIN 0.02 WAVELENGTH RMS OVER THE CLEAR APERTURE WHEN REFERENCED TO 0.6328 MICRON LIGHT.

7.1 THE CLEAR APERTURE OF SURFACES 3 & 4 SHALL BE *.

7.2 SURFACES 3 & 4 TO BE POLISHED, ALL OTHER SURFACES ARE TO BE GROUND TO A FINISH EQUIVALENT TO A 120 GRIT OR BETTER AND FELT POLISHED.

7.3 SURFACE QUALITY - 50/30 IN ACCORDANCE WITH MIL-O-13830A.

7.4 SURFACE 3 SHALL CONFORM TO NOTE 7.0 AFTER COATING. SURFACE 3 SHALL HAVE A REFLECTANCE COATING APPLIED. THE MINIMUM AVERAGE REFLECTANCE OF THE SURFACE 3 COATING SHALL BE 60% AT THE SPECTRAL WAVELENGTH OF 0.6328 MICRONS WHEN MEASURED NORMAL TO THE SURFACE.

7.5 SURFACES 3 & 4 CLEANING SHALL BE IN ACCORDANCE WITH PROCEDURE *.

7.6 SURFACES 3 & 4 SHALL BE SPHERICAL FIGURES OF REVOLUTION WITH NOMINAL SPHERICAL VERTEX RADII OF 23.4330 ± *.

8.0 A LINE THROUGH INTERFEROMETER FOCI POINT #3 AND THE MECHANICAL CENTER OF SURFACE 3 MUST PASS THROUGH THE SECONDARY MIRROR SURFACE WITHIN * OF THE MECHANICAL CENTER.

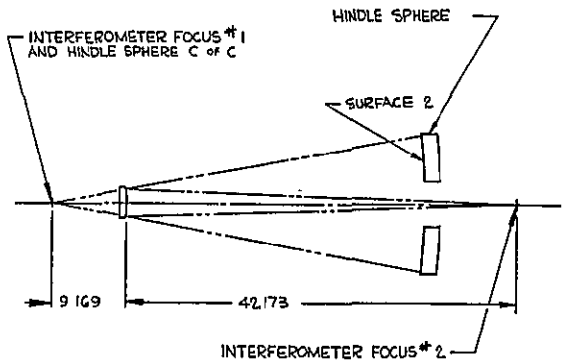

CONFIGURATION #1
(HINDLE)

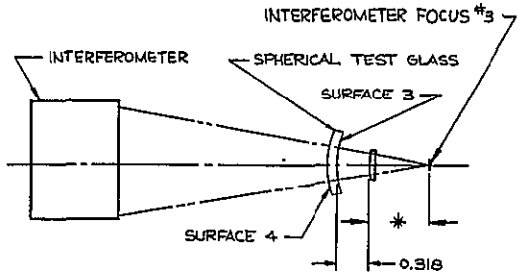

CONFIGURATION #2
(FIZEAU)

* = To Be Determined

ORIGINAL PAGE IS OF POOR QUALITY

NO.	REVISIONS	DR. BY APPR.

UNLESS OTHERWISE SPECIFIED
LINEAR TOLERANCE ±
ANGULAR TOLERANCE ±
DIMENSIONS ARE IN CENTIMETERS
DIMENSIONS APPLY AFTER FINISH WHERE TOTAL TOLERANCE IS .001 (.DECIMAL) OR LESS AND ON ALL THREADS. IN ALL OTHER PLACES DIMENSIONS APPLY BEFORE FINISH.
KAD PRODUCT DESIGN STANDARDS APPLY
THIRD ANGLE PROJECTION

MATERIAL
FINISH
SCALE OF ORIG. DWG. NONE

EASTMAN KODAK CO.
KODAK APPARATUS DIVISION
ROCHESTER, N.Y.

DR. Thrwett DATE 1/2/79
CK. DES. ENG. P.A. JONES
MFG. MFG. ENG.
CONT. CHG. NO.
APPROVED

PART USED ON
NAME PLANETARY CAMERA SECONDARY MIRROR ACCEPTANCE TEST CONFIGURATION, WF/PC
SKETCH NO. SIZE D
NO. D 231-129

219